

ISSN 2187-2260

**Proceedings of the 19<sup>th</sup> Meeting of  
Japan CF Research Society  
JCF19**

**November 9-10, 2018**

**Ginga Hall, Iwate University**

**Japan CF-Research Society**

**Edited by Katsuaki Tanabe**

Copyright © 2018 by Japan CF Research Society

*All rights reserved. No part of this publication may be reproduced, stored in a retrieval system, or transmitted, in any form or by any means, electronic, mechanical, photocopying, recording or otherwise, without the prior permission of the copyright owner.*

## PREFACE

This is the proceedings of the 19<sup>th</sup> Meeting of Japan CF-Research Society (JCF19), which was held on November 9-10, 2018 at Ginga Hall, Iwate University, Morioka, Japan. In this meeting, 17 presentations were given and 12 papers were submitted to the editorial board. They have been peer reviewed by the referees, and revised for the publication as the proceedings.

For all meetings, JCF1 through JCF18, we published the Proceedings. For the meetings after JCF4, we published electronic versions of the proceedings on our web-site [http://jcfrs.org/proc\\_jcf.html](http://jcfrs.org/proc_jcf.html) in addition to their printed versions. In view of low efficiency and low effectiveness in distributing information, we decided to discontinue the printed version for the meetings, JCF12. Only the electronic versions have been published thereafter. Any questions and comments are welcome for the proceedings.

Finally, we would like to thank all the participants and the people who have collaborated in organizing this meeting.

*Editor-in-Chief*

*Katsuaki Tanabe, Kyoto University*

*May 2019*

## CONTENTS

Preface: K. Tanabe .....	i
Repeated Calcination and AHE by PNZ6 Sample <i>A. Takahashi, K. Takahashi, R. Seto, T. Yokose, A. Kitamura, Y. Furuyama</i>	----- 1
Anomalous Heat Burst by CNZ7 Sample and H-Gas <i>T. Yokose, A. Takahashi, K. Takahashi, Y. Furuyama</i>	----- 18
Computer Simulation Approaches to Hydrogen Cohesion inside the Metal Surface <i>H. Miura</i>	----- 36
Thermal Properties of Pd–Zr and Pd–Ni–Zr Complex Sample in Deuterium Diffusion Process <i>M. Endo, Y. Sato, S. Kikuchi, K. Ota, K. Negishi, S. Narita</i>	----- 53
Search for Nuclear Reaction in Deuterium Discharge Experiment Using Pd/PdO Cathode <i>S. Kikuchi, T. Nejo, Y. Sato, K. Ota, M. Takahashi, S. Narita, K. Negishi</i>	----- 66
A Theoretical Study on the Possible Change of the Phonon Dispersion Relation due to the Nuclear Reaction in Two-Dimensional Lattice <i>K. Tsuchiya</i>	----- 77
Inductive Logic and Meta-Analysis in the Cold Fusion Research <i>H. Kozima</i>	----- 85

Development of the Solid State-Nuclear Physics

*H. Kozima*

----- 112

Microstructure of Pd Rod Electrode during Long-Term Electrolysis in 0.1 M LiOD and during Repeated Cathodic and Anodic Electrolysis in Glycerin-Phosphoric Acid: Behavior of Void Related with Vacancy-Cluster

*H. Numata*

----- 148

Note

Characteristics of the Nuclear Reactions in the Cold Fusion Phenomenon

*H. Kozima, H. Yamada*

----- 165

## Repeated Calcination and AHE by PNZ6 Sample

Akito Takahashi<sup>1\*</sup>, Koh Takahashi<sup>1</sup>, Reiko Seto<sup>1</sup>,  
Toyoshi Yokose<sup>2</sup>, Akira Kitamura<sup>2</sup>, Yuichi Furuyama<sup>2</sup>

<sup>1</sup> Technova Inc., 100-0011 Japan,

<sup>2</sup> Graduate School of Maritime Sciences, Kobe University, 658-0022 Japan

\*Corresponding author

**Abstract** Repeatability of anomalous heat effect (AHE) by the interaction of nano-composite PNZ6 (Pd<sub>1</sub>Ni<sub>10</sub>/zirconia) sample and D-gas at ca. 300°C RC (reaction chamber) condition was studied by making repeated calcination of sample after D-charging experimental runs. D-loading ratios (D/Ni) at room temperature changed as 3.5, 0.8 and 0.08 for the first, second and third calcined PNZ6 sample, respectively with big decrease of integrated amount of heat. AHE at elevated temperature was repeatedly observed with 7-11 W level by re-calcination, and excess power was sustained for several weeks. Large increase (over 100°C cf. blank run) of local temperatures in RC was observed by the #1-2 run with the third calcined sample PNZ6rr. It is equivalent to excess power of 55 W in the local zone along central vertical line of RC. Strange oscillatory change of TC4 temperature at gas-inlet/outlet point of RC and much increased inside temperatures by 4 RTDs were recorded in #1-2 run of PNZ6rr sample.

We make summary as: Re-calcination is effective to change D-loading at room temperature; namely to drastically small absorption of D. After third calcination, PNZ6rr sample (ca.100g) gave significant (ca. 100°C) temperature rise in local RC zone and sustainable excess heat over 10W for several weeks. Oxygen content increased to ca. 20% in weight for PNZ6rr by the third calcination. Low oxidized sample PNZ10 (under trial for AHE scale-up) with poor control of fat melt-spun ribbon thickness can be treated by re-calcination after use and we may try retest, for confirming possible enhancement of AHE.

**Index Terms** – Anomalous heat effect, Pd-Ni nanocomposite, Repeated calcination, D-loading, Sustainable excess heat, 10 W level, local excess heat.

### I. INTRODUCTION

The anomalous heat effect (AHE) by experiments of hydrogen-gas charged nickel-based nano-composite samples as Pd-Ni/zirconia (PNZ) powder samples has been studied intensively [1,2] under the NEDO-MHE project in 2015-2017 [3], for verifying the existing of the phenomenon and finding conditions of excess power generation in controllable way. As reviewed in ref. [4], the 8 year-long (2008-2015) series of study on anomalous heat effects by interaction of metal nanoparticles and D(H)-gas under the collaboration of Technova Inc. and Kobe University has become the basis for the collaborative research of NEDO-MHE. The reports of results by the project were first published in Proceedings of ICCF20 Conference [5, 6].

In the present work, anomalous heat effect (AHE) by the interaction of nano-composite PNZ6 (Pd<sub>1</sub>Ni<sub>10</sub>/zirconia) sample and D-gas at ca. 300°C RC (reaction chamber) condition was studied by making the third repeated calcination of sample after D-charging experimental runs and by comparing data with the previous experiments by the first and second calcined samples. After describing experimental procedure and results, we will summarize as: Re-calcination is effective to change D-loading at room temperature; namely to drastically small absorption of D. After third calcination, PNZ6rr sample (ca.100g) gave significant (ca. 100°C) temperature rise in local RC zone and sustainable excess heat over 10W for several weeks. Oxygen content increased to ca. 20% in weight for PNZ6rr by the third calcination. Low oxidized sample PNZ10 (under trial for AHE scale-up) with poor control of fat melt-spun ribbon

thickness is to treat by re-calcination after use and we may try retest, for confirming possible enhancement of AHE.

## II. EXPERIMENTAL PROCEDURE AND SAMPLES

For fabricating Pd-Ni nano-composite samples, design guideline from the theoretical view of TSC model [7, 8] was useful. In the TSC theory, AHE is thought to take place by the CCF (condensed cluster fusion) of deuterons (or protons plus electron) at SNHs (sub-nano-holes) like surface defects which may work as surface catalytic sites of binary metal nano-composite islands. The formation probability of TSC (tetrahedral symmetric condensate) may be drastically enhanced at SNHs under high flux incoming or out-going isotopic hydrogen molecules. Therefore CCF reactions may take place under some net D (or H) desorption condition as well as net slow absorption condition. This condition will be attained at elevated sample temperature after saturation of D (or H) absorption into core (Ni nano-core is the case) of binary nano-composite islands. In Fig.1, we show again the image of working AHE sample configuration for nano-composite sample islands supported by nano-pores of ceramics as zirconia or silica.

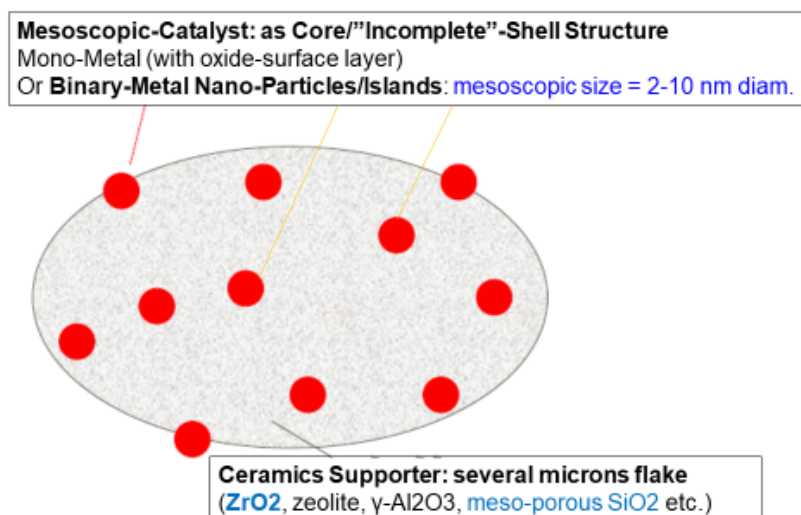


Fig.1 Image of working binary-metal nano-composite sample for fabrication

To realize the nano-core/incomplete shell structure with 2-10 nm nano-islands in ceramics supporter flake (several microns), atomic ratio of minor outer shell element (Pd in our case) and inner core (Ni in our case) may have optimum value around Pd/Ni = 1/7. The PNZ6 sample for the present work has Pd/Ni = 1/10 [1, 2]. Confirmation of nano-islands has been made by the STEM/EDS analysis [3, 4].

For fabricating PNZ6 sample, the melt-spinning-and-calcination method was used. In Fig.2, schematic procedure of fabrication is shown. First, Pd-Ni-Zr alloy with designated atomic ratio of Pd<sub>0.032</sub>Ni<sub>0.318</sub>Zr<sub>0.65</sub> was produced by arc-melting apparatus. Rod of alloy was melt again in graphite crucible by RF heating, and liquid was ejected onto rotating copper belt to make several micron thick amorphous ribbons. Amorphous

ribbons were calcined at 450°C for 60 hours. Pd<sub>1</sub>Ni<sub>10</sub> nano-islands would have been formed in homogeneous oxidized zirconium (zirconia). Powdering of sample was made by usual way of mortar processing.

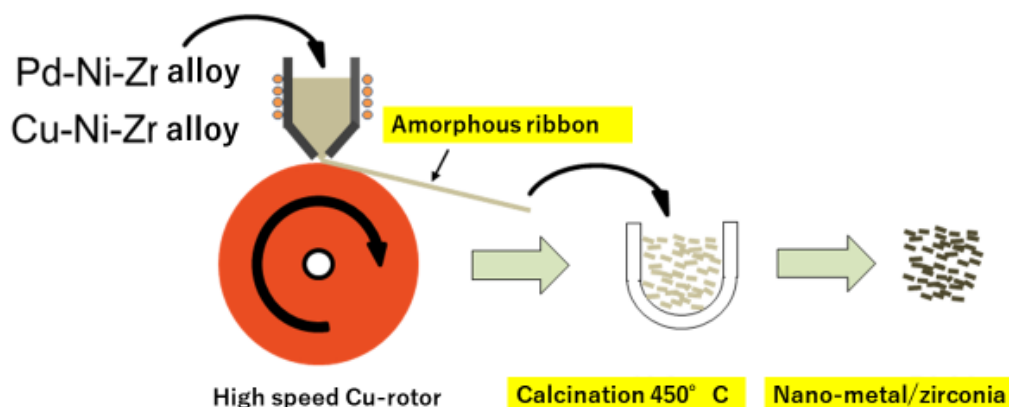


Fig.2 Procedure of sample fabrication for AHE experiment

Re-calcination of used sample (ca. 100 g) with D-gas charging at elevated temperatures [1, 2] was made at 450°C for 60 hours by using electric oven. We labelled as PNZ6, PNZ6r and PNZ6rr, respectively for the first, the second and the third calcined sample. In the present report, we add some preliminary data by large amount sample PNZ10 (Pd<sub>1</sub>Ni<sub>10</sub>/zirconia) after the first calcination only. Amount of oxygen content was estimated from the weight difference before and after the calcination/re-calcination. Data of oxygen contents for PNZ6, PNZ6r and PNZ6rr samples will be given in later section (Table-2).

A schematic of the D(H)-gas-charging-calorimetry system C<sub>1</sub> at Kobe University is shown in Fig. 3. Refer to the references [1, 2] for detailed description of the system. Calibration of the flow calorimetry with a flow rate of nominal 20 cc/min was performed using the 1500 g pure ZrO<sub>2</sub> filler. During real experimental runs, flow rate of coolant oil was varying from time to time in the range of 18.2 to 18.6 cc per minute. We adopted the flow rate correction [1, 2] to normalize to the flow rate of blank calibration run with dummy sample of pure zirconia filler. The heat conversion coefficient from the power to the oil-outlet temperature  $T_{C2}$  at TC2,  $dT_{C2}/dW = 1.57$  °C/W or 0.82 °C/W, was obtained at near room temperature (RT) or at elevated temperature around 300 °C of averaged 4 RTDs in RC, respectively. The test PNZ sample (ca. 100 g) was set in reaction chamber (RC) mixed with ca.1.3 kg ZrO<sub>2</sub> filler powder of 1-mm diameter zirconia particles. About 95% of 500 cc volume of the reaction chamber was filled mostly with the zirconia filler, and only about 5% was occupied by the mixed PNZ test sample for AHE measurement. Time constant of flow calorimetry (about 40 min around 300°C RC temperature) and heat transfer dynamics in RC was very close between each PNZ foreground run and zirconia blank run, consequently. Inside RC, we have 4 RTD-sensors (RTD1, RTD2, RTD3 and RTD4)

which are located at 3 cm, 6 cm, 9 cm and 12 cm height from the bottom of RC. Net height of inner volume of RC is 20 cm. The inner heater W2 is located at ca. 5 cm from the RC bottom and along the vertical centre line. The outer heater W1 is wound spirally outer face of RC. Therefore, evolution of averaged RC temperature during elevated temperature (ET) run can be roughly monitored by temperature of RTD4 at near mid-point of RC.

To remove impurity gas (mostly moisture) of sample, we made so called baking run at 200-250°C RTD temperatures under evacuation until when RC gas pressure  $P_r$  became less than 0.1 Pa. Baking was also done between #1, #2, #3, etc. runs, for changing experimental conditions of AHE observation. D-gas is once stored in storage tank (ST), typically with 1.0 MPa. We start RT (room temperature) run #1-1, #2-1, #3-1, etc. by slowly feeding D-gas through super needle valve (valve with vertical arrow in Fig.3). We accumulated time-evolution data of many items. Our measuring items were D-loading ratios (estimated from change of storage tank pressure  $P_s$  and RC pressure  $P_r$ ), 4 temperatures by RTDs in RC, oil inlet temperatures by TC5 and TC6, oil outlet temperatures by TC1, TC2 and TC2', temperature of D-gas inlet/outlet point by TC4, oil flow rate  $F_r$ , neutron monitor counts (by He-3 counter surrounded by polyethylene moderator) and gamma-ray counts/spectra by NaI detector, respectively. Data accumulation procedure was same for ET (elevated temperature) runs by heating with [W1, W2] resistive heaters. TC2' is set at "same place" together with TC2.

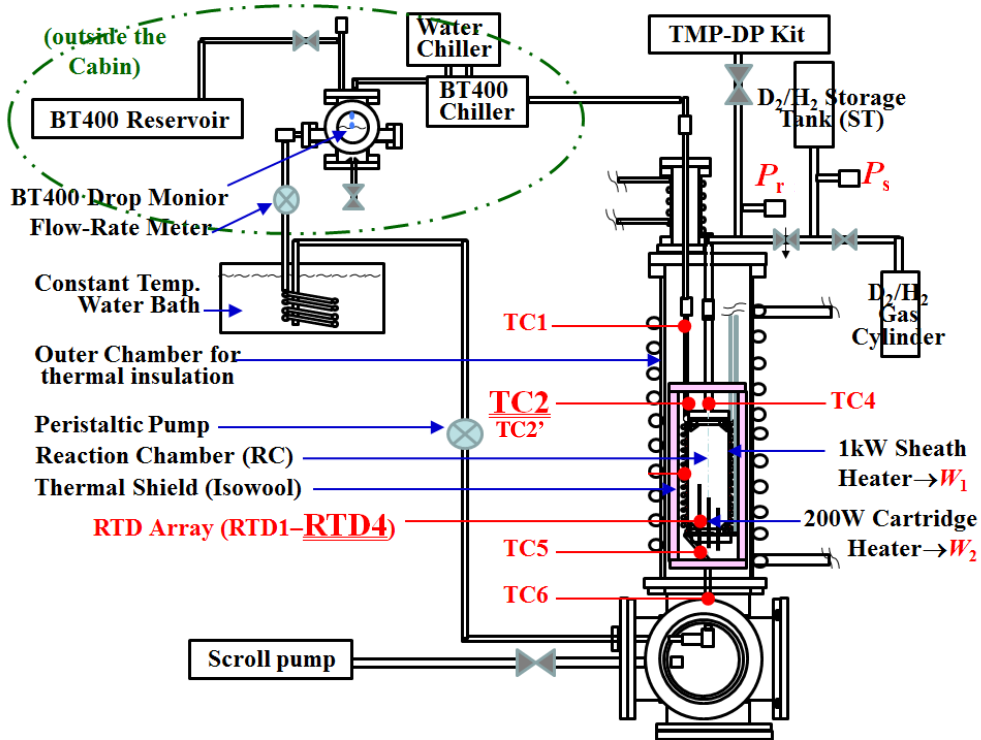


Fig. 3. Schematic of  $C_1$  absorption system equipped with oil-flow-calorimeter system with flow-rate-monitors and dual heaters.

### III. RESULTS AND DISCUSSIONS

#### 3.1 Comparison of Raw Data

Data for the PNZ6 sample were given in our previous paper [1, 2]. Due to the LOCA (loss of coolant accident) during the PNZ6#1 runs, experimental conditions were complex and time evolution data of temperatures, D-gas pressure and loading ratio  $L_M = D/Ni$  were complicated. During later experiments by PNZ6r and PNZ6rr samples, we had no LOCA accidents and observed rather stable time-evolution data to be preferable for comparison purpose.

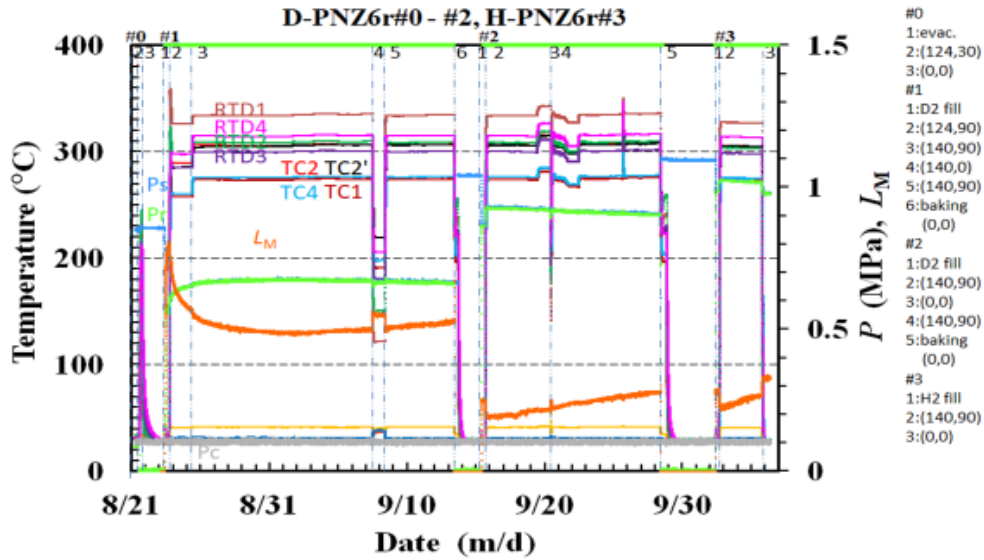


Fig.4 Raw data observed in PNZ6r#1, 2 and 3 runs

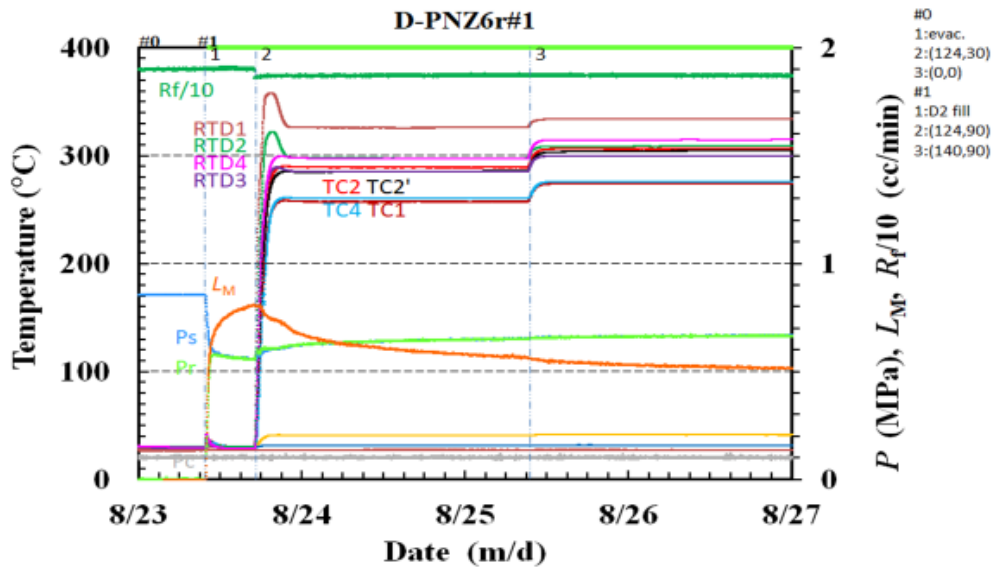


Fig.5 Expanded view of raw data for PNZ6r#-1-1, -2 and -3 runs

In Fig.4, all raw data by PNZ6r#1 runs are shown. Each measurement term (RTD1-4, TC1-6, Ps, Pr, LM or Rf) and graph is drawn with same color. Heating conditions (in bracket) by W1 and W2 heaters, baking and D-gas filling are inserted in very right of the figure. Expanded processed data of RT run (PNZ6r#1-1) will be shown in the next section. Behaviors of temperatures in RC and oil outlet point (by TC2) are smoothly lasted, except for beginning humps of RTDs by PNZ6r#1-2 run and artificial flow rate changes (to take flow rate correction data) in PNZ6r#2-3 and -4 runs. D-loading ratios  $LM = D/M$  are changed drastically in runs. Here  $D/M$  is  $D/((Pd + 10Ni)/11)$  and is roughly a measure of  $D/Ni$ . By RT run PNZ6r#1-1,  $LM$  saturated with ca. 0.80. In the next ET run PNZ6r#1-2,  $LM$  decreased (namely desorption of  $D_s$ ) significantly in a week and slowly increased (namely absorption of  $D_s$ ). We observed AHE with 10 W level excess thermal power in the total interval of PNZ6r1-2 run, even under the  $D$ -desorption condition. Runs after two baking treatments, namely between PNZ6r#2 and 3, slow  $D$  (or  $H$  for #2-3) absorption continued with smaller loading ratios.

In Fig.5, data of PNZ6r#1-2 in expanded time span are shown. By initial ET condition, small temperatures humps are seen in RTD data. Amplitudes of humps are larger for RTD1 and RTD2 than RTD3 and RTD4. This fact may reflect in possible enhanced AHE in higher RC local temperatures near W2 heating. We will see similar trend in Fig.9 for PNZ6rr run. The loading ratios  $LM$  are decreasing drastically in the corresponding time span. Exothermic heat spike by the humps is mysterious because we do not know any exothermic hydrogen desorption phenomena in chemistry. Heat power data will be shown in later section. Rather steady excess thermal power continued for ca. 4 days, under the slow  $D$ -desorption condition.

In Figs. 6-9, raw data by PNZ6rr runs are shown. Same color is used for each term and corresponding graph.

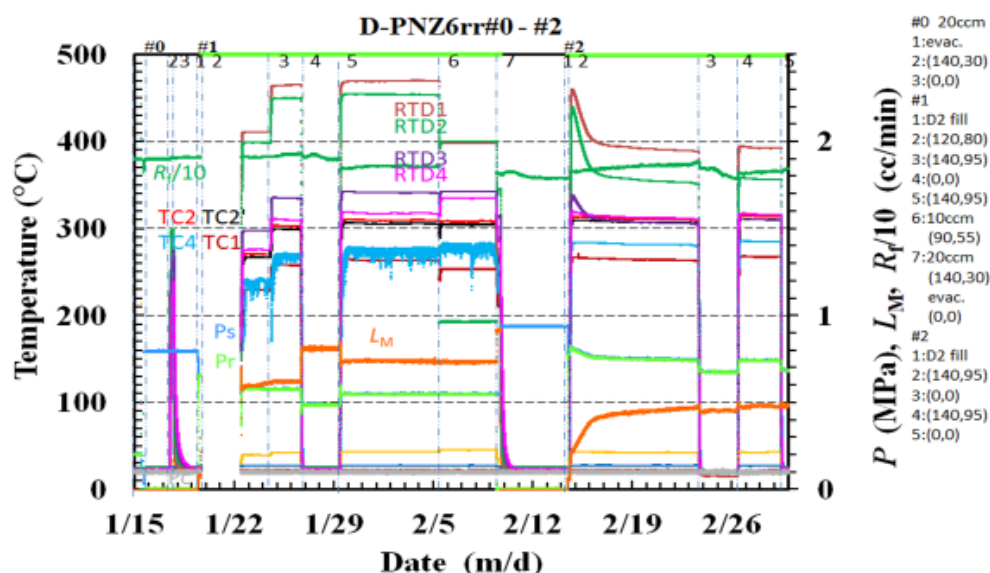


Fig.6 Full raw data of PNZ6rr#1 and PNZ6rr#2 runs

In Fig.6, full raw data are plotted for PNZ6rr#1 and PNZ6rr#2 runs. Variation of loading ratios was very small for PNZ6rr#1 ET runs, as well as rather small change in PNZ6rr#2 runs. Significantly high local RC temperatures by RTDs were observed in PNZ6rr#1-2 and -5 runs, which are ca. 100°C higher than compared data with PNZ6rr#2-2 and -4 runs, although heating conditions were just the same [W1, W2] = (140, 95) watts. Local RC temperatures by RTDs decreased steeply at the beginning of PNZ6rr#2-2 run. The reason of these behaviors is not understood well. Mysterious fluctuations of TC4 data at inlet/outlet point of D-gas were observed correspondingly to the local high temperatures of RTDs. This phenomenon may be similar to the frequent heat and pressure spikes observed by Iwamura et al [6] for CNZ5 and CNZ6 (Cu<sub>1</sub>Ni<sub>7</sub>/zirconia) ET runs. Also, the observation of very big heat burst event with big TC4 variation data for the CNZ7 1kg sample ET run CNZ7#1-2, by Yokose et al [9], may be the same phenomenon.

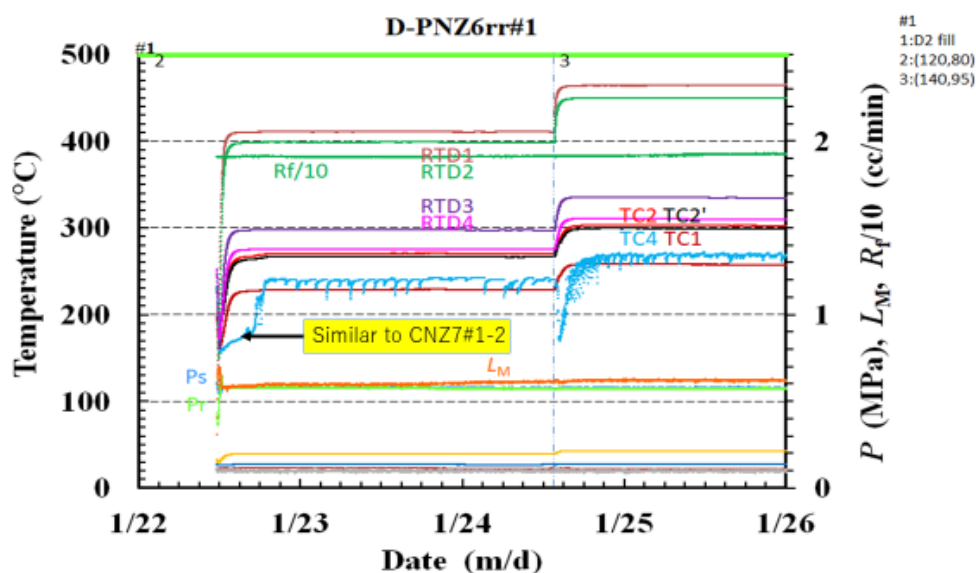


Fig.7 View in expanded time-span for PNZ6rr#1-2 and -3 raw data

In Fig.7, view in expanded time-span for PNZ6rr#1-2 and -3 runs is shown. Loading ratios D/M are very slightly increasing (very slow net absorption) around 0.6. AHE with ca. 10 W excess thermal power level was observed (see later section) during this time-span of several days. Local temperatures by RTDs in RC changed rather smoothly. Strange behavior is interestingly seen in frequent fluctuations of TC4 temperature curve. Especially, about 6 hours long plateau with significantly lower temperatures (cf. other temperature data of coolant oil and RC) were observed by TC4 at D-gas inlet/outlet point (see Fig.3). This plateau behavior of TC4 may be the same phenomenon as observed by the big heat burst event of CNZ7#1-2 run [9]. Fluctuation of temperature by TC4 ended when out-gassing of sample in RC was made by baking under evacuation, as shown in Fig.8. We wondered if some contact failure of thermocouple TC4 happened. However, it was not the case.

In PNZ6rr#2-2 run, we observed again (as it was in PNZ6r#1-2 run: see Fig.5) significant temperature humps of RTDs in RC, as shown in Fig.9. Under net slow D-

absorption process (see D/M loading ratio curve), the exothermic humps of RTDs data happened. During this time-span, we obtained rather flat AHE data with ca. 10 W excess thermal power evolution, as shown in later section.

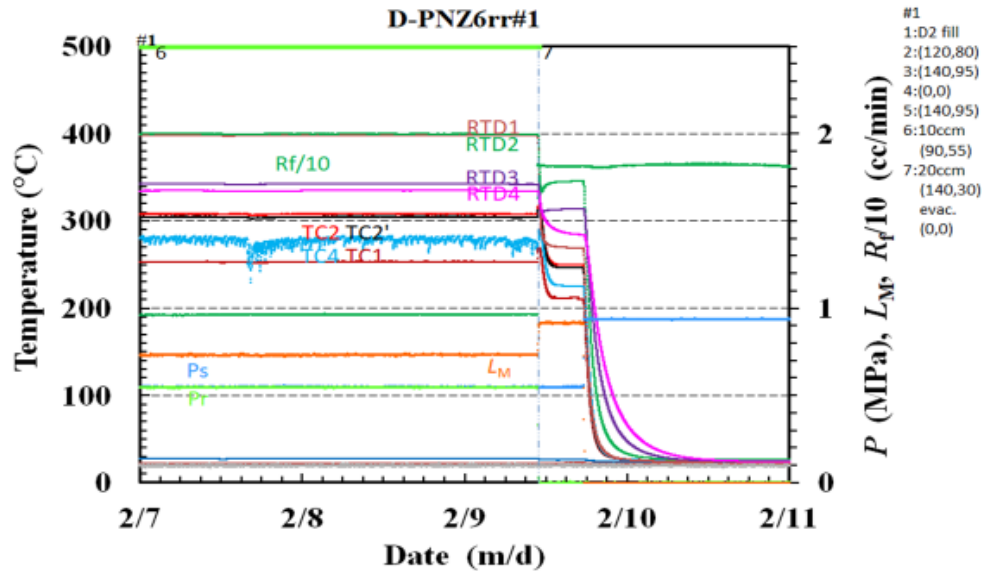


Fig.8 Raw data for PNZ6rr#1-6 ET run and PNZ6rr#1-7 baking run

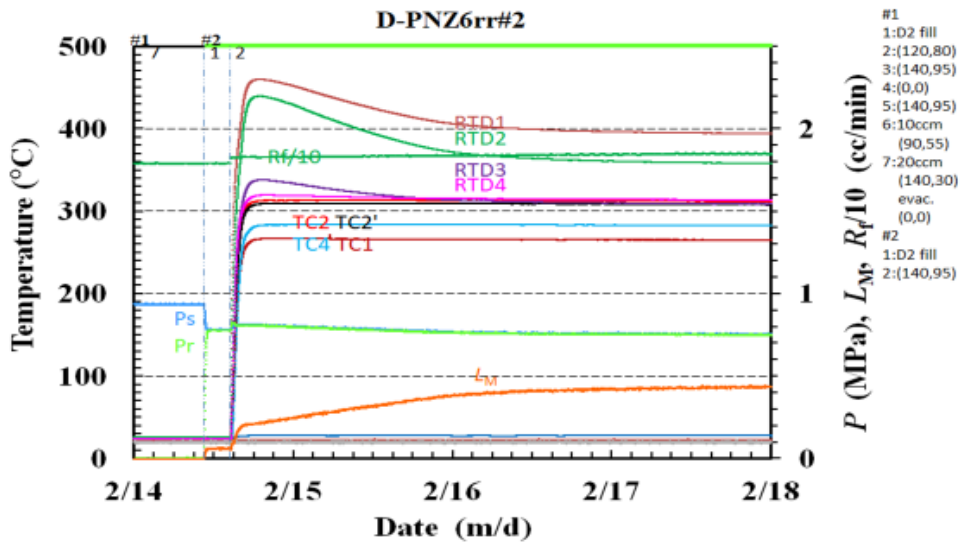


Fig.9 View of expanded time-span for PNZ6rr#2-2 ET run

In Fig.9, amplitudes of start-up humps are larger for RTD1 and RTD2 than RTD3 and RTD4. This fact may reflect in possible enhanced AHE in higher RC local temperatures near W2 heating. We saw similar trend in Fig.5 for PNZ6r run.

### 3-2 DATA BY RT RUNS

It was conclusively discussed in Ref [4] that the isotopic effect of D (or H) absorption in nano-metal powder at RT runs was not large. We reported that typically, about 30 percent (in average) larger specific reaction energy ( $\eta$ -value) for D than those for H was concluded. The  $\eta$ -data for nano-Pd/ceramics powder were around 0.5 eV/D, although loading ratio D(or H)/Pd could reach very large value as 3.5 at maximum. We know that D (or H)/Pd for bulk sample saturates usually with ca. 0.7 with  $\eta$ -value of 0.22 eV/D(or H). With PNZ type powder sample, D(H) absorption is thought to take place into Ni nano-core of composite binary metal islands.

In Figs. 10-12, observed data of thermal power, integrated exothermic energy,  $\eta$ -value and loading ratio are shown, respectively for RT runs of PNZ6#1-1, PNZ6r#1-1 and PNZ6rr#1-1.

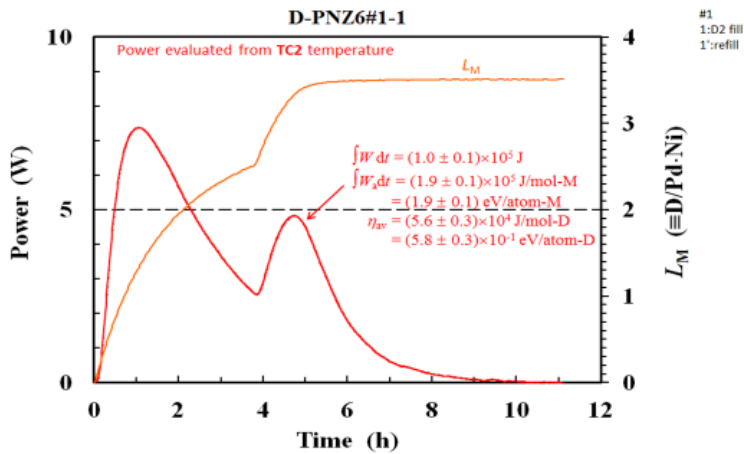


Fig. 10 Observed thermal power and D/M loading ratio for PNZ6#1-1 RT run

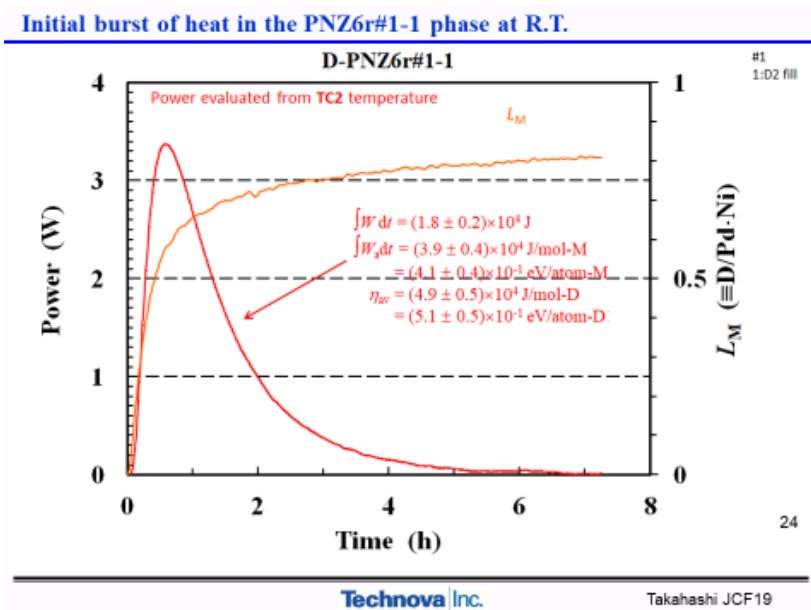


Fig. 11 Observed thermal power and D/M loading ratio for PNZ6r#1-1 RT run

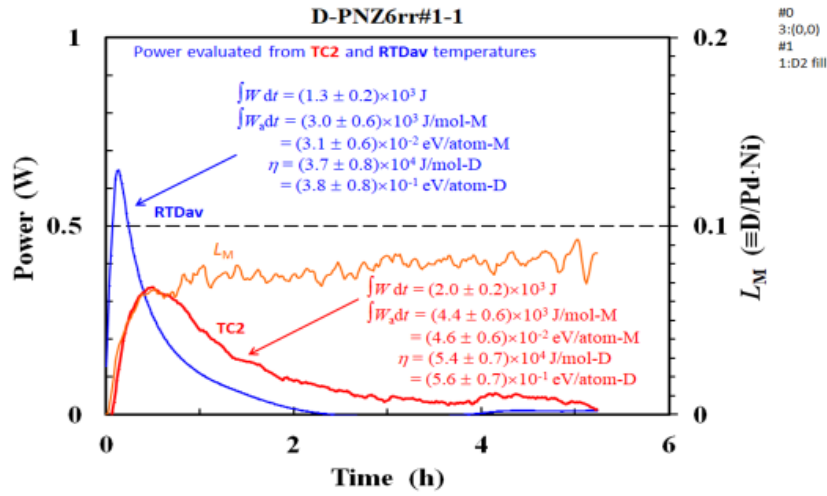


Fig. 12 Observed thermal power and D/M loading ratio for PNZ6rr#1-1 RT run

We summarize integrated data in Table-1.

Table-1 Integrated performance data of PNZ6, PNZ6r and PNZ6rr at RT

Sample	Maximum Loading Ratio; D/M	Integrated Heat (kJ)	Specific Reaction Energy (eV/D)
PNZ6	3.60	100	0.58
PNZ6r	0.80	18	0.51
PNZ6rr	0.08	2.0	0.56

Evidently, repeated calcination made very negative effect for D-absorption at RT. Loading ratios D/M decreased drastically from very large value 3.60 for PNZ6 to 0.80 for PNZ6r and 0.08 for PNZ6rr. As we show later in Table-2, oxygen contents increased drastically by the second and the third calcination. If the heat generation by PNZ6 at RT is from reduction of calcined sample (namely from formation of D<sub>2</sub>O water by D<sub>2</sub> + O reactions), we should have observed very increased integrated heat and “apparent” increase of loading ratio values. Evidently, it is not the case. We can conclude that reduction process is negligibly small for D (H) absorption runs of PNZ-type samples. Since specific reaction energies are observed as almost same values (0.55 eV/D in average), microscopic reaction mechanism seems common in three samples. We regard that D-absorption is into Ni nano-cores mostly because of 1/10 minor Pd content. About 0.55 eV/D for nickel is considerably large exothermic value at RT.

### 3.3 AHE by ET Runs

Most interested and important aspect of present work is of anomalous heat effect (AHE) at elevated RC temperatures. AHE data by PNZ6 and PNZ6r samples at ET can be seen in already published papers [1, 2]. However, several figures are copied below for the sake of easy comparison, in Figs. 13-16.

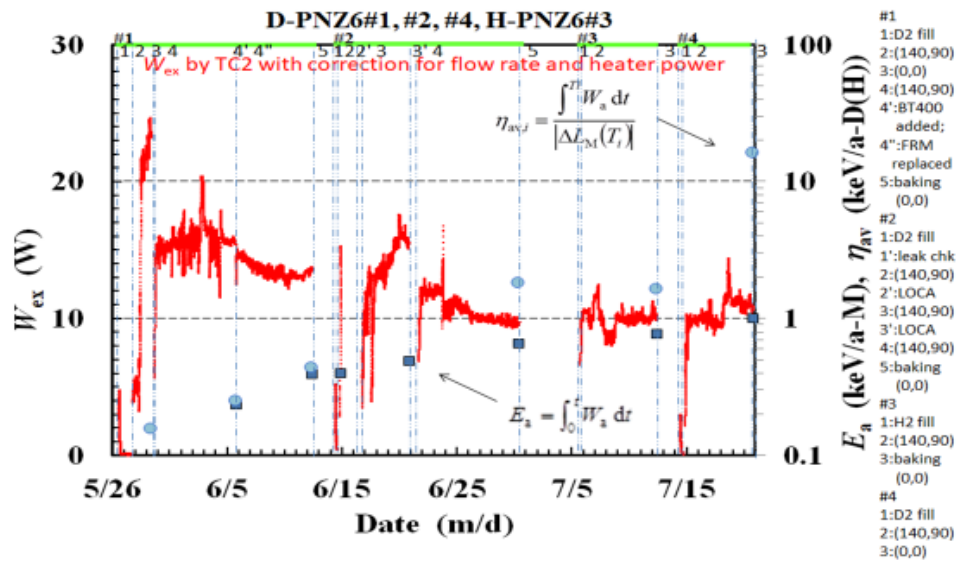


Fig. 13 Processed data of excess thermal power (red graph), integrated heat energy per M (blue square) and eta value (sky blue circle) for PNZ6 ET runs around 300 °C RC temperature, obtained by TC2-TC6 data of flow calorimetry

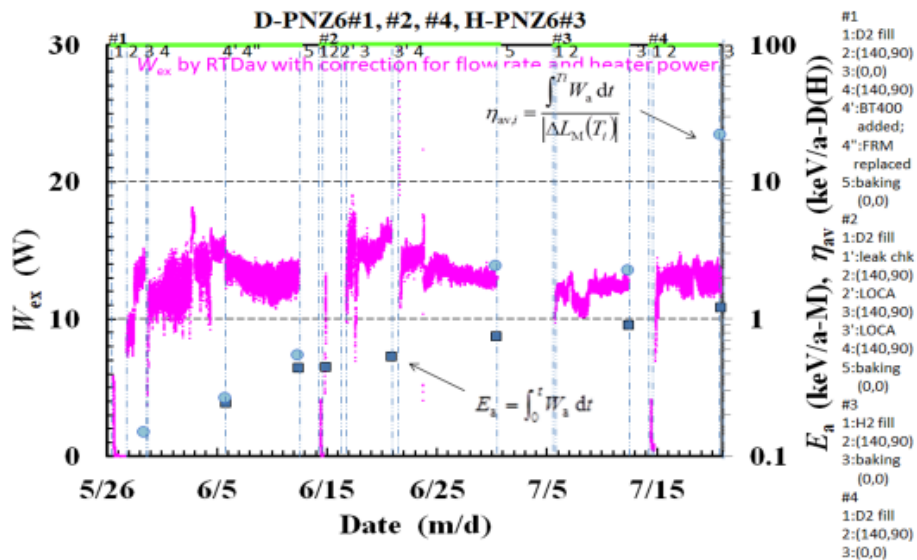


Fig. 14 Processed data of excess thermal power (red graph), integrated heat energy per M (blue square) and eta value (sky blue circle) for PNZ6 ET runs around 300 °C RC temperature, obtained by RTD-average data

In PNZ6#1-2 run, excess thermal power by TC2-TC6 increased suddenly from ca. 5 W to 20W in early time stage. The reason is unknown. Looking at excess thermal power data processed from RTD-average temperatures in Fig.15, we notice that local heat along central line of RC in the early time stage is near 10 W level. This fact may

infer that larger excess thermal power was locally generated in upper zone and peripheral region of RC, where no RTD sensors are set up.

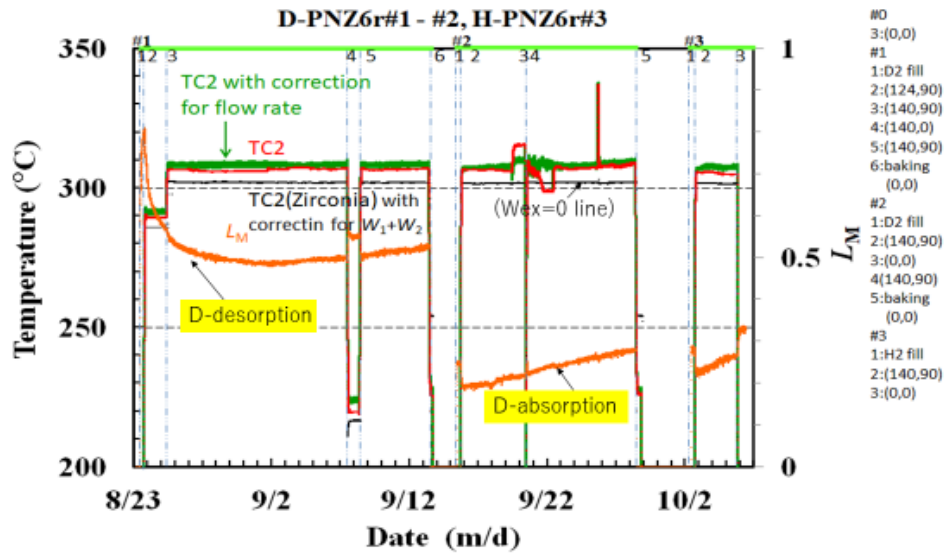


Fig. 15 Temperature evolution (green) of oil outlet point by TC2, compared with calibration line by blank sample (zirconia) run (black line) and loading ratio variation

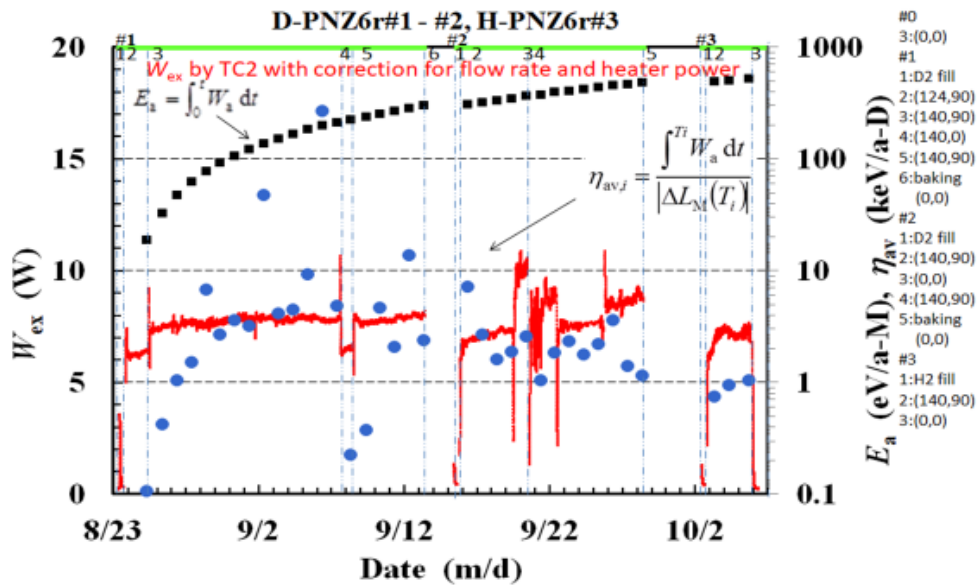


Fig. 16 Processed data of excess thermal power (red graph), integrated heat energy per M (black square) and eta value (sky blue circle) for PNZ6r ET runs around 300 °C RC temperature, obtained by TC2-TC6 data of flow calorimetry

From Figs. 15 and 16, we see that around 8 W excess thermal power, sustainable over a month, was observed under slow D-desorption or absorption conditions. We do not

know exactly how much D atoms were burnt by the AHE reactions. Rate of consumed D atoms can be regarded as much less than differential variation of loading ratios. We can calculate daily variation of D loading ratio and corresponding amount of D-atoms transferred. Temporarily we adopted daily amount of transferred D-atoms for a measure of burnt D-atoms, knowing that this is very overestimation, to deduce specific reaction energy per D ( $\eta$ -values, sky-blue circles in figures). Estimated  $\eta$ -values are scattered between 1keV/D to several 100 keV/D. Most values are of several keV/D. Comparing with 0.55 eV/D at RT by D-absorption (see Table-1),  $\eta$ -values at ET are too large to explain by chemical binding energy of electrons. The gap is more than three orders of magnitude. Energy density (accumulated excess heat) for several weeks run is also large as 500 eV/Ni-atom or ca. 26 MJ for PNZ6r ET runs.

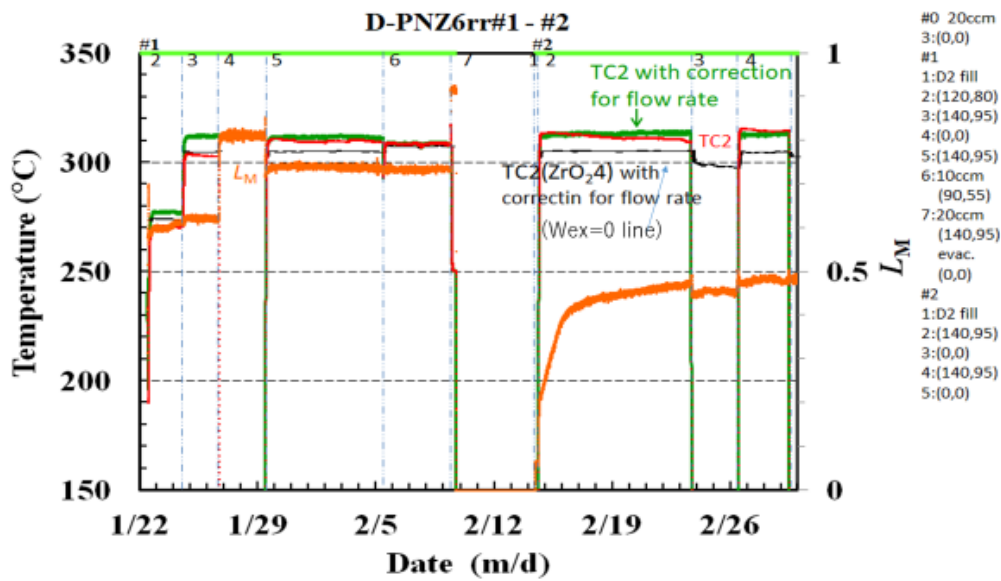


Fig. 17 TC2 data (green) by PNZ6rr#1 and PNZ6rr#2 runs are compared with calorimetry calibration line (black) by blank zirconia sample and evolution of D-loading ratios

Newly obtained AHE data by Technova-Kobe-U group, after the NEDO-MHE project, are shown in Figs. 17-20. Figs. 17 and 18 show temperature data for calorimetry.

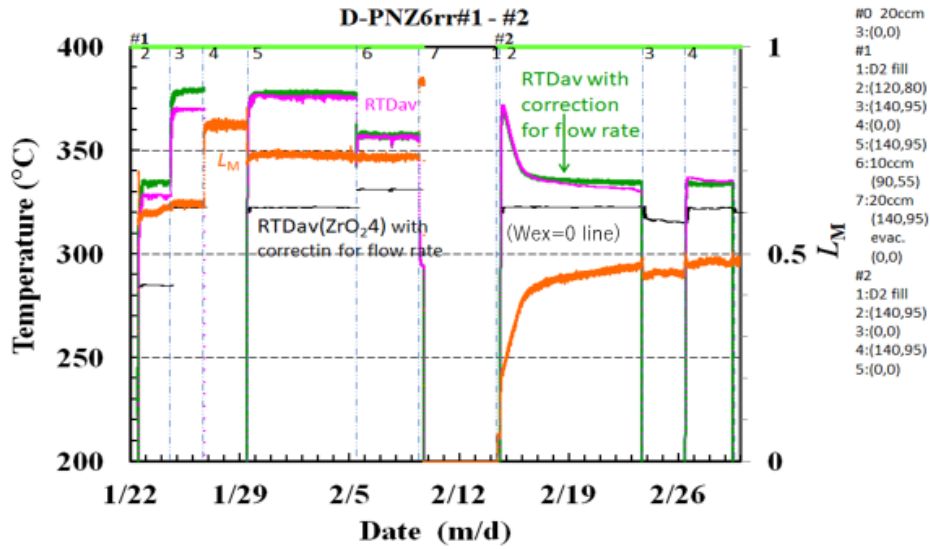


Fig. 18 Temperature data by RTDs for PNZ6rr#1 and PNZ6rr#2 runs

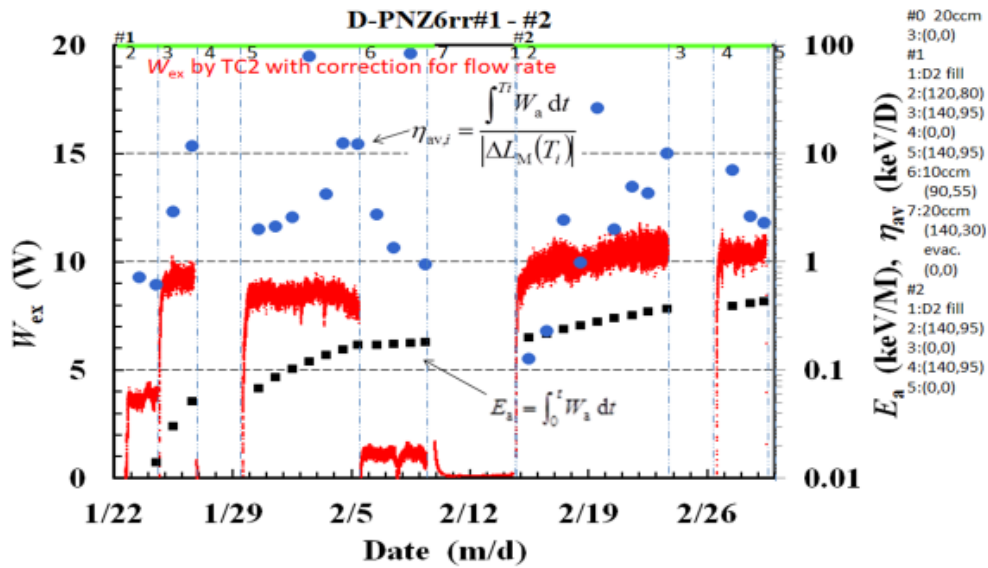


Fig. 19 Processed data of excess thermal power (red graph), integrated heat energy per M (black square) and eta value (sky blue circle) for PNZ6rr ET runs around 300 °C RC temperature, obtained by TC2-TC6 data of flow calorimetry

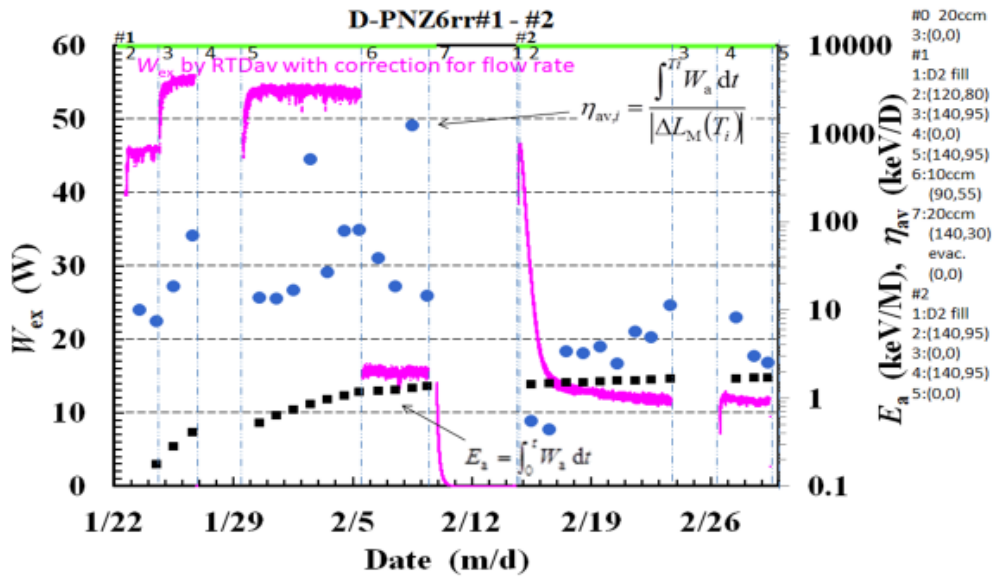


FIG. 20 Processed data of excess thermal power (pink graph), integrated heat energy per M (black square) and  $\eta$ -value (sky blue circle) for PNZ6rr ET runs around 300 °C RC temperature, obtained by RTD-average data

AHE with excess thermal power around 10 W, sustainable for several weeks, was repeatedly observed, as seen with data by oil flow calorimetry (TC2-TC6 data). In this case, daily D-transfer rates estimated from variation of loading ratios were relatively so small (see Fig.17) that larger  $\eta$ -values as around 10 keV/D were obtained. Largest  $\eta$ -values are close to 1,000 keV/D (namely 1 MeV/D) that is really of “nuclear reaction” signature. Significant high local excess power level as 55 W was observed in central zone of RC (see Fig.20), though total heat recovery data by oil flow showed near 10 W level. Probably local heat generation in peripheral region of cylindrical RC chamber was smaller than that in central vertical zone. This will suggest that we will be able to increase total excess heat of oil flow recovery, by using improved MHE system to homogenize D-gas feeding and RC local temperature distribution.

In Table-2 we summarize integrated key data for AHE by repeated calcination. Preliminary data for PNZ10 (Pd<sub>1</sub>Ni<sub>10</sub>/zirconia) ca. 1kg sample by the first calcination only are added for comparison.

We can summarize as follows: Re-calcination is effective to change D-loading at room temperature; namely to drastically small absorption of D. After third calcination, PNZ6rr sample (ca.100g) gave significant (ca. 100°C) temperature rise in local RC zone and sustainable excess heat over 10W for several weeks. Oxygen content increased to ca. 20% in weight for PNZ6rr by the third calcination. Low oxidized sample PNZ10 (under trial for AHE scale-up) with poor control of fat melt-spun ribbon thickness can be better treated by re-calcination after use and we may try retest, for confirming possible enhancement of AHE. No significant increase of neutron and gamma-ray counts over natural background were observed during present experiments.

Table-2 Key Integrated Data of AHE by Repeated Calcination

Sample	PNZ10	PNZ6	PNZ6r	PNZ6rr
Total (g)	956.1	120.0	131.9	129.8
Oxygen content (%)	2.44	4.51	16.86	20.64
Wex (watt) at ET	7, 14 18 (#1) (#2) (#3) AHTB	24, 15 (#1) (#2)	8, 10 (#1) (#2)	9, 11 (#1) (#2)

AHTB: after higher temperature baking

## VI SUMMARY AND CONCLUDING REMARKS

Re-calcination is effective to change D-loading at room temperature; to drastically small absorption of D.

After third calcination, PNZ6rr sample gave significant (ca. 100°C) temperature rise in local RC and sustainable excess heat over 10W for weeks.

Strange oscillatory behavior of TC4 temperature evolution was observed. The phenomenon is similar to the observation by Yokose et al [9].

Oxygen content increased to ca. 20% in weight for PNZ6rr by the third calcination (similar value to DSC Kyushu experiments [3]).

Specific Reaction Energy ( $\eta$ -value) is very large as 10 keV to 1,000 keV per D-transferred, which infers heat generation mechanism as nuclear-like origin.

Low oxidized sample PNZ10 with poor control of melt-spun ribbon thickness should be re-calcined.

### References

- [1] Akira Kitamura, Akito Takahashi, Koh Takahashi, Reiko Seto, Takeshi Hatano, Yasuhiro Iwamura, Takehiko Itoh, Jirohta Kasagi, Masanori Nakamura, Masanobu Uchimura, Hidekazu Takahashi, Shunsuke Sumitomo, Tatsumi Hioki, Tomoyoshi Motohiro, Yuichi Furuyama, Masahiro Kishida, Hideki Matsune, “Comparison of excess heat evolution from zirconia-supported Pd-Ni nanocomposite samples with different Pd/Ni ratio under exposure to hydrogen isotope gases”, Proc. JCF18, pp. 14-31, 2018
- [2] Akira Kitamura, Akito Takahashi, Koh Takahashi, Reiko Seto, Takeshi Hatano, Yasuhiro Iwamura, Takehiko Itoh, Jirohta Kasagi, Masanori Nakamura, Masanobu Uchimura, Hidekazu Takahashi, Shunsuke Sumitomo, Tatsumi Hioki,

- Tomoyoshi Motohiro, Yuichi Furuyama, Masahiro Kishida, Hideki Matsune; “Excess heat evolution from nanocomposite samples under exposure to hydrogen isotope gases”, *Int. J. Hydrogen Energy*, 43 (2018) 16187-16200
- [3] Akito Takahashi, Akira Kitamura, Koh Takahashi, Reiko Seto, Takeshi Hatano, Yasuhiro Iwamura, Takehiko Itoh, Jirohta Kasagi, Masanori Nakamura, Masanobu Uchimura, Hidekazu Takahashi, Shunsuke Sumitomo, Tatsumi Hioki, Tomoyoshi Motohiro, Yuichi Furuyama, Masahiro Kishida, Hideki Matsune; “Phenomenology and Controllability of New Exothermic Reaction between Metal and Hydrogen”, Technical report uploaded at Research Gate: [https://www.researchgate.net/publication/322160963\\_Brief\\_Summary\\_Report\\_of\\_MHE\\_Project\\_Phenomenology\\_and\\_Controllability\\_of\\_New\\_Exothermic\\_Reaction\\_between\\_Metal\\_and\\_Hydrogen](https://www.researchgate.net/publication/322160963_Brief_Summary_Report_of_MHE_Project_Phenomenology_and_Controllability_of_New_Exothermic_Reaction_between_Metal_and_Hydrogen)
- [4] A. Takahashi, A. Kitamura, K. Takahashi, R. Seto, T. Yokose, A. Taniike and Y. Furuyama, “Anomalous Heat Effects by Interaction of Nano-metals and D(H)-gas”, Proc. ICCF20, Tohoku University (2016), downloadable at Research-Gate: [https://www.researchgate.net/publication/313310565\\_Anomalous\\_Heat\\_Effects\\_by\\_Interaction\\_of\\_Nano-Metals\\_and\\_HD-Gas](https://www.researchgate.net/publication/313310565_Anomalous_Heat_Effects_by_Interaction_of_Nano-Metals_and_HD-Gas)
- [5] Akira Kitamura, Akito Takahashi, Koh Takahashi, Reiko Seto, Yuki Matsuda, Yasuhiro Iwamura, Takehiko Itoh, Jirohta Kasagi, Masanori Nakamura, Masanobu Uchimura, Hidekazu Takahashi, Tatsumi Hioki, Tomoyoshi Motohiro, Yuichi Furuyama, Masahiro Kishida, “Collaborative Examination on Anomalous Heat Effect Using Nickel-Based Binary Nanocomposites Supported by Zirconia”, *J. Condensed Matter Nucl. Sci.*, 24, 202-213 (2017).
- [6] Yasuhiro Iwamura, Takehiko Itoh, Jirohta Kasagi, Akira Kitamura, Akito Takahashi, Koh Takahashi, Reiko Seto, “Replication Experiments at Tohoku University on Anomalous Heat Generation Using Nickel-based Binary Nanocomposites and Hydrogen Isotope Gas”, *J. Condensed Matter Nucl. Sci.*, 24, 191-201 (2017)
- [7] Akito Takahashi, “Physics of Cold Fusion by TSC Theory”, *J. Condensed Matter Nucl. Sci.*, 13, 565-578 (2014)
- [8] Akito Takahashi, “Background for Condensed Cluster Fusion”, Proceedings of JCF-15 JCFRS, pp.63-90, (2014)
- [9] Toyoshi Yokose, Akito Takahashi, Koh Takahashi, Yuichi Furuyama, “Anomalous Heat Burst by CNZ7 Sample and H-Gas”, Proceedings of JCF19, JCFRS, to be published in 2019

# Anomalous Heat Burst by CNZ7 Sample and H-Gas

Toyoshi Yokose<sup>2</sup>, Akito Takahashi<sup>1\*</sup>, Koh Takahashi<sup>1</sup>, Yuichi Furuyama<sup>2</sup>

<sup>1</sup> Technova Inc., 100-0011 Japan,

<sup>2</sup> Graduate School of Maritime Sciences, Kobe University, 658-0022 Japan

\*Corresponding author

**Abstract** We have been studying anomalous heat effect (AHE) by the interaction of nano-composite CNZ (Cu<sub>1</sub>Ni<sub>7</sub>/zirconia) sample and H-gas at 200- 300°C RC (reaction chamber) condition. In this paper, we report a large heat burst (ca. 130 W peak by oil-flow calorimetry) event by CNZ7 sample (ca. 1kg, Cu<sub>1</sub>Ni<sub>7</sub>/Zirconia) and H-gas interaction under elevated temperature. Specific energy of reaction seems very much larger than 6.5 eV/H-transferred. From the rise time data of RTD4, TC2 and Pr for the heat burst, we conclude that the main part of heat pulse occurred in ca.100s and real peak power was ca.3 kW. After the heat burst event, small (2-3 W) excess power level sustained for a day. Then we increased the H-gas pressure of SC (storage chamber) to ca. 1.0MPa to feed to RC with [120, 80] W heaters condition; we then started to observe rather slow H-absorption with significant endothermic condition. After saturation of H/Ni ratio, we increased RC temperature to have observed weeks-sustaining excess thermal power (ca. 12-14W in earlier weeks).

**Index Terms** – Anomalous heat burst, Cu-Ni nanocomposite, H-gas, Sustainable excess heat, Elevated temperature

## I. INTRODUCTION

The anomalous heat effect (AHE) by experiments of hydrogen-gas charged nickel-based nano-composite samples as Pd-Ni/zirconia (PNZ) and Cu-Ni/zirconia (CNZ) powder samples has been studied intensively [1, 2] under the NEDO-MHE project in 2015-2017 [3], for verifying the existence of the phenomenon and finding conditions of excess power generation in controllable way. As reviewed in ref. [4], the 8 year-long (2008-2015) series of study on anomalous heat effects by interaction of PNZ and CNZ metal nanoparticles and D(H)-gas, under the collaboration of Technova Inc. and Kobe University, has become the basis for the previous collaborative research of NEDO-MHE. The reports of results by the project were first published in Proceedings of ICCF20 Conference [5, 6]. Especially, sustainable excess thermal power generation by CNZ-type nano-composite metal powder under light hydrogen (H) gas charging is of great interest. CNZ-type does not contain expensive precious metal as Pd. H-gas is much cheaper than D-gas. If we will prove that sustainable generation of several kW thermal power is realistic by a small size device of CNZ + H-gas reaction system, it must be breakthrough toward industrialization of new distributed type energy devices operated with high energy density, high power density, radiation-free eco-friendly condition and very small amount of H-gas consumption. Based on the results of NEDO-MHE project, we expect to implement scale-up experiments by increasing amount of CNZ sample and improving fabrication process of nano-composite metal samples.

Repeatability of anomalous heat effect (AHE) by the interaction of nano-composite CNZ (Cu<sub>1</sub>Ni<sub>7</sub>/zirconia) sample and H-gas at 200 - 300°C RC (reaction chamber) condition has been studied intensively in previous works [1-6]. In this paper, we report a large heat burst (ca. 130 W peak by oil-flow calorimetry) event by CNZ7 sample (ca. 1kg, Cu<sub>1</sub>Ni<sub>7</sub>/Zirconia) and H-gas interaction under elevated temperature. From the rise time data of excess thermal power burst and desorbed H-gas pressure spike for the heat burst event, we conclude that the main part of heat pulse occurred in ca.100s and real

peak power was ca.3 kW. After the burst event, we have observed ca. 14 W level excess thermal power continuing for several weeks.

## II. EXPERIMENTAL PROCEDURE

CNZ7 sample was made by calcination (450°C x 60hr) of melt-spun ribbons. CNZ7 sample of 1137g with 1mm diameter zirconia filler of 439g was set in the reaction chamber (500 cc) of Kobe-U MHE calorimetry system (see Figs. 1 and 2).

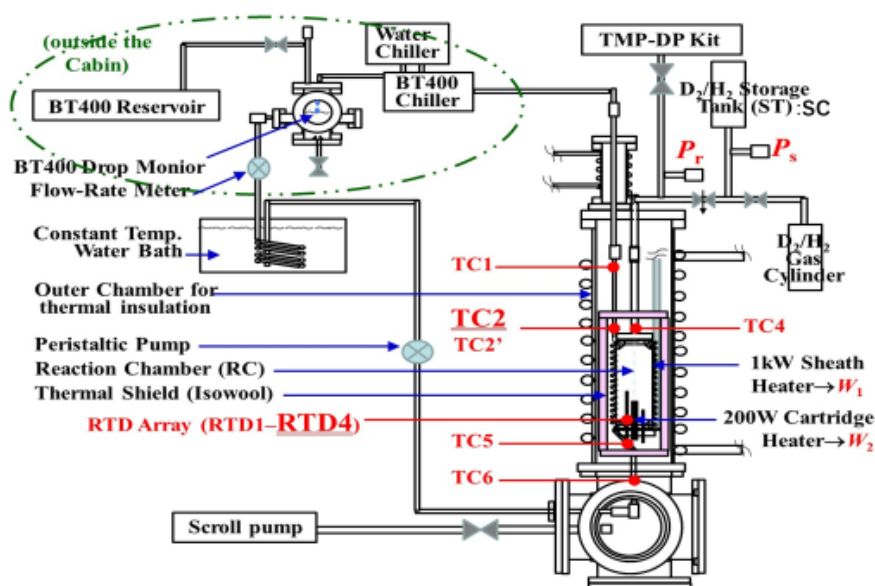


Fig.1 Schematics of MHE calorimetry system at Kobe University

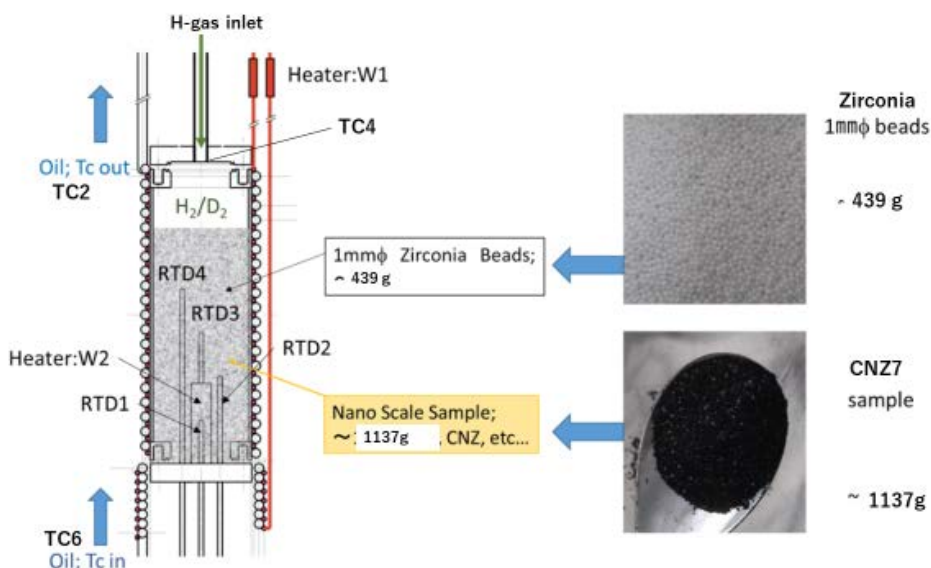


Fig.2 Reaction chamber (RC) with oil-cooling, temperature measuring and heating systems and image of sample powder and dummy filler

Positions of 4 RTDs in RC are at 3 cm, 6 cm, 9 cm and 12 cm from the bottom of RC chamber. Net height of RC volume is 20 cm. CNZ7 sample mixed with zirconia filler occupied fully the RC inner volume (ca. 500 cc). The inner heater W2 locates between RTD1 and RTD2. Two thermocouples TC6 and TC5 monitor temperatures of oil inlet line. Upper three thermocouples TC2, TC2' and TC1 are for monitoring temperatures of oil outlet points. TC4 thermocouple is for monitoring temperature of the H-gas inlet/outlet point (near middle of upper flange of RC).

The sample was first baked at round 300-500°C of RC temperatures (monitoring by 4 RTDs) for a few days and cooled down to room temperature (25°C). The #1-1 RT (room temperature) run with H-gas feed was done in a day to have H-loading ratio of 0.35 H/Ni and heat of ca. 20Wx2hrs (124 kJ). Data will be shown in Section 3.2.

Next run #1-2 under elevated temperature (ET) was started with [W1, W2] = [120, 80] W heating condition. After ca. 90 min of the ET-run start, we suddenly observed large heat burst event (data will be shown in Section 3.1); Temperature at about middle height (by RTD4) of RC increased from 210°C to 475°C. And we saw ca. 130 W peak-heat power by coolant-oil outlet temperature (TC2) of 350°C (increased from 237°C). In coincidence with RTD4 temperature rise, pressure spike of ca. 0.8 MPa pulse increase of RC gas-pressure (Pr) and quick decrease was recorded. The pulse pressure increase was quickly transferred to ca. 4000 cc H-gas storage chamber (SC) at room temperature. Pressure increase in SC was 0.16 MPa by the event, which corresponded ca. 0.19 H/Ni decrease from sample, namely desorption of H-gas from the sample. Total released heat by the burst was ca. 365 kJ (see Section 3.1). Strange oscillatory behavior of TC4 (at RC gas outlet) was observed, which looks corresponding to the Iwamura observation [6] of frequent heat and pressure spikes observed by CNZ5 and CNZ6 samples, as well as similar oscillatory fluctuation of TC4 temperature in #1-2 run of PNZ6rr sample (Takahashi et al [9]). Detail description with discussions will be extended in Section 3.1.

Detail of MHE calorimetry and process method of excess thermal power deduction are described in our previous papers [1-6]. The latest improvement of MHE calorimetry is made by the usage of two Keithley constant power supplies for W1 and W2 heaters. Thermal power is estimated by oil flow calorimetry; namely, temperature difference between oil outlet (TC2) and oil inlet (TC6) and oil flow rate are used. Oil flow rate in the present work was kept to be constant as 18.4 cc per minute, as far as experimenter could adjust. Calorimetry calibration by blank runs with dummy zirconia sample was also adjusted to conditions of 18.4 cc per minute flow rate for different heater power. Consequently, flow rate corrections for calculating excess thermal power was negligible in the present experiment.

Theoretical aspects for making working binary metal nano-composite samples are explained in references [7, 8]. The 1/7 atomic ratio for Cu/Ni binary shell/core nano-islands was adopted by theoretical optimization of surface sub-nano holes (SNH) which are expected to work as surface catalytic sites to form TSC transient molecules of 4H/TSC.

Optimum procedures for calcination of melt-spun amorphous metal ribbons and mortaring degree are important, but will be disclosed in future due time.

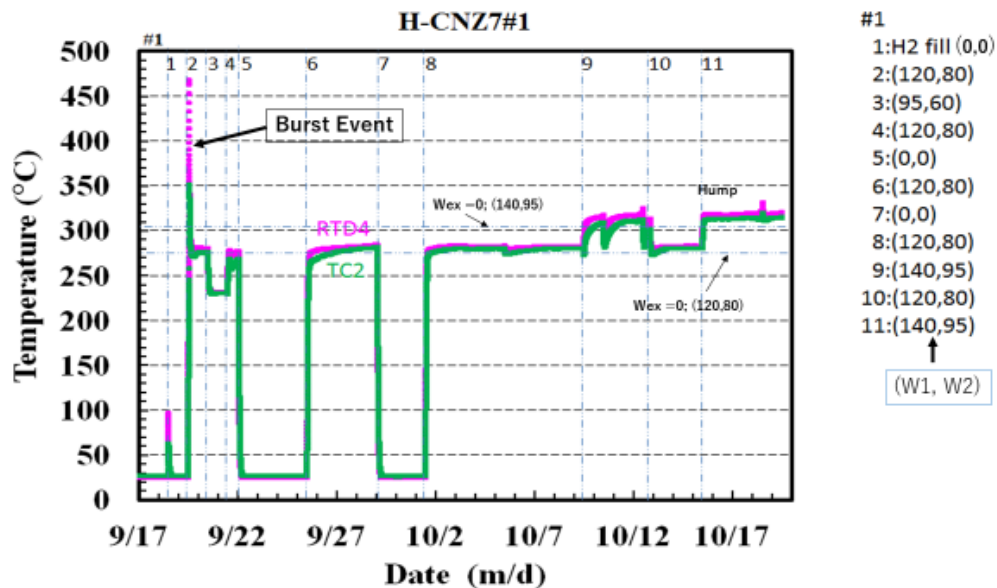


Fig.3 Quick view of experimental procedure for the first month period

For a quick view of experimental procedure in the first one month of series runs, we show evolution data of oil outlet temperature (TC2) and near midpoint temperature (RTD4) of RC, in Fig.3. Experiments at elevated temperature (ET) has continued for further months by observing around 15 W level excess thermal power sustainably, but we will report these results in separate paper in future. On 9/18, you see the peaks by CNZ7#1-1 RT run (detail in Section 3.2). On 9/19, we encountered the anomalous heat burst event. For further runs with heater condition of [120, 80] watts, CNZ7#1-4, 6, 8 and heater condition of [140, 95] watts, CNZ7#1-9, 11 followed in a month.

### III. RESULTS AND DISCUSSIONS

#### 3.1 Anomalous Heat Burst Event

In Fig.4, raw data of #1-2 run are plotted. Each measuring term (temperature by RTD1, RTD2, RTD3, RTD4, TC1, TC2 or TC4, pressure by Ps or Pr) and corresponding data-curve are drawn by same color. The anomalous burst peaks took place near at 12:15 of 9/19 (September 19, 2018). Before noon (12:00), temperatures in various points were elevating smoothly, except for the “flat” evolution of TC4 temperature. The flat TC4 evolution is mysterious, and we will discuss later. Pressure spike of Pr at around 12:15 decayed quickly, and we see pressure equilibrium between Ps and Pr, which was kept almost constant as ca. 0.5 MPa for about 6 hours. At around 18:40, Ps and Pr started to decrease slowly, probably by H-absorption of endothermic condition as we see slight decrease of inner temperatures of RC (see RTD1, 2 and 3). Coincidentally, “strange fluctuation” of TC4 temperature ended. These behaviors are mysterious and interesting. The burst event was very clear and undeniable phenomenon, even if we say that it is yet to reproduce. Some novel reaction may be there.

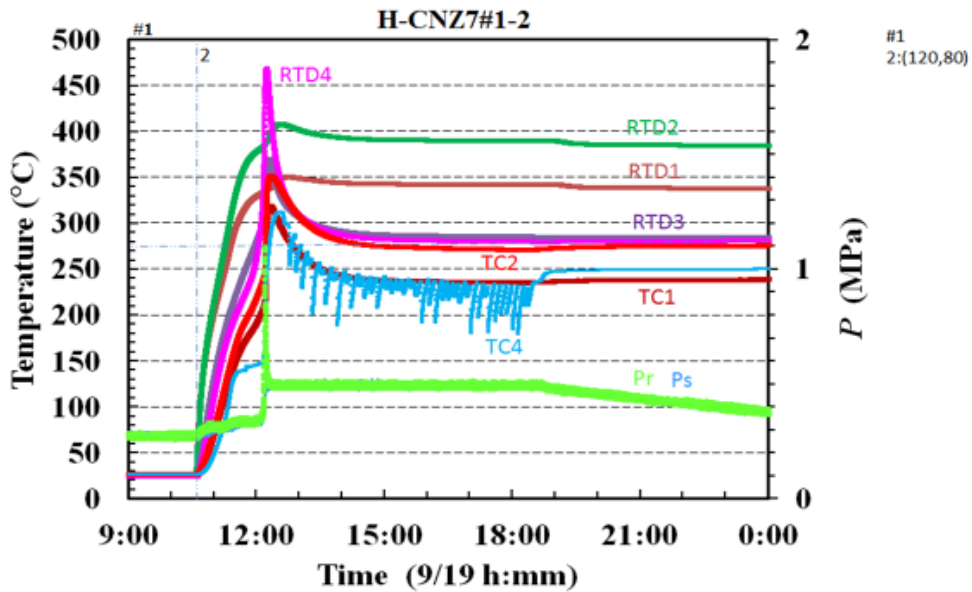


Fig.4 Raw data of inner temperatures of RC (by RTD1-4), temperatures of coolant oil outlet (by TC2 and TC1), temperature at H-gas inlet/outlet point (by TC4), and gas pressures of H-gas storage chamber (by Ps) and RC chamber (Pr)

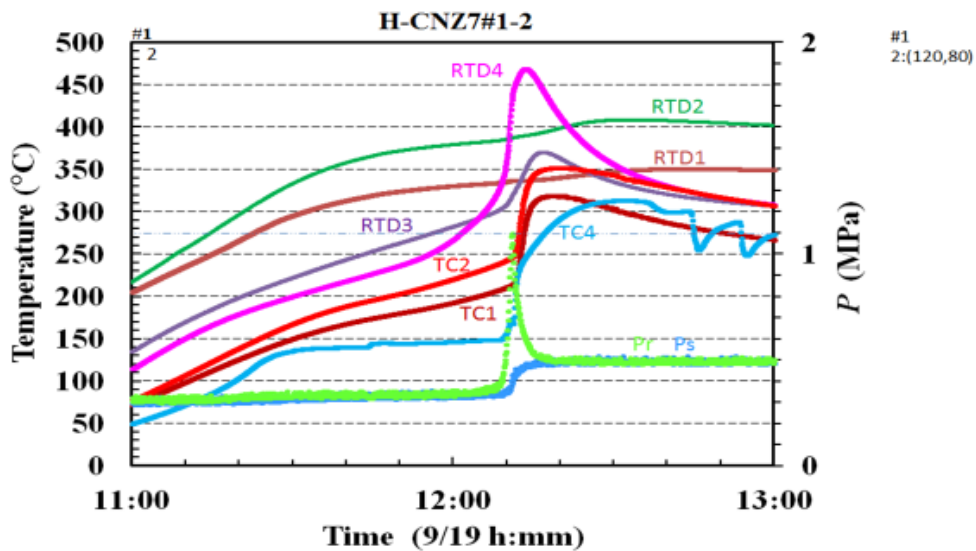


Fig.5 Expanded view of raw data around the burst peak

In Fig.5, expanded view of data around the burst peak is drawn. The plateau of TC4 temperature for about 40 min is obvious, while temperatures at other points are increasing smoothly in the corresponding time-interval. The pressure spike of Pr (light green) disappeared shortly. Probably, desorbed H-gas transferred quickly (due to over 1 MPa high pressure) to storage chamber (SC) via super needle valve.

In Fig.6, we show simplified scheme of Kobe-MHE system for gas pressure balance between source chamber (SC) at room temperature (25 °C) and reaction chamber (RC) at elevated temperature.

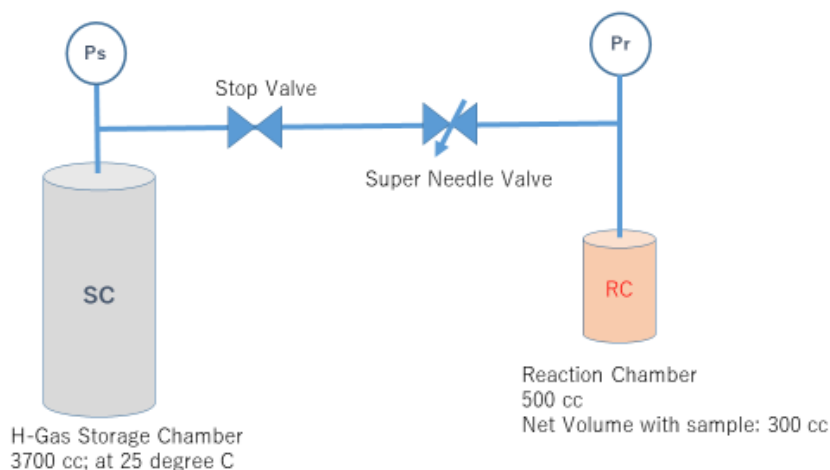


Fig.6 Scheme of Kobe-MHE system for gas pressure balance between source chamber (SC) at room temperature (25 °C) and reaction chamber (RC) at elevated temperature

Before feeding H-gas from SC to RC, we fill SC with 1.0 MPa (maximum) to 0.1 MPa (minimum) pressure from high pressure H<sub>2</sub>-gas cylinder placed outside the temperature controlled room of MHE system. We set designated gas flow rate to RC by the super needle valve (SNV). By opening the stop valve, we start to feed H-gas to RC. In the case of zirconia dummy sample (blank run) in RC, gas filling saturates in about 60 min with 2.13 dial setting of SNV: this is usual condition for #1-1 RT run at the beginning of series experiments. Net volume of SC is 3700 cc and net volume of RC with sample is ca. 300 cc for gas space. When we start to elevate temperature of RC by [W1, W2] heaters, pressure in RC increases gradually (by  $PV = RT$  law) and backward gas flow via SNV to SC takes place to balance both pressures of SC and RC. During the elevated temperature runs for CNZ7, we opened more SNV dial to be 4.13: with which setting, time for pressure balance between RC and SC shortens to be ca. a few minutes.

In Fig.7, we show comparison of evolution data around the anomalous heat burst peak, for RC local temperature at upper zone (by RTD4) and both gas-pressures of RC (Pr) and SC (Ps). Pressure spike with 1.08 MPa peak in Pr decayed in about 5 min to make equilibrium pressure ca. 0.5 MPa in both of Pr and Ps. Increment of Ps pressure was ca. 0.16 MPa. SC/RC volume ratio =  $3700/300 = 12.3$ . At pressure equilibrium ( $P_s = P_r$ ), most H-gas locates in SC. Equilibrium reaches in a few minutes by SNV dial 4.12 as mentioned above. Pressure spike (1.08 MPa at peak) gas moved quickly to SC to increase SC pressure from 0.32 MPa to 0.486 MPa, which was sustained constant for ca. 6 hours. Transferred gas by the heat burst is ca. 0.27 mol-H<sub>2</sub>; namely 0.54 mol-

H. We can regard 0.54 mol H is desorbed hydrogen amount from CNZ7, and it corresponds to 0.19 H/Ni decrease of H-loading in CNZ7 sample.

If feeding H-gas induced chemical reduction process as  $H_2 + O \rightarrow H_2O + 2.96 \text{ eV}$  (143 kJ/mol-H),  $H_2O$  vapor in SC should have condensed to liquid and caused SC pressure decrease. This is because of low vapor pressure 3.13 kPa of water at 25 °C, which causes saturation amount of water vapor 23.06 g/m<sup>3</sup> (or 0.092 g/4000cc, namely ca. 0.01 mol H in SC.) This reduction process has never happened, because the transferred gas amount is 0.54 mol in SC at room temperature.

We will show soon that integrated heat by the burst is 365 kJ. If it were H-desorption energy (though we have to assume exothermic desorption!), it corresponds to 6.5 eV/desorbed-H. However, happening of exothermic H-desorption is very hard to conceive in known chemistry. In the burst event, RTD4 temperature started to rapidly increase at about 15 min before the RC gas pressure spike: consequently, we have to conceive that AHE was observed before the thought H-desorption spike! About 265 °C anomalous temperature rise was observed at upper zone of RC (by RTD4), in the burst event. As we will show soon that the calorimetry conversion factor by RTD-average temperature under elevated temperature of 250-300 °C is 1.0 W/°C, local thermal power at RTD4 (12 cm from bottom of RC with 20 cm height) was as large as 265 W in the burst peak.

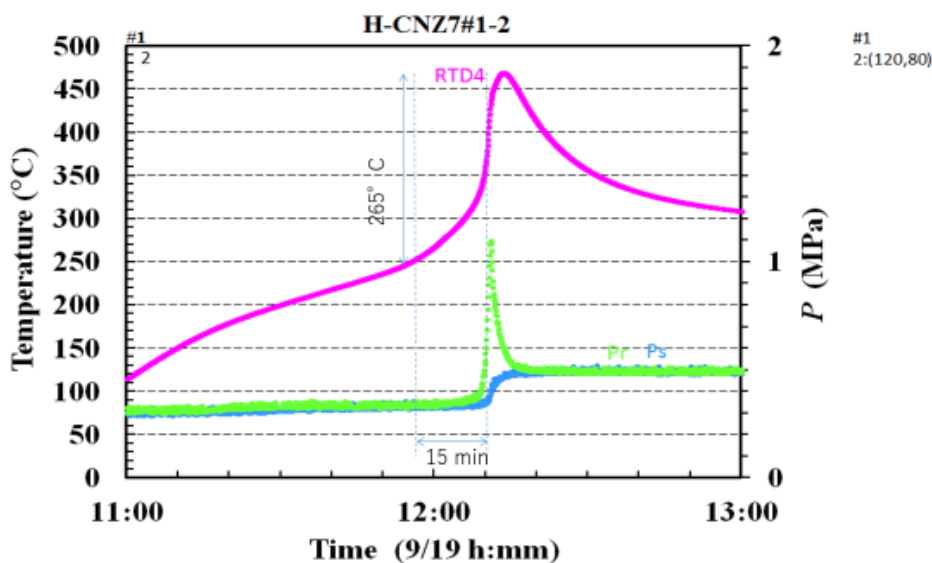


Fig.7 Comparison of RC temperature at upper zone (by RTD4) and gas pressures of RC (Pr) and SC (Ps), around the anomalous heat burst peak

In Fig.8, we compare time response of oil flow calorimetry (by TC2 temperature rise) with local temperature evolution by RTD4 and gas-spike. About 110 °C rise (ca. 130 W) of TC2 (coolant outlet temp.) with delay by calorimetry response is seen. Rise times are ca. 100s for RTD4, TC2 and Pr at the burst. Here, data are plotted in every 5 s. Time-constant of TC2 indicial response of calorimetry is ca. 40min, so that 100s is too short to correlate with slow heat generation as step-function! We see also that the shape of gas spike is very short. We need to investigate about impulsive heat generation.

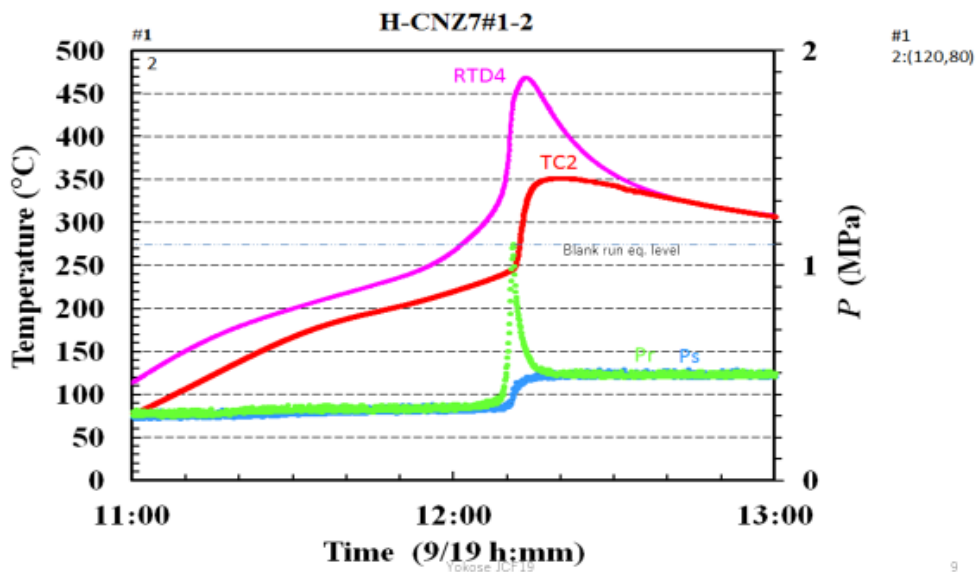


Fig.8 Comparison of time-response of oil flow calorimetry (by TC2), with time response of local temperature (by RTD4) and gas spike

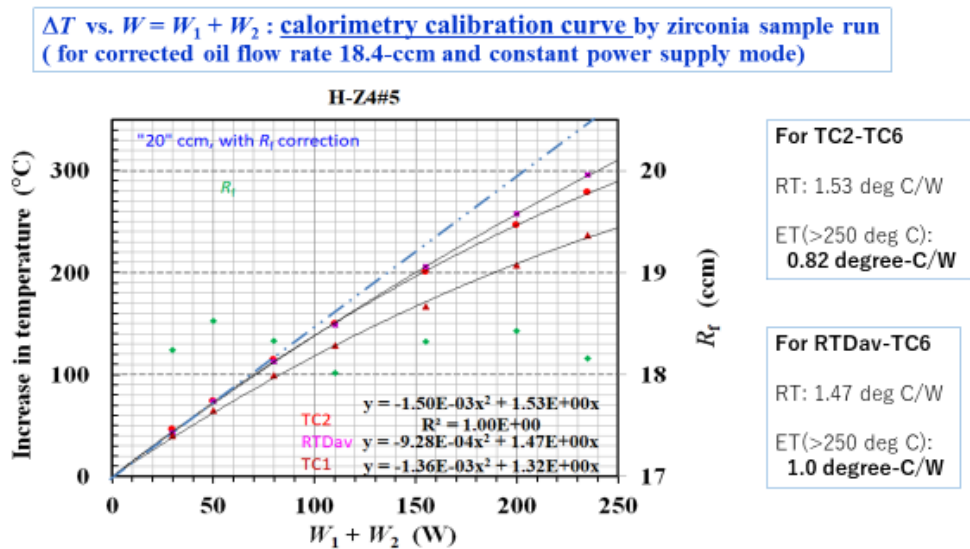


Fig.9 Calibration data for calorimetry of Kobe MHE system, by blank runs with dummy zirconia sample in RC

In Fig.9, we show calibration data for calorimetry, by ET runs with dummy zirconia sample in RC [1, 2]. Dial of peristaltic pump for oil flow was set to “20 ccm” nominal value. Actual flow rates were around 18.4 ccm (cc per minute), and data were corrected to those of 18.4 ccm flow rate. Conversion ratio was 0.82 °C/W for oil flow calorimetry by TC2 – TC6, and 1.0 °C/W for RTD-average method, respectively at ET runs of more than 250°C.

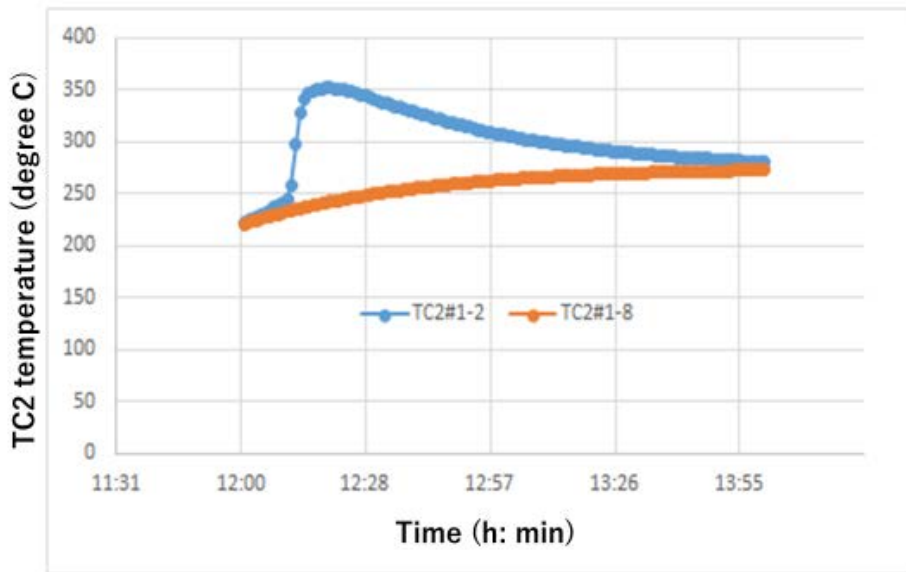


Fig.10 Comparison of time-evolution of TC2 temperature data between CNZ7#1-2 run and CNZ7#1-6 run, around the heat burst interval of #1-2

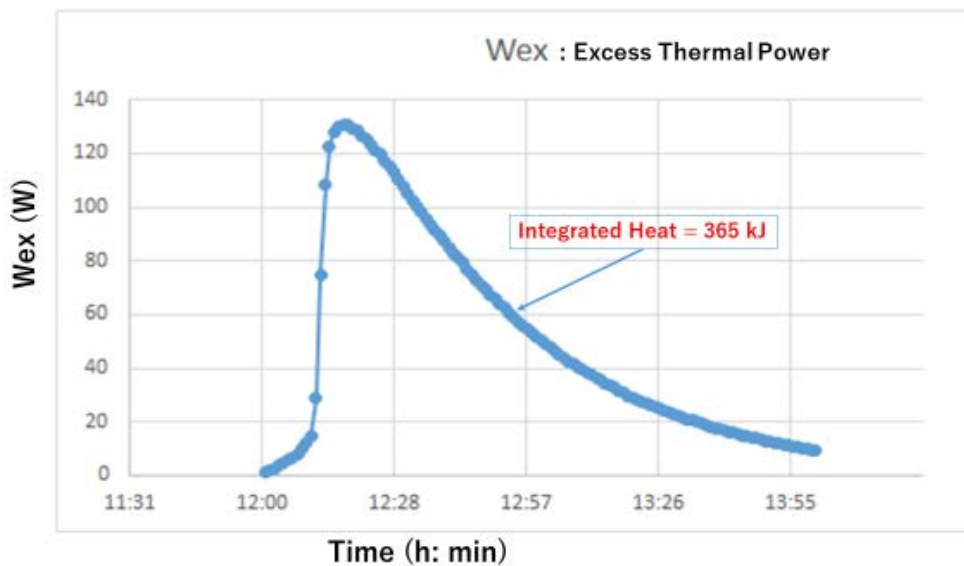


Fig.11 Time evolution data of excess thermal power for the anomalous heat burst of CNZ7#1-2 ET run, data plotted in every 1 min

The heat burst of CNZ7#1-2 run happened in transient time interval of oil mass flow calorimetry which had ca. 40 min time constant. With step function input of two heater powers [W1, W2], we observed that about 4 hours were needed to get to temperature equilibrium in  $\pm 0.1$  °C variation per hour, by the blank calibration run. The heat burst event happened in about 90 min after the start of ET run CNZ7#1-2. We have to use temperature (TC2) rising curve data of blank run with [120, 80] W heater

setting to estimate excess increase of TC2 temperature of CNZ7#1-2 run. Since temperature rising curve (dynamic) of CNZ7 sample in RC may be considerably different from that of the zirconia blank run, we adopted the TC2 temperature rising data of CNZ7#1-6 run with [120, 80] W heater setting (see Fig.3), because we could regard that the data were very close to the zirconia blank run. In Fig.10, we show comparison of time-evolution data of TC2 temperatures between CNZ7#1-2 run and CNZ7#1-6 run, by adjusting the starting time of heating. We see about 110 °C sudden increase of TC2 by the burst event. The peak excess thermal power of observation is ca. 130 W as shown below.

In Fig.11, we plot time-evolution data of excess thermal power of the burst event. Power rise is very steep as it gets to near maximum in ca. 3 min (180 s). The steep rise of main part happened in ca. 100s. After the peak of 132 W, thermal power decays slowly. The decaying curve shape is close to  $\exp(-t/\tau)$  with  $\tau = 34$  min. Namely the thermal power of the burst decayed nearly with the time constant 40 min of oil flow calorimetry calibration by zirconia blank run at around 300°C. This fact infers that the observed time-evolution data of the burst is close to the impulse response of MHE calorimetry. In other words, the heat burst happened impulsively within about 100 s. Total heat by the burst is 365 kJ. Consequently, we can conclude that the anomalous heat event took place in short time-interval as 100 s with ca. 3 kW peak power. Why such a big power was generated is of mystery at this stage.

In correlation with the heat burst, we observed very strange behavior of temperature data at TC4 (H-gas inlet/outlet point). In Fig.12, we show time-evolution data of TC4 temperature before and after the heat burst.

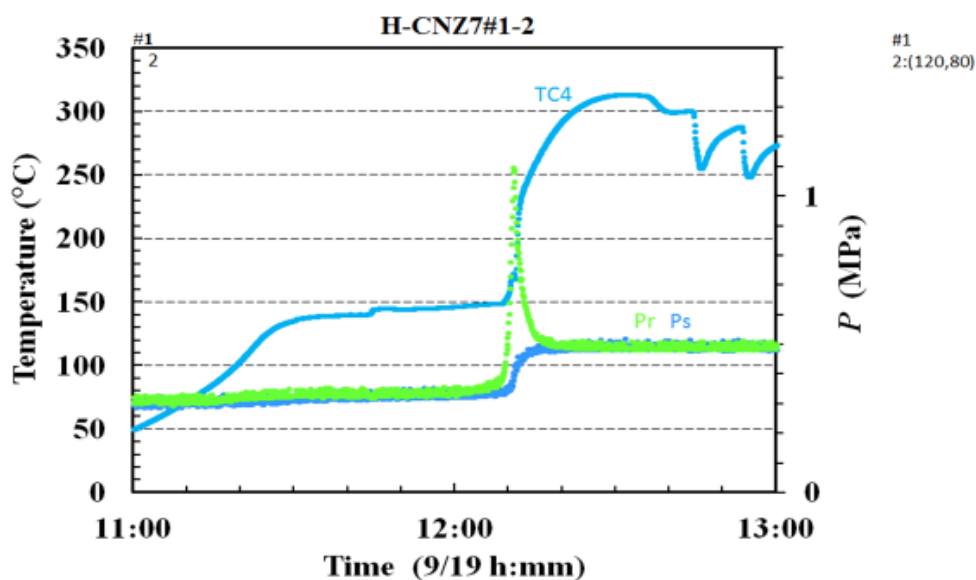


Fig.12 Comparison of TC4 temperature evolution around the heat burst, compared with H-gas pressure spike

H-absorption by CNZ7 is endothermic in 140-250 °C (See Fig.4 and Section 3.3). TC4 locates at the H-gas inlet point of RC, which is set on the upper flange center of

RC. Powder density of CNZ7 is so high that H-gas penetration from top to bottom takes time and H-gas pressure gradient in RC might be steep vertically. Above conditions may induce very localized endothermic H-absorption near H-gas inlet region, in the early time phase of H-gas feeding to RC. Due to endothermic H-absorption, TC4 temperature becomes significantly lower than oil outlet temperature TC2 or TC1 and may keep flat evolution (“plateau”) until when local H-absorption will saturate. After local H-saturation of CNZ7 sample, nuclear events like 4H/TSC WS fusion [8, 9] may have been locally enhanced to heat much the upper sample region of RC. This condition may lead to heat burst in the upper region of RC. After the heat burst, strange fluctuation of TC4 temperature repeated with smaller amplitude as shown in Fig.13.

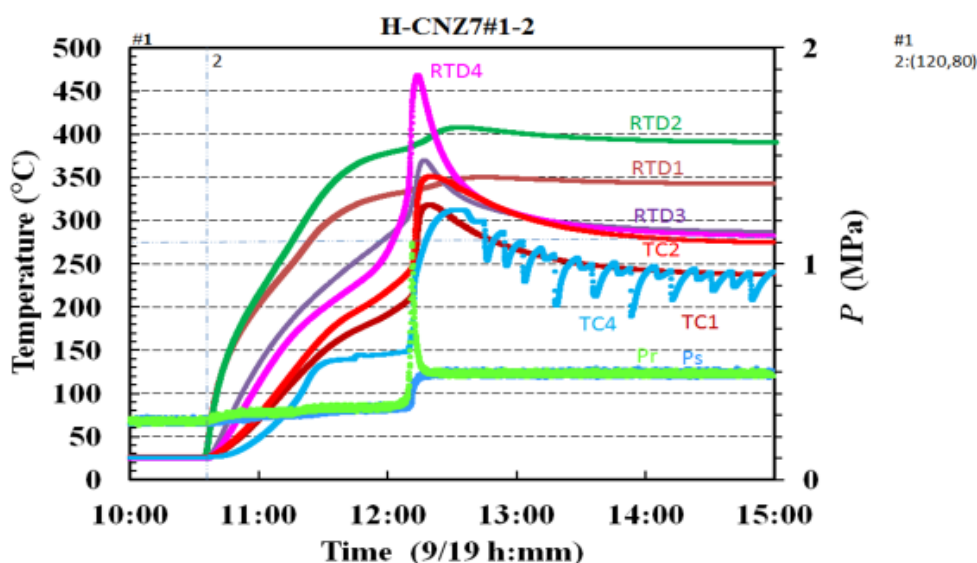


Fig.13 Expanded view of raw data around and after the heat burst

Strange and frequent oscillatory behavior of TC4 (at RC gas outlet) temperature was observed after the burst event. The phenomenon seems to be corresponding to the Iwamura observation of frequent heat and pressure spikes observed by CNZ5 and CNZ6 samples [6], as well as similar oscillatory fluctuation of TC4 temperature in #1-2 run of PNZ6rr sample (Takahashi et al [9]). We conceive that much smaller scale local heat bursts may continue as local saturation of H-absorption goes down in large volume of CNZ7 sample zone in RC.

In Fig.14, we show again view of local temperature in RC. We see that the heat burst happened first in upper zone of RC, as RTD4 data show, and went downward as RTD3, RTD2 and RTD1 data show. Before the burst, however, local temperatures at RTD1, RTD2 and RTD3 were already much higher than those of CNZ7#1-3, -6 and -8 runs. Comparable data by CNZ7#1-6 were 249, 275.6, 218.0 and 211.2 °C, respectively for RTD1, RTD2, RTD3 and RTD4, at 60 min after the start of [120, 80] W heating. For the CNZ7#1-2 run at 60 min after the start of heating, data were 325, 375, 270 and 230 °C, respectively for RTD1, RTD2, RTD3 and RTD4. Quite similar increment of local temperatures in RC was observed by the re-calcined PNZ6rr sample

[9]. Something like AHE seems to have happened in the interaction of nano-composite metals and H-gas.

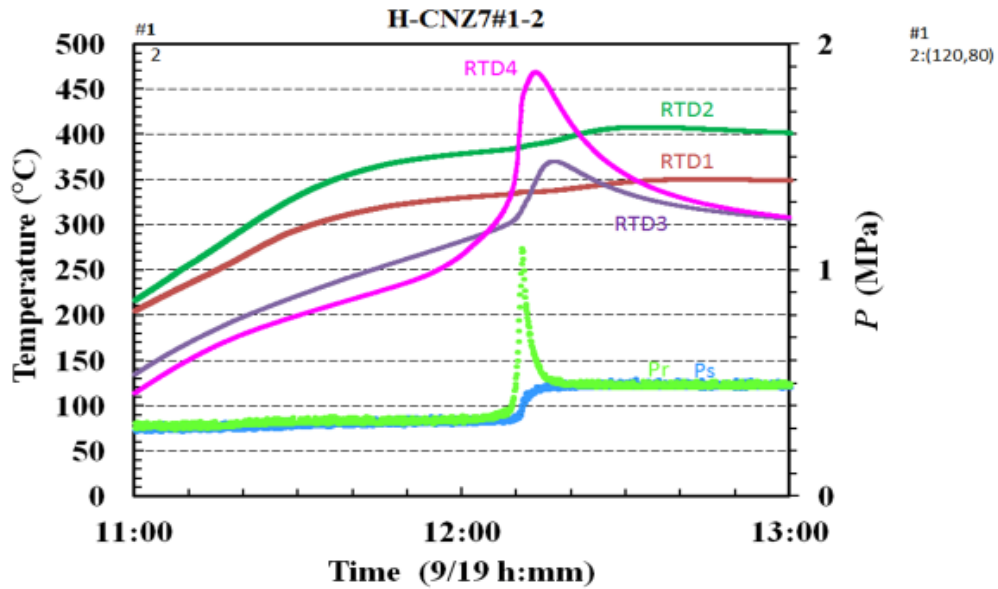


Fig.14 Evolution of local temperatures (by RTDs) in RC around the burst

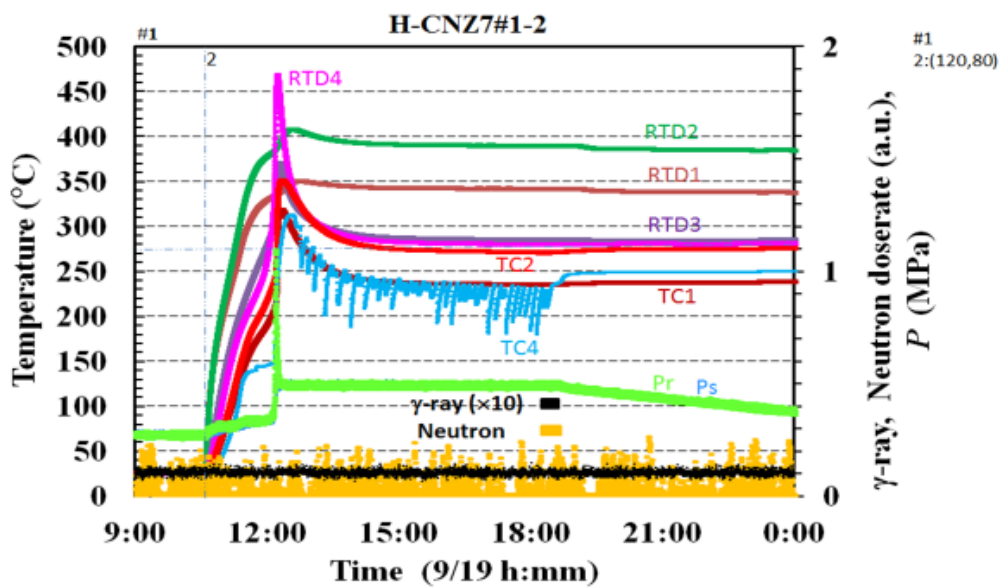
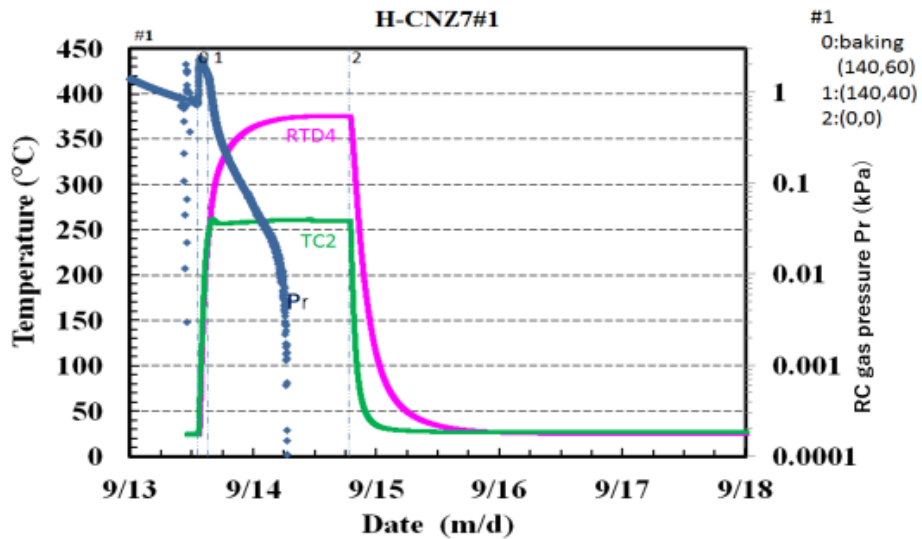


Fig.15 Neutron and gamma counting levels during CNZ7#1-2 run

As shown in Fig.15, no obvious correlations between the heat burst and neutron and gamma-ray counting were observed. Radiation levels were within statistics of natural background. Almost radiation-less “condensed matter nuclear reactions” as the thought heat source of the burst event are not in contradiction with the CCF/TSC theory prediction of nuclear products [10].

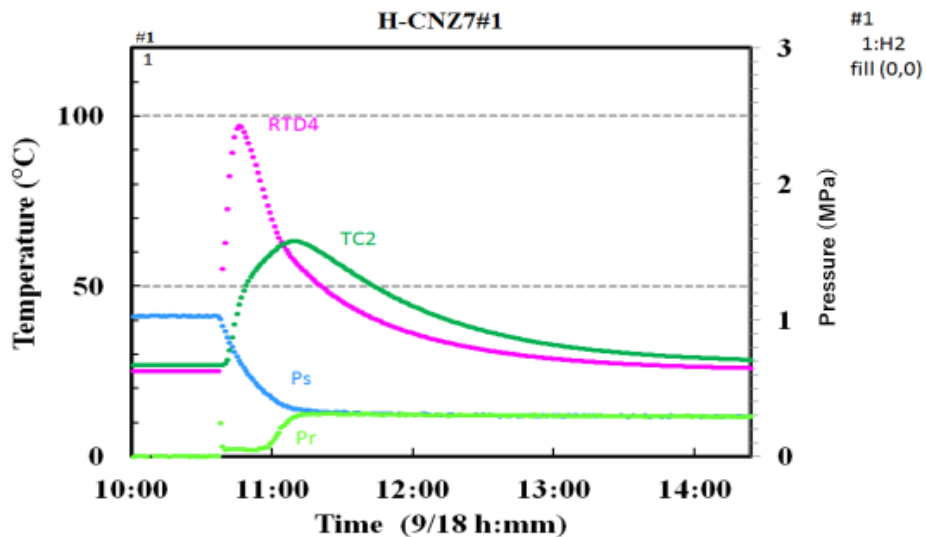
### 3-2 DATA BY RT RUNS

In Figs.16 and 17, raw data are shown for the initial baking under evacuation and the first room temperature H-loading run CNZ7#1-1.



15

Fig. 16 Initial baking data, RC pressure Pr and temperatures of RTD4 and TC2



16

Fig.17 Raw data of initial RT H-loading run CNZ7#1-1

In the present work, we elevated average RC temperature (represented by RTD4) over 300 °C, for baking. We used to set around 200 °C in our previous works [1-6]. We have found some positive indication to increase AHE (the case of PNZ10

experiment [9]), by elevating more baking temperature, and we tried the same here in this work.

As shown in Fig.17, feeding of 1.05 MPa x 3700 cc H<sub>2</sub> gas at SC was started to RC with ca. 1kg CNZ7 (Cu<sub>1</sub>Ni<sub>7</sub>/ZrO<sub>2</sub>) powder sample. Net amount of nickel was ca. 3 mol (namely ca. 180 g). About 1.0 mol H-gas was absorbed by CNZ7 sample in ca. 60 min. Saturated H-loading ratio was H/Ni = ca. 0.35. As shown in Fig.18, total heat of 124 kJ by H-absorption was obtained. Decay of thermal power followed the calorimetry response function  $exp(-t/\tau)$  with  $\tau = 62$  min, which is close to 60 min by zirconia calibration run around room temperature. Specific H-absorption energy (eta value) was ca. 1.2 eV/H, which is considerably large in usual sense of H-absorption, as we obtained 0.55 eV/D for PNZ6 (Pd<sub>1</sub>Ni<sub>7</sub>/zirconia) sample at RT [9].

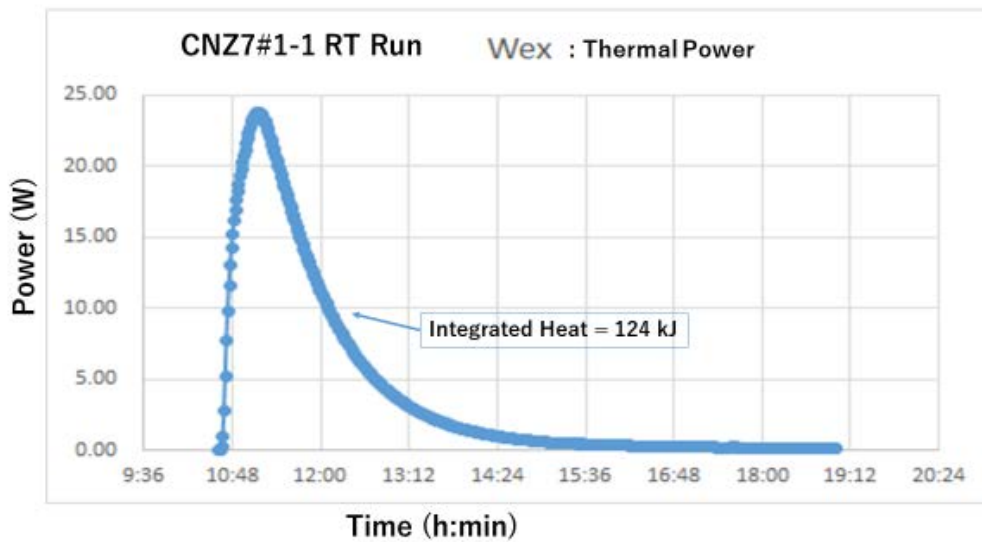


Fig.18 Thermal power evolution by H-loading to CNZ7 sample at room temperature

### 3.3 Sustainable AHE by ET Runs

After seeing the heat burst event, experiments at ET conditions have continued for a few months. In the present paper, we show data in the first month and some preliminary discussions.

In Fig.19, we show evolution of temperatures by RTD4 and TC2 for CNZ7#1-2 and -4 data with [120, 80] W heating condition. Broken line is Wex (excess power) = zero level by the blank run with zirconia. After the heat burst event of CNZ#1-2, slight excess power in 2-3 W continued for 17 hours. We once decreased heater power to [90, 50] to confirm Wex = 0. In the second [120, 80] W run, we added H<sub>2</sub>-gas to RC and saw significantly endothermic effect by H-absorption.

In Fig.20, we show data by CNZ7#1-9 and -10 with [140, 95] W heating condition. TC2 temperature decrease below Wex = 0 line are seen after we refilled H-gas. It seems that endothermic H-absorption evolved for about 12 hours after each refill of H-gas and

exothermic reactions are gradually increasing to generate excess power, which reached to 9-12 W. We can conceive that there happened competing process between endothermic H-absorption and some exothermic reaction.

In Fig.21, we show data by CNZ#1-11. Wex on the level of ca. 14 W is continuing for about 4 days. When we refilled H-gas (0.16 MPa), Wex increased to ca. 19 W for a few hours. Total excess energy for ca. 4 days is ca. 4.8 MJ.

Experiments will be continuing further for a few months. We will report summarized results including H-loading ratio data and excess power evolution graphs in forthcoming scientific meetings.

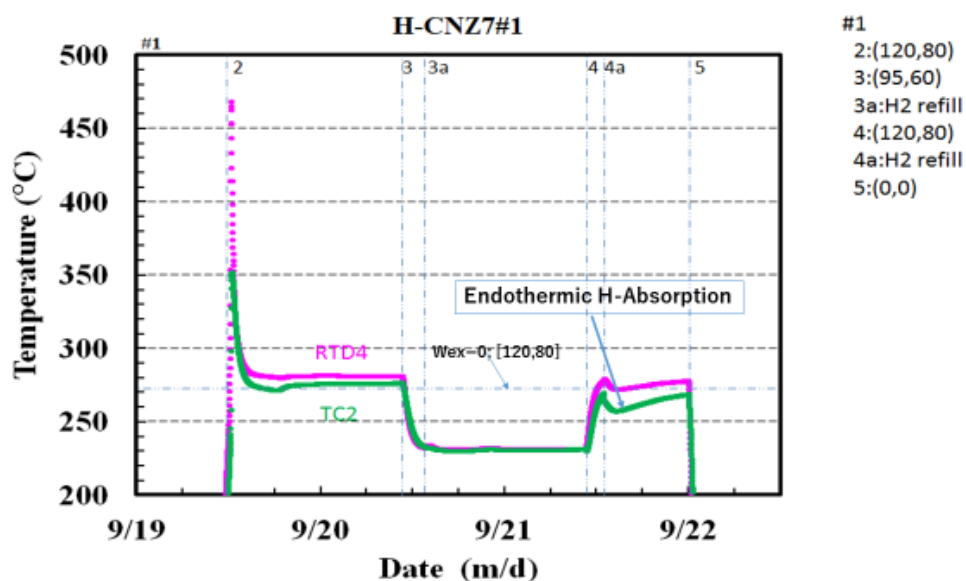


Fig.19 Brief view of ET runs of CNZ7#1-2, -3 and -4, for typical evolution of temperatures

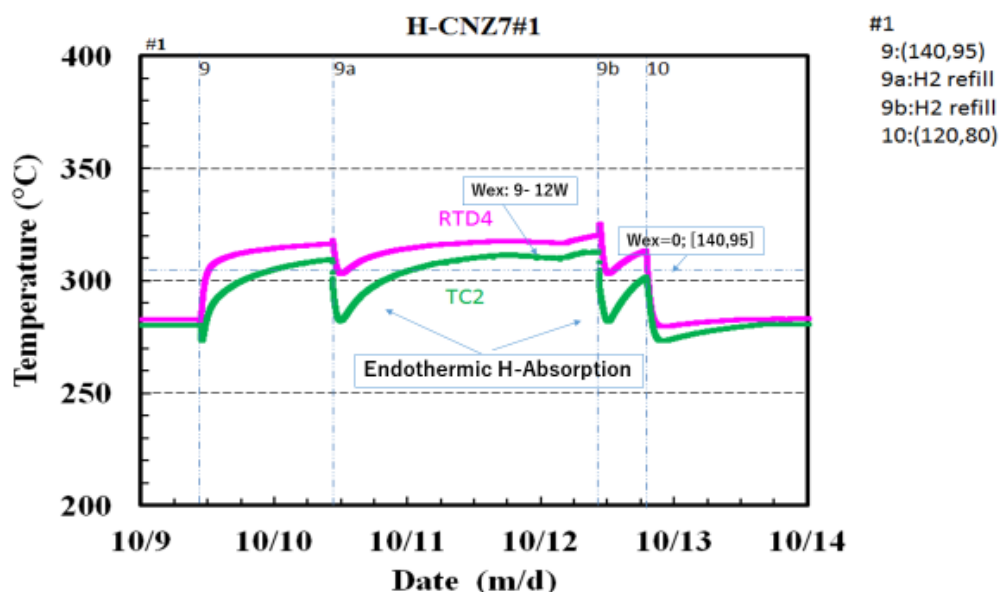


Fig.20 Brief view of ET runs of CNZ7#1-9 and -10, for typical evolution of temperatures

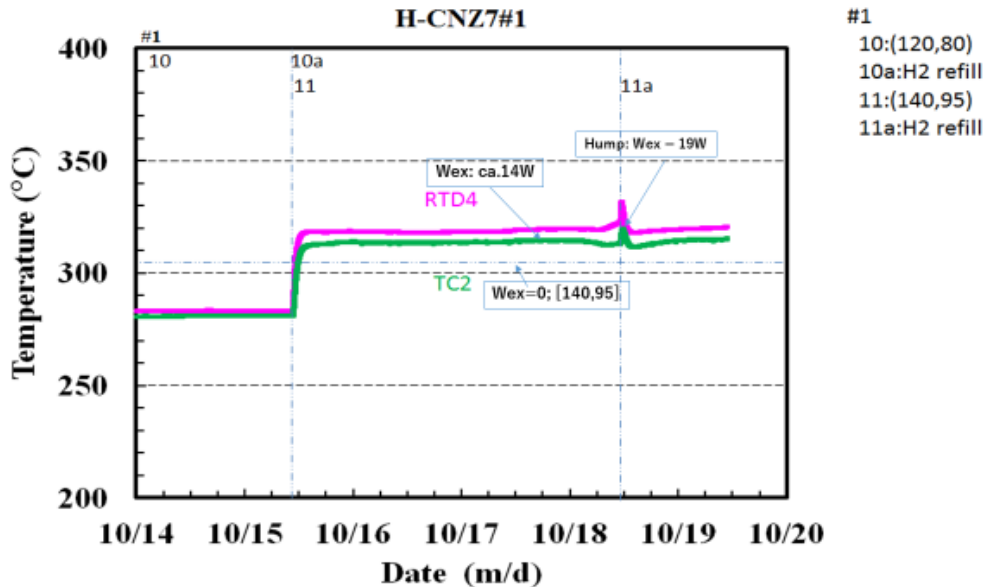


Fig.21 Brief view of ET runs of CNZ7#1-9 and -10, for typical evolution of temperatures

## VI SUMMARY AND CONCLUDING REMARKS

Anomalous heat burst with ca.130W peak power and ca. 365kJ total heat was observed by ca. 1kg CNZ7 sample under elevation of temperature. Heat pulse occurred in ca. 100s with ca. 3 kW peak power. It happened in the upper zone of RC when local H-absorption looked saturated.

Strange oscillatory evolution of temperature was observed at gas-outlet/inlet point of RC, which may be the same phenomena as Iwamura et al reported first at ICCF20.

H-absorption at elevated temperature by CNZ7 is endothermic and has reached at near-saturation state in a few days.

After saturation of H-absorption, sustaining excess power in earlier weeks was observed with 12-14 W. Small hump with 19 W excess was observed by re-filling H-gas of ca. 0.16 MPa into RC.

The anomalous heat burst event was observed only at the beginning ET run. However various data (as local temperatures in RC, coolant oil outlet temperatures, temperature behavior of gas inlet/outlet point and H-gas spike and quick balance) are very clear and consistent each other. The existence of very large thermal power generation must be real. How to elongate time-interval of large heat power will be of key issue toward the industrial application.

## References

- [1] Akira Kitamura, Akito Takahashi, Koh Takahashi, Reiko Seto, Takeshi Hatano, Yasuhiro Iwamura, Takehiko Itoh, Jirohta Kasagi, Masanori Nakamura, Masanobu Uchimura, Hidekazu Takahashi, Shunsuke Sumitomo, Tatsumi Hioki, Tomoyoshi Motohiro, Yuichi Furuyama, Masahiro Kishida, Hideki Matsune; “Comparison of excess heat evolution from zirconia-supported Pd-Ni nanocomposite samples with different Pd/Ni ratio under exposure to hydrogen isotope gases”, Proc. JCF18, pp. 14-31, 2018
- [2] Akira Kitamura, Akito Takahashi, Koh Takahashi, Reiko Seto, Takeshi Hatano, Yasuhiro Iwamura, Takehiko Itoh, Jirohta Kasagi, Masanori Nakamura, Masanobu Uchimura, Hidekazu Takahashi, Shunsuke Sumitomo, Tatsumi Hioki, Tomoyoshi Motohiro, Yuichi Furuyama, Masahiro Kishida, Hideki Matsune, “Excess heat evolution from nanocomposite samples under exposure to hydrogen isotope gases”, *Int. J. Hydrogen Energy*, 43 (2018) 16187-16200
- [3] Akito Takahashi, Akira Kitamura, Koh Takahashi, Reiko Seto, Takeshi Hatano, Yasuhiro Iwamura, Takehiko Itoh, Jirohta Kasagi, Masanori Nakamura, Masanobu Uchimura, Hidekazu Takahashi, Shunsuke Sumitomo, Tatsumi Hioki, Tomoyoshi Motohiro, Yuichi Furuyama, Masahiro Kishida, Hideki Matsune; “Phenomenology and Controllability of New Exothermic Reaction between Metal and Hydrogen”, Technical report uploaded at Research Gate: [https://www.researchgate.net/publication/322160963\\_Brief\\_Summary\\_Report\\_of\\_MHE\\_Project\\_Phenomenology\\_and\\_Controllability\\_of\\_New\\_Exothermic\\_Reaction\\_between\\_Metal\\_and\\_Hydrogen](https://www.researchgate.net/publication/322160963_Brief_Summary_Report_of_MHE_Project_Phenomenology_and_Controllability_of_New_Exothermic_Reaction_between_Metal_and_Hydrogen)
- [4] A. Takahashi, A. Kitamura, K. Takahashi, R. Seto, T. Yokose, A. Taniike and Y. Furuyama, “Anomalous Heat Effects by Interaction of Nano-metals and D(H)-gas”, Proc. ICCF20, Tohoku University (2016), downloadable at Research-Gate: [https://www.researchgate.net/publication/313310565\\_Anomalous\\_Heat\\_Effects\\_by\\_Interaction\\_of\\_Nano-Metals\\_and\\_HD-Gas](https://www.researchgate.net/publication/313310565_Anomalous_Heat_Effects_by_Interaction_of_Nano-Metals_and_HD-Gas)
- [5] Akira Kitamura, Akito Takahashi, Koh Takahashi, Reiko Seto, Yuki Matsuda, Yasuhiro Iwamura, Takehiko Itoh, Jirohta Kasagi, Masanori Nakamura, Masanobu Uchimura, Hidekazu Takahashi, Tatsumi Hioki, Tomoyoshi Motohiro, Yuichi Furuyama, Masahiro Kishida, “Collaborative Examination on Anomalous Heat Effect Using Nickel-Based Binary Nanocomposites Supported by Zirconia”, *J. Condensed Matter Nucl. Sci.*, 24, 202-213 (2017).
- [6] Yasuhiro Iwamura, Takehiko Itoh, Jirohta Kasagi, Akira Kitamura, Akito Takahashi, Koh Takahashi, Reiko Seto, “Replication Experiments at Tohoku University on Anomalous Heat Generation Using Nickel-based Binary Nanocomposites and Hydrogen Isotope Gas”, *J. Condensed Matter Nucl. Sci.*, 24, 191-201 (2017)
- [7] Akito Takahashi, “Physics of Cold Fusion by TSC Theory”, *J. Condensed Matter Nucl. Sci.*, 13, 565-578 (2014)
- [8] Akito Takahashi, “Background for Condensed Cluster Fusion”, Proceedings of JCF-15, pp.63-90, (2014)
- [9] Akito Takahashi, Koh Takahashi, Reiko Seto, Toyoshi Yokose, Akira Kitamura, Yuichi Furuyama, “Repeated Calcination and AHE by PNZ6 Sample”, Proceedings of JCF19, JCFRS, to be published in 2019

- [10] Akito Takahashi, “Nuclear Products of Cold Fusion by TSC Theory”, *J. Condensed Matter Nucl. Sci.*, 25, 11-25 (2015)

# Computer Simulation Approaches to Hydrogen Cohesion inside the Metal Surface

Hidemi Miura  
Izumi-ku, Sendai. 981-3109, Japan

**Abstract:** There have been a lot of studies about the generation of excess heat and elements related to nuclear fusion and nuclear transmutation in metals. Hydrogen (H) or deuterium (D) atoms probably gather to generate high density cohesion state in the diffusion process of H or D atoms inside the metal surface prior to the condensation of proton (p) or deuteron (d) to occur nuclear fusion and/or nuclear transmutation. We investigated the transition energy (the difference of total energy) when an H atom transited between T sites and O sites in aluminum (Al) metal lattice by computer simulation. As a result, when some H atoms had entered T sites or O sites of Al metal lattice, the transition energy of the H atom decreased about half of no H atom had entered and the total energy from hollow site to T site right inside the surface decreased where the cohesion state of H atoms seemed to be formed. Furthermore, when some H atoms had entered O sites of Al metal lattice, the changing pattern of total energy lost the periodicity of metal lattice to probably cause the decrease of transition energy deep inside the metal lattice. It implies that the H atom surrounded by the other H atoms could more easily transit. Then domains where H atoms transit fast or slow would appear and H atoms are shoved inside the fast diffusion domains in front of the slow ones to form the cohesion state of H atoms as long as H atoms continuously enter the metal surface.

**Keywords:** computer simulation, NEB method, transition energy, cohesion state, hydrogen, aluminum

## 1. Introduction

Since the excess heat by electrolysis of heavy water with palladium (Pd) cathode has been reported, there have been a lot of studies about the generation of excess heat and elements related to nuclear fusion and nuclear transmutation in metals. These contain electrolysis of light water with nickel (Ni) cathode, deuterium gas permeation through the composite membrane of Pd and calcium oxide (CaO), deuterium gas occlusion into the nanoparticle of Pd or palladium oxide (PdO), and so on. In recent years, it has been reported that anomalous heat is detected when some metal alloys of Pd, Ni and other metals or some binary powder systems of Ni, aluminum (Al) and other metals are heated in hydrogen (H) or deuterium (D) gas, and various elements are

generated under vibratory agitation of the pure water or aqueous electrolyte solutions such as metal-chloride by Pd plating vibration blades<sup>1)</sup>, and so on.

For occurring nuclear fusion and/or nuclear transmutation in metal lattices, two or more nuclei (proton (p) or deuteron (d)) of H or D atoms have condensed. However, H or D atoms entered the metals transit between one site and another neighboring site due to thermal lattice vibration and diffuse. Then, we investigated whether H or D atoms gather to generate high density cohesion state inside the metal surface during the diffusion process of H or D atoms prior to the condensation of p or d to occur nuclear fusion and/or nuclear transmutation. As for a method, we estimated the transition energy (the differences of total energy) when an H atom transited between tetrahedral (T) sites and octahedral (O) sites in Al metal lattice by computer simulation. Calculations were carried out by using Nudged Elastic Band (NEB) method on a computer simulation program Quantum ESPRESSO (opEn-Source Package for Research in Electronic Structure, Simulation, and Optimization) of the first principle molecular dynamics, imposed periodic boundary conditions on two slab-structural calculation units of (0 0 1) and (1 1 1) surfaces of Al metal lattice, for three cases when (1) no H atom had entered the other T sites or O sites and (2) some H atoms had entered the other T sites and (3) had entered the other O sites.

As a result, when some H atoms had entered T sites of Al metal lattice, the total energy from hollow site to T site right inside the surface decreased, and when some H atoms had entered O sites, according to the calculation conversed with the surface relaxation structurally optimized three surface atomic layers to the direction of depth (Z axis), the total energy from hollow site to T site right inside the surface decreased. These imply when H atoms enter the metal lattice, first of all they are trapped between hollow site and T site right inside the surface of metal lattice to form the H atom cohesion state.

Furthermore, when some H atoms have entered O sites of Al metal lattice, the transition energy of the H atom between T sites and O sites decreased about half when no H atom had entered, and the changing pattern of total energy lost the periodicity of metal lattice. The transition energy would possibly more decrease when the H atoms entered the many other different places. It implies that the H atom surrounded by the other H atoms could more easily transit, that is to say the diffusion rate of H atoms increase, than that surrounded by no other H atoms. Then H atom would diffuse fast in the domains where some H atoms have entered or slow in the domains where no H atom have entered, and cause to form the cohesion state of H atoms shoved inside the fast diffusion domains in front of the slow ones as long as H atoms continuously enter

the metal surface. This suggests that the H/D atom cohesion states would be locally generated in the front of H/D diffusion domains inside the metal surfaces of electrolysis cathode, gas permeation membrane and gas occlusion nanoparticle, when H/D atoms enter the metal lattice at higher rate than the diffusion rate of H/D atoms. Those would be generated also inside the metal surfaces of vibration blade, high voltage cathode or high pressure gas permeation membrane.

However, for occurring nuclear fusion and/or nuclear transmutation in metal lattices, these H/D atom cohesion states must become higher density p or d condensation states overcoming the repulsion force between p or d particles.

The similar calculations would be need for other metals to estimate whether these large decreases of total energy or transition energy of the H atom transit near other H atoms were characteristic of soft Al metal lattice. The feature of H/D atom cohesion states would be investigated to search what cause the condensation of p or d particles.

## 2. Calculations

### 2.1 Method, Hardware and Software Used for Calculation

As for the simulation of transition of an H atom in metal lattices, the transition energy (the differences of total energy) arisen from the transition of the H atom between two sites of metal lattice were investigated by using NEB method<sup>2)</sup> on a computer simulation program Quantum ESPRESSO (Ver. 5)<sup>3)</sup> based on the density functional theory of the first principle molecular dynamics on a personal computer (PC) which had 4 cores / 8 ways CPU with 32 GB main memory. This computer simulation program was working on the molecular computation support system program Winmoster<sup>TM 4)</sup> which assisted in exchanging atomic kinds and changing atomic coordinates, and in immediately showing lattice structures of metals and outputting graphics of calculated total energies, and so on.

### 2.2 Calculated Metal lattices

Calculations were carried out for three cases (1) when no H atom had entered the other T sites and O sites, (2) some H atoms had entered T sites, and (3) some H atoms had entered O sites, imposed the periodic boundary conditions on two slab-structural calculation units of (0 0 1) and (1 1 1) surfaces Al metal lattice. Al metal was applied first because it was one of the face centered cubic lattice such as Pd, Ni, Cu metals using in experiments and was possible easily to be calculated by NEB method on the PC. Slab-structural calculation unit of (0 0 1) surface of Al metal lattice was composed of 2x2x2 layered conventional simple cubic cells of four Al atoms and had 25 Å thick

vacuum layer. And that of (1 1 1) surface of Al metal lattice was composed of 2x3x1 layered ones and the same vacuum layer.

NEB method finds the minimum energy paths between known reactants by optimizing a number of intermediate images along the reaction path. By using NEB method, total energies on the transition path of H atom in two slab-structural calculation units were calculated as follows:

- (1) Transition of one H atom when no H atom had entered the other T sites or O sites
  - Between on-top sites, bridge sites and hollow sites on the metal surface
  - Between T sites or O sites inside the metal surface and the sites mentioned above
  - Between T sites and O sites each other mentioned above
- (2) Transition of one H atom when other H atoms had entered some T sites
  - Between the same sites mentioned at (1)
- (3) Transition of one H atom when other H atoms had entered some O sites
  - Between the same sites mentioned at (1)

Three H atoms per calculation unit cell are lower than 0.1 concentrations to Al atoms and locally about 0.5 concentrations. For an example, (0 0 1) surface slab-structural calculation unit of the Al metal lattice is shown in Fig. 1.

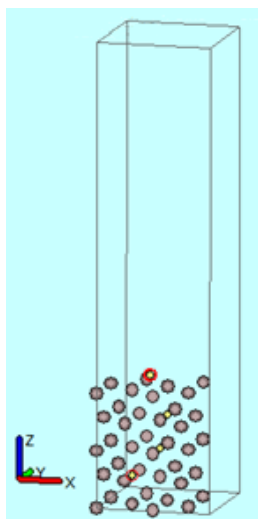


Fig.1 (0 0 1) surface slab-structural calculation unit of Al metal lattice

Calculated sites were named as illustrated in Fig. 2 and Fig. 3. (These figures are for Cu metal lattices prepared to calculate in similar way as the Al metal lattice.) These calculated sites were selected for an H atom to get into the Al metal lattice from a surface bridge or a hollow site to a T site and deeply by repeated transitions between T sites and O sites. For the NEB calculations, the short distances between sites on the

surface were divided into three equal parts (four steps) and the long distances between T sites and O sites inside the surface were divided into six equal parts (seven steps). The H atom on each site of the surface was set away from the surface about 1 Å optimized to the perpendicular or depth direction (Z axis).

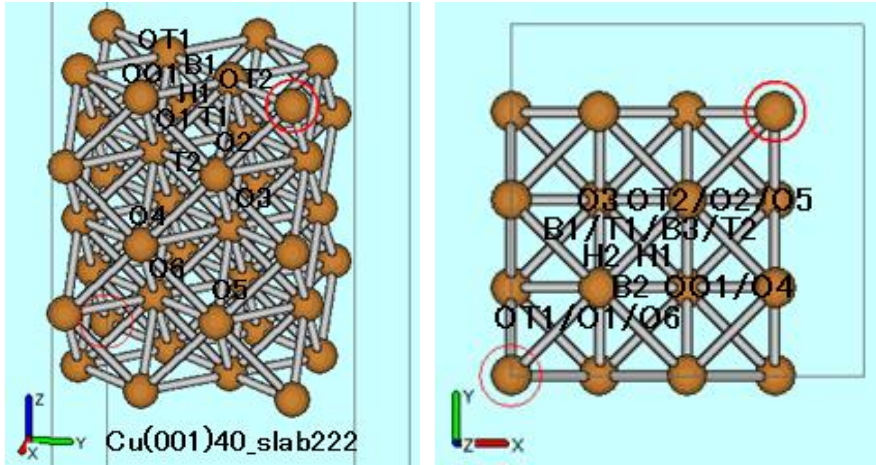
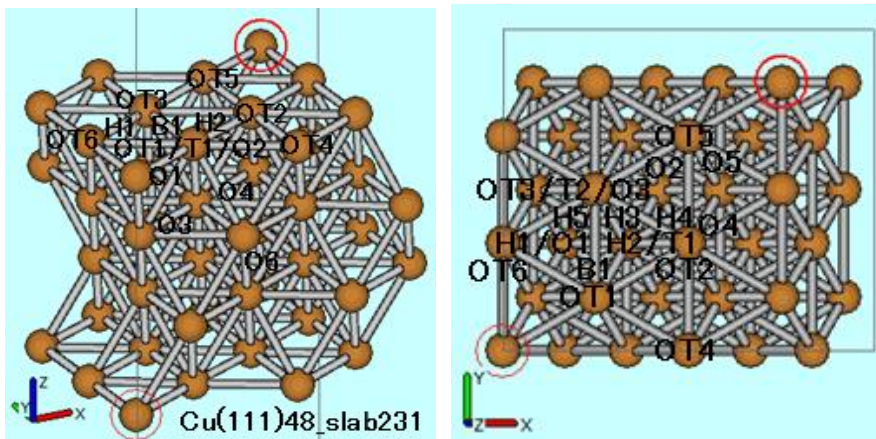


Fig. 2 Sites naming of (0 0 1) surface slab-structural calculation unit



metal lattice shown in Fig. 1 and named as Fig. 2.

The whole calculation results were shown in Fig. 4. The total energy of H atom at bridge site (B1) on the surface of Al metal lattice was the lowest of the all calculated sites. There are three layers of O sites in the calculation unit cell to the direction of depth (Z axis) then the graphs of calculated total energy on O1-T2-O3-T3-O5 sites symmetrize at the center O site (O3) to the direction of depth (opposite direction of Z axis in Fig. 1 or the horizontal axis in Fig. 4). The total energy on the third layer O site (O5) which contact with the bottom surface became the nearly same value on the first layer O site (O1) which contact with the upper surface. Since the transition energy (the difference of total energy) of an H atom through bridge sites is more than twice large as that through hollow sites, almost all H atoms seem to transit between T sites and O sites through hollow sites.

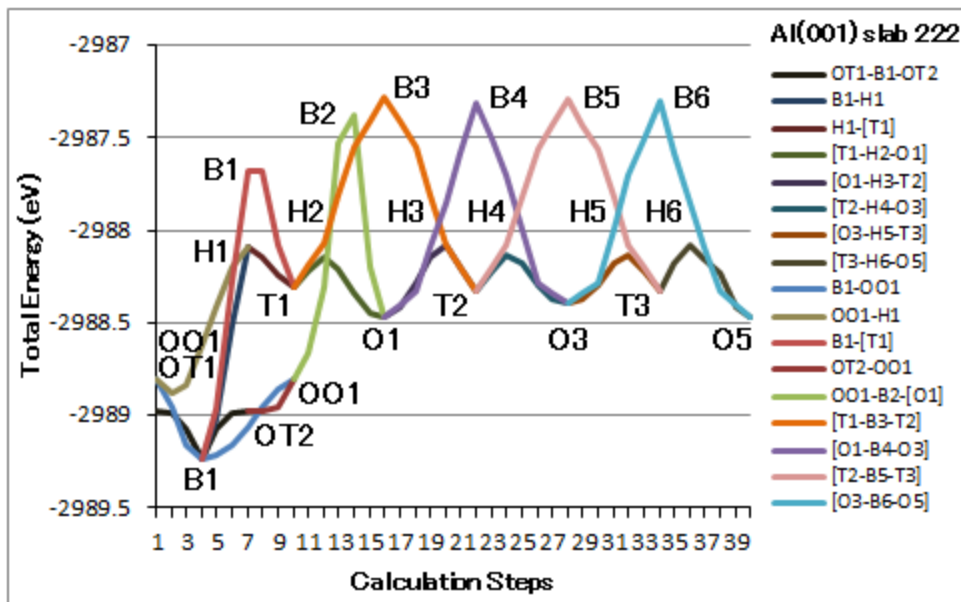


Fig. 4 Total energy of an H atom at each site of (0 0 1) surface slab-structure Al metal lattice [ ] indicate sites inside the surface

Fig. 5 shows the total energy for transitions between B1-H1-T1-O1-T2-O3-T3 sites when the surface relaxation of Al metal lattice by the structural optimization of surface atomic layers to the direction of depth (Z axis) and the surface relaxation or lattice expansion to all directions except the lowest one were carried out. Dotted lines indicate calculations without the surface relaxation of Al metal lattice (shown again some of the same graphs in Fig. 4), dashed lines indicate those with the surface relaxation by the structural optimization of one surface atomic layer to the direction of

depth (Z axis), broken lines indicate those with the surface relaxation of two surface atomic layers, long broken lines indicate those with the surface relaxation of three surface atomic layers, and solid lines indicate those with the surface relaxation or lattice expansion to all directions of surface atomic layers except the lowest one, respectively.

When the surface relaxation of one, two or three surface atomic layers was carried out, the total energy of an H atom of two groups of hollow site, T site and another hollow site (H1-T1-H2, H3-T2-H4), seemed to decrease one after another but slowly on the deep sites of later group. It can be presumed that the Al metal lattice is structurally optimized not only by the surface relaxation but also by the lattice expansion when the H atom enters the surface of Al metal lattice.

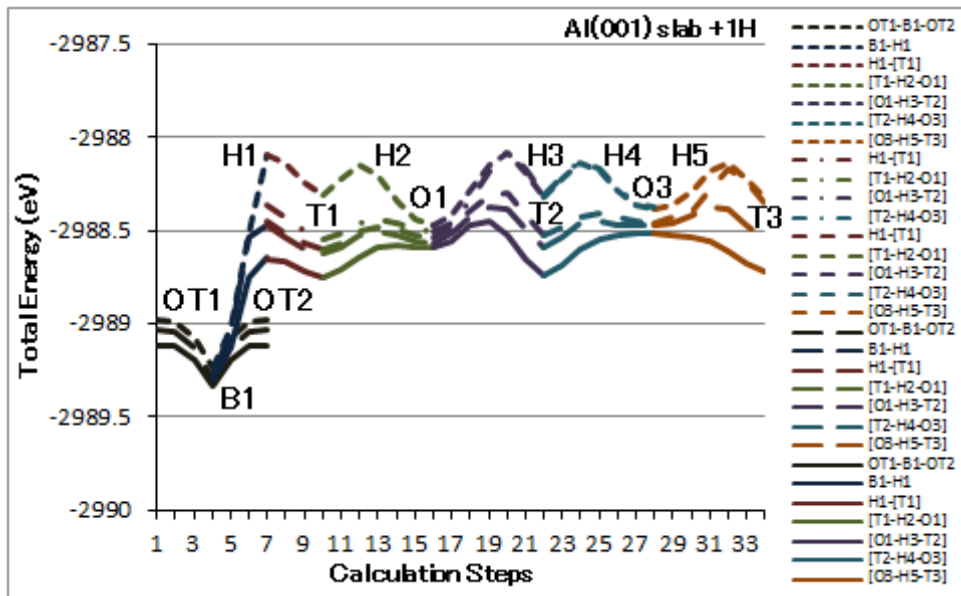


Fig. 5 Total energy of an H atom at each site of (0 0 1) surface slab-structure Al metal lattice

[ ] indicate sites inside the surface

Dotted lines indicate the total energy without the surface relaxation, and dashed lines indicate those with the surface relaxation of one surface atomic layer to the direction of depth (Z axis), and broken lines indicate those with the surface relaxation of two surface atomic layers, and long broken lines indicate those with the surface relaxation of three surface atomic layers, and solid lines indicate those with the surface relaxation or lattice expansion to all directions of surface atomic layers except the lowest one, respectively.

The total energy from hollow site (H1) to T site (T1) and to hollow site (H2) and next from hollow site (H3) to T site (T2) and to hollow site (H4) with the surface

relaxation or lattice expansion (solid lines in Fig. 5) became lower about 0.5 eV than those without them (dotted lines in Fig. 5). The transition barrier (the transition energy) of hollow site (H2) between T site and O site (T1-O1) and hollow site (H3) between O site and T site (O1-T2) became about 0.15 eV by the decrease of total energy from T site to O site and T site (T1-O1-T2) nearest to the surface, but the transition barrier (transition energy) of hollow sites (H4) between T site and O site (T2-O3-T3) did not change about 0.25 eV and wide by the increase of total energy of O site (O3) in the next below layer. When the H atom which enters T site (T1) or O site (O1) oscillates at two or three multiple frequency resonating with the thermal vibration (about 0.03 eV) of Al metal lattice<sup>5)</sup> and takes also the zero-point vibration, it could transit between T site and O site (T1-O1) and between O site and T site (O1-T2) right inside the surface of Al metal lattice. However, the H atom which enters T site (T2) seems to be difficult to easily overcome the transition barrier of hollow site and O site (H4-O3-H5) between T site and T site (T2-T3) slightly deep under the surface of Al metal lattice.

(2) Transition of one H atom when other H atoms had entered some T sites

Total energy was calculated when an H atom transited between on-top sites, bridge sites and hollow sites, between those sites and T sites or O sites and between those T sites and O sites in the (0 0 1) surface slab-structural calculation unit of Al metal lattice shown in Fig. 1 and named as Fig. 2, in which three H atoms had already entered three T sites.

Fig. 6 shows the total energy of the H atom for transitions between B1-H1-T1-O1-T2-O3-T3 sites without the surface relaxation of Al metal lattice indicated by dotted lines, those with the surface relaxation structurally optimized three surface atomic layers to the direction of depth (Z axis) indicated by long broken lines, and those with the surface relaxation or lattice expansion to all directions of surface atomic layers except the lowest one indicated by solid lines, respectively. Because the NEB calculation became hard to converge when some H atoms had entered T sites (and also O sites) with the surface relaxation structurally optimized to the direction of depth (Z axis) or to all directions of Al metal lattice, the whole calculations were not carried out (long broken lines and solid lines in Fig.6).

The transition energy (the difference of total energy) of the H atom when some H atoms had entered T sites was similar to that when no H atom had entered (dotted lines in Fig. 5 and Fig. 6).

When calculations with the surface relaxation structurally optimized three surface atomic layers to the direction of depth (Z axis) of Al metal lattice were carried out, the

total energy of the H atom between hollow site (H1) and T site (T1) right inside the surface decreased significantly (long broken lines in Fig. 6). Furthermore, the transition energy (the difference of total energy) of the H atom between T site (T1) and O site (O1), or the transition barrier of hollow site (H2), right inside the surface of Al metal lattice decreased and was about 0.1 eV, and the transition barrier of hollow site (H3) between O site (O1) and T site (T2) decreased but remained about 0.25 eV.

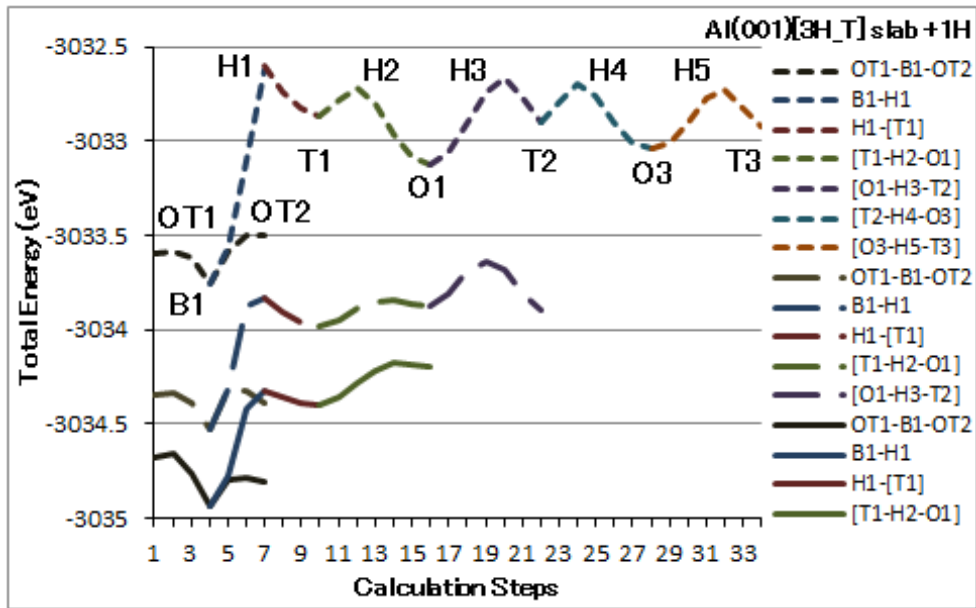


Fig. 6 Total energy of an H atom at each site of (0 0 1) surface slab-structure Al metal lattice when other H atoms have entered O sites

[ ] indicate sites inside the surface

Dotted lines indicate the total energy without the surface relaxation, and long broken lines indicate those with the surface relaxation of three surface atomic layers to the direction of depth (Z axis), and solid lines indicate those with the surface relaxation or lattice expansion to all directions of surface atomic layers except the lowest one, respectively.

When calculations with the surface relaxation structurally optimized to all directions of surface atomic layers except the lowest one of Al metal lattice were carried out, the total energy of the H atom decreased 0.3 - 0.5 eV lower (solid lines in Fig. 6) than that with the surface relaxation structurally optimized three surface atomic layers to the direction of depth (Z axis) (long broken lines in Fig. 6). The total energy of the H atom seemed to more decrease by the expansion of Al lattice due to H atoms entered T sites.

These decreases of total energy of the H atom possibly suggests that the Al metal lattice with some H atoms on T sites has a thin stable layer structure to trap H atom right inside the surface.

(3) Transition of one H atom when other H atoms had entered some O sites

Total energy was calculated when an H atom transited between on-top sites, bridge sites and hollow sites, between those sites and T sites or O sites and between those T sites and O sites in the (0 0 1) surface slab-structural calculation unit of Al metal lattice shown in Fig. 1 and named as Fig. 2, in which three H atoms had already entered three O sites.

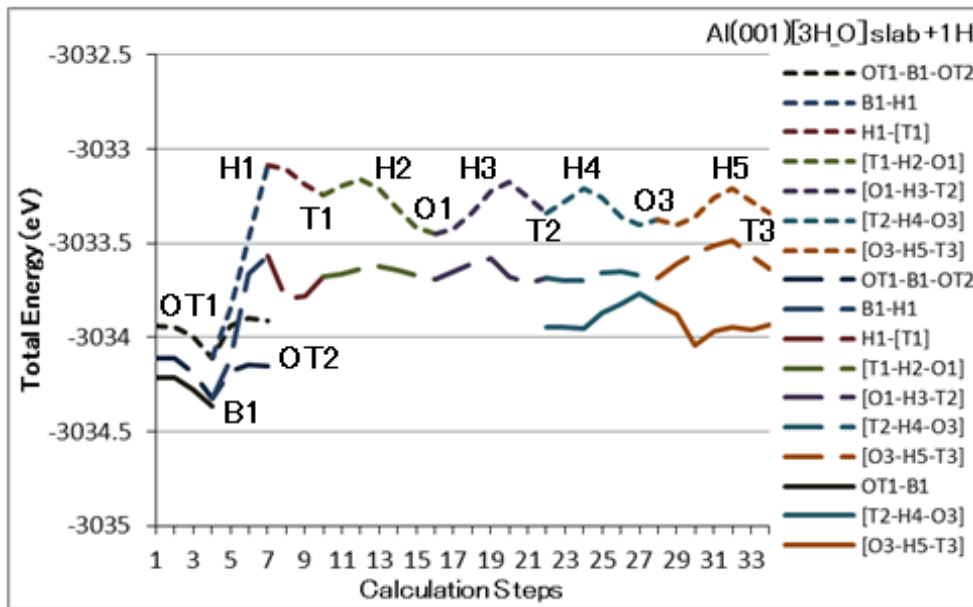


Fig. 7 Total energy of an H atom at each site of (0 0 1) surface slab-structure Al metal lattice when other H atoms have entered O sites

[ ] indicate sites inside the surface

Dotted lines indicate the total energy without the surface relaxation, and long broken lines indicate those with the surface relaxation of three surface atomic layers to the direction of depth (Z axis), and solid lines indicate those with the surface relaxation or lattice expansion to all directions of surface atomic layers except the lowest one, respectively.

Fig. 7 shows the total energy of the H atom for transitions between B1-H1-T1-O1-T2-O3-T3 sites without the surface relaxation of Al metal lattice indicated by dotted lines, those with the surface relaxation structurally optimized three

surface atomic layers to the direction of depth (Z axis) indicated by long broken lines, and those with the surface relaxation or lattice expansion to all directions of surface atomic layers except the lowest one indicated by solid lines, respectively. Because the NEB calculation became hard to converge when some H atoms had entered O sites (and also T sites) with the surface relaxation structurally optimized to the direction of depth (Z axis) or to all directions of Al metal lattice, the whole calculations were not carried out (long broken lines and solid lines in Fig. 7).

The transition energy (the difference of total energy) when some H atoms had entered O sites of Al metal lattice the transition energy of the H atom between H1-T1-O1-T2-O3-T3 sites decreased about half when no H atom had entered (dotted lines in Fig. 7 and Fig. 5). This decrease of the transition energy of the H atom was not clear, but the H atoms already entered O sites were observed to move inside the own sites when the transition H atom moved.

When calculations with the surface relaxation structurally optimized three surface atomic layers to the direction of depth (Z axis) of Al metal lattice were carried out, the total energy of the H atom between hollow site (H1) on the surface and T site (T1) nearest to the surface decreased significantly (long broken lines in Fig. 7). The NEB calculation converged with the surface relaxation structurally optimized three surface atomic layers to the direction of depth (Z axis), although that did not converged with the surface relaxation to all directions of surface atomic layers except the lowest one. This possibly suggests that the Al metal lattice with some H atoms has a thin layer structure stable to the direction of depth (Z axis) but unstable to the parallel direction of surface (X/Y axis) to trap H atom right inside the surface similarly to the case when other H atoms have entered some T sites.

Calculations were carried out for only so thin three O site layers that no information for transition energy (the difference of total energy) of the H atom between the deep sites was obtained. However, the transition energy of the H atom between the deep sites with the surface relaxation structurally optimized to all directions of surface atomic layers except the lowest one of Al metal lattice would be similar to the transition energy between T2-O3-T3 sites (solid lines in Fig. 5 and Fig. 7). When some H atoms had entered the O sites of Al metal lattice, the changing pattern of total energy (solid lines in Fig. 7) was different from that of when no H atom had entered (solid lines in Fig. 5), which lost the periodicity of metal lattice. The changing pattern of total energy would depend on the number and the places of entered H atoms, therefore when H atoms enter many different places of O sites, the transition energy of H atom would be averaged, and the diffusion rate of H atom in the metal lattice would increase.

When the calculation with the surface relaxation structurally optimized to all directions of surface atomic layers except the lowest one was not converged due to the instability of calculated Al metal lattice, H atoms were observed to leap out from O sites,. This suggests connections with the collective motion of H atoms in the metal lattice.

### 3.2 Al slab-structural calculation unit of (1 1 1) surface

The total energy were calculated when an H atom transited between on-top sites, bridge sites and hollow sites, between those sites and T sites or O sites and between those T sites and O sites in the (1 1 1) surface slab-structural calculation unit of Al metal lattice similar as shown in Fig. 1 of the (0 0 1) surface and named as Fig. 3. Calculations were carried out without the surface relaxation or structural optimization of Al metal lattice for H atom entered it.

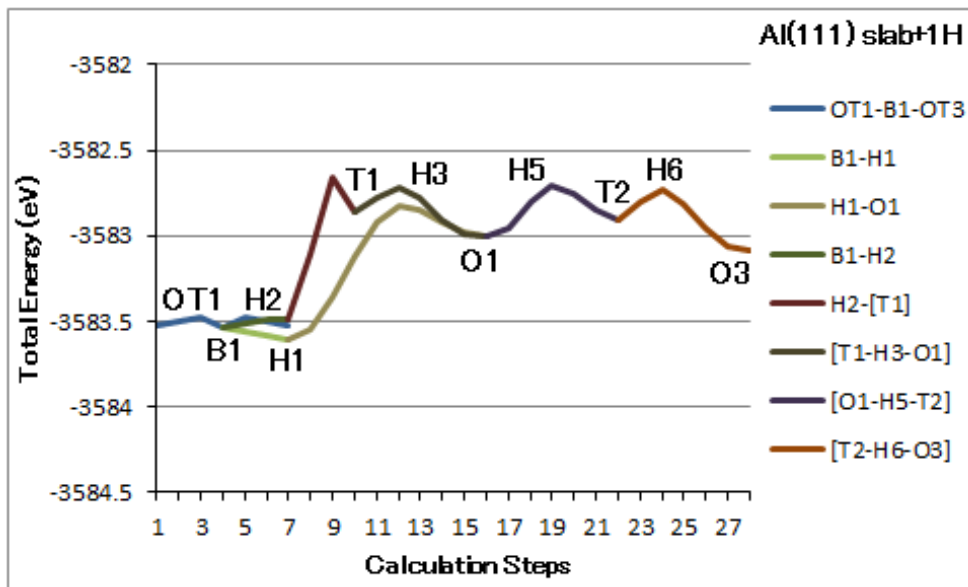


Fig. 8 Total energy of an H atom at each site of (1 1 1) surface slab-structure Al metal lattice [ ] indicate sites inside the surface

The calculation results were shown in Fig. 8 corresponded to the graphs of dotted line in Fig. 5. There are three layers of O sites in the calculation unit cell to the direction of depth (Z axis) then the graphs of calculated total energies on O1-T2-O3 sites symmetrize at the center O site (O3) to the direction of depth (Z axis or the horizontal axis in Fig. (8)). Total energy of hollow sites (H1, H2) on the surface were lower than those of the case of (0 0 1) surface slab-structure, however the change of

total energy on T sites, hollow sites and O sites (T1-H3-O1-H5-T2-H6-O3) under the surface was nearly same as that of the case of (0 0 1) surface slab-structure. Calculations for the (1 1 1) surface slab-structure Al metal lattice become difficult with surface relaxation and structural optimization of Al metal lattice for H atom entered, because of more Al atoms are there in the calculation unit of it.

### 3.3 Possibility of Generating of H Cohesion State

Total energy was calculated when an H atom transited between on-top sites, bridge sites, hollow sites and T sites or O sites on or inside the surface of Al metal lattice with the surface relaxation or lattice expansion structurally optimized to all directions, and calculations suggested the generation of cohesion state of H atoms.

In these calculations, the total energy from hollow site to T site right inside the surface observed to decrease, and when some H atoms had entered O sites of Al metal lattice, the changing pattern of total energy lost the periodicity of metal lattice. The similar calculations would be need for the other metals to estimate whether these large decreases of total energy of the H atom by the surface relaxation and the loss of periodicity in the changing pattern of total energy of the H atom near the other H atoms were characteristic of soft Al metal lattice.

#### (1) H Atom Cohesion State Generated around T Sites right inside Surface

When some H atoms had entered T sites of Al metal lattice, the total energy from hollow site to T site right inside the surface decreased with the surface relaxation structurally optimized to all directions. When some H atoms had entered the O sites of Al metal lattice, although calculations of total energy for the sites on or right inside the surface could not converge, the total energy from hollow site to T site right inside the surface decreased. These decreases of total energy of the H atom possibly suggests that the Al metal lattice with some H atoms on T sites has a thin stable layer structure to trap H atom right inside the surface.

Since T site (T1) has tetrahedral symmetry, there are two symmetrical decrease points of total energy from hollow site to T site right inside the surface. The other H atoms could enter these two symmetrical points or directions from the opposite O site symmetrical to T site (T1). Then four H cohesion state would be generated in and around T site right inside the surface, which could relate to the theory of condensation of four protons/deuterons <sup>6)</sup>. This H cohesion state could be continued to exit by feeding H atoms through the surface of Al metal lattice.

## (2) H Atom Cohesion State Generated by Increase of Diffusion Rate

When some H atoms had entered O sites of Al metal lattice, the transition energy (the difference of total energy) of the H atom decreased about half when no H atom had entered, and the changing pattern of total energy was different from that of when no H atom had entered, which lost the periodicity of metal lattice. The transition energy would possibly more decrease when the H atoms entered the many other different places. When the transition energy of H atom decreased, the diffusion rate of H atom in the metal lattice would increase.

This increase of the diffusion rate of H atom could not occur in the deep layer of the metal lattice where no H atom arrived. On the other hand, if too many H atoms entered almost all of the O sites and T sites of metal lattice locally, H atom could not transit between O sites and T sites and could not diffuse smoothly any more there. H atoms would diffuse fast in the domains where some H atoms had entered or slow in the domains where no H atom had entered, and these domains would move and expand in the metal lattice. Then H atoms are shoved inside the fast diffusion domains in front of the slow ones to form the cohesion state of H atoms as long as H atoms continuously entered the metal surface, which would also move and expand in the metal lattice and would be generated periodically or occasionally.

The NEB calculation of quantum mechanics (Quantum ESPRESSO) was carried out for the transitions of an H atom between T sites and O sites on this time. The researches using molecular dynamics simulation of classical mechanics have been reported that the diffusion coefficient increases in the region of concentration of H atoms 0.2 - 0.8<sup>7)</sup>.

## (3) Relation to Experiments

• Excess Heat Generation (Nuclear Fusion) or Nuclear Transmutation by Electrolysis of Light/Heavy Water or Deuterium Gas Permeation and Occlusion

In the electrolysis of light/heavy water, deuterium gas permeation through the membrane and deuterium gas occlusion in the nanoparticles or metal alloys or powder binary systems, first of all H/D atoms enter the surface of metal lattice and then the H/D atom cohesion state could be generated between the hollow site and T site right inside the surface of metal lattice. Furthermore, when the H/D atoms enter the metal lattice faster than the diffusion rate of them, the H/D atom cohesion state could be generated locally inside the fast diffusion domains in front of the slow ones of H/D atoms.

The similar H/D atom cohesion state could be generated near the connected

surface of two metals of different diffusion rate, when H atoms move from the higher diffusion rate to the lower one.

- Generation of Elements under Vibratory Agitation

It would be supposed that some spherical bubbles are generated and collapse near the pressurized surface of vibration blade when it moves periodically. The water cage cluster of nucleus in the collapsing spherical bubble would be pressed by water molecules which flow into the collapsing spherical bubble to form the high density water cage cluster of double cubic ice mutually insert each other. Then the high density water cage cluster would collide to the surface of vibration blade to cause the generation of elements <sup>1)</sup>.

The high density water cage cluster would probably collide randomly on the surface of vibration blade under vibration agitation. Then H/D atoms and O atoms or the other metal atoms which compose the large mass of high density water cage cluster would collide to the surface of vibration blade one after another in a short time, and the light H/D atoms which collide prior to the other heavy atoms would be squeezed into the surface of metal lattice of vibration blade by them. Locally inside the surface of vibration blade each where the high density water cage cluster collide, the H/D atom cohesion state could be generated. This H/D atom cohesion state would be generated in the region where the squeezing rate of H/D atoms into the metal lattice of vibration blade is larger than the diffusion rate of them.

- From H/D Cohesion State To p/d Condensation State

Even if either H/D cohesion state could be generated, no nuclear fusion and/or nuclear transmutation related to the generation of excess heat and elements occur only by it. For occurring nuclear fusion and/or nuclear transmutation, H/D cohesion state generated in the metal lattice scale would have to become high density p/d condensation state overcoming the Coulomb repulsion force of p/d in the nucleon scale. The problem seems lie in the reaction how the H/D cohesion state being applied for electrolysis voltage, permeation/occlusion gas pressure, or colliding speed interacts with own H/D atoms, metal lattice atoms and/or impurity atoms inside/entered the metal lattice. Some easy solutions for this problem might be the screening of Coulomb repulsion force, the generation of neutron by electron capture of H atom, the generation of pseudo-neutron by reduction of H atom electron orbit or something else which could be probably caused by the transition of H/D atoms through the bridge sites of high barrier energy or by the collision of them to the metal lattice atoms moving

strongly in the dynamic H/D cohesion state. However, because these phenomena have not been observed in experiments, the researches of vibration state and transition process of individual H/D atom or collective vibration state and dynamical collision process of H/D atom cohesion state would be established by computer simulation for the present.

#### 4. Summary

H or D atoms probably need to gather to generate high density cohesion state inside the metal surface during the diffusion process prior to the condensation of p or d to occur nuclear fusion and/or nuclear transmutation. Therefore, the transition energy (the differences of total energy) when an H atom transited between T sites and O sites in Al metal lattice was investigated by computer simulation to search the H cohesion state. Calculations were carried out by using NEB method on a computer simulation program Quantum ESPRESSO of the first principle molecular dynamics, imposed periodic boundary conditions mainly on a slab-structural calculation units of (0 0 1) surfaces of Al metal lattice, for three cases when no H atom had entered, some H atoms entered T sites, and some H atoms had entered the other O sites.

As a result, when some H atoms had entered T sites of Al metal lattice, the total energy from hollow site to T site right inside the surface decreased with the surface relaxation structurally optimized to all directions to form a thin stable layer structure and H cohesion state. Furthermore, when some H atoms had entered O sites of Al metal lattice, the transition energy (the difference of total energy) of the H atom between T sites and O sites was observed to be lower than when no H atom had entered them, and the changing pattern of total energy lost the periodicity of metal lattice to probably cause the decrease of transition energy deep inside the metal lattice.

The thin layer structure and the decrease of total energy near the surface implies when H atoms enter the metal lattice, first of all they are trapped between hollow site and T site right inside the surface of metal lattice, and then the H atom cohesion state could be generated there. Furthermore, the decrease of transition energy of the H atom when some H atoms have entered O sites of Al metal lattice implies that the H atom surrounded by the other H atoms could more easily transit than that surrounded by no other H atoms, that is to say the diffusion rate of H atoms increases. Then domains where H atoms transit fast or slow would appear and H atoms are shoved inside the fast diffusion domains in front of the slow ones to form the cohesion state of H atoms as long as H atoms continuously entered the metal surface.

This suggests that the H/D atom cohesion states would be locally generated in

front of the H/D diffusion domains inside the metal surfaces of electrolysis cathode, gas permeation membrane, gas occlusion nanoparticle when H/D atoms enter the metal lattice at higher rate than the diffusion rate of H/D atoms. Those would be generated also inside the metal surfaces of vibration blade, high voltage cathode or high pressure gas permeation membrane.

However, for occurring nuclear fusion and/or nuclear transmutation in metal lattices, these H/D atom cohesion states must become more high density p or d condensation states overcoming the repulsion force between p or d particles.

The similar calculations would be need for the other metals to estimate whether these large decreases of total energy of the H atom and the loss of periodicity in changing pattern of total energy of the H atom near the other H atoms were characteristic of soft Al metal lattice. The feature of H/D atom cohesion state will be investigated to search what cause the condensation of p or d particles.

## Acknowledgements

The author wishes to thank Japan Techno Co., Ltd. for providing many valuable data about vibration agitation and related phenomena.

## References

- 1) H. Miura, Water Clusters Related to OHMASA-GAS, Proc. of JCF18, 93 (2017).
- 2) H. Jonsson, G Mills, and K. W. Jacobsen, in Classical and Quantum Dynamics in Condensed Phase Simulations, edited by B. J. Berne, G. Ciccotti, and D. F. Coker (World Scientific, Singapore, 1998), p. 385.
- 3) P. Giannozzi et al., Quantum ESPRESSO: a modular and open-source software project for quantum simulations of materials, Journal of Physics: Condensed Matter, **21** (39), 395502 (2009).
- 4) N. Chida, Development of molecular computation support system Winmostar, Idemitsu technical report, **49**, 106 (2006).
- 5) H. Miura, Computer Simulation of Hydrogen Phonon States in Face Centered Cubic Lattice Metals, Proc. of JCF16, 92 (2015).
- 6) A. Takahashi, Chronicle of Condensed Cluster Fusion Models, Proc. of JCF8, 51 (2007).
- 7) K. Nishimura and K. Miyake, Molecular Dynamics Study on Hydrogen Diffusion in Pd and Pd-Ag Alloys, Journal of the Society of Material Science, **67**, 235(2018).

# Thermal properties of Pd–Zr and Pd–Ni–Zr complex sample in deuterium diffusion process

M. Endo\*, Y. Sato, S. Kikuchi, K. Ota, K. Negishi, S. Narita

Faculty of Engineering, Iwate University  
Morioka, Iwate, 020-8551, Japan  
\*t0315015@iwate-u.ac.jp

## Abstract

Deuterium desorption experiments were performed using various types of multi-layered Pd complex samples, and their deuterium diffusion behavior was investigated. Pd–Zr and Pd–Ni–Zr samples, as well as a sample with a fine-structured interface, were tested. For the Pd–Ni–Zr sample with a fine-structured interface, a continuous short-period fluctuation in temperature of the sample was observed. This phenomenon was also observed for the Pd–Ni sample with a fine-structured interface. The temperature fluctuation was not correlated with the pressure behavior. It is possible that deuterium diffusion from Pd to Ni and from Ni to Pd occurred alternately at the interface in this period and that endothermic and exothermic phenomena associated with the heat of solution repeatedly occurred owing to deuterium transport between the two metals.

## 1. Introduction

In deuterium absorption/desorption process for nanocomposite of Pd–Ni–Zr anomalous heat evolution that cannot be explained by chemical reaction has been observed [1,2]. In addition, a deuterium absorption and desorption experiment has been conducted using Pd-based metal complex samples, which were fabricated by depositing a metal membrane, such as Ni, Ag, Ti, and Zr, onto Pd foil. Then, an anomalous heat behavior was observed in the desorption process [3, 4]. These phenomena are supposed to be caused by the unique properties of deuterium diffusion in complex metals with a submicron/nano-scaled fine structure. Moreover, the anomalous phenomenon has been assumed to result from a condensed-matter nuclear reaction, and a specific sample condition in the experiments may be crucial for triggering the reaction.

For the Pd–Zr and Pd–Ni–Zr samples with and without a fine-structured interface were tested, and a continuous short-period fluctuation in temperature of the sample was observed that was not correlated with the pressure behavior [5]. In addition, a simultaneous increase of the temperature and the electrical resistance of the sample was observed during the desorption for several runs.

In this study, those results are reviewed, and further considerations are reported to clarify the mechanism that causes the phenomena.

## 2. Experiment

### Sample preparation

For this deuterium absorption/desorption experiment, four types of samples were tested: Pd–Zr and Pd–Ni–Zr samples with and without a fine-structured interface. These samples were fabricated by depositing Zr or Ni membrane onto the Pd foil ( $10 \times 10 \times 0.1$  mm) by using Ar beam sputtering. The thickness of the membrane was  $\sim 100$  nm. The fine-structured interface was formed by etching the Pd foil surface with an Ar ion beam before depositing the Zr or Ni membrane.

The surface of the Pd foil was analyzed using an atomic force microscope (AFM). Figure 1 shows the morphology of the surface before and after etching. It was found that the etched sample has an uneven shape with a height of 200 nm and width of approximately  $2 \mu\text{m}$ .

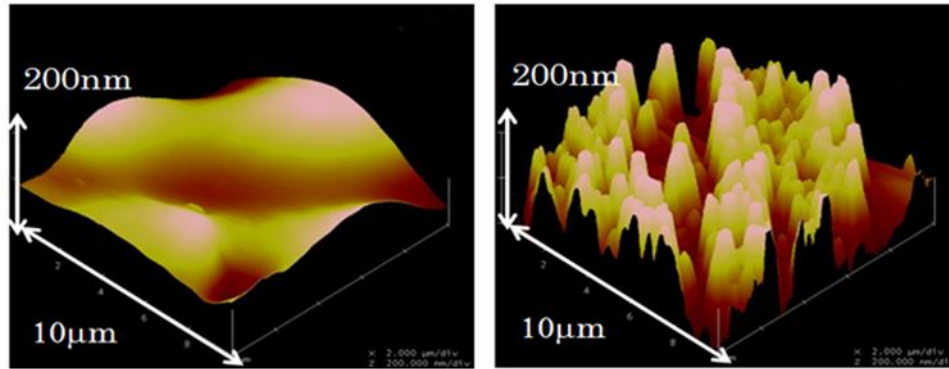


Fig. 1. Surface morphology before (left) and after (right) etching, observed by AFM

The sample surface was also analyzed by transmission electron microscopy (TEM) to evaluate a closer structure. A semispherical shape with a size of 50–200 nm was found.

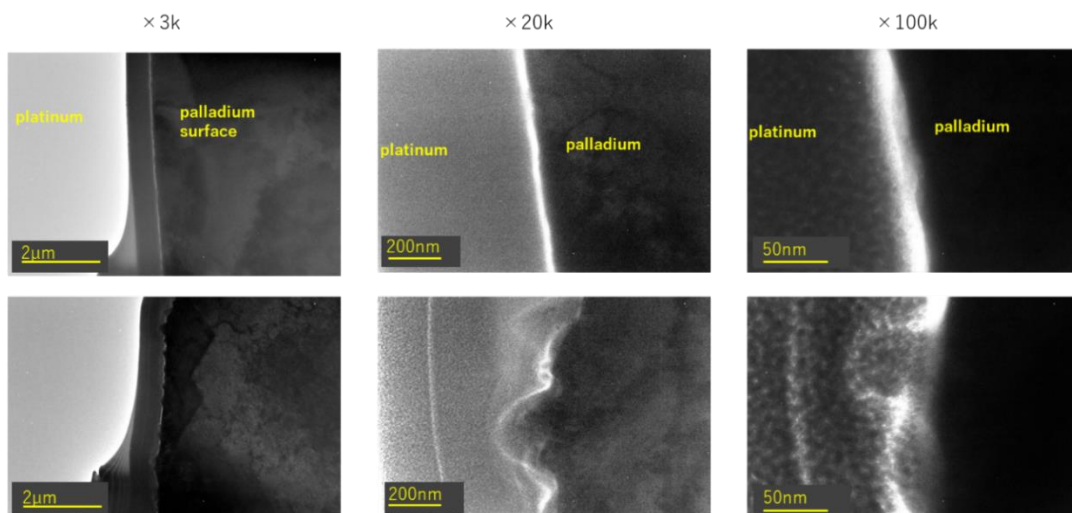


Fig. 2. TEM images for the sample etched — the sample surface was coated with Pt for protection in TEM analysis

In addition, the chemical composition of the Zr membrane was considered, because it can be easily oxidized, and the deoxidation by activated deuterium may affect the thermal behavior in the deuterium desorption experiment. The Zr membrane was analyzed by X-ray photoelectron spectroscopy (XPS). Figure 3 shows the XPS spectrum obtained. Since oxygen signal was observed as in the spectrum, Pd or Zr were supposed to be oxidized.

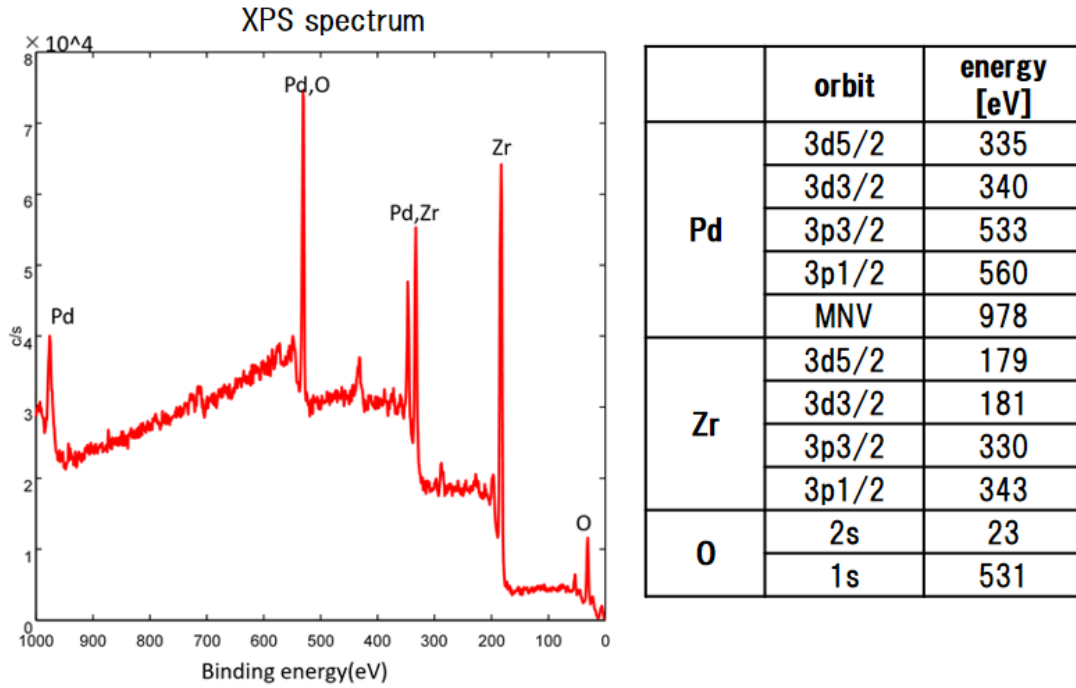


Fig. 3. XPS spectrum

### Deuterium loading

The fabricated multi-layered samples were exposed to deuterium gases at 5 atm for ~24 h to load deuterium. The weight of the sample was measured before and after loading, and the loading ratio (D/Pd) was calculated from the weight difference. Figure 4 shows the loading ratio for each of the samples, and their average values are also indicated. The average loading ratio was found to be 0.65–0.70 for most samples, and no significant difference in D/Pd values of each sample was seen.

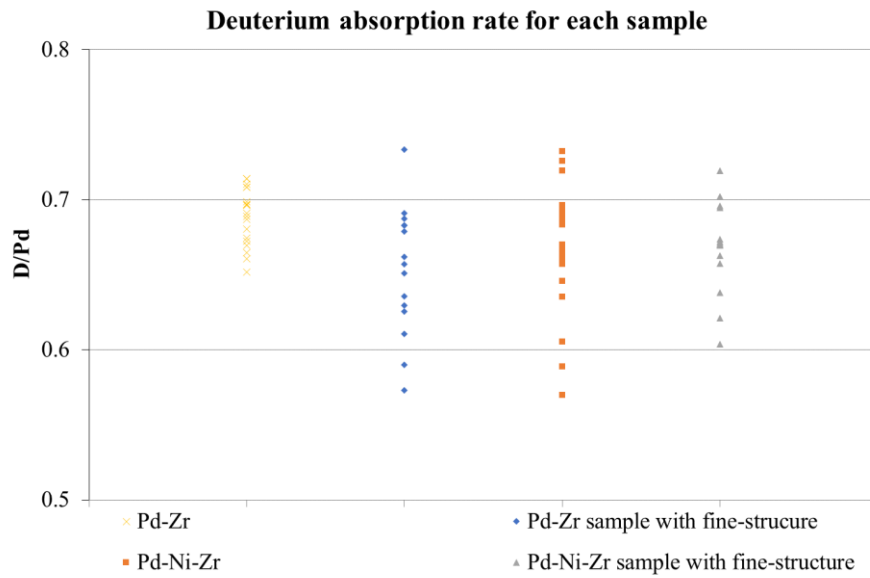


Fig. 4. Deuterium loading ratio(D/Pd) for each sample

### Deuterium desorption

In the desorption experiment, the sample was set into the chamber which has a cylindrical shape with volume of 880 cm<sup>3</sup> equipped with a turbo-molecular pump to be evacuated ( $\sim 10^{-4}$ Pa). the pressure in the chamber was measured by an ionization vacuum gauge. A DC power supplier supplied constant current to the sample through chrome clips in the chamber to stimulate deuterium out-diffusion from the sample. The sample temperature was measured by a thermocouple with an accuracy of  $\pm 1$  °C. The experimental apparatus is shown in Fig. 5.

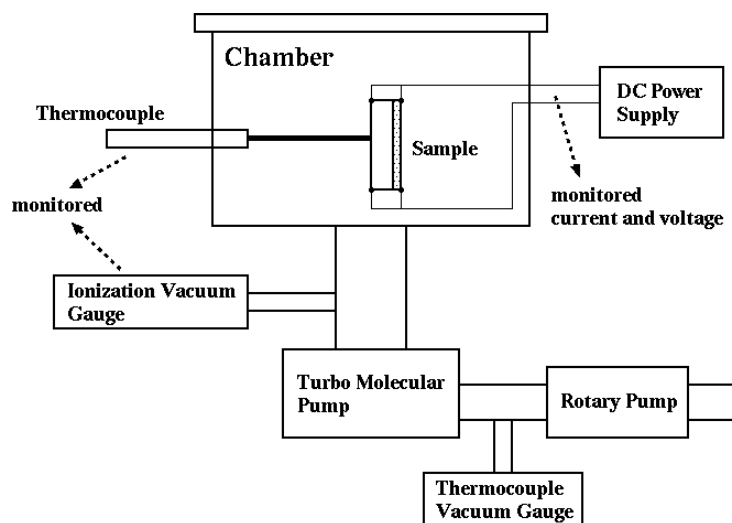
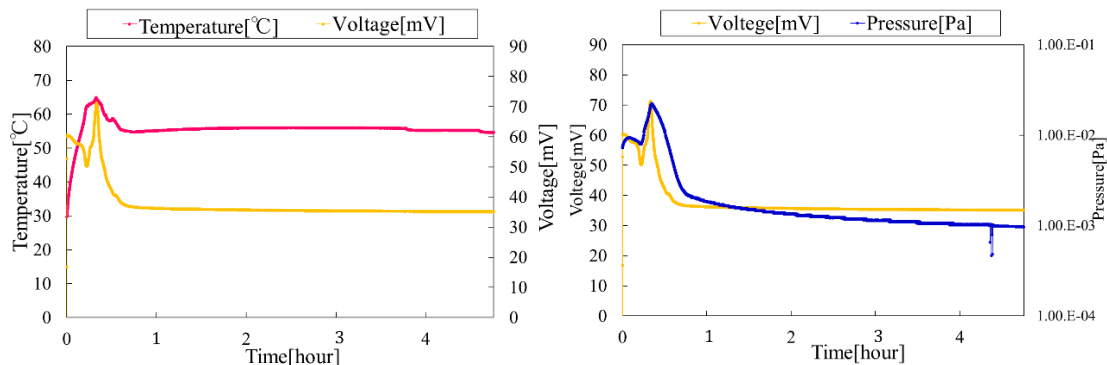


Fig. 5. Experimental apparatus

### 3. Results and Discussion

The thermal behaviors in deuterium diffusion for the Pd–Zr and Pd–Ni–Zr samples have been reported in Ref [4, 5]. Here, the distinctive results are reviewed and further discussed.



**Fig. 6.** Temperature and applied voltage vs. time (left) and applied voltage and chamber pressure vs. time (right) for Pd–Zr sample without fine structure

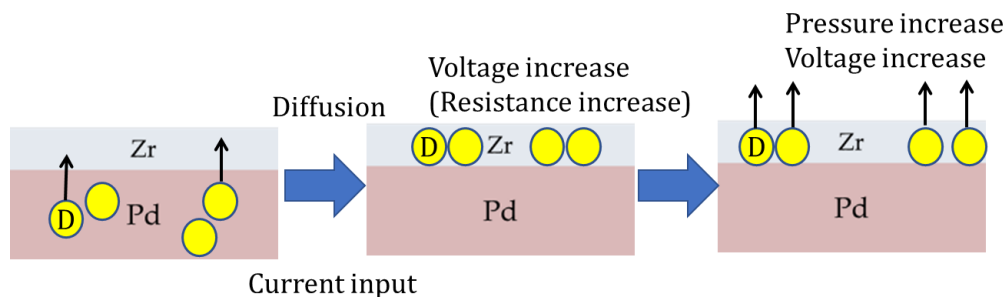


**Fig. 7.** Schematic view of deuterium diffusion/desorption in the Pd–Zr sample

In the Pd–Zr sample without a fine-structured interface, a simultaneous increase in the temperature and the voltage was observed, as shown in Fig. 6. This behavior was observed in 11 out of 13 runs. This temperature increase is regarded as the result of Joule heating caused by the increase in the voltage. Because the DC is constant for the Zr membrane side of the sample, the applied voltage depends on the resistance of the Zr membrane — that is, the deuterium content of the Zr membrane. Moreover, the correlation between the change in voltage and the change in pressure was observed simultaneously, as shown in Fig. 6 (right). The following scenario is a possible explanation for this behavior. After a DC was applied to the sample, the sample temperature increased, and deuterium diffused in the sample. Subsequently, the deuterium was stored in the Zr membrane, and the electric resistance of the Zr membrane increased according to the increase of the applied voltage. Once the deuterium density in the membrane reached a certain level, the deuterium was desorbed, resulting in an increase in pressure and decrease in voltage. A schematic view for this scenario of deuterium diffusion is shown in Fig. 7.

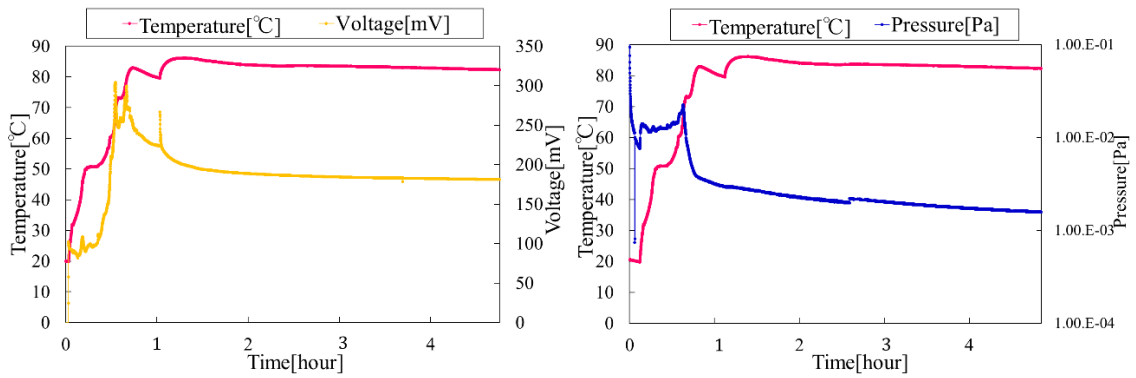


**Fig. 8.** Temperature and applied voltage vs. time (left) and applied voltage and chamber pressure vs. time (right) for Pd-Zr sample with a fine structure

A similar behavior to that of the Pd-Zr sample was observed for the Pd-Zr with a fine-structured interface in 8 out of 10 runs. Among them, an increase of temperature and voltage was observed several times in 4 out of 10 runs, as shown in Fig. 8. This phenomenon is regarded as the result of deuterium diffusion occurring from Pd to Zr, where deuterium is desorbed intermittently.

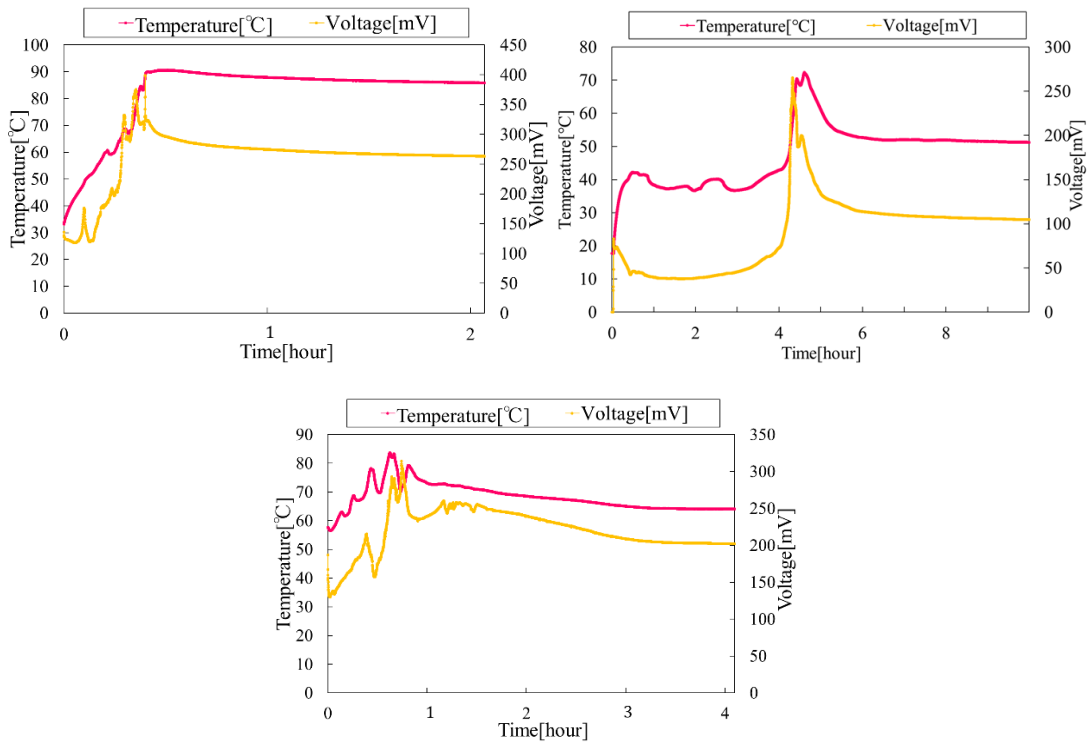


**Fig. 9.** Temperature and applied voltage vs. time for Pd-Zr-Ni sample without a fine structure

A simultaneous increase of the temperature and voltage was observed in 16 out of 18 runs for the Pd–Ni–Zr sample without a fine structure, although the variation patterns differed in each run, as shown in Fig.9. If these phenomena are the result of a specific deuterium diffusion, such as that shown in Fig. 7, it indicates that a slight difference in the condition of the membrane structure or the composition of the Pd–Ni–Zr complex can affect the behavior of deuterium diffusion, which results in different thermal behaviors. Note that we have examined different Pd-Ni-Zr samples for each runs.

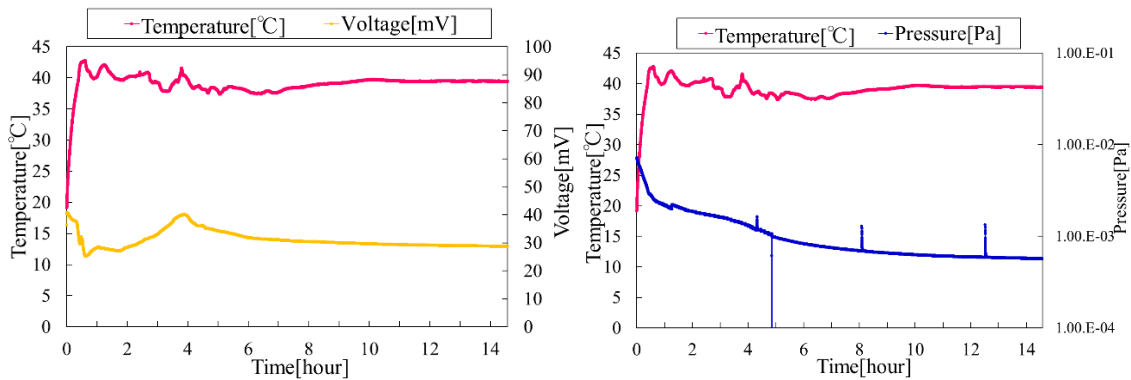


**Fig. 10.** Temperature and applied voltage vs. time (left) and applied voltage and chamber pressure vs. time (right) for Pd-Ni-Zr sample with fine structure

A short period fluctuation in temperature in the range of 1-6 h was observed six times out of 11 runs in the Pd–Ni–Zr sample with a fine structure. However, a significant variation of the pressure inside the chamber was not observed during the continuous temperature fluctuation, which suggests that a significant quantity of deuterium atoms was not desorbed from the sample. It is possible that deuterium diffusion from Pd to Zr and from Zr to Pd occurred alternately in this period resulting in occurring the endothermic and exothermic phenomena associated with the heat of the solution. Similar temperature behavior has been observed for the Pd–Ni sample with a fine-structured interface [3]. Because this temperature behavior was observed frequently in the sample with a fine structure between Pd and Ni, such an interface structure may promote deuterium diffusion in the region.

### Thermal estimation

Here, the heat balance for the observed temperature increase is evaluated quantitatively. The following quantities are defined.

$J$ : Heat derived from the observed temperature increase,  $mC\Delta T$

$m$ : weight of Pd foil,  $C$ : the specific heat of Pd

$J_1$ : Joule heating due to fluctuation of the electric power applied

$J_2$ : Heat by deuterium dissolution into Pd

$J_3$ : Heat of the solution/dissolution associated with deuterium diffusion from Pd into Ni layer, from Ni to Zr and other processes including nuclear reaction.

$J$  can be written as

$$J = mC\Delta T = J_1 + J_2 + J_3 \quad (1)$$

where  $m$  is the weight of Pd foil, and  $C$  is the specific heat of Pd.  $J_1$  can be estimated by the relationship between the change of the input power and the sample temperature. A calibration test was performed to obtain it in advance.  $J_2$  can be calculated by the amount of deuterium desorbed simultaneously with the temperature increase, which can be obtained by the change of the pressure monitored. In this calculation, it was assumed that deuterium desorbs from either of the surfaces — that is, the Pd side or Zr side. Then, one can derive  $J_3$ .

Figures 11 to 16 show  $J_3$  obtained from the results for Pd–Ni–Zr without a fine structure assuming deuterium desorbs from Pd side or Zr side.  $J_3$  was found to be between  $-1$  J and  $+1$  J. These are not significant to prove the anomaly in the thermal behavior. Figures 17 to 20 show  $J_3$  for Pd–Ni–Zr with a fine structure. For those samples also, anomalously large heat evolution was not found.

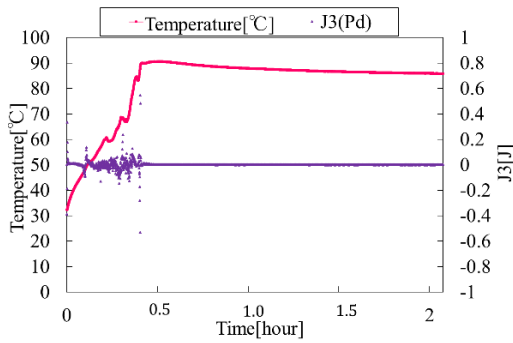


**Fig. 11.** Heat balance,  $J_3$ , assuming that deuterium desorbs from Pd side for Pd–Ni–Zr sample without fine structure (a)

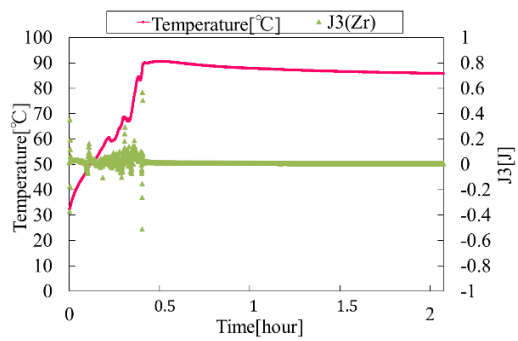


**Fig. 12.** Heat balance,  $J_3$ , assuming that deuterium desorbs from Zr side for Pd–Ni–Zr sample without fine structure (a)

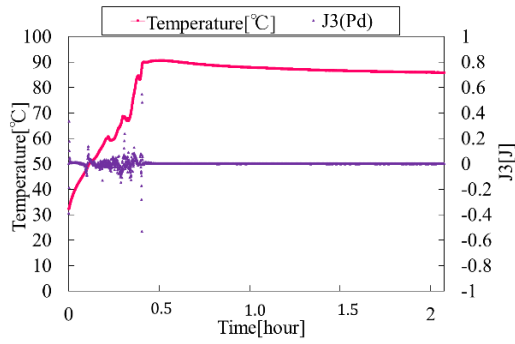


**Fig. 13.** Heat balance,  $J_3$ , assuming that deuterium desorbs from Pd side for Pd-Ni-Zr sample without fine structure (b)

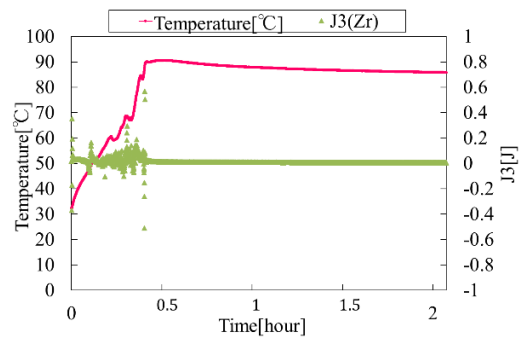


**Fig. 14.** Heat balance,  $J_3$ , assuming that deuterium desorbs from Zr side for Pd-Ni-Zr sample without fine structure (b)

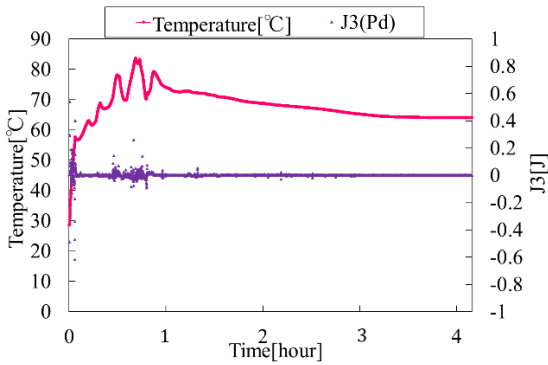


**Fig. 15.** Heat balance,  $J_3$ , assuming that deuterium desorbs from Pd side for Pd-Ni-Zr sample without fine structure (c)

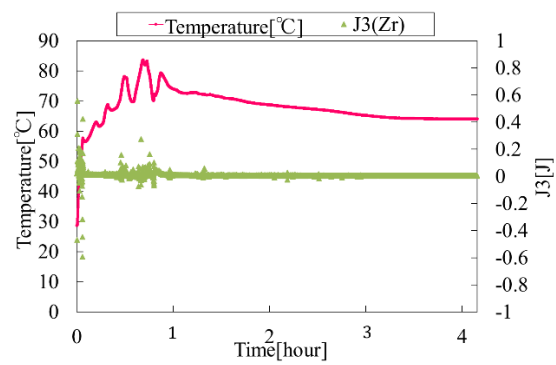


**Fig. 16.** Heat balance,  $J_3$ , assuming that deuterium desorbs from Zr side for Pd-Ni-Zr sample without fine structure (c)

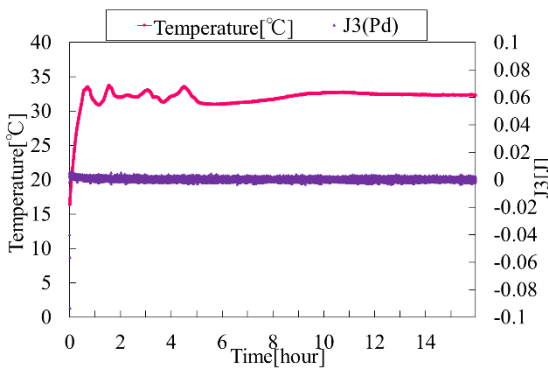


**Fig. 17.** Heat balance,  $J_3$ , assuming that deuterium desorbs from Pd side for Pd-Ni-Zr sample with fine structure (a)

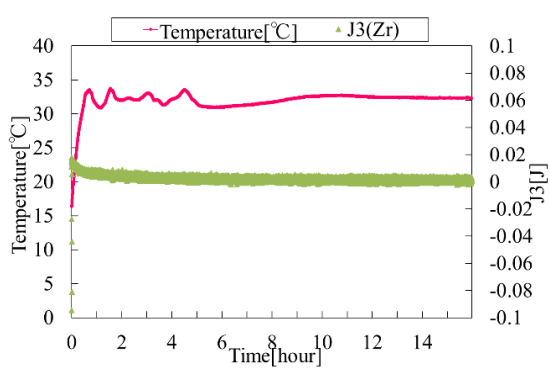


**Fig. 18.** Heat balance,  $J_3$ , assuming that deuterium desorbs from Zr side for Pd-Ni-Zr sample with fine structure (a)

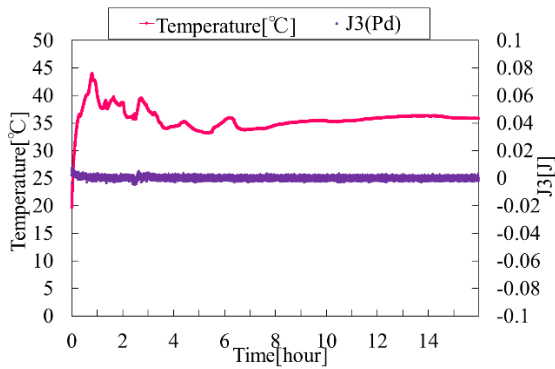


**Fig. 19.** Heat balance,  $J_3$ , assuming that deuterium desorbs from Pd side for Pd–Ni–Zr sample with fine structure (b)

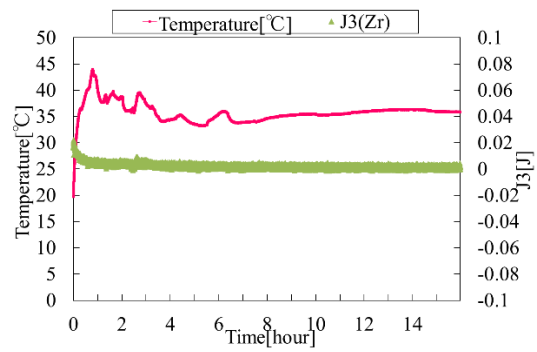
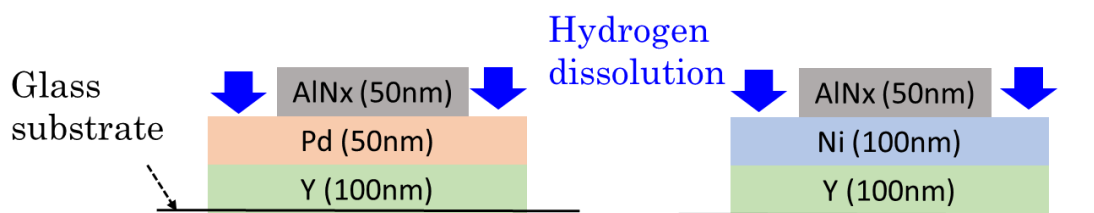


**Fig. 20.** Heat balance  $J_3$ , assuming that deuterium desorbs from Zr side for Pd–Ni–Zr sample with fine structure (b)

$J_3$  is approximately  $-0.1$  to  $0.1$  [J] at most, which is thought to be the result of measurement error and heat of dissolution at the interface. Therefore, no significant excessive heat was confirmed in this experiment.

### Hydrogen diffuse experiment

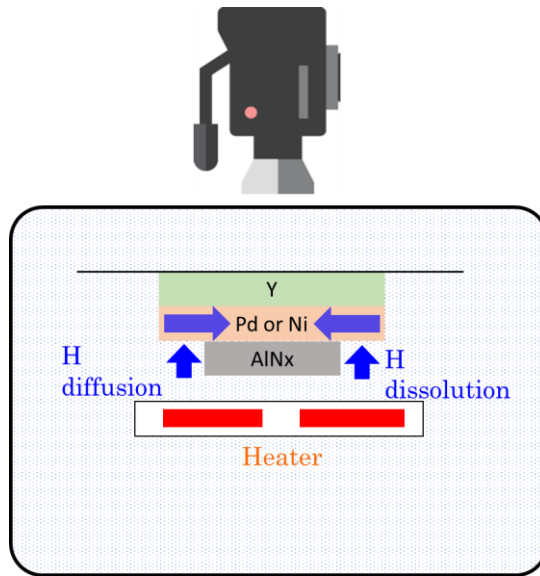
Although the anomaly in the origin of the heat evolution in the deuterium process was not clearly confirmed, it is still interesting to investigate the hydrogen diffusion characteristics in thin metal membrane. In the experiment, Pd or Ni membrane was deposited onto Y (yttrium) membrane (100 nm thickness). Then, aluminum nitride (AlN<sub>x</sub>) membrane (50 nm thickness) was deposited onto part of the Pd or Ni surface, as shown in Fig. 21.



**Fig. 21.** Samples used for hydrogen diffusion experiment (sectional view)

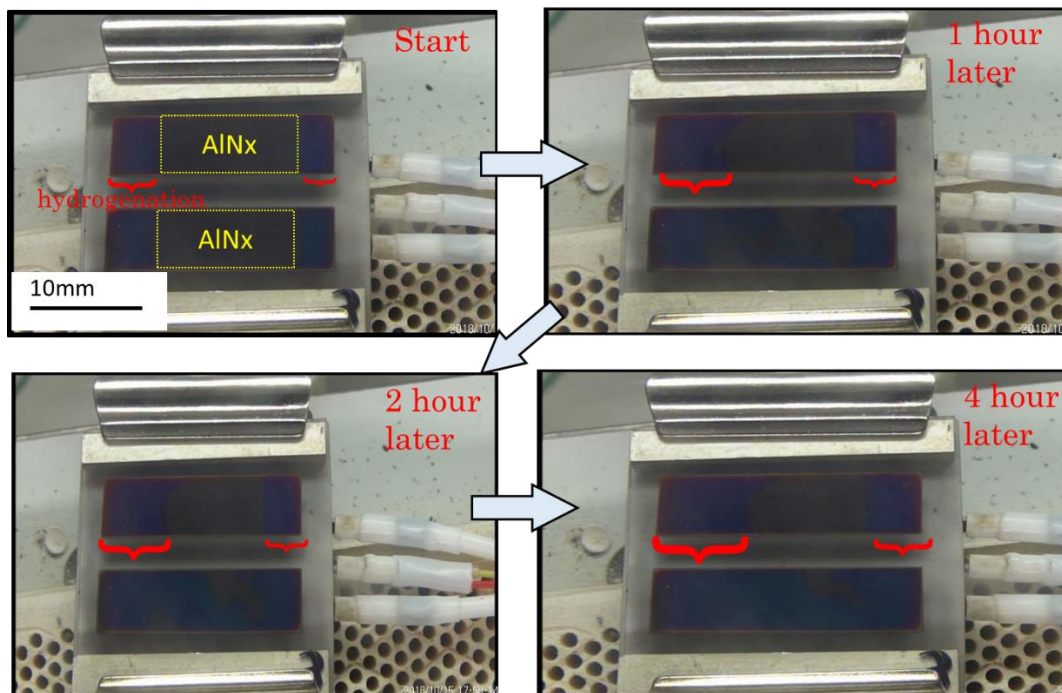
AlN<sub>x</sub> does not absorb hydrogen, so hydrogen dissolves into the Pd or Ni membrane from the area where is not covered by AlN<sub>x</sub> and diffuses horizontally. Because the light transmittance of Y depends on the hydrogen concentration, hydrogen diffusion behavior can be observed by the camera to record the change of the shading area of Y.

Figure 22 is a schematic diagram of the experimental apparatus. In this experiment, the sample was heated to 70 °C to promote the hydrogen diffusion.



**Fig. 22.** Observation of hydrogen diffusion

Figures 23 and 24 show the time dependence of the picture of the Y surface for the Pd and Ni membranes, respectively. The thickness of the Pd membrane was 50 nm, and that of the Ni was 100 nm for the present experiment, and various conditions are still being investigated.



**Fig. 23.** Experimental result on Y-Pd(50 nm)-AlN<sub>x</sub> sample

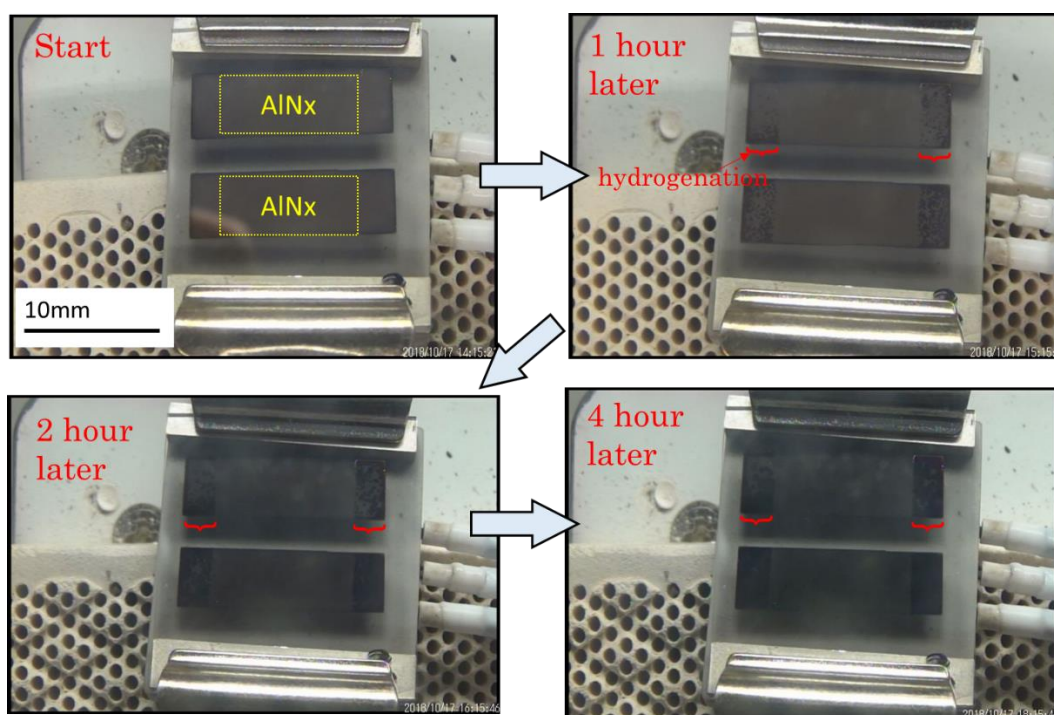


**Fig. 24.** Experimental result on Y–Ni(100 nm)–AlN<sub>x</sub> sample

From the time evolution of the hydrogenated area of Y, the diffusion coefficient of the Pd membrane was calculated, and it was found to be  $3.8 \times 10^{-10} \text{ m}^2/\text{s}$  at 343 K. It was larger than that reported elsewhere [6],  $1.2 \times 10^{-10} \text{ m}^2/\text{s}$  at 343 K. This difference may be primarily caused by the characteristics of the thin membrane.

For the Ni membrane, the diffusion coefficient was found to be  $<6.4 \times 10^{-14} \text{ m}^2/\text{s}$ . Measurement of the hydrogen diffusion coefficient for a multi-layered metal complex is planned to clarify the process observed in the deuterium diffusion experiment.

#### 4. Summary

Deuterium absorption/desorption experiments were conducted using various types of Pd-based metal complex samples. Unique temperature behavior was observed in the deuterium diffusion process for Pd–Zr and Pd–Ni–Zr samples. The combination of Pd and Zr may promote diffusion from Pd to Zr, and the deuterium may be densified in Zr and desorbed. The heat balance by the possible process during the desorption experiment was estimated, and significant heat evolution was not found, which may suggest the occurrence of a nuclear phenomenon. An attempt has begun to measure the hydrogen diffusion coefficient in a metal membrane in order to understand the deuterium diffusion behavior in Pd-based complexes that contain the metal membrane. The value for a Pd

membrane was preliminarily obtained, and it was  $3.8 \times 10^{-10}$  m<sup>2</sup>/s and much larger than that measured for a bulk Pd. This prompt diffusion behavior in a membrane may be related to a unique property in multi-metal systems, such as the sample used in the desorption experiment. Further measurement is planned with various metals and multi-layered membranes.

## Reference

- [1] A. Kitamura, A. Takahashi, R. Seto, Y. Fujita, A. Taniike and Y. Furuyama, “Comparison of some Ni-based nano-composite samples with respect to excess heat evolution under exposure to hydrogen isotope gases,” Proc of JCF15 (2015) 1.
- [2] A. Kitamura, E. F. Marano, A. Takahashi, R. Seto, T. Yokose, A. Taniike, and Y. Furuyama, “Heat evolution from zirconia-supported Ni-based nanocomposite samples under exposure to hydrogen isotope gas,” Proc of JCF16 (2016) 1.
- [3] S. Kataoka, H. Kudou, K. Ota, and S. Narita, “Deuterium desorption experiments using multi-layered metal samples with fine-structured surface,” Proc of JCF16 (2016) 29.
- [4] S. Narita, K. Kataoka, Y. Sato, K. Negishi, K. Ota, “Characterization of deuterium in multilayered metal samples,” Proc. of JCF17 (2017) 28.
- [5] Y. Sato, K. Ota, K. Negishi, S. Narita, “Deuterium desorption experiments using Pd-Zr and Pd-Ni-Zr multi-layered samples,” Proc of JCF18 (2017) 1.
- [6] Y. Fukai, K. Nakata, Y. Utida, “Suiso-to-Kinzoku” (1998) (in Japanese), “Utidaroukakuho,” 29.

# Search for Nuclear Reaction in Deuterium Discharge Experiment Using Pd/PdO Cathode

S.Kikuchi\*, T.Nejo, Y.Sato, K.Ota, M.Takahashi, S.Narita, K.Negishi

Iwate University  
Morioka, Iwate, 020-8551, Japan  
\*g0318055@iwate-u.ac.jp

## ABSTRACT

To study the occurrence of a low-energy nuclear reaction, we conducted deuterium discharge experiment using a Pd/PdO sample as a cathode. In the experiment, we investigated the sample with and without etching the interface between the Pd layer and PdO layer to observe the effect of the nanostructure for inducing nuclear reaction. The surfaces of the samples post-experiments were analyzed by TOF-SIMS, and nuclear reaction products were searched. Consequently, signals of mass numbers 51 and 55, which cannot be identified as contaminating impurities, were observed for the sample with a fine-structured interface.

## 1. Introduction

We observed possible nuclear products, which suggest occurrence of a low-energy nuclear reaction, in deuterium discharge using a Pd-based metal complex cathode [1-3]. Lipson et al. observed charged particle emission in the deuterium discharge using a Pd/PdO cathode [4]. In addition, it has been reported that anomalous heat evolution is observed in deuterium desorption experiments with nanoparticles of binary or ternary metal complex [5]. These phenomena could be attributed to specific properties of metal complex materials along with the fine structure of the sample. Considering these results of experiments, we tested the Pd/PdO sample with a fine-structured interface as a cathode in deuterium discharge and searched for nuclear products on the sample surface.

## 2. Experiment

We prepared the Pd/PdO sample using the following procedure. On the Pd substrate, nanostructures were formed by Ar<sup>+</sup> beam sputtering at an RF power of 20 W and Ar gas pressure of 0.5 Pa, and subsequently, an oxide film was formed on the surface by annealing at 800 °C in air.

To study the effect of the fine structure of a sample for inducing a condensed matter nuclear reaction, we also prepared a sample with the surface etched by an Ar<sup>+</sup> beam. Figure 1 shows the surface morphology before and after etching using atomic force microscopy (AFM) analysis. The etched surface has a projected shape with a width of approximately 2 μm and a height of 200 nm. Figure 2 shows a comprehensive observation of the above sample by TEM and an observed shape with a height of 50–200 nm.

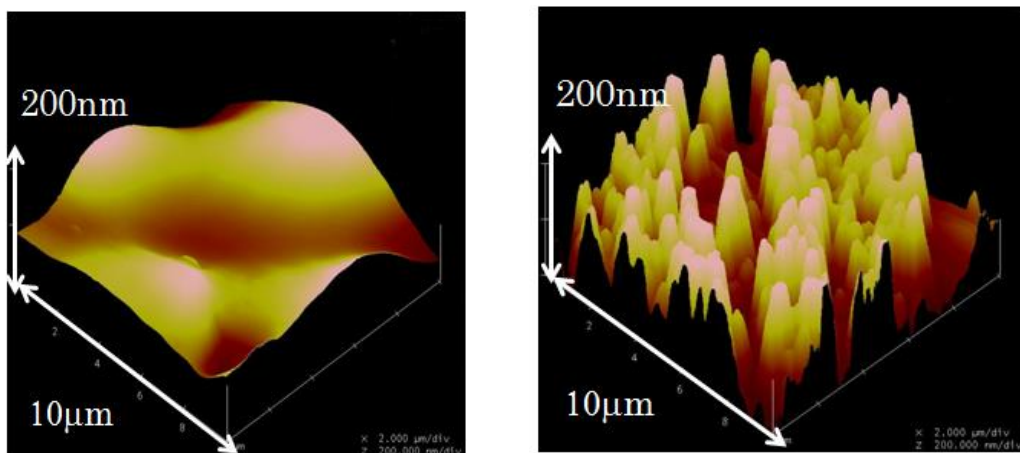


Fig.1 Surface morphology before (left) and after (right) etching, observed by AFM

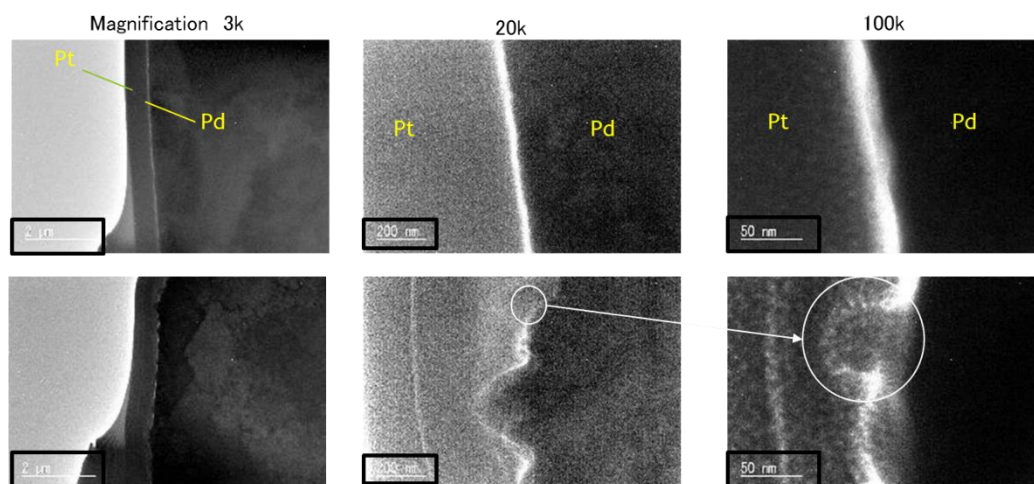


Fig.2 Surface morphology before (top) and after (bottom) etching, observed by TEM

Figure 3 shows the experimental apparatus. The fabricated sample was put into the discharge cell as the cathode. A stainless anode was used, and the gap between the electrodes was set at a distance of  $\sim 10$  mm. After evacuating the cell to  $<10^{-2}$  Torr, the deuterium gas was supplied until the inside pressure reached 1000 Pa. Then, DC voltage was applied to expose the Pd/PdO sample to discharge, which typically required a voltage and current of  $\sim 400$  V and  $\sim 2$  mA, respectively. The discharge experiment was performed for 3 h. Figure 4 shows the typical time dependence of the monitored voltage and current. During the experiment, the applied voltage was continuously adjusted to sustain the discharge.

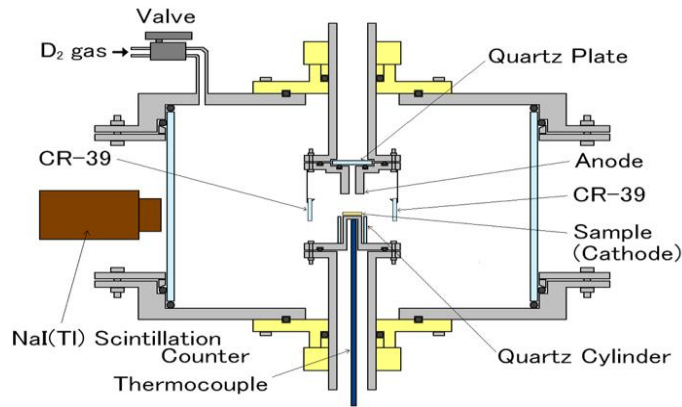


Fig.3 Experimental equipment

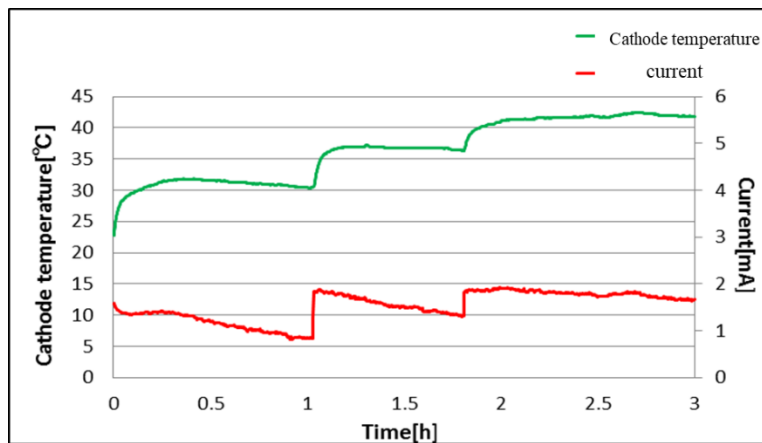


Fig.4 Typical current-temperature results

During the discharge experiment, measurements of cathode temperature using thermocouple, charged particles using CR-39, and  $\gamma$ -ray using an NaI scintillation counter were also performed. We conducted 10 runs for each sample with and without the fine structure. Following the discharge, the element composition of the cathode was analyzed by TOF-SIMS, and we searched for newly produced elements as well as anomalies in isotopic abundance for the detected elements. We analyzed the surface area on each spot as well as a considerably deeper region within the same spot where contaminants were removed by sputtering with a DC  $\text{Bi}^+$  beam for 30 s (namely, sputter cleaning process). To evaluate the effect of environmental contaminants, we prepared a control sample that was exposed to the discharge in nitrogen atmosphere.

### 3. Results and discussion

#### Pd/PdO fine-structured interface

We surveyed the mass spectrum obtained by TOF-SIMS analysis and identified the signal with significantly larger intensity compared to the spectrum for the reference sample. Figure 5 shows the mass number and intensity of the signal found for the Pd/PdO with a fine-structured interface. The red plots indicate the results for the sample exposed to the deuterium discharge, and the blue plots indicate the results for the reference sample. Table 1 shows the number of runs out of 10 runs, wherein each signal of mass was observed. The corresponding elements are also shown. Among them, signals of mass numbers 39 and 41 were, in particular, frequently detected. Figures 6 and 7 show the spectra of mass numbers around 39 and 41.

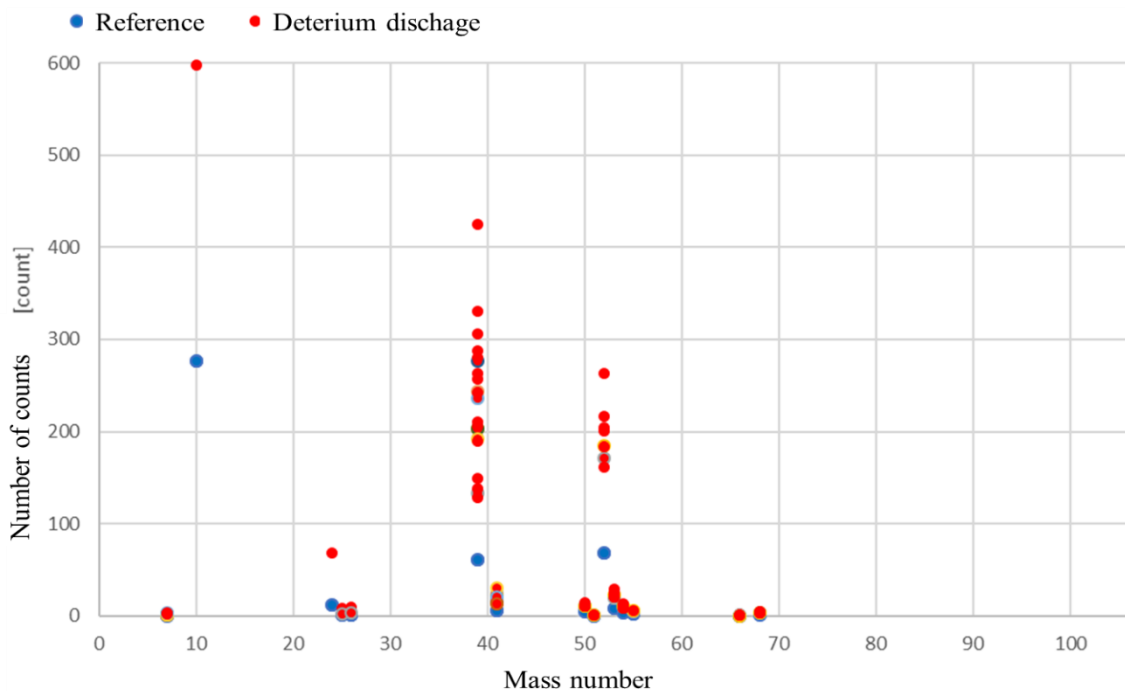


Fig.5 Mass number and intensity of signals observed by TOF-SIMS

Table.1 Mass number and the number of detections out of 10 runs

Mass number (corresponding elements)	Number of detections out of 10 runs
7 (Li)	7
10 (B)	1
24 (Mg)	1
25 (Mg)	2
26 (Mg)	2
39 (K)	8
41 (K)	8
50 (Cr, Ti V)	5
51 (V)	5
52 (Cr)	4
53 (Cr)	4
54 (Cr, Fe)	4
55 (Mn)	2
66 (Zn)	3
68 (Zn)	4

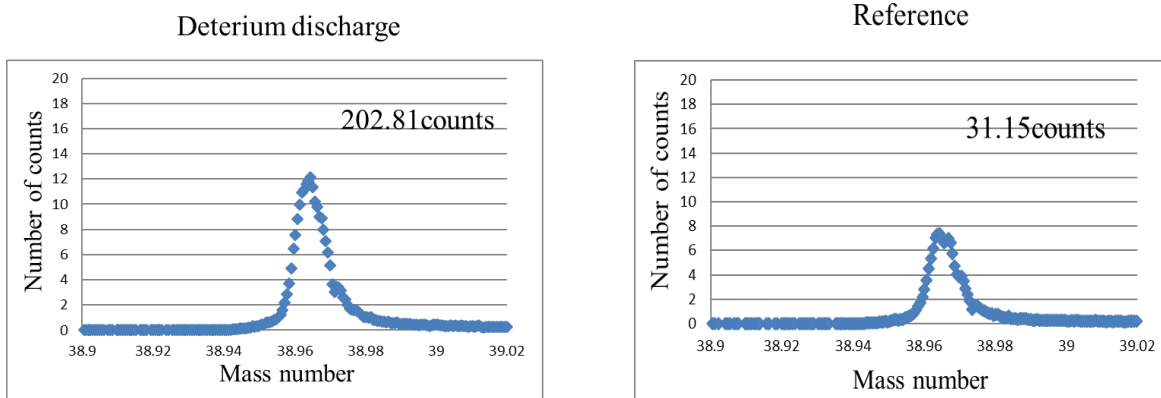


Fig.6 Spectrum of mass number around 39 for the sample for deuterium discharge (left) and reference sample (right)

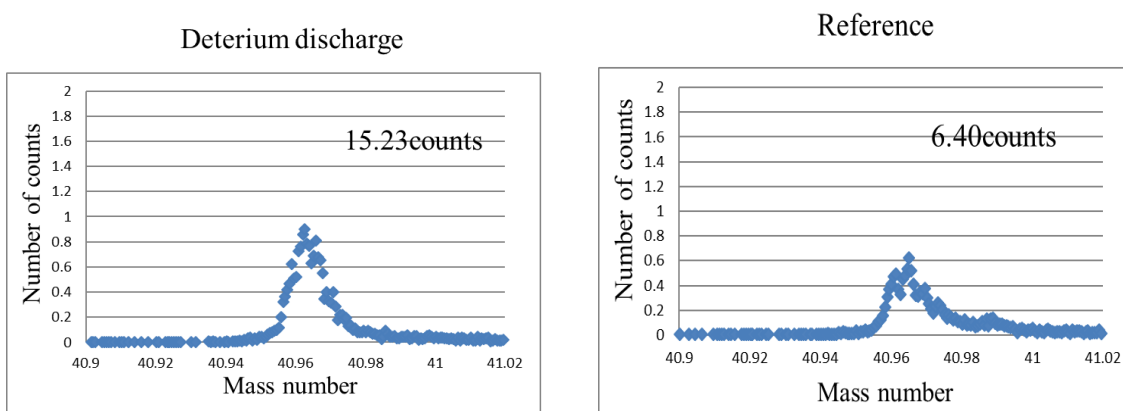


Fig.7 Spectrum of mass number around 41 for the sample for deuterium discharge (left) and reference sample (right)

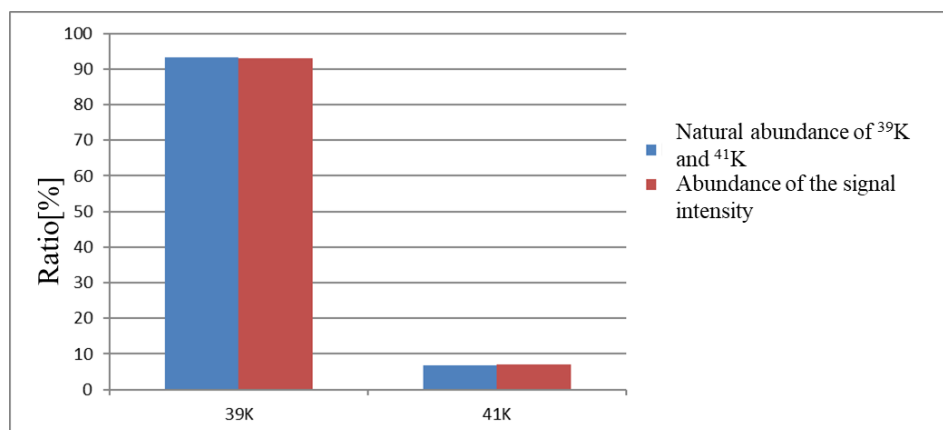


Fig.8 Abundance of the signal intensity of mass numbers 39 and 41 (in red). The natural abundance of  $^{39}\text{K}$  and  $^{41}\text{K}$  are also shown (in blue)

Significant signals were observed at mass numbers 39 and 41 in comparison to the reference sample. To examine if these signals were incidentally contaminated from the environment, we investigated the abundance of these signals assuming they are caused by potassium isotopes. Figure 8 shows the abundance of the signal intensity of mass numbers 39 and 41 compared to the natural abundance of  $^{39}\text{K}$  and  $^{41}\text{K}$ , and they conformed well. Thus, it can be assumed that the signal on these masses were not nuclear products. For other signals detected, the ratio of intensity was compared with the natural abundance of the corresponding isotopes. We found conformance between them except for the signals at mass numbers 50, 51, and 55. Figures 9 and 10 show the spectra of mass numbers around 50 and 51, respectively.

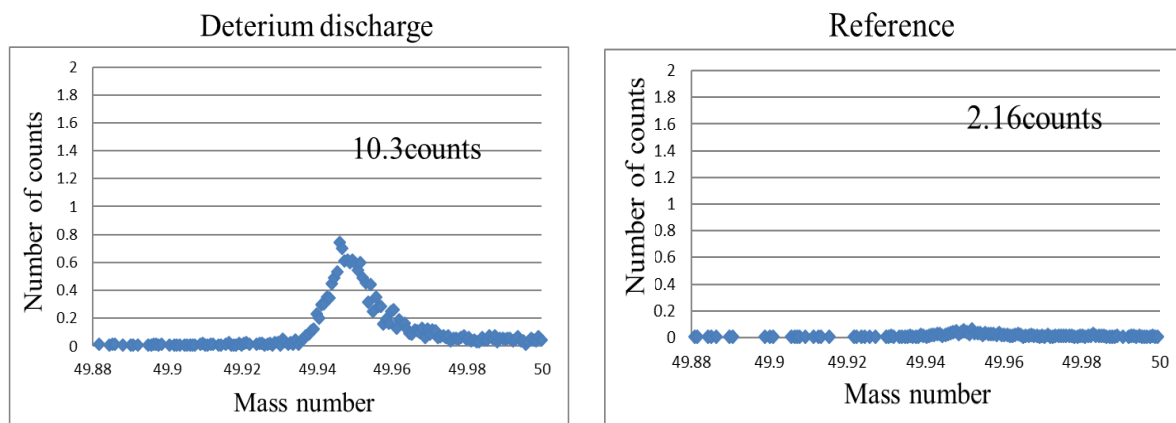


Fig.9 Spectrum of mass number around 50 for the sample for deuterium discharge (left) and reference sample (right)

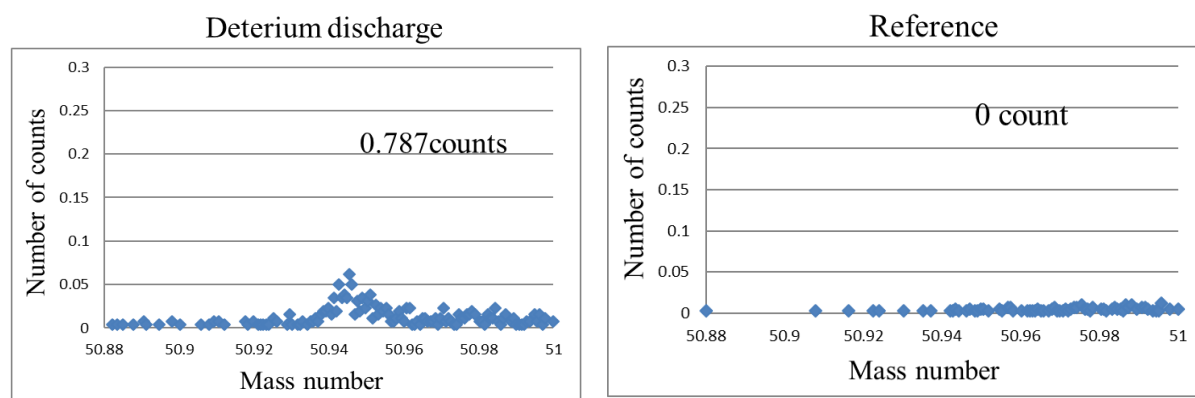


Fig.10 Spectrum of mass number around 51 for the sample for deuterium discharge (left) and reference sample (right)

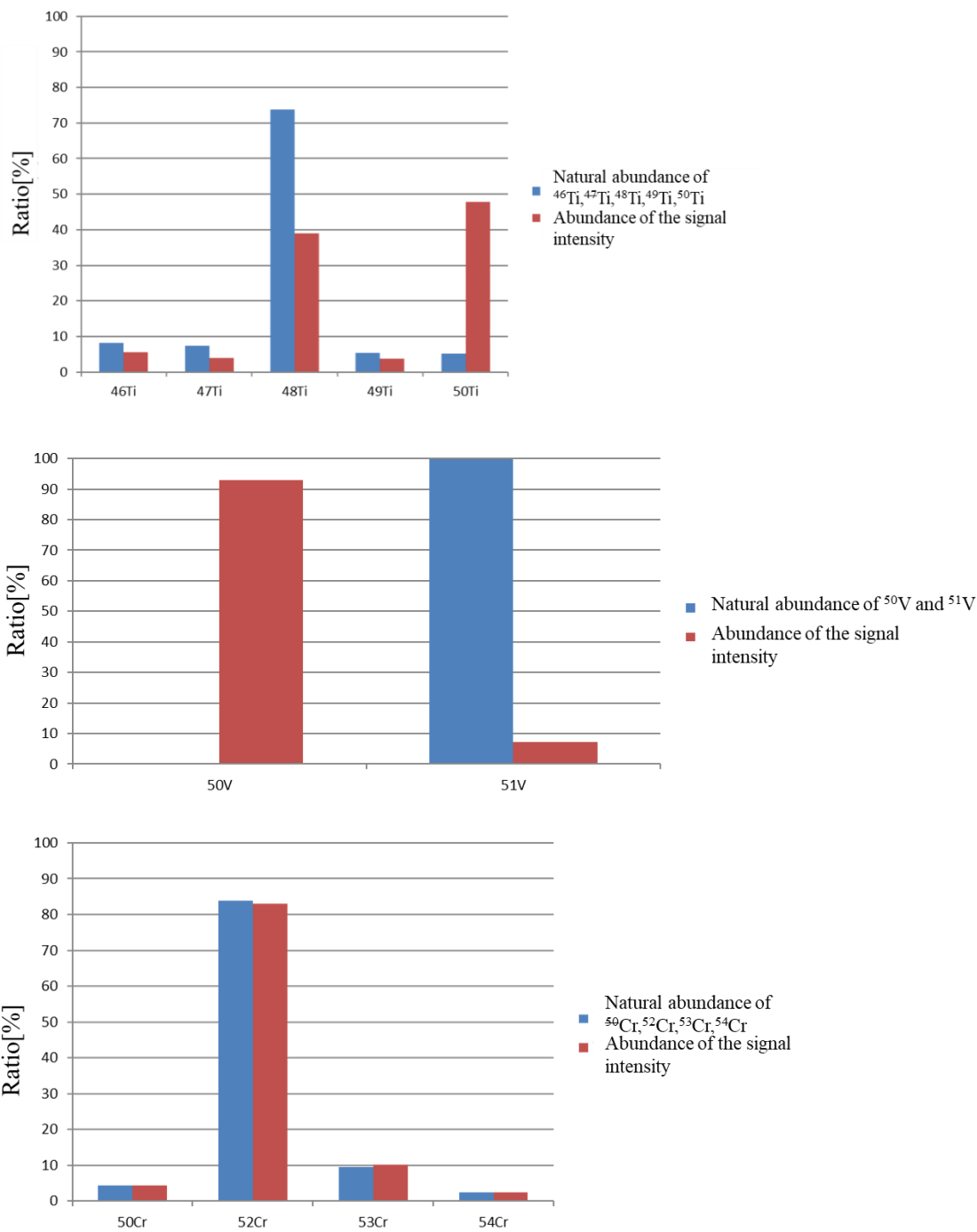


Fig.11 Comparison of the abundance of signal intensity and natural abundance for Ti (top), V (middle), Cr (bottom)

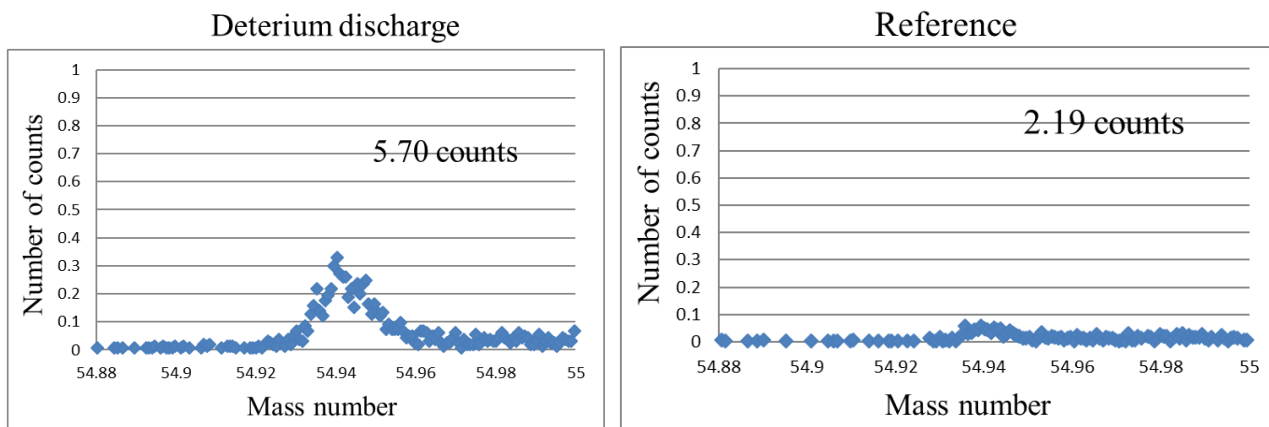


Fig.12 Spectrum of mass number around 55 for the sample for deuterium discharge (left) and reference sample (right)

It is possible that the signal of mass number 50 corresponds to Ti, Cr, or V isotopes, and the signal of mass number 51 corresponds to V. Then, we compared the abundance of the intensity of the signal found with the natural abundance of each element as shown in Fig. 11. The abundance of the signal intensity of masses 50, 52, 53, and 54 is consistent with that of natural abundance for Cr isotopes. Therefore, the signal of mass number 50 should be from Cr contaminants, and possibly this signal may be unexpectedly observed with lowered intensity. If this signal is due to  $^{50}\text{Cr}$ , we cannot identify the origin of the signal of mass number 51 from the abundance of masses 50 and 51 compared to the natural abundance of V because the natural abundance of  $^{50}\text{V}$  is much smaller than that of  $^{51}\text{V}$ .

We found that the signal of mass number 55 for the sample in the discharge experiment is significantly larger than that of the reference sample as shown in Fig. 12. Mn is the only corresponding stable isotope, and we are unable to identify the signal because of the presence of contaminants by the natural abundance. Thus, Mn is one more candidate that can be considered as a nuclear product.

### **$\gamma$ - ray measurement and charged particle measurement result**

In these experiments, we measured  $\gamma$ -ray measurements. Figure 13 shows the mass spectrum for the experiment in which signals with mass numbers 51 and 55 were obtained. The spectrum for the reference run is also plotted. It indicates that there was no significant difference from the reference experiment, and no result suggesting nuclear reaction was obtained. In addition, charged particle emission by CR-39 was not confirmed.

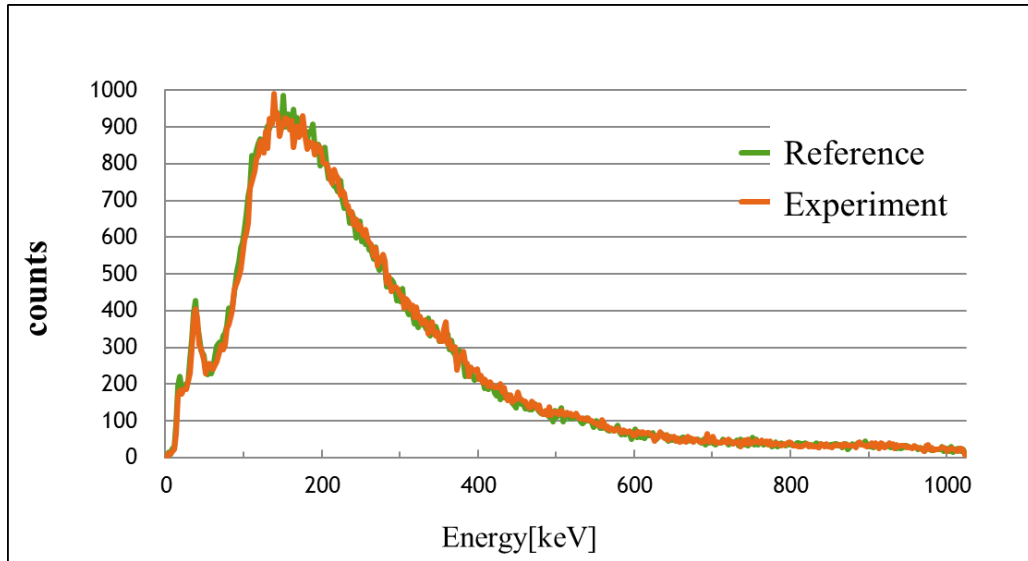


Fig.13  $\gamma$ -ray measurement result

Table. 2 Mass number and the number of detections out of 10 runs

Mass number (corresponding elements)	Number of detections out of 10 runs
6 (Li)	5
7 (Li)	5
27 (Al)	7
39 (K)	6
41 (K)	4

### **Pd/PdO without fine-structured interface**

Table 2 shows the corresponding element of mass and the number of runs performed in 10 runs, in which each signal of mass was observed. Analysis of the signal obtained by TOF-SIMS was conducted in a similar manner to the Pd/PdO samples with fine-structured interface, that is, the abundance of these signals was investigated assuming they were caused by corresponding isotopes. Consequently, results suggesting the possibility of a nuclear reaction product were not obtained. In addition, we did not observe signals for  $\gamma$ -ray or charged particle emission.

#### 4. Summary

In this study, deuterium aerial discharge experiments were conducted on Pd/PdO samples with a fine-structured interface, and thereafter elemental analysis was performed on the surface of the sample, and the nuclear reaction was examined. Consequently, signals of mass numbers 51 and 55 that cannot be determined as contaminating impurities were observed as those that were fine-structured. In samples without microstructures, possible signals of nuclear reaction products were not observed. It might be possible that the fine structure of the sample surface enhanced the efficiency of inducing a nuclear reaction. Further systematic study to verify the phenomena and test different metal complex sample may lead us to understand the effects and the mechanism of the reaction.

#### Reference

- [1] S. Narita et al., Proc. of ICCF, 12 (2006) 188.
- [2] S. Narita et al., Proc. of JCF, 6 (2005) 43.
- [3] H. Ougida et al., Proc. of JCF, 11 (2011) 23.
- [4] A. G. Lipson et al., Proc. of ICCF, 12 (2005) 26.
- [5] A. Kitamura et al., Proc. of JCF, 16 (2016) 1.

# A theoretical study on the possible change of the phonon dispersion relation due to the nuclear reaction in two-dimensional lattice

Ken-ichi TSUCHIYA

*Department of Chemical Science and Engineering,  
National Institute of Technology, Tokyo College,  
1220-2 Kunugida, Hachioji, Tokyo 193-0997, Japan*

E-mail: tsuchiya@tokyo-ct.ac.jp

## Abstract

In this study, we tried to show the method how to find the change of phonon dispersion relation due to the nuclear reaction in solid. In our previous works, we considered the change of phonon dispersion relations due to the nuclear reaction by assuming ions and impurities arranged in one dimension. In those studies, we considered the changes of crystal structure due to the nuclear reactions, and estimated their effects to the phonon dispersion relations. However, in one-dimensional lattices, it is unlikely that a collision of two impurities will happen, a host ion exists between two impurities. In this study, we used two-dimensional models and estimated the nuclear reactions in solids. If some impurity ions get closer through the lattice gaps and nuclear reactions occur, the structures of the crystal will change and it makes changes of phonon dispersion relations.

(**keywords;** phonon dispersion relations, nuclear reaction in solids )

## 1 Introduction

Many studies on the nuclear reactions in solids have been done since Fleischmann and Pons [1]. In order to detect them, we should detect gamma ray, heat generation, neutron, helium, and so on. In our study, we introduce new method to find nuclear reaction in solids. If nuclear reactions happen in solids, the crystal structures of the solids are changed because the number of the impurity ions are changed due to the reactions, which affect the phonon dispersion relations. Therefore, we can detect nuclear reactions in solids through the observation of phonon dispersion relations.

This study shows the first step for theoretical approach. In Sec.2, we show brief explanation on the basic formulas for lattice vibrations. In Secs.3 and 4, we show some examples by using two-dimensional cubic lattice. In our previous work on these studies, one-dimensional lattice was used as the simplest model [2]. However, one-dimensional model is not easy to understand the nuclear collision between an impurity trapped in a cell and another impurity included in the neighborhood cell. We used two-dimensional model with a natural structure to happen nuclear collisions moving through the gaps in the lattice.

## 2 Basic formulas for lattice vibrations

If we define  $\mathbf{u}_{nm}$  as a displacement vector of the ion whose equilibrium position is the  $m$ -th lattice point in the  $n$ -th cell and denote  $j$  component of the vector by  $u_{nm}^j$ , Lagrangian  $L$  satisfies

$$\frac{d}{dt} \frac{\partial L}{\partial \dot{u}_{nm}^j} = \frac{\partial L}{\partial u_{nm}^j} . \quad (1)$$

The Lagrangian is given by  $K - V$  where  $K$  and  $V$  mean kinetic and potential energy, respectively. The kinetic energy of the system is given by

$$K = \frac{1}{2} \sum_{nmj} M_m (\dot{u}_{nm}^j)^2 , \quad (2)$$

where  $M_m$  means the mass of the  $m$ -th ion in the cell. And the potential energy of the system in the form of Maclaurin expansion is written as

$$V = V_0 + \sum_{nmj} \left[ \frac{\partial V}{\partial u_{nm}^j} \right]_0 u_{nm}^j + \frac{1}{2} \sum_{nmj} \sum_{n'm'j'} \left[ \frac{\partial^2 V}{\partial u_{nm}^j \partial u_{n'm'}^{j'}} \right]_0 u_{nm}^j u_{n'm'}^{j'} + \dots , \quad (3)$$

where  $[ ]_0$  means the value at equilibrium position. Here we can omit the first order terms because  $\left[ \frac{\partial V}{\partial u_{nm}^j} \right]_0$  corresponds to the force acting on the ions in the equilibrium position. Therefore, the potential within the second order approximation is written as

$$V = V_0 + \frac{1}{2} \sum_{nmj} \sum_{n'm'j'} C_{nmn'm'}^{jj'} u_{nm}^j u_{n'm'}^{j'} . \quad (4)$$

Substituting Eq.(2) and Eq.(4) into Eq.(1), we obtain

$$M_m \ddot{u}_{nm}^j = - \sum_{n'm'j'} C_{nmn'm'}^{jj'} u_{n'm'}^{j'} . \quad (5)$$

This is an equation of motion for the ion  $(n, m)$  with a following vibrating solution as

$$u_{nm}^j(t) = e^{-i\omega t} u_{nm}^j(0) , \quad (6)$$

where  $\omega$  means angular frequency. Furthermore, we can reduce the solution with considering symmetry of the lattice. For example, the solution should satisfy Bloch's theorem which is written as

$$u_{nm}^j = e^{i\mathbf{q} \cdot \mathbf{r}_n} u_{0m}^j . \quad (7)$$

And the coefficients in Eq.(5) depend on the relative position vector  $\mathbf{r}_{n'} - \mathbf{r}_n$  between two cells. This is expressed as

$$C_{nmn'm'}^{jj'} = C_{mm'}^{jj'}(\mathbf{h}) \quad (\mathbf{h} = \mathbf{r}_{n'} - \mathbf{r}_n) . \quad (8)$$

Considering those things described above, we obtain the final equation for the lattice with  $M$  ions in a primitive cell which is written as

$$\sum_{m'=1}^M \sum_{j'=1}^3 G_{mm'}^{jj'}(\mathbf{q}) u_{0m'}^{j'}(0) = \omega^2 u_{0m}^j(0) \quad , \quad (9)$$

where the element  $G_{mm'}^{jj'}(\mathbf{q})$  is defined as

$$G_{mm'}^{jj'}(\mathbf{q}) = \sum_{\mathbf{h}} C_{mm'}^{jj'}(\mathbf{h}) e^{i\mathbf{q}\cdot\mathbf{h}} \quad . \quad (10)$$

This means that the final equation can be written by  $3M \times 3M$  type matrix. This is called Dynamical matrix. By solving this eigenvalue problem, we can obtain the relation between  $\omega$  and  $\mathbf{q}$  whose name is phonon dispersion relation.

### 3 Pure lattice

Firstly, we begin to consider one-dimensional monoatomic lattice whose degree of freedom for each ion is three. The eigenvalue problem for this case is written as

$$\begin{pmatrix} G^{11} & G^{12} & G^{13} \\ G^{21} & G^{22} & G^{23} \\ G^{31} & G^{32} & G^{33} \end{pmatrix} \begin{pmatrix} u^1 \\ u^2 \\ u^3 \end{pmatrix} = \omega^2 \begin{pmatrix} u^1 \\ u^2 \\ u^3 \end{pmatrix} \quad . \quad (11)$$

The sketch of phonon dispersion relation estimated from Eq.(11) is shown in Fig.1.

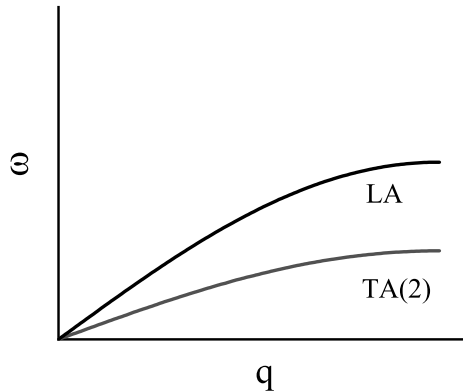


Fig. 1. Phonon dispersion relation of monoatomic one-dimensional lattice. TA(2) and LA mean doubly degenerated transverse and longitudinal acoustic modes, respectively.

In Fig.1, longitudinal mode LA is the wave propagating along the lattice line. And the doubly degenerated transverse modes TA(2) are the wave whose amplitude vec-

tors are orthogonal to the lattice line. If the degree of freedom for each ion is one, transverse modes disappear.

For the case of diatomic one-dimensional lattice moving in the three dimensional space, dynamical matrix becomes  $6 \times 6$  type

$$\begin{pmatrix} G_{11}^{11} & G_{11}^{12} & G_{11}^{13} & G_{12}^{11} & G_{12}^{12} & G_{12}^{13} \\ G_{11}^{21} & G_{11}^{22} & G_{11}^{23} & G_{12}^{21} & G_{12}^{22} & G_{12}^{23} \\ G_{11}^{31} & G_{11}^{32} & G_{11}^{33} & G_{12}^{31} & G_{12}^{32} & G_{12}^{33} \\ G_{21}^{11} & G_{21}^{12} & G_{21}^{13} & G_{33}^{11} & G_{33}^{12} & G_{33}^{13} \\ G_{21}^{21} & G_{21}^{22} & G_{21}^{23} & G_{33}^{21} & G_{33}^{22} & G_{33}^{23} \\ G_{21}^{31} & G_{21}^{32} & G_{21}^{33} & G_{33}^{31} & G_{33}^{32} & G_{33}^{33} \end{pmatrix} \begin{pmatrix} u_1^1 \\ u_1^2 \\ u_1^3 \\ u_2^1 \\ u_2^2 \\ u_2^3 \end{pmatrix} = \omega^2 \begin{pmatrix} u_1^1 \\ u_1^2 \\ u_1^3 \\ u_2^1 \\ u_2^2 \\ u_2^3 \end{pmatrix}. \quad (12)$$

The sketch of phonon dispersion relation estimated from Eq.(12) is shown in Fig.2. In this case, there are three optical modes whose values at  $q = 0$  are not zero.

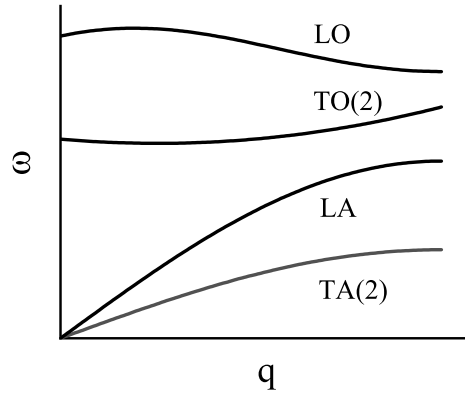


Fig. 2. Phonon dispersion relation of diatomic one-dimensional lattice. TA(2) and LA mean doubly degenerated transverse acoustic and longitudinal acoustic modes, respectively. TO(2) and LO mean doubly degenerated transverse optical and longitudinal acoustic modes, respectively.

In two-dimensional lattice whose degree of freedom for each ion is three, lattice vibration propagates along the lattice plane and the directions of amplitude have three possibilities. One is along the wave propagation, others are orthogonal to it. Unlike the case of one-dimensional lattice, transverse modes are not degenerated, because directions orthogonal to the lattice plane is different from that of parallel. The monoatomic two-dimensional lattice and its phonon dispersion relations are sketched in Figs.3 and 4, respectively.

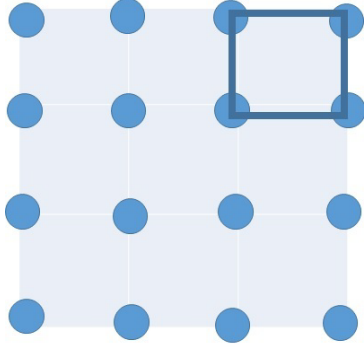


Fig. 3. Monoatomic two-dimensional cubic lattice. The primitive cell is shown by thick lines. The circles mean ions of host metal.

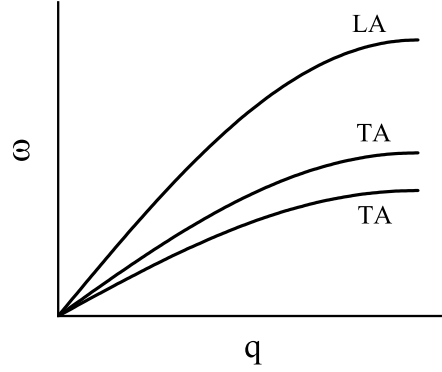


Fig. 4. Phonon dispersion relation of monoatomic two-dimensional cubic lattice. TA and LA mean transverse and longitudinal acoustic modes, respectively.

#### 4 Hydrogen storage lattice

Firstly, we consider the change of the phonon dispersion relation due to the hydrogen storage and its nuclear reaction. We show the deuterium storage two-dimensional lattice sketched in Fig.5. The primitive cell of this lattice contains one host ion and one deuteron. Therefore, this is a case of diatomic two-dimensional lattice with  $6 \times 6$  type dynamical matrix. Adding three optical modes to Fig.4, we obtain phonon dispersion relation of this case sketched in Fig.6.

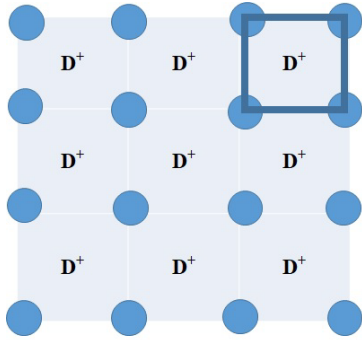


Fig. 5. Diatomic two-dimensional cubic lattice including deuterons. The primitive cell is shown by thick lines. The circles mean ions of host metal.

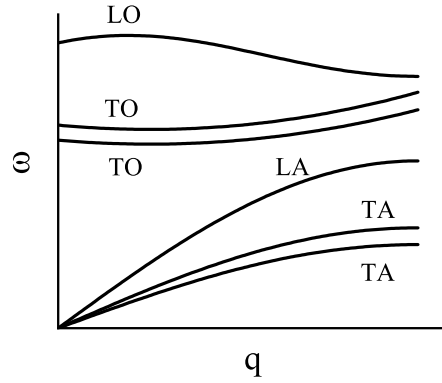


Fig. 6. Phonon dispersion relation of diatomic two-dimensional cubic lattice. TA and LA mean transverse and longitudinal acoustic modes, respectively. TO and LO mean transverse and longitudinal optical modes, respectively.

Comparing Figs.4 and 6, we can find the effect of hydrogen storage through the existence of optical mode.

Secondly, we consider DD reactions in the hydrogen storage lattice sketched in Fig.5. As the simplest example, we assume the case that all reaction occurs simultaneously to induce the change of the lattice in Fig.7 to the lattice shown in Fig.8. In this study, we do not consider the exact collision processes, however the nuclear fusions between deuterons moving through the gaps in the lattice are assumed. The migrations of deuterons are shown by the purple arrows in the left hand side of Fig.7. After the reactions, all deuterons become helium atoms which is shown in the right hand side of Fig.7. Seeing Fig.7, primitive cell before the reaction contains one host ion and one deuteron, therefore dynamical matrix is  $6 \times 6$  type. On the other hand, primitive cell after the reaction contains two host ions and one helium atom, therefore it has  $9 \times 9$  type dynamical matrix. This means that the number of the vibrational modes increases from 6 to 9 due to the nuclear fusion in the lattice. Therefore, we can know the reaction by finding such a change in phonon dispersion relation. After the reaction shown in the right side of Fig.7, the number of deuterons and helium atoms are same, and also the vacant stable sites exit in the same rate with deuteron and helium atom.

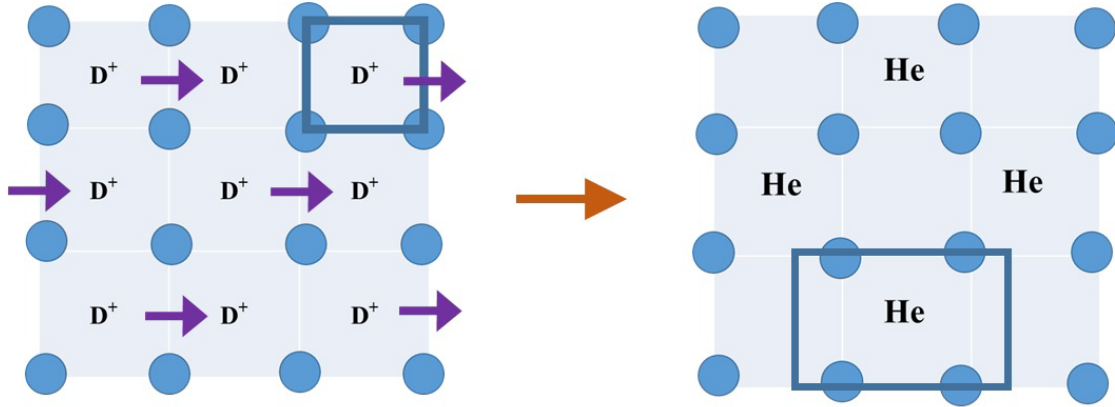


Fig. 7. An example of DD reactions in two-dimensional lattice, where 1/2 deuterons migrate and all deuterons happen to react. In the left hand side of the figure, the deuterons stored in the two-dimensional lattice are drawn and the migration through the gaps of the lattice are shown by the purple arrows. In the right hand side of the figure, He atoms and vacant stable sites created by the nuclear fusions are shown. In both sides of the figure, the primitive cells are shown by the thick lines.

Thirdly, we consider another type reactions. In Fig.8, we show the case that 1/3 deuterons migrate and 2/3 deuterons cause nuclear fusions and become helium atoms. Here, we do not consider the mechanism why 2/3 of them happen to react, however we assume simultaneous migrations and the reactions at definite site as

drawn in the left side of Fig.8. In the same consideration with the previous example, we can understand that the number of the vibrational modes increase from 6 to 15, because the primitive cell after the reaction contains three host ions, one deuteron and one helium. We also know such a reaction by finding this change in phonon dispersion relation.

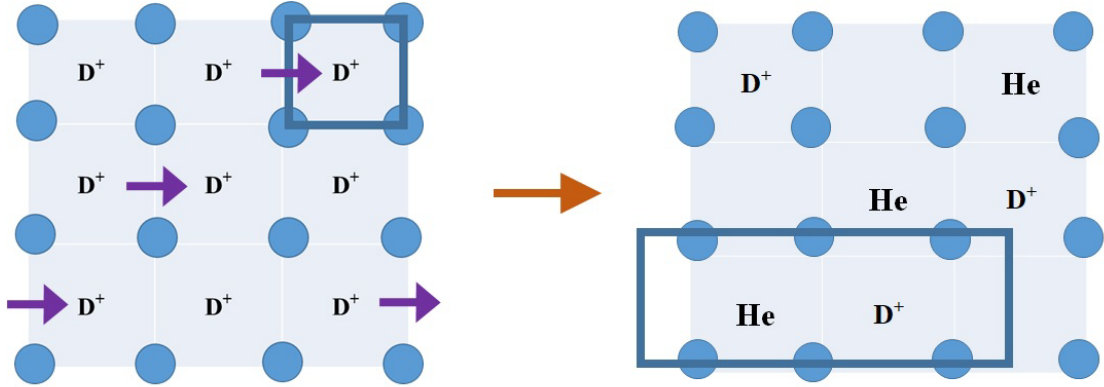


Fig. 8. Another example of DD reactions in two-dimensional lattice, where  $1/3$  deuterons migrate and  $2/3$  deuterons happen to react. In the left hand side of the figure, the deuterons stored in the two-dimensional lattice are drawn and the migration through the gaps of the lattice are shown by the purple arrows. In the right hand side of the figure, He atoms and vacant stable sites created by the nuclear fusions are shown. In both sides of the figure, the primitive cells are shown by the thick lines.

## 5 Conclusions

In this paper, the changes of phonon dispersion relations due to the nuclear reactions in solids was shown by using the limited simple models. We can know that nuclear reactions happen in the solids when you find the same kind of change. However, phonon dispersion relations depend on the macroscopic lattice structure, while nuclear reactions are known to happen at local space in the lattice. Therefore, this is not the perfect method but we can use it in assistance for the detection of nuclear reaction in solids.

The model we used here was hydrogen storage two-dimensional cubic lattice. This gives a more visible image than the one-dimensional model. However, we should consider the change of phonon dispersion relations using three-dimensional hydrogen storage fcc Pd. We will do it in near future.

Lastly, we emphasize that the experimental data on past phonon dispersion relations may give the evidences of nuclear reactions in solids by using our method. However, exact correspondence between the nuclear reaction and phonon dispersion relation is unknown now. Therefore, we should show more cases in future works.

## Acknowledgements

I would like to express my gratitude to Dr. Hiroshi Yamada (Prof. Emeritus of Iwate Univ.) for his long-term encouragements to our study. I would also like to thank my grandson Kazushi Kurosawa for his nice smile.

## References

- [1]M.Fleishman, S.Pons and M.J.Hawkins, 'Electrochemically Induced Nuclear Fusion of Deuterium', J. Electroanal. Chem. **261**(1989)301
- [2]K.Tsuchiya, 'A theoretical study on the possible change of the phonon dispersion relation due to the nuclear reaction in solid', Proc of JCF9, p80

## **Inductive Logic and Meta-analysis in the Cold Fusion Research**

Hideo Kozima

Cold Fusion Research Laboratory, Shizuoka, Japan

E-mail: [hjrfq930@ybb.ne.jp](mailto:hjrfq930@ybb.ne.jp)

### **Abstract**

The cold fusion phenomenon (CFP) has been a wonderful and inexplicable phenomenon where occur nuclear reactions in materials composed of host elements and hydrogen isotopes at near-room temperature environment without any acceleration mechanism. The variety of the experimental data has been also mysterious to understand it in the traditional solid-state physics and the nuclear physics. To understand the complex experimental data obtained in the CFP consistently, we have to depend on the phenomenological approach with a model and then on the quantum mechanics to investigate the premises assumed in the model. We have presented a successful model (the TNCF model) for the CFP in 1994 and the analysis of the experimental data by the model revealed clearly participation of neutrons in the nuclear reactions in the materials (CF materials) where the CFP has been observed.

Looking back to the methodology used in the explanation of the CFP by the TNCF model, we notice that there are resemblance of the logic in the explanation of the CFP by the TNCF model to the meta-analysis and more widely to the inductive logic prevalent in the natural history before the science revolution occurred in the 17<sup>th</sup> century.

It is valuable to point out the use of the meta-analysis in astronomy in the 18<sup>th</sup> century and in such complex situations as medical fields where they call the analysis “EBM” (evidence based medicines) or “Systematic Review” in the modern medicine. The analysis of the data sets in the CFP performed in our works could be classified into a kind of the meta-analysis. It is also noticed that the logic used in our phenomenological explanation of the CFP by the TNCF model is classified into the inductive logic rather than the deductive logic extensively used in the modern science developed after the 17<sup>th</sup> century when the Newtonian mechanics was established.

In a complex system where the nonlinear dynamics governs the behavior of components of the system, we are not able to prepare exactly the same state of a sample in the microscopic sense by using the identical macroscopic experimental conditions; therefore we are not able to predict the effect after a macroscopic initial condition.

Furthermore, we have to notice that the CF material changes its structure drastically by the large liberated energy in the process of the CFP; the nuclear energy liberated in the nuclear reactions is, in general, about 8 orders of magnitude larger than the thermal energy of particles of the CF material

where occurs the CFP. The liberated nuclear energy is distributed among particles around the reaction sites and the temperature of that region becomes very high up sometimes to melt the CF material there. The change of the structure by the nuclear reaction in the CFP also makes it impossible to obtain the same result again for the sample under the same macroscopic experimental initial condition.

Therefore, the ordinary concept and the deductive logic in the analysis of experimental data fail to give a definite image and a definite history of the system. The cold fusion phenomenon (CFP) is just the case we have to depend on the meta-analysis and on the inductive logic to describe the development of the system. We show the important roles of the inductive logic and the meta-analysis in the researches of the cold fusion phenomenon.

**Keywords:** cold fusion phenomenon, phenomenological approach, inductive logic, meta-analysis, TNCF model, ND model, complexity,

## 1. Introduction

It is interesting to notice that any activity of human beings is based on their subjective experience. Even if the natural science seems to treat very objective observables, the confidence in facts observed and obtained by experiments influences strongly on subjective relation with the facts.

In the background of the severe battle fought between people in favor of CFP and those opposed to have been differences of their experience obtained in doing their experiments. The author understands very well this subtle circumstance partly explained in a previous paper [Kozima 2017b] by his humble experience on the experimental study of the CFP [Kozima 1990]. We had observed neutron emission from PdD<sub>x</sub> samples performed with collaboration of a electrochemist Dr. S. Oe and two chemists in the radiochemistry Dr. K. Hasebawa and Dr. H. Suganuma in 1990. This experience has supported the author's effort for 30 years to establish the science of the CFP to explain various facts inexplicable in the existing frameworks in physics. The lack of quantitative reproducibility, one of the controversial points taken up in the logical battle referred above, is the common experience of researchers in this field and should be understood as the qualitative reproducibility accompanied by the complexity in the CFP [Koziam 2013].

We have noticed also the problem of logical framework applied to the explanation of the various experimental facts obtained in the CFP. Looking into the history of spiritual activities of humanbeings, we have many excellent ideas developed in various cultures since the Greek culture flourished 2500 years ago. In Appendix A, we have given a brief overview on the logical principles to be applied to our mental activity in pursuit of the truth behind complicated facts.

Thus, a new inductive axiom has to be set out or assumed when there are inconsistencies of facts with a logical system to reconcile them with a system of principles as explained in *Phaedo* by Plato [Plato P (p. 101d)]. Such processes had historically been achieved as Euclidian geometry and Newtonian mechanics. As we know well, the examples of this axiom had, furthermore, been developed in the modern sciences in the 20<sup>th</sup> century e.g. as Relativistic Mechanics and Quantum Mechanics.

It was an unhappy history for the science of the CFP since its discovery in 1989 by M. Fleischmann et al. in PdD<sub>x</sub> system [Fleischmann 1989] to know that there has been no recognition of the necessity of a new paradigm or a system of principles for the solid state-nuclear physics suggested by the CFP. The logic and the method of analysis in this field were inconsistent with those popular in the established fields of modern natural science. The success of the modern science in the microscopic world developed on the Newtonian mechanics and later on the quantum mechanics has forced scientists participated in this field to work mainly on the deductive reasoning. The logical battle fought between supporters (pros) and critiques (cons) of the CFP has been on the same ground inappropriate for this new science as we have shown in books [Kozima 1998, 2006a] and a paper published before [Kozima 2017b].

We have to start our investigation of the science of the CFP on the experimental facts honestly not bothered by the established knowledge of the nuclear physics mainly in free space and of the solid state physics independent of the nuclear force between relevant particles. In short, we should have to face the experimental facts with *knowledge of modern physics* guided by the *inductive reasoning* as people used to do so when they had faced new phenomena outside of their power since the dawn of the culture in the 5 century B.C.

We had shown the success of the phenomenological approach using a model with an adjustable parameter assuming participation of neutrons to induce nuclear reactions in the CF materials, i.e. materials where occurs the CFP [Kozima 1998, 2006a]. Then, the premises of the model had been justified by quantum mechanical investigation of the states of neutrons in the CF materials [Kozima 2006a, 2013]. The evidence of the success of the inductive reasoning by the TNCF model is best illustrated by the discovery of the three laws (or regularities) in the CFP as explained in Appendix B. The success of our phenomenological approach had been shown in our books and papers for about 25 years as summarized in the recent paper presented at this Conference [Kozima 2019b]. However, we have not discussed the meaning of the phenomenological approach and the use of a model in this field from the general point of view in terms of the logic and the method of analysis in the science. Now, it is the time to take up these phases of science in this

complex field of the CFP for the further development of this field.

In this paper, we give a general discussion of the logic and the method of analysis used in science that is not necessarily governed by linear but nonlinear dynamics. We will be able to understand that the success of the phenomenological approach by the TNCF model and the ND (neutron drop) model is justified by the methodology of science in general.

## **2. Inductive and Deductive Logics in Modern Science**

In the research in a truly new field where we need revolutionarily novel ideas, it is necessary to use whole facts obtained in it and to explore a new framework for them. When we investigate events difficult to explain in the framework of existing science, we collect as many events as possible. Then, we contemplate them to make an image covering them as a whole. Furthermore, we look for qualitative concepts based on principles of science to take the image into our scientific framework.

About the importance of the imagination, Albert Einstein once told his opinion as follows; "Imagination is more important than knowledge. For knowledge is limited, whereas imagination embraces the entire world, stimulating progress, giving birth to evolution." [Einstein 1929]

In front of the bizarre events of the CFP, Martin Fleischmann had expressed his thought on the importance of the qualitative approach as follows;

"In the development of any new area of research (and especially in one likely to arouse controversy!), it is desirable to achieve first of all a qualitative demonstration of the phenomena invoked in the explanation of the observations. It is the qualitative demonstrations which are unambiguous: the quantitative analyses of the experimental results can be the subject of debate but, if these quantitative analyses stand in opposition to the qualitative demonstration, then these methods of analysis must be judged to be incorrect." [Fleischmann 1991 (p. 476)]

In addition to these general thinking about the necessity of imagination and qualitative thinking in the research of new science, it is very important to understand the characteristics of complexity revealed in nonlinear dynamics. We can not overvalue the importance of complexity and its meaning for the development of a system governed by nonlinear dynamics as expressed by I. Prigogine;

"The world of dynamics, be it classical or quantum, is a reversible world. As we have emphasized in Chapter VIII, no evolution can be ascribed to this world; the "information" expressed in terms of dynamical units remains constant. It is therefore of great importance that the existence of an evolutionary paradigm can now be established in physics—not

only on the level of macroscopic description but also on all levels.

Of course, there are conditions for it: as we have seen, a minimum complexity is necessary. But the immense importance of irreversible processes shows that this requirement is satisfied for most systems of interest. Remarkably, the perception of oriented time increases as the level of biological organization increases and probably reaches its culminating point in human consciousness.” [Prigogine 1984 (The Evolutionary Paradigm pp. 297 – 298)] (Partly italicized in the sentence at citation)

It will be not necessary to refer to these words cited above to recognize the importance of the conclusion attained by the phenomenological approach to the CFP that the physics of the CFP is governed by the complexity and related to self-organization of the optimum conditions of the superlattice formation [Kozima 2013].

To see the flow of progress of the solid state physics in relation to the interactions other than the electromagnetic one including the nuclear interaction (strong interaction among nucleons), we made a brief chart of the developments of the solid state physics and the nuclear physics including the solid state-nuclear physics in between them as shown in Appendix C (Fig. C1). This flowchart shows that there had been several tips of physics induced by interactions other than the electromagnetic interaction in the solid state physics prior to the discovery of the cold fusion phenomenon (CFP).

We have to recognize the fact that there is scarce tradition of inductive logic or reasoning in physics since the Newtonian mechanics was compiled as the “Principia” (1687) in the 17th century which had been too effective to treat physics described by the linear dynamics. As Prigogine described in his sentence cited above, we need to extend our consideration to the world governed by the nonlinear dynamics.

### **3. The Cold Fusion Phenomenon as Described by a Phenomenological Model –Inductive Logic and Effective Use of Meta-analysis**

To understand the general feature of the development of the science of the CFP, a flow chart of the solid state-nuclear physics is given in the Appendix C (Fig. C1). As we can see in the Fig. C1, there have been observed events belonging to the solid state-nuclear physics (SSNP), i.e. events induced by the nuclear force in the solid state physics and those influenced by the electromagnetic force from surrounding environment in the nuclear physics, before the explicit recognition of the vast realm of the SSNP by the discovery of the CFP since the year of 1989.

It should be noticed that acceptance of the experimental facts telling us the occurrence of the CFP, i.e. the nuclear reactions in solids at near room temperature without specific

acceleration mechanism, is strongly dependent on the personal experience of the researchers themselves. Once we observe such an events showing the CFP, we believe in the existence of the nuclear reactions even if the reproducibility is qualitative but not quantitative. The personal experience the author had is common to all researchers in this field. We observed neutron emission from Pd/LiOH + D<sub>2</sub>O/Pt systems in 1989 – 1990 and was convinced of existence of the CFP [Kozima 1990].

The CF materials, i.e. systems where the CFP has been observed, are composed of several component elements where is dynamically constructed a state that is optimum to induce nuclear reactions resulting in the CFP [Kozima 2013]. The dynamical process in formation of the optimum state includes necessarily the process that we call complexity well known in nonlinear dynamics. We can not expect realization of the same microscopic state from the same macroscopic condition that we could arrange. This is a conclusion of the theory of complexity and also of our experience, e.g. the elaborate experimental result obtained by McKubre et al. [McKubre 1993] gives one of the best examples. In their experiment, they obtained various CF materials with different average D/Pd values and measured different excess powers for the same D/Pd value (e.g. as shown in their Fig. 7).

The irreproducibility, or rather the qualitative reproducibility of events in the CFP shown in their experiment [McKubre 1993] is a common characteristic of phenomenon in this field and we have to explain it in the science of the CFP.

This fact demands to abandon the deductive approach to the CFP if we want to establish the science of the solid state-nuclear physics where the CFP should take its appropriate position.

As explained in our books [Kozima 1998, 2006a] and papers (e.g. [Kozima 2005, 2013]), the phenomenological approach to the CFP using the TNCF model (and the ND model) has been successful to give a unified explanation for the various events observed in the CFP. The three laws or regularities in experimental data are explicit evidences of the successful phenomenological approach [Kozima 2011] which are briefly explained in Appendix B.

In the application of the models to events in the CFP, we have made several assumptions in analyses of the experimental data; the assumptions unintentionally used were classified into an inductive logic and also the meta-analysis examined from the viewpoint of the methodology of data analysis. In this section, we give several examples in the geophysics and the medical science which show the resemblance of the data analysis used in the CFP.

### **3.1 Phenomenological Approach is a Typical Inductive Logic**

As briefly mentioned in Introduction, the three laws or regularities discovered in the CFP have been induced from many experimental data sets obtained by different investigators and in different CF materials [Kozima 2011]. The process of the induction of these laws are the typical meta-analysis used frequently in the modern medical science (cf. Appendix E). This point is discussed in Section 3.2.

The similarity of the medical science and the cold fusion phenomenon is discussed in Section 3.3. The investigation of the characteristics of both sciences regitimate the use of the meta-analysis in the CFP.

### **3.2 The Stability Law and the Inverse-Power Law in the CFP are induced by the Meta-analysis**

It is shown in this section that the stability law for the elemental transmutation and the inverse-power law for the excess power [Kozima 2011] briefly explained in Appendix B are established using the meta-analysis.

It will be helpful to see the correspondence of a physics in complex materials and a disease in human beings to understand the statistical relation between the cold fusion phenomenon (CFP) in the solid state-nuclear physics and the lung cancer in the human disease. We have shown the characteristics of the lung cancer and the CFP in Appendix E (Table E1). This table clearly shows that the situation we have been in the CFP has strong similarity with that in the medical science at the *variety* in patients in the latter which is a natural result of individuals in a society and in CF materials in the former which is induced by the complexity in the process of formation of the sample.

As we show in Appendix B, there are three laws in the CFP induced from experimental facts obtained by many researchers. The treatment of the data in the process of induction of these laws is essentially the application of the meta-analysis developed and used effectively in the medical science in recent years (cf. Appendix E). Especially, the inductions of the inverse-power law by Lietz [Lietz 2008] and the stability law for the generation of the new elements [Kozima 2011] are the typical cases of the application of the meta-analysis.

The essential point showing the adequacy of the induction of the three laws from experimental data obtained by various researchers is seen from a criterion of the meta-analysis [Walker 2008] (cited in Appendix E):

“Meta-analysis is an analytical technique designed to summarize the results of multiple studies.

By combining studies, a meta-analysis increases the sample size and thus the power to study effects of interest.

There are many caveats in performing a valid meta-analysis, and in some cases a meta-analysis is not appropriate and the results can be misleading.” [Walker 2008 (Key points)].

In the application of the meta-analysis to the CFP, we have to care about the third point in the above citation and discuss it in Section 3.4 below.

We give fundamental literatures of the meta-analysis in Appendix E.

### **3.3 Another Example of the Phenomenological Approach in the Physical Science – The Continental Drift Theory**

There are several successful examples of the phenomenological approach in the physical science, too. The most famous one of them may be the continental drift theory introduced in Appendix D. The huge amount of evidences in geology, biology, paleontology and others suggesting the drift of continents had been neglected by physicists in the main stream science just due to the lack of the driving force to induce the drift of continents. This is a typical example that the deductive logic denied the inductive logic based on the observed facts. We had to accept the fact and then look for the driving force for the continental drift to promote geophysics faster than the history as it was.

After almost 40 years from the proposal of the continental drift in a definite form by Wegener, the idea of continental drift has been subsumed by the theory of plate tectonics, which explains how the continents move.

### **3.4 From the Phenomenological Model to the Physics**

The history of the investigation of the CFP has shown that their complex facts observed in the CF materials have similarity to the data treated in the medical science as shown in Fig. 3.1. Figure 3.1 (a) shows a subset of systematic reviews in the medical science; a method for systematically combining pertinent qualitative and quantitative study data from several selected studies to develop a single conclusion that has greater statistical power. Figure 3.1 (b) shows a tentative scheme of the analysis in the CFP formulated according to the scheme used in the medical science shown in Fig. 3.1 (a).

So, it is useful to investigate the characteristics of the events in the CFP in relation to the symptoms in the medical science and refer to the guide line of the application of the meta-analysis in the latter..

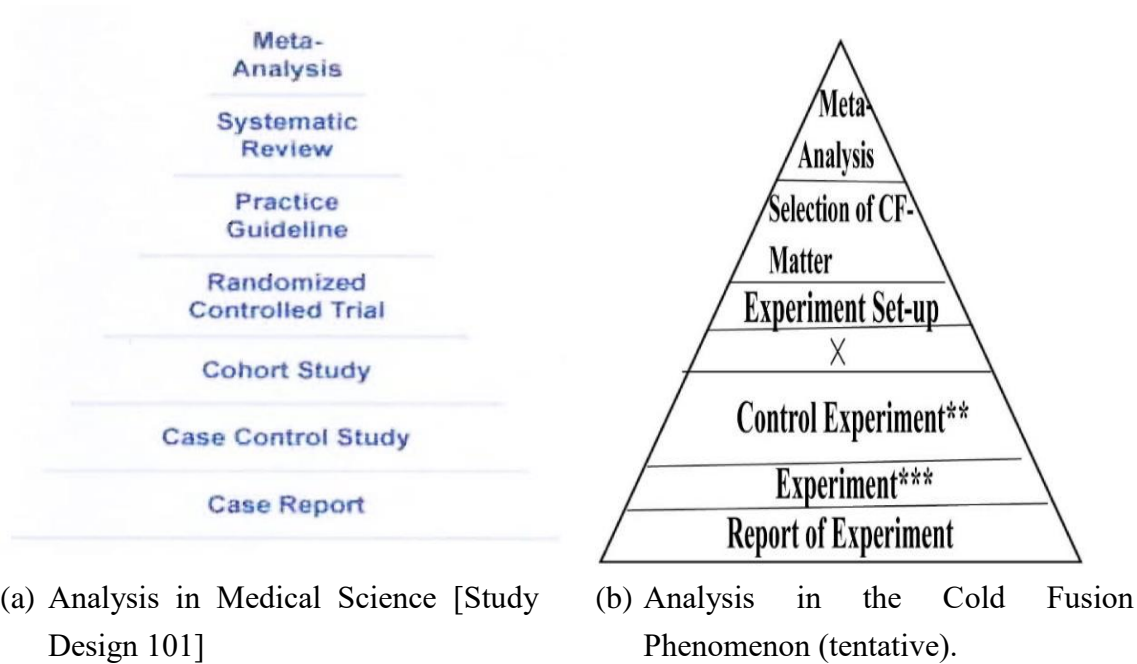


Fig. 3.1 Meta-analysis (a) in Medical Science and (b) in the CFP (tentative). In the tentative scheme for the CFP, *\*\*Control Experiment* means the experiments with no hydrogen isotopes and *\*\*\*Experiment* means experiments with hydrogen isotope H or D to measure NT (nuclear transmutation),  $Q$  (excess heat),  $n$  (neutron emission),  $t$  (tritium),  ${}^4_2\text{He}$  (helium 4), etc.

The most important and crucial point in application of the meta-analysis to the CFP may be the selection bias. This point is discussed in detail in Appendix E-2.

Fundamental difficulty in application of the meta-analysis to the CFP is, needless to say, the scarceness of the number of data sets compared to the medical cases. For instance, there are 63,552 patients (Appendix E-4-1) and 86,092 patients (Appendix E-4-2) are included in the cases of the “cardiovascular risk factors” (Appendix E-4-1) and of the “coronary heart disease” (Appendix E-4-2), respectively. Therefore, we have to use rather arbitrary criterion in the CFP than the objective criteria proposed by Walker (Appendix E-2 (Selection bias)).

This arbitrariness in the selection of the data sets in our analyses in the CFP may result in a larger errors in the induced result and should be improved as soon as possible even if we can infer the global tendencies in the phenomenon from our result.

#### **4. Restoration of the Inductive Logic in Modern Science**

The pursuits of a mechanism for the  $d-d$  fusion reactions in CF materials in the framework of the solid state physics and the nuclear physics done thus far seem to belong to the deductive logic in which explanation for the various events in the CFP is given by the mechanism thus found. The phenomenological approach using a model based on the experimental data will be classified to the inductive logic to find a new mechanism for explanation of various events as a whole.

The success of our phenomenological approach using the TNCF and ND models to the CFP [Kozima 1998, 2005, 2006a, 2011, 2013] is an example of efficacy of the inductive explanation for the phenomenon including the complexity conditioned by the nonlinear interaction among components in the system.

It will instructive to recollect another example of the success of the inductive logic in modern science, the continental drift model (e.g. [Gould 1977]) to explain the many facts suggesting the drift of continents; topographical, geophysical, geological, paleontological, biogeographical and paleoclimatology. Details of this case is discussed in Appendix D in relation to our phenomenological approach to the science of the CFP using the TNCF model [Kozima 1998].

#### **5. Conclusion**

It was noticed more than 2500 years ago that the inductive reasoning was effective for the phenomenon difficult to explain it by a simple cause. Many logical systems of the science including the meta-physical and physical systems had been established on principles thus induced from facts using logical processes. Once a science was established, however, the deductive reasoning was prevalently used to settle the science as a solid system of explanation for facts experienced in the realm of the science as far as the limit of the science is not encountered. Repetitions of this kind of logical process composed of extensions and innovations have formed the history of human knowledge. A small example of the innovation seems to be experienced now in the solid state-nuclear physics as surveyed in this and the another paper [Kozima 2019b] presented at this Conference.

The meta-analysis is useful in the analysis of such complex data encountered in the CFP as Walker et al. explained its characteristic in their paper [Walker 2008] as cited below.

*“A meta-analysis is a statistical analysis that combines the results of multiple scientific studies. The basic tenet behind meta-analyses is that there is a common truth behind all conceptually similar scientific studies, but which has been measured with a certain error within individual studies. The aim then is to use approaches from statistics to derive a*

*pooled estimate closest to the unknown common truth based on how this error is perceived.*" [Walker 2008]

It has been a riddle that the wonderful phenomenon of the super-diffusivity (the extraordinary high diffusivity of hydrogen in some transition metals and alloys) noticed more than 150 years ago [Graham 1866] has not been fully understood until now. The explanation of the CFP by the ND model based on the neutron energy band [Kozima 2006] had supplied a possible explanation of the super-diffusivity as explained in another paper presented at this Conference [Kozima 2019b].

One of the reasons of the lack of appropriate explanation for this phenomenon is the overwhelming popularity of the deductive logic in the modern science since the 17<sup>th</sup> century as pointed out in this paper. People have tried to explain the super-diffusivity using the first principle and only knowledge known in the solid state physics not considering the possible interaction of protons and lattice nuclei by the nuclear force. The nuclear transmutations observed in the CFP shed light at this nuclear interaction between protons/deuterons and neutrons in lattice nuclei [Kozima 2006a, 2006b, 2013].

The super-nuclear interaction between neutrons in different lattice nuclei mediated by protons/deuterons at interstitial sites has given a possibility to form the neutron energy bands where neutrons are trapped as neutron Bloch waves. Conversely, the nuclear interaction of protons/deuterons with lattice nuclei lowers the energy of the interstitial protons/deuterons making them more stable. This stabilization of the interstitial protons/deuterons may be the fundamental factor resulting in the super-diffusivity of protons/deuterons in some transition metals and alloys.

The development of the nonlinear dynamics assisted by use of the computer has given an effective point of view to resolve the riddle of the CFP and also the super-diffusivity of hydrogen isotopes. Without the knowledge of complexity, the qualitative reproducibility of the CFP has remained a tumbling stone for the development of the physics of the CFP and therefore the solid state-nuclear physics.

The success of our phenomenological approach to the CFP is a triumph of the inductive logic over the deductive logic in systems where the complexity is an essential factor to induce the phenomenon. The discovery of the first (the stability law) and the second (the inverse-power dependence) laws in the three laws of the CFP, explained in Appendix B, was based on the use of induction from the experimental data using unintentionally the meta-analysis at the time when the laws were formulated [Kozima 2005, 2006a, 2006c, 2011, Lietz 2008].

It is possible to say that the neglect of the inductive logic and the meta-analysis in the CFP made the 30 years of theoretical investigation almost a waste of time except only

one exception of our phenomenological approach. Using these approach adequate for the complicated data obtained in the CFP, we will be able to make another great progress of the physics of the CFP bringing the whole data obtained in these 30 years back to life initiated by our trial using the TNCF and the ND models.

## Appendices

A. *Logical Development of Inquiry into Questions*

B. *Three Laws of the Cold Fusion Phenomenon*

C. *Development of the Solid State-Nuclear Physics*

D. *Continental Drift Theory – An Example of Induction vs. Deduction in the Science*

E. *Meta-Analysis in the Fields where are Plural Trials*

E1 **The Principle of the Arithmetic Mean** [Plackett 1958]

E2 **Meta-analysis: Its Strengths and Limitations** [Walker 2008]

E3 **The Process of the Meta-Analysis** [Tsutani 2003]

E4 **Examples of Meta-Aalysis in the Medical Science**

## Appendix A. Logical Development of Inquiry into Questions

It is interesting to notice that Aristotle named Socrates as the innovator of the inductive reasoning as follows; “*There are two innovations which may fairly be ascribed to Socrates: inductive reasoning and general definition. Both of these are associated with the starting-point of scientific knowledge.*” [Aristotle M (1078b 27 – 29)]. It should be noticed also that he explained Socrates as a moralist rather than a scientist as follows; “*And when Socrates, disregarding the physical universe and confining his study to moral questions, sought in this sphere for the universal and was the first to concentrate upon definition, Plato followed him and assumed that the problem of definition is concerned not with any sensible thing but with entities of another kind; for the reason that there can be no general definition of sensible things which are always changing. These entities he called "Ideas," and held that all sensible things are named after them sensible and in virtue of their relation to them; for the plurality of things which bear the same name as the Forms exist by participation in them.*” [Aristotle M (987b 1 – 2)].

As Aristotle said as above on Socrates and Plato, Plato had written a sentence on the inductive reasoning as follows;

“*You would say: I will let alone puzzles of division and addition—wiser heads than mine may answer them; inexperienced as I am, and ready to start, as the proverb says, at my own shadow, I cannot afford to give up the sure ground of a principle. And if any one*

*assails you there, you would not mind him, or answer him, until you had seen whether the consequences which follow agree with one another or not, and when you are further required to give an explanation of this principle, you would go on to assume a higher principle, and a higher; until you found a resting-place in the best of the higher; but you would not confuse the principle and the consequences in your reasoning, like the Eristics—at least if you wanted to discover real existence. Not that this confusion signifies to them, who never care or think about the matter at all, for they have the wit to be well pleased with themselves however great may be the turmoil of their ideas. But you, if you are a philosopher, will certainly do as I say.” [Plato P (101d-e)] (Some sentences are colored at citation for emphasis).*

If we accept the Aristotle’s first statement and the saying in Phaedo [Plato P (101d)], it is a natural conclusion that the method of “hypothesis” used by Platonic School (Academia) had generated the Platonism, first of all, that had scarcely remained in the books “*The Dialogues of Plato*” published by Plato based on his diverse experience in his eventful life. And then the Euclidean Geometry compiled as the “*Elements*” had been built on the definitions and axioms in 300 B.C. and finally Newtonian Mechanics compiled as the “*Principia*” (1687) similarly constructed in the 17<sup>th</sup> century.

## **Appendix B. Three Laws of the Cold Fusion Phenomenon**

The three laws (regularities) of the cold fusion phenomenon were discovered by investigation of experimental data sets as a whole [Kozima 2011].

They are formulated as follows in the recent explanation:

- 1) The First Law; The stability law for elemental transmutation products**
  - 1-1 Corollary 1. Production of a nuclide  ${}^{A'}_{Z+1}X'$  from a nuclide  ${}^A_ZX$  in the system.
  - 1-2 Corollary 2. Stabilization and Decay time shortening of unstable nuclei in the system.
- 2) The Second Law; The inverse power dependence of the frequency on the intensity of the excess heat production**
- 3) The Third Law; Bifurcation of the intensity of events (neutron emission and excess heat production) in time**

The first law was noticed in 2005 [Kozima 2005, 2006b] by comparison of the cumulative data of nuclear transmutations in the CFP from 40 data sets obtained in 1996 – 2003 [Kozima 2006b] with the data of abundance of the elements in universe [Suess 1956]. The second law was found out from the data by McKubre et al. [McKubre 1993] counting elaborately the correspondence of the numbers of data for a definite value of excess energy in their Fig. 6 [Kozima 2005a, 2006c]. The fundamental point of view in our phenomenological approach has been the inductive logic looking back logically now.

Furthermore, we notice that the analyses used in these works are classified in the meta-analysis using the name used in the medical science.

It is necessary to remind two words the “house” and the “building stones” to construct a house as H. Poincare stated appropriately;

*“The man of science must work with method. Science is built up of facts, as a house is built of stones; but an accumulation of facts is no more a science than a heap of stones is a house. Most important of all, the man of science must exhibit foresight.”* [Poincare 1902 (p. 141)]

We have to consider the building stones when we see such grandiose cathedrals as Platonism, Euclidean Geometry and Newtonian Mechanics and not only to worship the resultant Principles.

Thus, all our spiritual products are based on the experience we have had obtained in our communication with outside world, natural and social. All products reflect the experience. The Euclidian geometry reflects all geometrical experience obtained by the time Euclid compiled them in the *Elements* under the definitions and theorems. The Newtonian mechanics reflects all physical experience obtained by the time Newton compiled them in the *Principia* under the definitions and laws. Even the Platonian philosophy reflects all spiritual experience suffered by Plato until he compiled them in *The Dialogues of plato* even if it was said that Plato told always the written materials could not convey truth at all. We always have to have our base of investigation on facts even if we tend to easily rely on principles established already on the past facts and testified by experience after their settlement.

### **Appendix C. Development of the Solid State-Nuclear Physics**

The solid state-nuclear physics has been developed drastically in these 30 years by the investigation of nuclear reactions in the cold fusion phenomenon (CFP) where complexity plays a decisive role to generate various and profound events not known before [Kozima 2019b]. In Fig. C1, we have shown the development of the solid state-nuclear physics in relation to the solid state physics and the nuclear physics.

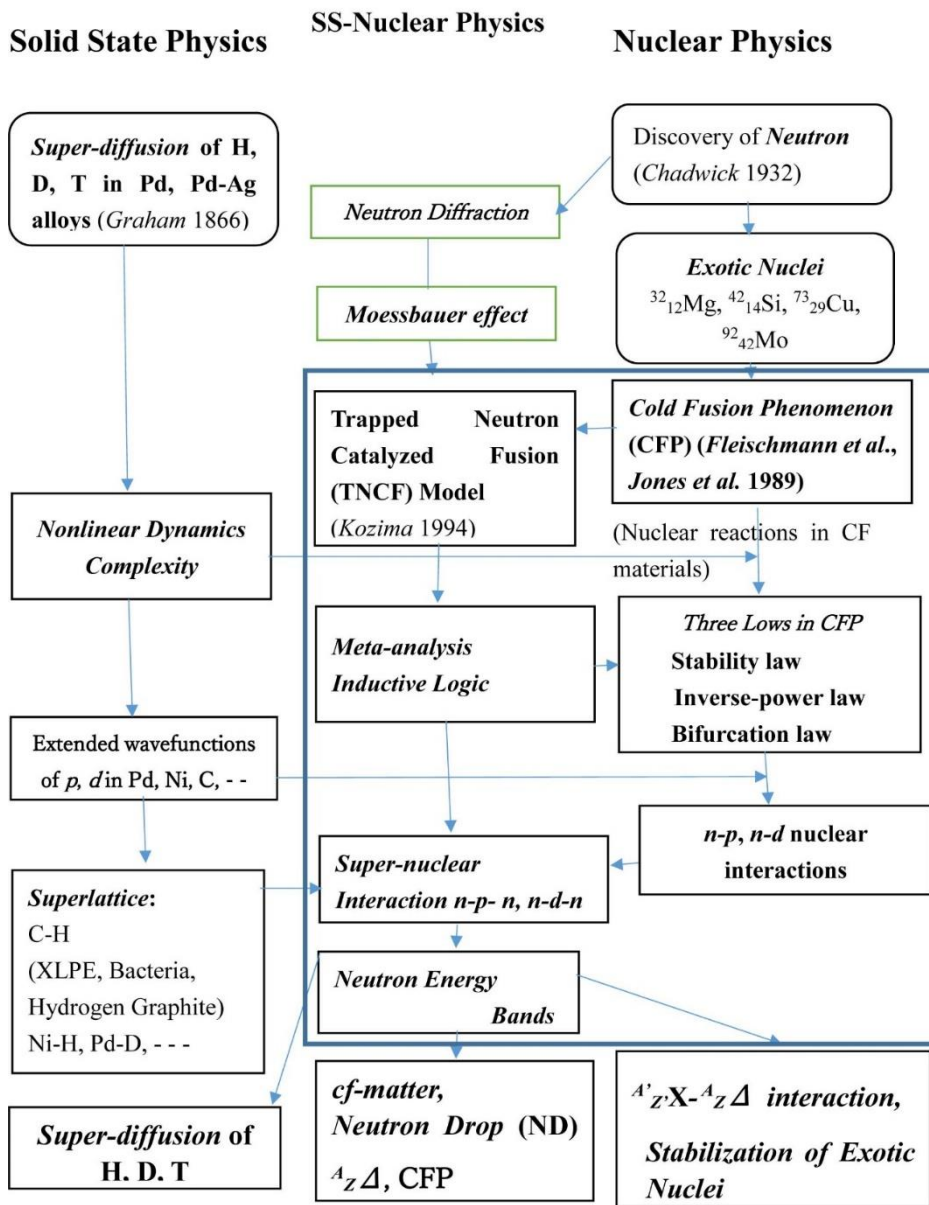


Fig. C1 Flow chart of the development of the solid state-nuclear physics mediated by the progress of the cold fusion phenomenon (CFP) since the work by Fleischmann et al. in 1989 [Fleischmann 1989].

### Appendix D. Continental Drift Theory – An Example of Induction vs. Deduction in the Science (cf. [Gould 1977 (Chapter 20. *The Validation of Continental Drift*)])

The history of the evolution started in the 19<sup>th</sup> century. In the mid-19th century, Charles Darwin formulated the scientific theory of evolution by natural selection,

published in his book *On the Origin of Species* (1859). Evolution by natural selection is a process first demonstrated by the observation that often, more offspring are produced than can possibly survive. This is followed by three observable facts about living organisms: 1) traits vary among individuals with respect to morphology, physiology, and behaviour (phenotypic variation), 2) different traits confer different rates of survival and reproduction (differential fitness), and 3) traits can be passed from generation to generation (heritability of fitness). Fortunately enough in biology, there was no principles governing the biological world at that time and the idea was accepted gradually among scientists in this field.

The history of the idea about the continental drift shows defect of the physical science too biased to deduction by the success of classical mechanics since the 18<sup>th</sup> century: “*The concept was independently and more fully developed by Alfred Wegener in 1912, but his theory was rejected by some for lack of a mechanism (though this was supplied later by Arthur Holmes). The idea of continental drift has been subsumed by the theory of plate tectonics, which explains how the continents move.*” (Continent drift from Wikipedia) As we know well now, the concept of the continental drift by A. Wegener was developed inductively on the many facts suggesting the drift of continents; topographical, geophysical, geological, paleontological, biogeographical and paleoclimatology. However, he was unable to provide a convincing explanation for the physical processes which might have caused this drift (e.g. [Gould 1977]).

“*We now have a new, mobilist orthodoxy, as definite and uncompromising as the staticism it replaced. In its light, the classical data for drift have been exhumed and proclaimed as proof positive. Yet these data played no role in validating the notion of wandering continents; drift triumphed only when it became the necessary consequence of a new theory.*” [Gould 1977 (p. 166)]

The explanation of the mechanism for the continental drift was given now by the theory of plate tectonics very well. People believes the fact of the continental drift based on the plate tectonics as it gives a deductive explanation from more general theory. However, *the idea is more important than theory* in this case, too; we have had too deep credit to the mechanism of the continental drift than the fact revealed by natural historical observation. We had to accept the idea of the continental drift concluded inductively from many facts and then had to look for geophysical mechanisms for the drift. Then, the history of geophysics might be very different and fast to understand the physics of the Earth.

# Continental Drift and the Cold Fusion Phenomenon

## Continental Drift

## Cold Fusion Phenomenon

### 1. Phenomenon

1. The complementary arrangement of the facing sides of South America and Africa
2. Similar plant and animal fossils are found around the shores of different continents
3. The same animals being found on two continents
4. Widespread distribution of Permo-Carboniferous glacial sediments

1. Space distribution of Nuclear Transmutation products  $NT(r)$
2. Neutron energy spectrum  $n(\epsilon)$
3. Stabilization of unstable nuclei
4. Decrease of decay constants
5. Enormous excess energy  $Q$
6. Lowering of fission threshold energy

### 2. Phenomenological Explanation

**Continental drift**

1. TNCF Model and
2. Neutron Drop (ND) Model

### 3. Physical Bases of the Explanation

The theory of plate tectonics explains all following facts, including the movement of the continents, better than Wegener's theory:

There are two kinds of crust: continental crust and oceanic crust. Continental crust is inherently lighter and its composition is different from oceanic crust, but both kinds reside above a much deeper "plastic" mantle. Oceanic crust is created at spreading centers, and this, along with subduction, drives the system of plates in a chaotic manner, resulting in continuous orogeny and areas of isostatic imbalance.

1. Super-nuclear interaction of neutrons at lattice nuclei mediated by interstitial protons or deuterons
2. Formation of neutron energy bands
3. Generation of the cf-matter at boundary regions
4. Formation of neutron drops in the cf-matter  $A_Z \Delta$
5. Interaction of neutrons in the energy bands and nuclei at irregular positions
6. TNCF and ND models explain almost all experimental data in CFP

Fig. D1 Explanation of the logical structure of the continental drift theory (left) in contrast to the case of the cold fusion phenomenon (CFP) (right).

We are able to understand the present status of the cold fusion research by a comparison of the Continental Drift and the CFP as shown in Fig. D1.

The necessity of the inductive logic is recognized by many people who know the failure of deductive logic due to the existence of evolutionary paradigm based on the complexity as described by Prigogine and Stengers [Prigogine 1984] and K. Nakamura [Nakamura 1993] as follows.

*“The world of dynamics, be it classical or quantum, is a reversible world. As we have emphasized in Chapter VIII, no evolution can be ascribed to this world; the “information” expressed in terms of dynamical units remains constant. It is therefore of great importance that the existence of an evolutionary paradigm can now be established in physics—not only on the level of macroscopic description but also on all levels. Of course, there are conditions: as we have seen, a minimum complexity is necessary. But the immense importance of irreversible processes shows that this requirement is satisfied for most systems of interest. Remarkably, the perception of oriented time increases as the level of biological organization increases and probably reaches its culminating point in human consciousness.”* [Prigogine 1984 (pp. 297 – 298)]

*“While I had been working in the field of the life science, I noticed the existence of the natural history of life, or biohistory, and determined to work in this new field. The recognition of the transfer from science to history occurred in the middle of 1980s.”* [Nakamura 1993 (p. 8)]

*“I have started from the molecular biology and arrived at the biohistory through the biological science.”* (p. 179).

*“In Noya’s opinion, the trend of R. Bacon, G.B. Vico, and J.W. Goethe who tried to organize intellectual works from the view point of natural history should be taken up as another trend of G. Galilei, R. Descarte, and I. Newton who composed the main stream of modern science. Especially, Noya had taken up Bacon as a person who tried to reform the Medieval rhetoric into new one to use it for reformation of the natural history into the modern science. Noya insisted that his “induction” should be revalued from such a point of view.”* [Nakamura 1993 (p. 209)]

## Appendix E. Meta-Analysis in the Fields where are Plural Trials

It is interesting to compare the cold fusion phenomenon (CFP) with a disease (e.g. the lung cancer) in their characteristics as shown in Table E1. We notice many similarities in both cases, the lung cancer vs. the CFP, from the variety of *Patients* vs. *CF Materials* to the *Symptoms* vs. *Events*. We can concentrate on the individual symptom (event) or look for the common cause of these symptoms (events).

Table E1. Comparison of the characteristics of the Lung Cancer (left) and the Cold Fusion Phenomenon (right)

<b><i>Lung cancer or lung carcinoma</i></b>	<b><i>Cold Fusion Phenomenon (CFP)</i></b>
<b>Symptoms of a patient</b>	<b>Events of a CF material</b>
Coughing (including coughing up blood),	Nuclear transmutation
Weight loss,	Neutron emission
Shortness of breath,	Tritium generation
Chest pains	$^4_2\text{He}$ generation
	Excess energy generation
<b>Types</b>	<b>CF materials</b>
Small-cell lung carcinoma (SCLC),	Transition metal hydrides and deuterides
Non-small-cell lung carcinoma (NSCLC)	Hydrogen graphite
	XLPE
	Microorganism
<b>Risk factors</b>	<b>Necessary conditions for the CFP</b>
Tobacco smoking,	Existence of solid state host materials M
Genetic factors,	Existence of hydrogen isotopes H or D
Radon gas,	Large ratio of H/M or D/M close to 1
Asbestos,	Formation of superlattice MH or MD
Air pollution	Existence of heterogeneous Nuclei M' or disordered nuclei M
<b>Diagnostic</b>	<b>Mechanism for the phenomenon</b>
Medical imaging,	$n + M'$ reaction (neutron-M' reaction)
Tissue biopsy	$^A_Z\text{A} + M'$ reaction (neutron drop-M' reaction)

We may consider such a trial to look for a *d-d* fusion mechanism in CF materials to that of treatment on the individual symptom (e.g. coughing in the lung cancer).

In the following subsections E-1 to E-4, we show several examples of meta-analyses used in the medical science which will be helpful to analyze experimental data obtained in the CFP even if where experimental data are little in number and poor in quality compared with patients in the medical science taken up in the following Appendices.

**E-1.** *The Principle of the Arithmetic Mean* [Plackett 1958]

**E-2.** *Meta-analysis: Its Strengths and Limitations* [Walker 2008]

**E-3.** *The Process of the Meta-Analysis* [Tsutani 2003]

**E-4.** *Examples of Meta-Analysis in the Medical Science*

### **E-1. The Principle of the Arithmetic Mean** [Plackett 1958]

“The history of the problem of combining a set of independent observations on the same quantity is traced from antiquity to the appearance in the eighteenth century of the arithmetic mean as a statistical concept.” (p. 121)

“The technique of repeating and combining observations made on the same quantity appears to have been introduced into scientific method by Tycho Brahe towards the end of the sixteenth century.” (p. 122)

“A third example illustrates the combination of data from different observers. During 1736 – 7, a French expedition under Maupertuis was sent to Lapland in order to measure the length of a degree of latitude and, by comparing it with the corresponding length in France, to decide whether the earth was flattened at the poles, - - , or at the equator, - - -.” (p. 124).

“At this interval of time, we can recognize the last part of Lagrange’s memoir as a starting point of the theory of integral transforms, although its merits were scarcely visible to Todhunter, writing in 1865. However, they were at once appreciated by Laplace, who refers to ‘la belle méthode que vous donnez’ in a letter written to Lagrange on 11 August 1780, and who subsequently made the technique a basic part of his attack on the problem of combining observations.” (pp. 125 – 126)

### **E-2. Meta-analysis: Its Strengths and Limitations** [Walker 2008]

To help make sense of the information, we are seeing more and more review articles that pool the results of multiple studies. When certain principles are followed and the data are quantitatively analyzed, these reviews are called meta-analyses. A PubMed search of

the word “meta-analysis” in the title yielded 1,473 articles in the year 2007.

Combining available information to generate an integrated result seems reasonable and can save a considerable amount of resources. Nowadays, meta-analyses are being used to design future research, to provide evidence in the regulatory process, and even to modify clinical practice.

Meta-analysis is powerful but also controversial—controversial because several conditions are critical to a sound meta-analysis, and small violations of those conditions can lead to misleading results. Summarizing large amounts of varied information using a single number is another controversial aspect of meta-analysis. Under scrutiny, some meta-analyses have been inappropriate, and their conclusions not fully warranted.

This article introduces the basic concepts of meta-analysis and discusses its caveats, with the aim of helping clinicians assess the merits of the results. We will use several recent meta-analyses to illustrate the issues, including a controversial one<sup>4</sup> with potentially far-reaching consequences. [Walker 2008]

A meta-analysis is a statistical analysis that combines the results of multiple scientific studies. The basic tenet behind meta-analyses is that there is a common truth behind all conceptually similar scientific studies, but which has been measured with a certain error within individual studies. The aim then is to use approaches from statistics to derive a pooled estimate closest to the unknown common truth based on how this error is perceived. In essence, all existing methods yield a weighted average from the results of the individual studies and what differs is the manner in which these weights are allocated and also the manner in which the uncertainty is computed around the point estimate thus generated. In addition to providing an estimate of the unknown common truth, meta-analysis has the capacity to contrast results from different studies and identify patterns among study results, sources of disagreement among those results, or other interesting relationships that may come to light in the context of multiple studies [Wikipedia].

### **(1) Objectives of Meta-Analysis**

The main objectives of a meta-analysis are to:

- Summarize and integrate results from a number of individual studies
- Analyze differences in the results among studies
- Overcome small sample sizes of individual studies to detect effects of interest, and analyze end points that require larger sample sizes
- Increase precision in estimating effects
- Evaluate effects in subsets of patients

- Determine if new studies are needed to further investigate an issue
- Generate new hypotheses for future studies.

These lofty objectives can only be achieved when the meta-analysis satisfactorily addresses certain critical issues, which we will discuss next.

## **(2) Critical Issues in Meta-Analysis Design**

1. Identification and selection of studies
2. Heterogeneity of results
3. Availability of information
4. Analysis of the data

The most important one in these four critical issues listed up by Walker [Walker 2008], the first is essential in the application of this method to the CFP. The meaning of the first issue is explained as follows:

“The outcome of a meta-analysis depends on the studies included. The critical aspect of selecting studies to be included in a meta-analysis consists of two phases. The first is the identification phase or **literature search**, in which potential studies are identified. In the second phase, further criteria are used to create **a list of studies for inclusion**. Three insidious problems plague this aspect of meta-analysis: 1. publication bias and 2. search bias in the identification phase, and 3. selection bias in the selection phase. These biases are discussed below.” [Walker 2008 (p. 432)]

The critically important problem in the application of meta-analysis to the CFP is the selection bias explained as follows;

### **“Selection bias: Choosing the studies to be included**

The identification phase usually yields a long list of potential studies, many of which are not directly relevant to the topic of the meta-analysis.

This list is then subject to additional criteria to select the studies to be included.

This critical step is also designed to reduce differences among studies, eliminate replication of data or studies, and improve data quality, and thus enhance the validity of the results.

To reduce the possibility of selection bias in this phase, it is crucial for the criteria to be clearly defined and for the studies to be scored by more than one researcher, with the final list chosen by consensus.<sup>9,10</sup> Frequently used criteria in this phase are in the areas of:

- Objectives
- Populations studied
- Study design (eg, experimental vs observational)
- Sample size

- **Treatment** (eg, type and dosage)
- **Criteria for selection of controls**
- **Outcomes measured**
- **Quality of the data**
- **Analysis and reporting of results**
- Accounting and reporting of attrition rates
- Length of follow-up
- When the study was conducted.” [Walker 2008 (p. 433)]

The decisively important ones in the CFP will be those boldfaced criteria in the above list due to the lack of standards in a few experimental data compared to the case of the medical science. Even in this area, it happens to occur following instance; “In some cases, it is particularly difficult to find similar studies,<sup>10,11</sup> and sometimes the discrepancies and low quality of the studies can prevent a reasonable integration of results. In a systematic review of advanced lung cancer, Nicolucci et al<sup>12</sup> decided not to pool the results, in view of “systematic qualitative inadequacy of almost all trials” and lack of consistency in the studies and their methods.” [Walker 2008 (p. 433)]

Therefore, we have to use a subjective ones for these boldfaced criteria in the above list. This defect in the application of meta-analysis for the CFP will be remedied by accumulation of enough data sets in time.

### **E-3. The Process of the Meta-Analysis** [Tsutani 2003]

It is possible to define the Meta-Analysis as “The analysis of the data as a whole for a research question where are plural trials.” [Tsutani 2003 (p. 1418)]

#### **The Process of the Meta-Analysis** (pp. 1417 – 1418, Translated into English by H.K.)

There are 7 steps in the meta-analysis

(1) Set the Research Theme, i.e. the Research Question.

In the first step “Identification of the Problem” of the EBM, the four elements called “PECO” (i.e. patient, exposure, comparison, and outcome) are about a specific patient. In the identification of the problem at the meta-analysis, the generalized “name of disease” corresponds to the patient in the PECO.

(2) Collection of Researches without Exception.

This is a very important step. We have to collect as many trials as possible including unpublished ones to avoid the publication bias. Considering this point, it is very difficult to develop the systematic review at individual level. It is desirable to have supports by public organizations.

- (3) Evaluation of Values of Individual Researches
- (4) Summarization of the Result of the Evaluation
- (5) Systematic Analysis of the Result
- (6) Interpretation of the Result
- (7) Edit and Publication of the Result periodically

#### **E-4. Examples of Meta-Analysis in the Medical Science**

There are very many works used the meta-analysis to analyze the effect of some causes on the symptom in the medical science. We cite only two examples to show the use and effects of the meta-analysis to induce rather general conclusion from several experiments done with limited conditions.

##### **E-4-1 “Cardiovascular Risk Factors and Venous Thromboembolism: A Meta-Analysis,” [Ageno 2007]**

**“Methods and Results** – Medline and EMBASE databases were searched to identify studies that evaluated the prevalence of major cardiovascular risk factors in venous thromboembolism (VTE) patients and control subjects. Studies were selected using a priori defined criteria, and each study was reviewed by authors who abstracted data on study characteristics, study quality, and a random-effects model. Statistical heterogeneity was evaluated through the use of  $\chi^2$  and  $I^2$  statistics. Twenty-one case-control and cohort studies with a total of 63,552 patients (*from 21 sources*) met the inclusion criteria. - - - .”

**“Conclusions** – Cardiovascular risk factors are associated with VTE. This association is clinically relevant with respect to individual screening, risk factor modification, and primary and secondary prevention of VTE. Prospective studies should further investigate the underlying mechanisms of this relationship.” [Ageno 2007 (p. 93) (Italicized sentence in a parenthesis is added at citation.)

##### **E-4-2 “The Prevalence and Incidence of Coronary Heart Disease is Significantly Increased in Periodontitis: A Meta-Analysis,” [Bahekar 2007]**

**“Methods** A systematic review of the literature revealed 5 prospective cohort studies (follow-up >6 years), 5 case-control studies, and 5 cross-sectional studies that were eligible for meta-analysis. Individual studies were adjusted for confounding factors such as age, sex, diabetes mellitus, and smoking. The 3 study categories were homogeneous; therefore, the Mantel-Haenszel fixed-effect model was used to compute common relative risk and odds ratio (OR).”

**“Results** Meta-analysis of the 5 prospective cohort studies (86,092 patients) indicated that

individuals with periodontitis (PD) had a 1.14 times higher risk of developing coronary heart disease (CHD) than the controls - - - .”

“**Conclusions** This meta-analysis indicates that both the prevalence and incidence of CHD are significantly increased in PD. Therefore, PD may be a risk factor for CHD. Prospective studies are required to prove this assumption and evaluate risk reduction with the treatment of PD.” [Bahekar 2007 (p.830)]

## References

- [Ageno 2007] W. Ageno, C. Becattini, T. Brighton, R. Selby, and P.W. Kamphuisen, “Cardiovascular Risk Factors and Venous Thromboembolism: A Meta-Analysis,” *Circulation*. 2008; 117:93-102; originally published online December 17, 2007; doi:10.1161/CIRCULATIONAHA.107.709204.
- [Aristotle M] Aristotle, *Metaphysics*, translated by Hugh Tredennick, Cambridge, MA, Harvard University Press, London, William Heinemann Ltd., 1933, 1989.
- [Bahekar 2007] A.A. Bahekar S. Singh, S. Saha, J. Molnar and R. Arora, “The Prevalence and Incidence of Coronary Heart Disease is Significantly Increased in Periodontitis: A Meta-Analysis,” *American Heart Journal*, **154**, No. 5, pp. 830 – 837 (2007).
- [Einstein 1929] A. Einstein, “What Life means to Einstein : An Interview by George Sylvester Viereck,” *The Saturday Evening Post*, October 26, 1929.
- [Fleischmann 1989] M. Fleischmann, S. Pons and M. Hawkins, "Electrochemically induced Nuclear Fusion of Deuterium," *J. Electroanal. Chem.*, **261**, 301 – 308 (1989).
- [Fleischmann 1991] M. Fleischmann, “The Present Status of Research in Cold Fusion,” Proc. ICCF2, pp. 475 – 487 (1991). Published as *Conference Proceedings*, Vol. 33, *The Science of Cold Fusion*, Italian Physical Society, Bologna, Italy (1991), ISBN 88-7794-045-X.
- [Gould 1977] S.J. Gould, *Ever Since Darwin – Reflections in Natural History –*, W.W. Norton & Co., New York, 1977, ISBN 0-393-00917-3.
- [Graham 1866] [Graham 1866] T. Graham, *Philos. Trans. R. Soc. London*, **156**, p. 415 (1866).
- [Kozima 1990] H. Kozima, S. Oe, K. Hasegawa, H. Suganuma, M. Fujii, T. Onojima, K. Sekido and M. Yasuda, “Experimental Investigation of the Electrochemically Induced Nuclear Fusion,” *Report of Faculty of Science, Shizuoka University*, **24**, pp. 29 -34 (1990), ISSN 0583-0923.
- [Kozima 1998] H. Kozima, *Discovery of the Cold Fusion Phenomenon*, Ohtake Shuppan Inc., Tokyo, Japan, 1998. ISBN: 4-87186-044-2.

- [Kozima 2005] H. Kozima, "Cold Fusion Phenomenon," *Rep. Fac. Science, Shizuoka University*, 39, pp. 21 – 90 (2005), ISSN 05830923.
- [Kozima 2006a] H. Kozima, *The Science of the Cold Fusion Phenomenon*, Elsevier Science, 2006, ISBN-10: 0-08-045110-1.
- [Kozima 2006b] H. Kozima, "cf-Matter and the Cold Fusion Phenomenon," *Proc. ICCF10*, pp. 919 – 928 (2005), ISBN 981-256-564-7.
- [Kozima 2006c] H. Kozima, "Cold Fusion Phenomenon and Solid State Nuclear Physics," *Proc. ICCF11*, pp. 769 – 775 (2006), ISBN 981-256-640-6.
- [Kozima 2011] H. Kozima, "Three Laws in the Cold Fusion Phenomenon and Their Physical Meaning," *Proc. JCF17*, pp. 101 – 114 (2012), ISSN 2187-2260.
- [Kozima 2013] H. Kozima, "Cold Fusion Phenomenon in Open, Nonequilibrium, Multi-component Systems – Self-organization of Optimum Structure," *Proc. JCF13* **13-19**, pp. 134 - 157 (2013), ISSN 2187-2260, [http://jcfirs.org/proc\\_jcf.html](http://jcfirs.org/proc_jcf.html).
- [Kozima 2017a] H. Kozima, M. Ohmori and M. Ohta, "Nuclear Transmutations in Critical and Supra-critical Electrolysis with Graphite, Pd, W, Re, Pt and Au Cathodes Analyzed by the TNCF Model," *Proc. JCF17*, **17-12**, pp. 89-147 (2017), ISSN 2187-2260, [http://jcfirs.org/proc\\_jcf.html](http://jcfirs.org/proc_jcf.html).
- [Kozima 2017b] H. Kozima, "The Sociology of the Cold Fusion Phenomenon – An Essay –," *Proc. JCF17*, **17-13**, pp. 148 -219 (2017), ISSN 2187-2260, [http://jcfirs.org/proc\\_jcf.html](http://jcfirs.org/proc_jcf.html).
- [Kozima 2019a] H. Kozima, "Characteristics of Nuclear Reactions in the Cold Fusion Phenomenon," *Proc. JCF19*, **19-13** (2019) (to be submitted), ISSN 2187-2260.
- [Kozima 2019b] H. Kozima, "Development of the Solid State-Nuclear Physics," *Proc. JCF19*, **19-15** (2019) (to be submitted), ISSN 2187-2260.
- [Lietz 2008] H. Lietz, "Status of the Field of Condensed Matter Nuclear Science", Working Paper, Mittweida University, August 2008.
- [McKubre 1993] M.C.H. McKubre, S. Crouch-Baker, A.M. Riley, S.I. Smedley and F.L. Tanzella, "Excess Power Observed in Electrochemical Studies of the D/Pd System," *Proc. ICCF3* (Oct. 21 – 25, 1992, Nagoya, Japan), pp. 5 - 19, Universal Academy Press, Inc., Tokyo, 1993, ISBN: 4-946443-12-6.
- [Miley 1996a] G.H. Miley and J.A. Patterson, "Nuclear Transmutations in Thin-film Nickel Coatings undergoing Electrolysis," *J. New Energy*, **1**(3), pp. 5 – 38 (1996), ISSN 1086-8259.
- [Miley 1996b] G.H. Miley, G. Name, M.J.W. Williams, J.A. Patterson, J. Nix, D. Cravens and H. Hora, "Quantitative Observation of Transmutation Products occurring in Thin-film Coated Microspheres during Electrolysis," *Proc. ICCF6*, pp. 629 – 644 (1996).

- [Nakamura 1993] K. Nakamura, *Self-developing Life – A Story of Universality and Individuality* –, Tetsugaku-shobo, Tokyo, Japan, 1993, ISBN 4-88679-055-0 (Cited sentences are translated into English from original Japanese version by H.K.).
- [Plackett 1958] R.L. Plackett, “The Principle of the Arithmetic Mean,” *Biometrika*, **45**, Issue 1-2, pp. 130–135 (1958).
- [Plato P] Plato, *Phaedo*, translated into English by F. J. Church, The Liberal Arts Press, New York, First Edition, February, 1951, Reprinted, August, 1954. (And also B. Jowett, Volume 1, Macmillan Co., (1982).)
- [Poincare 1902] H. Poincaré, *Science and Hypothesis* (1902). Translated by W.J.G., Dover Publications Inc. 1952. Library of Congress Catalog Card Number 53-13673.
- [Prigogine 1984] I. Prigogine and I. Stengers, *Order out of Chaos – Man’s New Dialogue with Nature* –, Bantam Books, Toronto (1984), ISBN 0-553-34082-4.
- [Storms 2007] E. Storms, *The Science of Low Energy Nuclear Reaction – A Comprehensive Compilation of Evidence and Explanations about Cold Fusion* –, World Scientific, Singapore, 2007, ISBN-10 981-270-620-8
- [Study Design 101]  
<https://himmelfarb.gwu.edu/tutorials/studydesign101/metaanalyses.html>
- [Suess 1956] H.E. Suess and H.C. Urey, “Abundance of the Elements,” *Rev. Mod. Physics*, **28**, pp. 53 – 74 (1956).
- [Tsutani 2003] K. Tsutani, “Examination of Evidence in EBM,” *Therapeutic Research*, **24**, No. 8, pp. 1415 – 1422 (2003) (in Japanese).
- [Walker 2008] E. Walker, A.V. Hernandez and M.W. Kattan, “Meta-analysis: Its strengths and limitations”. *Cleve. Clinic. J. Med.* **75** (6): 431–9, (2008), PMID 18595551.

## **Development of the Solid State-Nuclear Physics**

Hideo Kozima

Cold Fusion Research Laboratory, Shizuoka, Japan

E-mail: hjrfq930@ybb.ne.jp

### **Abstract**

Investigation of the cold fusion phenomenon (CFP) for about 30 years since its discovery in PdD<sub>x</sub> by M. Fleischmann et al. in 1989 has revealed existence of nuclear reactions in specific solids (CF materials) at near room-temperature without any mechanism of acceleration for particles in the system. The *Cold Fusion Phenomenon* (CFP) is defined as a phenomenon including nuclear reactions observed in such materials (CF materials) composed of host elements and hydrogen isotopes as transition-metal hydrides and deuterides, hydrogen graphite, XLPE (cross-linked polyethylene) and microbial cultures. The diverse and complex experimental data, obtained in the CF materials and piled up in vast amounts in these years, have been riddles for almost all scientists. The experimental facts observed in this field, however, suggest existence of new mechanisms for nuclear reactions in the CF materials. The new mechanism for the CFP should be a fundamental element of a new physics, the solid state-nuclear physics (SSNP), in between solid state physics (condensed matter physics) and nuclear physics. It should be noticed that we have observed some effects belonging to the SSNP in solid state physics and in nuclear physics prior to the discovery of the CFP in which there are mechanisms related to the CFP.

We have developed a phenomenological approach to the CFP with a model (TNCF Model) to understand the complex data sets obtained in this field, as a whole. The approach has been successful to give a unified interpretation for the CFP and suggests an outline of the SSNP where neutrons in the CF materials play the leading role for realization of the nuclear reactions. The fundamental premises assumed in the TNCF model have been investigated quantum mechanically taking up properties of protons ( $p$ ) and deuterons ( $d$ ) in CF materials and also novel features of the nuclear structure of host elements ( $M$ ) in them. The extended wavefunctions of protons  $p$  (or deuterons  $d$ ) at interstitial sites and the intranuclear structure of nuclei at lattice sites (lattice nuclei) seem to be essential to the CFP when the interstitial protons (deuterons) and the lattice nuclei form a superlattice (metal-hydrogen superlattice).

The inductive reasoning and meta-analysis applicable to the complex experimental

data sets have given logical legitimation of our phenomenological approach performed using the TNCF model. The successes of the TNCF and the succeeding ND model to understand the CFP as a whole should be understood as an evidence of the fundamental role of neutrons assumed in the models to understand the CFP. The existence of neutron energy bands (neutron bands, for short) with neutrons in them, when there is a metal-hydrogen superlattice, is a new important fact in the solid state-nuclear physics discovered by the CFP. The neutrons in the CF materials are responsible not only to the CFP but also to the super-diffusivity of hydrogen in some transition metals observed for more than 100 years.

**Keywords:** solid state-nuclear physics, carbon-hydrogen superlattice, cold fusion phenomenon, nuclear transmutation, CF materials, metal-hydrogen superlattice, super-nuclear interaction, neutron energy band, cf-matter

## 1. Introduction

Quantum mechanical treatments of microscopic objects, atoms, nuclei and elementary particles, have a common difficulty related to the many-body problem common in classical mechanics and quantum mechanics; the three-body problem is, in general, impossible to solve exactly in the classical mechanics as well-known in the history of mechanics. The situation is the same in quantum mechanics; we have to depend on some approximations to treat the many-body system even if there are only linear but not nonlinear interactions between components. In the systems where are nonlinear interactions, we have to encounter with complexity leaving the fundamental equations applicable only to linear systems in classical and also in quantum mechanical objects.

Since 1920s when the quantum mechanics was established we have investigated the physical events occurring in the microscopic world around us at energy ranges from 1 K to  $10^4$  K on a temperature scale ( $1 \text{ K} = 1.38 \times 10^{-23} \text{ J}$ ) in nuclear physics and also in solid state physics (a part of the condensed matter physics).

Nuclear physics is the physics of a system where the principal interaction between components of the system is the nuclear force; the short-range, strong interaction between nucleons with some other characteristics. The other interactions such as electromagnetic and contact interactions work in such subordinate cases as the Knight shift and the electron capture by an unstable nucleus.

Solid state physics is the physics of a system composed of atomic nuclei and electrons where the principal interaction between particles is electromagnetic. The nuclear interaction works in such subordinate phenomena in this field as the neutron diffraction

and Moessbauer effect.

*Solid State-Nuclear Physics (SSNP)* in between the nuclear physics and the solid state physics may be defined as “the physics of a system composed of atomic nuclei, including protons and neutrons, and electrons in which the nuclear force between nucleons plays an essential role in addition to the electromagnetic force.” Though this definition includes some ambiguities, we have not much trouble with them in the following discussion.

It is convenient to define the cold fusion phenomenon as follows for further discussion. The *Cold Fusion Phenomenon (CFP)* is a phenomenon including nuclear reactions observed in such materials composed of host elements and hydrogen isotopes (CF materials) as transition-metal hydrides and deuterides, hydrogen graphite, XLPE (cross-linked polyethylene) and microbial cultures. It should be noticed that the CFP has given a decisive influence since its discovery on the establishment of the Solid State-Nuclear Physics as explained in this paper.

It is also emphasized that the investigation of the CFP revealed the restoration of the induction (or the inductive reasoning) superior over the deduction (or deductive reasoning) for such a problem in dynamical systems as the CFP where the behavior of particles interacting nonlinearly is governed by complexity. The deduction considered to be the most effective logic to deduce a conclusion starting from an established principle becomes ineffective when the principle does not define a logic leading to a conclusion but to indefinite conclusions with probabilities.

In Section 2, we briefly overview the microscopic world to understand the situation treated in atomic physics and nuclear physics developed in the 20<sup>th</sup> century. We also give examples of events belonging to the SSNP in solid state and nuclear physics investigated prior to the discovery of the CFP. The discovery of the CFP by chance in the search of new energy source have given a motivation to establish the solid state-nuclear physics as explained in this paper.

In Section 3, we explain that the novel feature of the SSNP revealed by the CFP has been explained by formation of a new state of neutrons, the *neutron energy band*, in the CF materials. The formation of the neutron energy band is realized when there is a *metal-hydrogen superlattice* [Bradley 1932] which is self-organized in a host lattice (transition metal or carbon) containing a hydrogen isotope (H or D) with high concentration. The *super-nuclear interaction* between neutrons in different lattice nuclei, mediated by protons/deuterons at interstices coupled with lattice nuclei through the nuclear interaction plays the principal role in the formation of the neutron energy band.

In Section 4, we discuss the meaning of the development of the solid state-nuclear physics in terms of logical structure of science in general. Possible applications of the

CFP will be discussed briefly.

## **2. Solid State Physics and Nuclear Physics in terms of the Cold Fusion Phenomenon**

In this section, we recollect the solid state physics and the nuclear physics from the viewpoint of the solid state-nuclear physics (SSNP) to notice that the effects of the nuclear force have appeared in the former and the effect of environments outside nucleus in the latter already prior to the discovery of the CFP. The fundamental characteristic of the CFP is the nuclear reaction occurring in the CF materials while there have been observed no events related to nuclear reactions in the SSNP before the year of 1989 even if the nuclear force works there in addition to the electromagnetic force.

To show the outline of the historical developments, a flowchart of the SSNP in relation to the solid state physics and the nuclear physics is given in Appendix A as Fig. A1.

### **2.1 Effects of the Nuclear Force in Solid State Physics**

The solid state physics is a science of atoms and molecules in the condensed state. It is inevitably a science of the many-body system where the leading actors are atoms and electrons interacting mainly with the long-range electromagnetic force and occasionally with other interactions like the hyperfine interaction between an electron and a nucleus and the strong interaction between nucleons. The latter interactions have given a few examples of the solid state-nuclear physics in the extended fields of the solid state physics.

It should be noticed here that the extraordinary large diffusivity (let us call it the *super-diffusivity*) of hydrogen isotopes in some transition metals and their alloys has been a riddle for more than 150 years since the phenomenon was observed by T. Graham [Graham 1866]. In the materials where occurs the super-diffusivity (e.g. [Voelkl (1978), Fukai (2005)]), there has been observed the CFP as we have noticed already [Kozima 2006 (Sec. 3.6), 2014 (Appendix A3)]. The close relation of the super-diffusivity and the CFP is discussed in Sec. 3 and it is suggested that the super-diffusivity should be treated as a phenomenon in the solid state-nuclear physics.

#### **2.1-1 Electromagnetic and Hyperfine Interactions**

Even if almost all phenomena occurring in condensed matters, solids and liquids, reflect the electromagnetic interaction among particles in the system, there are some effects reflecting the hyperfine interaction between a nucleus and an electron, such as the Knight shift [Knight 1949, 1956], and the nuclear interaction (strong force) between a proton and a neutron as pointed out in the next subsection.

## 2.1-2 Nuclear Interaction between Atoms and Nucleons in Solids

In a condensed matter, there occur sometimes the nuclear interactions between nuclei of host atoms and a nucleon or a nucleus of an exotic atom [Seitz 1956]. Most popular phenomena in this genre are the radiation damage and the Moessbauer effect. We give their brief explanation below from our present viewpoint.

### Radiation Damage

Since Silk and Barnes [Silk 1959] observed the tracks of uranium fission fragments on the mica films, the formation of latent tracks by heavy charged particles in solids has been recognized as one of fundamental phenomena of the radiation damage. And then, the investigation of the latent tracks became an important device for detection of charged particles by the success of etch-pit technique developed by Price and Walker [Pryce 1962]. The technique to identify incident charged particles using their latent tracks in target solid-state detectors, especially CR-39, has been developed enthusiastically and used widely in many fields of science including the CFP [Kozima 2013a].

Radiation damages are the most widely investigated theme in the solid state-nuclear physics due to their importance in modern world where various kinds of radiation are influencing human activities. Its importance will surely increase furthermore in future. We give only a glimpse on the present status of this theme leaving its further discussion elsewhere.

The radiation damages have been investigated mainly in three cases where one of three radiations, charged particles, electromagnetic waves (mainly X-rays and gamma rays) and neutrons, interacts with matter.

### Mössbauer Effect [Mössbauer 1958]

The **Mössbauer effect**, or **recoilless nuclear resonance fluorescence**, is a physical phenomenon discovered by R. Mössbauer in 1958. It involves the resonant and recoil-free emission and absorption of gamma radiation by atomic nuclei bound in a solid. Its main application is in Mössbauer spectroscopy [Frauenfelder 1962, Silsbee 1964].

In the Mössbauer effect, a narrow resonance for the nuclear gamma emission and absorption results from the momentum of recoil being delivered to a surrounding crystal lattice rather than to the emitting or absorbing nucleus alone. When this occurs, no gamma energy is lost to the kinetic energy of recoiling nuclei at either the emitting or absorbing end of a gamma transition; emission and absorption occur at the same energy, resulting

in strong, resonant absorption.

### 2.1-3 Neutron Diffraction and Neutron Waveguides

In addition to the above examples of the solid state-nuclear physics, we have an important genre of the solid state-nuclear physics caused by the interaction between a neutron and host nuclei in the solids (e.g. [Kothari 1959]). The neutron-nuclear interaction is most effectively investigated and utilized as the neutron diffraction [Shull 1956, 1995] for the structural analysis in solid state physics and recently as the neutron waveguide to guide a neutron beam from the source to a place where the beam is used.

Looking for historical basis of the neutron-solid interaction, we have noticed profound researches originating from the work by E. Fermi in 1936 [Fermi 1936, Golub 1990]. Especially interesting is the interaction of thermal neutrons with solids reviewed by Kothari and Singwi [Kothari 1959]. There have been many works on the neutrons in crystals interacting with lattice nuclei through the strong interaction [Scheckenhofer 1977, Steinhauser 1980] in addition to that due to the magnetic interaction [Hino 1998] as discussed in our paper [Kozima 2016a], however, lacking the formation of the neutron energy band we have noticed in our previous works [Kozima 1998a (Sec. 12.4), 1998b, 2004, 2006a (Sec. 3.7.2)], perhaps, due to the finite life of free neutrons. We will give our opinion on this problem and our answer in this paper (especially in Section 3.3).

In the metal-hydrogen superlattice in CF materials, the interaction of neutrons in host nuclei and protons/deuterons at interstices through the nuclear force should be treated as a many-body problem. In this paper, however, we have to consider the situation in a simplified manner using a single-particle approximation as a problem of neutron energy band formation mediated by the proton/deuteron sublattice in CF materials, a specific array of host elements and hydrogen isotopes [Kozima 2013b (Figs. 3.8 and 3.9), 2016a]. This situation reminds us the liquid drop and the shell models for the nucleus composed of nucleons interacting through the nuclear force. In our case, the correspondence to these models is many-body and single-particle approximations for the neutrons interacting with the super-nuclear interaction.

It is an obvious one-step by above investigations to attain the neutron energy band structure such as the electron energy band [Kozima 2016a (Fig. A3)] while the step is not traced due, perhaps, to the finite life time  $889 \pm 3$  s of the free neutron. However, it is easy to infer from the experimental data for neutron transmission obtained in the potential steps similar to the Kronig-Penny potential [Steinhauser 1980 (Fig. 3), Kozima 2016a (Fig. 5.3)] that the neutron energy band is formed in such a potential as the Kronig-Penny one for an electron [Kozima 2016a (Fig. A2)].

## 2.2 Effects of Environment to Nucleus in Nuclear Physics

The nuclear physics is a science of protons and neutrons in a close distance of about  $10^{-15}$  m (meter), mainly in a nucleus and at close encounters of nucleons and nuclei in free space (the scattering and the collision) (e.g. [Blatt 1952]). It is also a science of the many-body system but the number of participating particles is drastically few compared to that in the solid state physics. Another characteristic of this science is the shortness and large strength of the nuclear force – the force among protons and neutrons – with a range  $R_0$  of about 1 fm =  $10^{-15}$  m (meter) and energy/ $R_0$  of about 1 MeV/ $R_0$ . Another characteristic of the nuclear force is its saturation property – the number of particles with simultaneous interaction has a limit while the electromagnetic force in the solid state physics has no such limitation.

### 2.2-1 Stable and Unstable Nuclei

Atomic nuclei in their stable state with definite numbers of a proton number  $Z$  and a nucleon number  $A$  have been investigated extensively in these 100 years after their discovery. On the other hand, the atomic nuclei at their unstable or quasi-stable states are in their investigation especially if they are in the exotic composition with large imbalances of  $A$  and  $Z$  from their values of the stable nuclei. The exotic nuclei are in quasi-stable state but are able to participate new phenomena in the solid state-nuclear physics as shown in Section 3.3 and also discussed in Section 3.5. Several phases of the exotic nuclei is taken up in the next subsection.

### 2.2-2 Quasi-stable Nuclei

The exotic nuclei with large shifts of  $A$  or  $Z$  from those in stable nuclei have been extensively investigated recently [Caurier 2005, Cizewski 2010, Sharp 2013, Morfouace 2014, Sahin 2015, Stroberg 2015]. The properties of the exotic nuclei, especially their life time and distribution of neutrons in them, are interesting from our point of view in terms of the interaction between the interstitial proton/deuteron and neutrons in lattice nuclei in the CF material. The instability of the exotic nuclei may be decreased by their interaction with interstitial protons/deuterons in the CF material as discussed in our papers (e.g. [Kozima 2016a]).

### 2.2-3 Effects of Environment on the Nuclear Properties

In the nuclear physics, there are a few examples of events where the environment around a nuclear particle (a nucleus or a nucleon) affects the properties of the particle; the

electron capture (EC) by an unstable nucleus (a radioactive decay mode of unstable nuclei) (e.g. [Blatt 1952 (XIII, 3 Orbital electron capture)], the neutron trap and waveguide to confine neutrons [Kozima 2016a], the chain reaction of fission reactions of uranium or plutonium (e.g. [Anderson 1939]), the successive reaction of fusion reactions of hydrogen isotopes (e.g. [Chen 1974 (Chapter 9 Introduction to Controlled Fusion)]).

The Mössbauer Effect discussed in Section 2.1-2 is a process in which a nucleus emits or absorbs gamma rays without loss of energy to a nuclear recoil. It was discovered by the German physicist Rudolf L. Mössbauer in 1958 and has proved to be remarkably useful for basic research in physics and chemistry. It has been used, for instance, in precise measurement of small energy changes in nuclei, atoms, and crystals induced by electrical, magnetic, or gravitational fields.

These examples in the nuclear physics, however, are not necessarily recognized as the events in the solid state-nuclear physics due, perhaps, to the fact that this field is not established yet.

### **3. Solid State-Nuclear Physics (SSNP)**

The solid state-nuclear physics (SSNP) is the physics between the solid state physics and the nuclear physics, both of which have developed accompanied with the development of the quantum mechanics from the beginning of the 20<sup>th</sup> century. The solid state-nuclear physics developed faintly in between the two key branches of physics, the solid state physics and the nuclear physics, as described briefly in Sec. 2 until 1989, when astonishing phenomenon called the cold fusion phenomenon (CFP) including various events showing unexpected nuclear reactions in solids was discovered.

It is difficult to believe in occurrence of nuclear reactions in solids at near room temperature without any acceleration mechanism for particles in them if we have no own experience to detect events inexplicable without nuclear reactions in the solids. The author has had such an experience to observe neutron emission from an electrolytic system Pd/LiOH+D<sub>2</sub>O/Pt that gave him confidence in existence of the CFP [Kozima 1990].

We would like to emphasize the fact that the CF materials (i.e. the materials where occurs the CFP) are not confined to deuterium but also protium systems. And then, the CF materials are classified into two groups by the mechanism of formation of the active structure, the superlattice of the host element and hydrogen [Kozima 2013b], for the nuclear reaction in the CFP; (1) metal-hydrogen system; transition-metal hydrides (e.g. NiH<sub>x</sub>, AuH<sub>x</sub>) and deuterides (e.g. PdD<sub>x</sub>, TiD<sub>x</sub>) and hydrogen graphite (HC<sub>x</sub>), and (2) carbon-hydrogen system; XLPE, microorganisms, microbial cultures and biological

tissues.

In the first group (1), the *metal-hydrogen superlattice* (the metal includes transition metals and graphite in this division) responsible to the CFP is formed in the CF materials by the self-organization, a process characterized by complexity, in the dynamical process of component particles [Kozima 2013b]. In the second group (2), on the other hand, the carbon-hydrogen superlattice, i.e. C-H superlattice, is a rearranged ready-made structure in the hydrocarbons in the system [Kozima 2016b, 2018].

In the discussion of the quantum mechanical explanation of the CFP, it is convenient to use a word “*metal-hydrogen superlattice*” for the superlattice composed of a sublattice of the host element (C, Ti, Ni, Pd, - - -) and another of a hydrogen isotope (H, D, (T)). Carbon is classified usually into the non-metals with other elements silicon, germanium, tin, and lead in the same Group IVA. However, it is also well-known that graphite, one of carbon’s two allotropic forms, is unique among nonmetals showing a high conductivity [Sorum 1955 (p. 493)], a characteristic of the metal. Graphite is one of two forms of carbon where we have observed the CFP in addition to another ready-made superlattice in carbon-hydrogen system, XLPE and organic molecules in microorganism. Therefore, graphite shows similar characteristics to other metals, Ti, Ni, and Pd, in the CFP. Due to the property of carbon in the form of graphite, we may be able to classify the carbon, in the form of graphite, as a metal in our discussion of the neutron energy band for the basis of the TNCF model [Kozima 1998b, 2013b, 2015].

As we have discussed in a recent paper [Kozima 2018], the CFP in the CF materials belonging to the second group (2) is interesting in terms of the application of the nuclear transmutation. On the other hand, in the first group (1), there are many materials interesting in terms of the solid state physics. Therefore, we concentrate our discussion to them in this paper.

We have to notice two characteristics of the CFP. At first, it should be noticed that the energy scale we encounter in the CFP ranges very wide from 10 meV to 10 MeV on an electron volt scale: The outcome of the nuclear reactions of an order of 1 MeV has been enormously larger than the thermal energies of participating particles of an order of 25 meV by about nine orders of magnitude. This large difference of the liberated energy and the energy of environmental particles may have some decisive effects on the physics of the CFP. Secondly, one of the characteristics of the CFP we have to notice is the variety of products; we observed particles from neutron, helium-4, and various transmuted nuclei. These two extraordinary characteristics of the CFP opened a new perspective of the SSNP as we show in this section.

Because of the complex nature of the physics of the CFP related closely with the

complexity based on the nonlinear interactions among participating elements in the CF materials [Kozima 2013b], the essential nature of the events in the CFP had not been recognized at first just as the case of the continental drift theory in geophysics as illustrated in our recent paper [Kozima 2019a (Appendix B)]. A brief explanation of the situation by the figure is cited in Appendix B in this paper.

The success of a phenomenological approach using the TNCF model [Kozima 1998a, 2006a] as explained briefly in Sec. 3.2 and the quantum mechanical explanation of the premises of the model [Kozima 2006a, 2019b] as explained briefly in Sec. 3.3 have shown new features of the SSNP where the neutrons in host nuclei at lattice sites (lattice nuclei) and the hydrogen isotopes at interstices (interstitial hydrogens) play fundamental roles. This situation in the solid state-nuclear physics developed by the CFP is explained in Secs. 3.4 and 3.5.

### **3-1 Cold Fusion Phenomenon (CFP)**

In specific solid state materials at near room temperature, various observables have been measured which are explicable only by assuming nuclear reactions since 1989; the most typical observables have been neutrons and new nuclei different from those existed in the materials prior to the experiment. And then, therefore, the extravagant excess heat has been also observed which is inexplicable by chemical reactions and physical processes without nuclear reactions.

This phenomenon should be called the cold fusion phenomenon (CFP) to distinguish it from other events in the SSNP occurring in similar materials explicable physically without nuclear reactions. The phenomenon is fairly complex and it is necessary to explain them thorough investigation of experimental conditions for the CFP which are given in the next section.

It is well-known that the CFP defined above has had an unfortunate fate destined by its initial start at 1989. Details of this situation have been explained in a paper published in 2017 [Kozima 2017].

In the following sections, we give facts in the CFP revealed by experiments obtained in these about 30 years. We have given a unified explanation for the whole experimental data sets by a phenomenological approach with a model with an adjustable parameter (the TNCF model). Investigation of the bases of the TNCF model successful to give a unified explanation for the CFP is left to the next chapter.

#### **3-1-1 Experimental Facts of the CFP**

The CFP is characterized by events explained only by assuming nuclear reactions in

CF materials as briefly explained above. Furthermore, the events in this field are irreproducible or have no quantitative reproducibility and have only the qualitative reproducibility. This characteristic of the events in the CFP is best illustrated by the elaborate experimental result obtained by McKubre et al. [McKubre 1993]. In their experiment, they obtained various CF materials with different average D/Pd values and different excess powers for the same D/Pd value, for example as shown in their Fig. 7 [McKubre 1993 (Fig. 7)]. This characteristic of the CFP has been explained in our papers by the formation of the metal-hydrogen superlattice by the self-organization process of complexity (e.g. [Kozima 2013]).

It should be added another cause of irreproducibility of events in the CFP. As we have mentioned several times (e.g. [Kozima 1998a, 2006a]), the liberated energy in the nuclear reaction is in the energy range of about million electron volts (MeV) that is eight orders of magnitude larger than the thermal energy of particles in the CF material. Therefore, the liberated energy heat up the lattice around the reaction site over the melting points of the CF material. This phenomenon has been observed very often as shown in many papers, e.g. in our book [Kozima 2006a (Fig. 2.3)] and in a paper by Ohmori [Ohmori 2016 (Fig. 34)]. This phenomenon shows that the CF material is damaged badly by the liberated heat of the nuclear reactions and the metal-hydrogen superlattice responsible to the nuclear reactions is deteriorated by the loss of the *cf-matter* (cf. Section 3.3). Thus, the nuclear reaction of the CFP has a finite life and the CF material should be renovated to recover its ability for the CFP. This is another cause of the irreproducibility or qualitative reproducibility of the events in the CFP.

We explain fundamental characteristics of the CFP in the following subsections.

### 3-1-1a Characteristics of CF Materials or Necessary Conditions for the CFP

As we have shown in our books and papers (e.g. [Kozima 2006a, 2013]), the CF materials where observed the CFP have common characteristics that the concentrations of the host element and the hydrogen isotopes are comparable. Furthermore, the host elements are limited to some of the transition metals and carbon. We can list up the CF materials as follows;

- (a) Transition metal hydrides (and deuterides) with a ratio  $x_1$  of the concentration  $C_H$  of H (or D) and that  $C_M$  of the host element M (M = Ti, Ni, Pd, Au, Pt, - -),  $x_1 = C_H / C_M$ , larger than a threshold value  $x_1 \geq x_{1th} \approx 0.8$ . Typical CF materials in this group are PdD<sub>x</sub>, NiH<sub>x</sub>, AuH<sub>x</sub>, PtH<sub>x</sub>, - - - ( $x_1 \approx 1$ ). Let us call the ratio  $x_1$  the *concentration index*, or *Index 1*.
- (b) Hydrogen-Graphite

- CH<sub>x</sub> ( $x_1 \leq 1$  or  $\approx 1$ )
- (c) XLPE (cross-linked polyethylene)  
(C<sub>2</sub>H<sub>4</sub>)<sub>x</sub> ( $x = \infty$ ) ( $x_1 = 2$ )
- (d) Microorganisms  
Microbial cultures (microbiological culture), yeast, biological textures and organs. ( $x_1 = 1 - 2$ )

In other words, the characteristics of the CF materials listed up above in items (a) – (d) are the necessary conditions for the materials where the CFP occurs in them. *The concentration index, Index 1, should be close to or more than 1 for a material to be the CF material.*

As we have given a brief explanation at the beginning of Section 3, the CF materials listed up above are classified into two groups by another standard; (A) Metal-hydrogen system and (B) carbon-hydrogen system according to their characteristics in formation of the *superlattice*, a structure responsible for the CFP. Their characteristics are explained as follows;

(A) Metal-hydrogen system.

In this classification, the metal includes graphite in addition to such transition metals as Ti, Ni, Pd, Pt, and Au. In this system, the CF material is formed increasing the hydrogen isotopes to make the Index 1,  $x_1$ , close to or more than 1.

The *metal-hydrogen superlattice* in this group is composed of a sublattice of the host element M (i.e. C, Ti, Ni, Pd, Pt and others) and another of the hydrogen isotope (H or D) and is formed by the *self-organization* in the process of experiments.

(B) Carbon-hydrogen system.

The CF materials in this group include XLPE (cross-linked polyethylene) and microorganisms. In this system, the Index 1,  $x_1$ , is automatically larger than 1. The superlattice of C and H are formed by appropriate rearrangements of polymers composing the material. Therefore, it is easier to obtain the *carbon-hydrogen superlattice* responsible to the CFP compared to it in the case (A) where the concentration of M and H/D has to be adjusted to be comparable and the superlattice is formed by the self-organization, a process governed by complexity.

It is convenient to define the second index, *Index 2*,  $x_2$ , specifying the metal-hydrogen superlattice in the case (A) and the carbon-hydrogen superlattice in the case (B) for the CF material related to the realization of the CFP. The Index 2, the *superlattice index*  $x_2$ ,

is defined as the proportion of the superlattice to the whole CF material. It is essential to increase  $x_2$  in an experiment for realization of the CFP.

As a whole, there are two important indices characterizing the CF materials for the CFP;

- (1) *The concentration index*  $x_1$  (Index 1), defined as  $x_1 = C_H / C_M$  where  $C_H$  is the concentration of H (or D) and  $C_M$  is the concentration of the host element M (M = Ti, Ni, Pd, Au, Pt, - -). (Threshold value of  $x_1$  for the CFP is supposed to be  $x_{1th} \approx 0.8$ )
- (2) *The superlattice index*  $x_2$  (Index 2), defined as the proportion of the superlattice to the whole CF material. ( $0 \leq x_2 \leq 1$ )

### **3-1-1b Nuclear Structure of Specific Elements composing Host Lattices of the CF Materials**

The host elements in the CF materials for the CFP taken up in Sec. 3-1-1a are rearranged according to their physical characteristics as follows;

- (a) Transition metals,  
Ti, Ni, Pd, Au, Pt, - - -
- (b) Carbon in the following forms;
  - b-1 Graphite (C)
  - b-2 Polyethylene (C<sub>2</sub>H<sub>4</sub>)<sub>x</sub> ( $x = \infty$ )
  - b-3 Microbial (Microbiological) cultures

These elements, transition metals and carbon, have following common characteristics in their nuclear structure [Kozima 2004 (Sec. 2.4), 2006b, 2014a]; the neutron energy levels are located at around the evaporation level of their nuclei. These energy levels may be responsible to the formation of the superlattice through the neutron-proton/deuteron interaction discussed in Section 3.3.2.

### **3-1-2 Three Laws found in Experimental Data in the CFP**

We have induced three laws (or regularities) between observables from experimental data sets obtained in more than 20 years using the meta-analysis [Kozima 2006a (Sec. 3.8), 2012, 2019a]. The three laws are explained briefly as follows.

- 1) The First Law; The stability law for nuclear transmutation products

This law is induced using many experimental data obtained in various CF materials having different characteristics. The induction of this law is an example of the meta-analysis explained in another paper [Kozima 2019a] presented in this Conference. The

process inducing this law in our phenomenological approach gives also an example of the inductive logic rather than the deductive logic as explained there.

- 2) The Second Law; The inverse power dependence of the frequency on the intensity of the excess heat production

This law shows also the effectiveness of the meta-analysis in the CFP. The deduction of the inverse-power law by Lietz [Lietz 2008] had used 157 excess heat results obtained by different authors in various CF materials. This is a miniature meta-analysis for the process used in the medical science as illustrated in another paper presented in this Conference [Kozima 2019a].

- 3) The Third Law; Bifurcation of the intensity of events (neutron emission and excess heat production) in time

These laws and the necessary conditions for the CFP given in Sec. 3-1-1a tell us that the CFP is a phenomenon belonging to complexity induced by nonlinear interactions between agents in the open and nonequilibrium CF materials [Kozima 2013b]. The characteristics of the CF materials for the CFP are investigated using our knowledge of the microscopic structure of the CF materials consulting to the complexity investigated in the nonlinear dynamics in relation to the three laws explained above [Kozima 2013b]. A computer simulation is proposed to reproduce an essential feature of the CFP using a simplified model system (a superlattice) composed of two interlaced sublattices; one sublattice of host nuclei with extended neutron wavefunctions and another of protons/deuterons with non-localized wavefunctions [Kozima 2012].

### **3-2 Explanation of the CFP by Phenomenological Models (TNCF Model and ND Model)**

We have given a unified and comprehensive explanation for the vast experimental data sets in the CFP obtained hitherto since 1989 using a phenomenological approach with the TNCF (trapped neutron catalyzed fusion) model proposed in 1994 [Kozima 1994] and ND (neutron drop) model developed from the TNCF model in 2000 [Kozima 2000, 2004, 2006a]. Investigation of the foundation of these models are given in recent papers [Kozima 2014a, 2014b].

Flow chart for the development of the solid state-nuclear physics is given in Appendix A which gives an outline of the relation between the two models and the nuclear physics.

The brief explanation of the TNCF model and the ND model is given below.

#### **3-2-1 TNCF Model (Trapped Neutron Catalyzed Fusion Model)**

The TNCF model is a phenomenological model with an adjustable parameter  $n_n$ , assumed to be a density of trapped neutrons behaving as a free particle interacting with only nuclei at disordered position in the CF material. In the interaction, the absorption cross section  $\sigma_{nX}$  by a nucleus X is taken tentatively the same as that determined in nuclear physics [Kozima 1998a, 2006a]. Other premises of the model than the existence of neutrons are assumed based on the experimental data. Quantum mechanical justification of the premises in the TNCF model is introduced in Section 3.3.

### 3-2-1a Experimental Data explained by the TNCF Model

The experimental data sets obtained in the cold fusion experiments until 1998 had been explained by the TNCF model as tabulated in Tables 11.2 and 11.3 of our book [Kozima 1998a] which are cited in Appendix C as Tables C-1 and C-2.

These Tables show that the parameter  $n_n$  of the model takes appropriate values for various experiments (Sec. 3-2-1b) and the model gives the semi-quantitative explanation for the numerical relations among observables (Sec. 3-2-1c).

### 3-2-1b Value Range of the Parameter $n_n$

The values of  $n_n$  determined by the TNCF model for experimental data sets are in a range  $10^8 - 10^{12} \text{ cm}^{-3}$  as seen in Tables C-1 and C-2. This finite range of the value  $n_n$  might be an indirect evidence of the applicability of the model for the CFP.

### 3-2-1c Relations between Observables explained

Another evidence of the availability of the TNCF model for the CFP is the quantitative explanation of the numerical relations between several observables by the model [Kozima 2006a (Sec. 2.15.1)].

The experimental data sets showing nuclear transmutations along with other observables such as excess energy  $Q$ , the number and the energy of emitted neutrons  $n$ , and generated tritium  $t$ , had been analyzed by the TNCF model as shown in Tables C-1 and C-2. The results of the analyses had shown the applicability of the model to explain the CFP as a whole; the parameter  $n_n$  is determined as in between  $10^8 - 10^{12} \text{ cm}^{-3}$  as explained in Sec. 3-2-1b and the theoretical ratio  $N_a/N_b|_{\text{th}}$  of the numbers  $N_a$  and  $N_b$  of events  $a$  and  $b$  is in accordance with the experimental ratio  $N_a/N_b|_{\text{ex}}$  in a factor 3.

$$N_a/N_b|_{\text{th}} = m N_a/N_b|_{\text{ex}} (m \leq 3).$$

### 3-2-2 ND Model (Neutron Drop Model)

The experimental data sets had been explained by the TNCF model when there is a

single trapped neutron participating to the nuclear reactions in the CFP. While the model had given semi-quantitative explanations for many data in the CFP including the nuclear transmutations, there remained a large number of data sets where observed nuclear transmutations with large shifts of proton and neutron numbers from pre-existed nuclei. In these cases, we have to assume existence of neutron drops  ${}^A_Z\Delta$  consisted of several neutrons and protons [Kozima 2006a (Sec. 3.7)] in addition to the possibility of nuclear fissions as discussed already [Kozima 1998a (Sec. 9.2), 2014a (Sec. 2.4)]. In this paper, we concentrate to the development of the TNCF model to the ND (neutron drop) model as explained in the next Section.

### **3-3 Development of the Solid State-Nuclear Physics – Formation of the Metal-Hydrogen Superlattice and a New State realized by Neutron-Proton/Deuteron Interaction**

The experimental facts in the CFP and a unified phenomenological explanation for them have been given in the preceding section 3.2 using the TNCF model with an adjustable parameter  $n_n$ . The premises assumed in the TNCF model should be key concepts in the solid state-nuclear physics closely related to physics involved in the CFP if we consider the success of the model.

In this section, we investigate the physics of the CFP through the investigation of premises in relation to the physical properties of the CF materials where observed the CFP.

#### **3-3-1 Physical Foundation for the Parameter $n_n$ assumed in the TNCF Model – The cf-matter and the neutron drop**

The central premise of the TNCF model, existence of neutrons in the CF material is investigated quantum mechanically in the solid composed of a lattice of host element M and another lattice of hydrogen isotope (H or D) interlaced to the former. Because of the nonlinear interaction among M and H/D, the system is governed by complexity and we cannot expect the cause-effect correspondence existing in linear dynamical systems. Furthermore, there occur various processes inherent in the system governed by complexity. One of the interesting effects closely related to the CFP is the self-organization of a low energy state, in our case the superlattice of M and H/D [Kozima 2006a (Sections 2.4, 3.5 and 3.7), 2016a]. This point is summarized below in the next section 3-3-2 in terms of the CFP.

#### **3-3-2 Formation of the Metal-Hydrogen Superlattice and Origin of the Trapped**

## Neutrons

In the CF materials composed of a metal and hydrogen (metal-hydrogen system), the ordered array of the metal atom and proton (or deuteron) forms a stable structure, i.e. the metal occludes hydrogen (deuterium) [Wicke 1978]. Therefore, the metal-hydrogen superlattice may be realized there by the self-organization, a process of complexity, when the densities of both components are comparable.

The CF materials, thus, are classified into two materials, (1) the metal-hydrogen system and (2) the carbon-hydrogen system. And then, the situation proceeds as follows for the realization of the CFP;

- (1) In the metal-hydrogen system, the first process is *occlusion of H(D)* into the solid of host element  ${}^A_ZX$  up to a considerable (average) ratio of  $H(D)/X \geq H(D)/X|_{th} \approx 0.8$  by a dynamical process (electrolysis, gas contact, discharge, etc.).
- (2) Then, there is *the self-organization of the superlattice XH/D* composed of a sublattice X and another H/D at a region where the ratio  $H(D)/X \approx 1$  [Kozima 2013b]. The threshold value for the self-organization of the superlattice was given experimentally as  $D/Pd|_{th} \approx 0.85$  [McKubre 1993].

The following processes are common to both systems.

- (3) The nuclear interaction between a neutron in a lattice nucleus and a proton/deuteron at an interstice (the neutron-proton/deuteron interaction) results in *the super-nuclear interaction* between two neutrons in adjacent lattice nuclei.
- (4) Formation of *neutron energy bands* by the super-nuclear interaction between neutrons in lattice nuclei.
- (5) Formation of *high density neutrons* by accumulation of neutrons in the neutron energy bands at boundaries of the superlattice [Kozima 2006a (Sec. 3.7.3)].
- (6) Formation of *the cf-matter* of neutrons and protons including *neutron drops*  ${}^A_Z\Delta$  composed of Z protons and  $(A - Z)$  neutrons fed by the dynamical process. [Kozima 2006a (Sec. 3.7.4)]
- (7) Interaction of neutron drops with disordered nuclei at boundaries of and in the superlattice resulting in *nuclear reactions*; nuclear transmutations, emission of neutrons and charged particles, and liberation of excess energy (cf. Sec. 3-4 below).
- (8) Destruction of the optimum structure to realize the cf-matter by the nuclear products and liberated energy in the nuclear reactions.

We give brief explanations of these individual processes in the following subsections.

### 3-3-2a Self-organization of Metal-Hydrogen Superlattice [Kozima 2013b].

In the CF materials composed of a metal and hydrogen (metal-hydrogen system), the process (2) is responsible to the CFP. It should be noticed that the formation of the metal-hydrogen superlattice makes energy of the system lower than before and therefore realize stabilization of specific states such as exotic nuclei with large extents of neutron numbers and formation of interstitial hydrogens with largely extended wavefunctions. These effect are the cause of and also the result of the metal-hydrogen superlattice.

It should be noticed that the shape of the CF materials has essential importance for occlusion of hydrogen isotopes into and for formation of the metal-hydrogen superlattice in them. The former is related to the Index 1 and the latter to the Index 2 defined in Sec. 3-1-1a. It is easier to have a more homogeneous distribution of hydrogen isotopes and therefore to realize a metal-hydrogen superlattice in the CF material with smaller size as far as it is durable. This point is exemplified by many data sets such as Notoya et al. [Notoya 1993, 1994a, 1994b], Miley et al. [Miley 1996a, 1996b], Kitamura et al. [Kitamura 2016, 2018] and Iwamura et al. [Iwamura 2018] (cf. also [Kozima 1998a (Sec. 7 Cold Fusion occurs in Hydrated Materials, Too)]).

### **3-3-2b Materials formed of Units with Superlattice Structure**

On the other hand, there are the wonderful natural substances containing molecules composed of the regular arrays of C and H; the XLPE (cross-linked polyethylene) and also microorganisms contain carbon-hydrogen superlattice by itself, as shown in our papers [Kozima 2015, 2016b]. The hydrocarbons can form a carbon-hydrogen superlattice only by regular arrangement of polymers. The specific effects of these superlattice existing in nature, however, have not attracted our interest if there have not observed the CFP in the XLPE as the water tree generation and in the microorganisms as the biotransmutation [Kozima 2018].

It has been a riddle of two centuries to observe nuclear transmutations in biological systems since the discovery of the increase of CaO in the daily excretion of chicken by Vauquelin in 1799 [Kozima 1998a (Sec. 10.1)].

The CF materials composed of intrinsic superlattice of C and H have an advantage in application of the CFP because of the ease to form the cf-matter in them [Kozima 2018].

### **3-3-3 The Super-Nuclear Interaction – Indirect Neutron-Neutron Interaction mediated by Protons/Deuterons**

It is known that the interstitial proton/deuteron has an extended wavefunctions overlapping with the nuclei at the nearest neighbor lattice sites in some metals such as Pd [Kozima 2006a (Section 3.6)]. The non-local wavefunction of occluded proton/deuteron

seems to have close correlation with the super-diffusivity of hydrogen/deuterium [Kozima 2009]. In such a case, there appears the nuclear interaction between an interstitial proton/deuteron and neutrons in a lattice nucleus (the *nuclear proton/deuteron-neutron interaction*).

When there is a metal-hydrogen superlattice with the nuclear proton/deuteron-neutron interaction, the neutrons in lattice nuclei interact each other by the *indirect neutron-neutron interaction* mediated by interstitial protons/deuterons [Kozima 2006a (Sec. 3.7), 2016a]. This interaction is attractive and lowers the total energy of the system. One of the effects of this indirect neutron-neutron interaction is the lowering of the neutrons in lattice nuclei and the formation of the neutron energy bands in the single-particle approximation.

### 3-3-4 Neutron Energy Band and Neutron Drops

For the many-body system composed of neutrons in lattice nuclei and protons/deuterons at interstitial sites, we can use the single-particle approximation for neutrons connected with the super-nuclear interaction [Kozima 2006a (Section 3.7)] as used in the energy band theory of electrons in solid state physics (e.g. [Kittel 1976 (Chapter 7)]). As noticed above, this situation corresponds to the liquid drop and the shell models for the nucleons interacting with the nuclear force which may give indirect support for the single-particle approximation for our trapped neutrons and for the neutron band formation figured out in our papers.

#### 3-3-4a Neutron Energy Bands

Using the tight-binding approximation for the energy band formation, we have given a formal deduction of the *neutron energy bands* [Kozima 2006a (Sec. 3.5.2), 2016a]. This is a quantum mechanical justification of the premise of the trapped neutron assumed in the TNCF model [Kozima 1994].

The analyses of experimental data sets given in our papers and compiled in our book had shown that the density of neutrons in a neutron energy band  $n_n$  should be larger than a threshold value  $n_{n|th} \approx 10^8 \text{ cm}^{-3}$  in the region of CF materials where the nuclear reactions occurred.

#### 3-3-4b CF-Matter and Neutron Drops

To explain the experimental data where observed nuclear transmutations with large shifts of the proton number  $Z$  and the nucleon number  $A$ , we proposed extension of the TNCF model to the ND (neutron drop) model where we assumed existence of *neutron drops*  ${}^A_Z\Delta$  composed of  $Z$  protons and  $(A - Z)$  neutrons in the *cf-matter*. [Kozima 2000,

2006a (Sec. 3.7)]

The density of neutrons in an energy band increases at a boundary region where a neutron Bloch wave reflected coherently and reaches very high as assumed in the simulation for the neutron star matter [Negele 1973]. In analogy, we can assume possibility to have the cf-matter, a state of the neutron in the neutron energy bands with very high density at the boundary of the CF material, similar to the neutron star matter investigated in nuclear physics in terms of the neutron star formation [Negele 1973].

In the neutron star matter, there appeared the Coulomb lattice as the neutron density increased in a neutron star matter assumed at first as homogeneous [Negele 1973]. In the CF material, there are a sublattice of host nuclei from the beginning. This difference of the initial condition may influence the final distribution of the neutron drops in the cf-matter while we assumed just their existence and interaction with disordered nuclei. This point is a serious problem to be investigated in relation to the formation of the neutron drops in the cf-matter in the CF material.

### **3-3-5 New State composed of Neutrons and Protons/Deuterons**

The nuclear interaction among neutrons in lattice nuclei and interstitial protons/deuterons resulting in the neutron energy band discussed above should induce a new state composed of neutrons and protons/deuterons where the neutron energy band is only its component seen from the neutron phase. The new state may be seen to contain the proton/deuteron energy band in the single-particle approximation if we see from the phase of the occluded hydrogen isotope. Even if the single-particle approximation for the neutrons in the CF material has given a foundation of the TNCF and ND models, the extent of the applicability of the neutron energy band figured out by the single-particle approximation is not certain.

The new state, however, is essentially a many-body state composed of neutrons and protons/deuterons interacting nonlinearly each other. Therefore, the images of the neutron energy band and the proton/deuteron energy band as used in explanation of the CFP by the single-particle approximation may be spurious and at most be partial views. We have to investigate the new state as the many-body state composed of neutrons and protons/deuterons interacting nonlinearly each other. Then, we are able to induce nuclear and atomic properties to give explanations for observables (in CFP, super-diffusion, etc.) measured in the CF materials hitherto.

In the following discussion, we remain in the single-particle approximation leaving the many-body treatment elsewhere. The nuclear fission for the nuclear transmutation in the CFP considered in our explanation of some experimental data sets [Kozima 2006a

(Sec. 2.5.3)] may have close connection with the latter case.

### **3-4 Interaction between Neutrons and Disordered Nuclei in the Metal-Hydrogen Superlattice resulting in Nuclear Reactions responsible to the CFP**

Neutrons in a neutron energy band in perfect superlattice (without disordered lattice nuclei and disordered hydrogen isotopes) do not interact neither with a lattice nucleus nor with a proton/deuteron. On the other hand, when there are disordered lattice nuclei or disordered protons/deuterons in the CF material, then band neutrons interact with them. The most popular disordered lattice nuclei exist at boundaries of the CF material which result in nuclear transmutations observed very often there in CF experiments [Kozima 1998a, 2006a, 2011, 2018].

### **3-5 Solid State-Nuclear Physics**

The formation of the metal-hydrogen superlattice by the interaction of lattice nuclei and interstitial protons/deuterons results in the cold fusion phenomenon on one hand and in the super-diffusivity (the extraordinary large diffusivity) of H/D in the solid state physics on the other. These events are fully understood only when we understand the physics of the metal-hydrogen superlattice composed of the specific host nuclei and the interstitial protons/deuterons [Kozima 2013b].

The interaction between lattice nuclei at lattice points and hydrogen isotopes at interstitials results in lowering of the energy of the whole CF materials composed of lattice nuclei and interstitial protons/deuterons. The formation of the neutron energy bands is an example of this interaction by the super-nuclear interaction between neutrons in different lattice nuclei [Kozima 2006a].

Another possible result in the lattice nuclei may be the stabilization of exotic nuclei with far excess neutron numbers over that of stable nuclei [Kozima 2014a]. The exotic nuclei are quasi-stable in free space but may possibly be stabilized by the interaction with occluded protons/deuterons.

The interaction between lattice nuclei and interstitial protons/deuterons results in stabilization of protons/deuterons occluded in CF materials. It has been noticed for more than 150 years that hydrogen is occluded in such transition metals as Ti, Ni, Pd, and their alloys and shows an extremely large diffusivity [Graham 1866]. In the transition-metal hydrides, the interaction of protons/deuterons mediated by neutrons in lattice nuclei may generate the proton/deuteron energy bands. In the low density limit, the protons in the proton valence band will move with a large diffusivity without interaction with lattice as

observed by experiments.

We can cite several sentences by solid state physicists.

“Casella has suggested that the hydrogen states excited in neutron scattering are *wave-mechanical band states*, and shows this to be in accord with experimental findings.” [Puska 1984 (p. 5393)]

“On the other hand, according to the calculations, self-trapping in the tetrahedral site is improbable, and thus hydrogen would not be localized at the tetrahedral site during the activation process, but *its wave function should be spread over several interstices*.” [Puska 1984 (p. 5383)]

There are several interesting facts in the behavior of protons in transition-metal hydrides not explicable with common sense of solid state physics.

“The pronounced maximum appearing in the longitudinal optic branch indicates *strong second neighbor D-D interactions* whose strength is comparable to *the first neighbor D-D interaction*.” [Springer 1978 (p. 85)]

“Consequently, Burch introduced the idea of a *repulsion of H atoms on next-nearest neighbor sites*, which would overcompensate *the attraction of nearest neighbor H atoms at high concentrations*.” [Wicke 1978 (p. 101)]

We may be able to shed a light to these problems using the formation of the proton/deuteron energy band, a counterpart of the neutron energy band, realized by the interaction among lattice nuclei and protons/deuterons.

The neutron energy band and the proton/deuteron energy band are in the single-particle approximation for the many-body system as we know well in the theory of the electron energy band. Therefore, the explanation of the CFP by the TNCF model based on the neutron energy bands is not complete and we are aware of some missing factors remaining outside of our treatment by our model. It is desirable to develop a many-body treatment of the neutron-proton/deuteron system in the metal-hydrogen superlattice.

Finally, we have to give a word on the electronic contribution to the solid state-nuclear physics. In the discussions of the transition-metal hydrides and deuterides, it has been discussed the effect of electronic states on the energy of the system (e.g. [Wicke 1978 (Section 3.2)]). Therefore, the effect of electronic states on the solid state-nuclear physics is not negligible and should be taken into consideration in addition to the nuclear interactions among host elements and interstitial hydrogen isotopes emphasized in this paper.

## 4. Conclusion

In the history of science in the 20<sup>th</sup> century, the solid state physics has developed where the various phenomena occurring in solids have been explained by quantum mechanics considering mainly the electromagnetic interaction between particles in the solids (e.g. [Seitz 1940, Kittel 1976]). The physics of these treatments composes the solid state physics containing very wide fields of phenomena depending on the variety of materials, observables and environments in the energy range from  $10^{-3}$  K up to  $10^4$  K on a temperature scale, or  $10^{-7}$  eV up to 10 eV on an energy scale.

On the other hand, the nuclear physics has developed where the phenomena occurring in the nucleus and among nuclei are investigated by quantum mechanics also where the main interactions are the strong and the weak interactions between participating particles, nucleons and mesons (e.g. [Blatt 1952, Bohr 1969]). There are very many features of phenomena in the energy range from a few million electron volts (MeV) up to a few giga electron volts (GeV) in this field.

There have been investigated few phenomena observed and investigated by quantum mechanics in the solid state-nuclear physics, the interdisciplinary region between the solid state physics and the nuclear physics, as pointed out in the Introduction of this paper. However, the situation changed drastically by the discovery of the CFP, a phenomenon including various events explicable only by nuclear reactions, in CF materials, characteristic solids composed of specific host elements and hydrogen isotopes, at near room temperature without any acceleration mechanism for the particles in the system. We have used the name the “*CF material*” to designate the material where observed the CFP.

In the process of unified explanation of the CFP observed in the metal-hydrogen system defined in Section 3-1-1a using a phenomenological approach with a model, it has been noticed importance of neutrons in the CF materials composed of host metals (including carbon) and hydrogen isotopes. In the investigation of the basic premises of the model, we could develop a new phase of the solid state-nuclear physics, the physics of metal-hydrogen superlattice which has not been recognized in the solid state physics and the nuclear physics.

The phenomena in solid state-nuclear physics, explained by the super-nuclear interaction between neutrons at different lattice nuclei mediated by interstitial hydrogen isotopes through the strong neutron-proton/deuteron interaction, have been observed in CF materials with a ratio  $x_1$ , the Index 1, of concentrations H/D vs. host elements X (X = C, Ti, Ni, Pd, Au, Pt, - -) larger than a threshold value  $x_{th} \approx 0.8$  for the CFP;  $x_1 \geq x_{1th}$ . This fact should be emphasized that the CFP has been observed in CF materials with  $x_1 \geq x_{1th} \approx 0.8$ .

This characteristic of the CFP is explicable by the self-organization of the superlattice of the lattice nuclei and the interstitial protons/deuterons [Kozima 2013b]. The favor of deuterium than protium in palladium systems ( $\text{PdD}_x$  and  $\text{PdH}_x$ ) for the CFP was explained by the larger diffusivity of deuteron than that of proton [Kozima 2013b (Fig. 3.2)].

The characteristic of nickel systems ( $\text{NiH}_x$ ) where is observed a lot of nuclear transmutations than in  $\text{PdD}_x$  system might be explained, from our point of view, by the higher densities of trapped neutrons in the cf-matter in the former than in the latter which will be shown by detailed investigation of the structure of both systems; their lattice structures, states of hydrogen isotopes, nuclear levels of host elements, and so forth.

In addition to the metal-hydrogen system discussed in this paper, there is another group in the CF materials, the carbon-hydrogen system including the XLPE and the microorganisms, where the Index 1,  $x_I$ , is larger than 1 by nature [Kozima 2008, 2016b, 2018]. The CFP has been observed in this carbon-hydrogen system for long [Kozima 1998 (Sec. 10.1), 2018]. It is amazing to know that our phenomenological approach successful for the CFP in the metal-hydrogen system has been similarly successful in the carbon-hydrogen system [Kozima 2008, 2016b].

We have to notice that there are several characteristics of host nuclei and interstitial hydrogen isotopes for the realization of the CFP. The host nuclei seem desirable to have excited neutron levels at around the evaporation level as seen in our paper [Kozima 2016a (Fig. 4.1)]. On the other hand, the proton/deuteron at an interstice should have wavefunctions extended to lattice points surrounding the interstitial site [Kozima 2009]. These conditions for the component particles guarantee the occurrence of the CFP on one hand and the super-diffusivity of hydrogen/deuterium in the host lattice on the other.

Finally, we want to discuss the logical structure of reasoning in science. As we have shown in another paper presented at this Conference [Kozima 2019a], induction and deduction are two logical methods used in mental activities for more than 2500 years since the Greek culture. The physics of the CFP may be one of typical examples of the inductive reasoning. In the method of analysis, the analyses used in the phenomenological approach to the CFP might be classified into the meta-analysis used from the 18<sup>th</sup> Century in astronomy and frequently in modern EMB (the evidence-based medicine) [Plackett 1958, Tsutani 2003, Walker 2008]. We have given an extensive discussion on the meaning of the meta-analysis in another paper [Kozima 2019a].

We are able to add a word on the comparison of the continental drift and the CFP given in Appendix B. The famous example of the success of the inductive logic in modern science is the continental drift model (e.g. [Gould 1977]) to explain the many facts suggesting the drift of continents; topographical, geophysical, geological, paleontological,

biogeographical and paleoclimatology [Kozima 2019a]. In the continental drift, the problem is the unknown mechanism of driving force for the drift in addition to disbelief in the inductive reasoning. In the CFP, the problem is lack of recognition that the CFP is a problem of complexity in which we could not expect the quantitative reproducibility.

The success of the phenomenological approach with the TNCF and ND models has been the natural result of approach based on the experimental results and unintentionally use of inductive logic and the meta-analysis in the investigation of the science of the CFP as a part of the solid state-nuclear physics.

In conclusion, the knowledge of neutrons in the CF materials we have had through the investigation of the CFP will give a first step to the science of the metal-hydrogen and the carbon-hydrogen systems in the solid state-nuclear physics. We can expect abundant fruits in this field where the investigation has just started.

## **Appendices**

Appendix A. *Flow Chart of the History of the Solid State Physics, the Nuclear Physics and the Solid State-Nuclear Physics*

Appendix B. *Continental Drift vs. Cold Fusion Phenomenon*

Appendix C. *Experimental Data Sets Explained by the TNCF Model*

## Appendix A. Flow Chart of the History of the Solid State Physics, the Nuclear Physics and the Solid State-Nuclear Physics

The development of the solid state-nuclear physics in relation to those of the solid state physics and the nuclear physics is shown in the flowchart in Fig. A1.

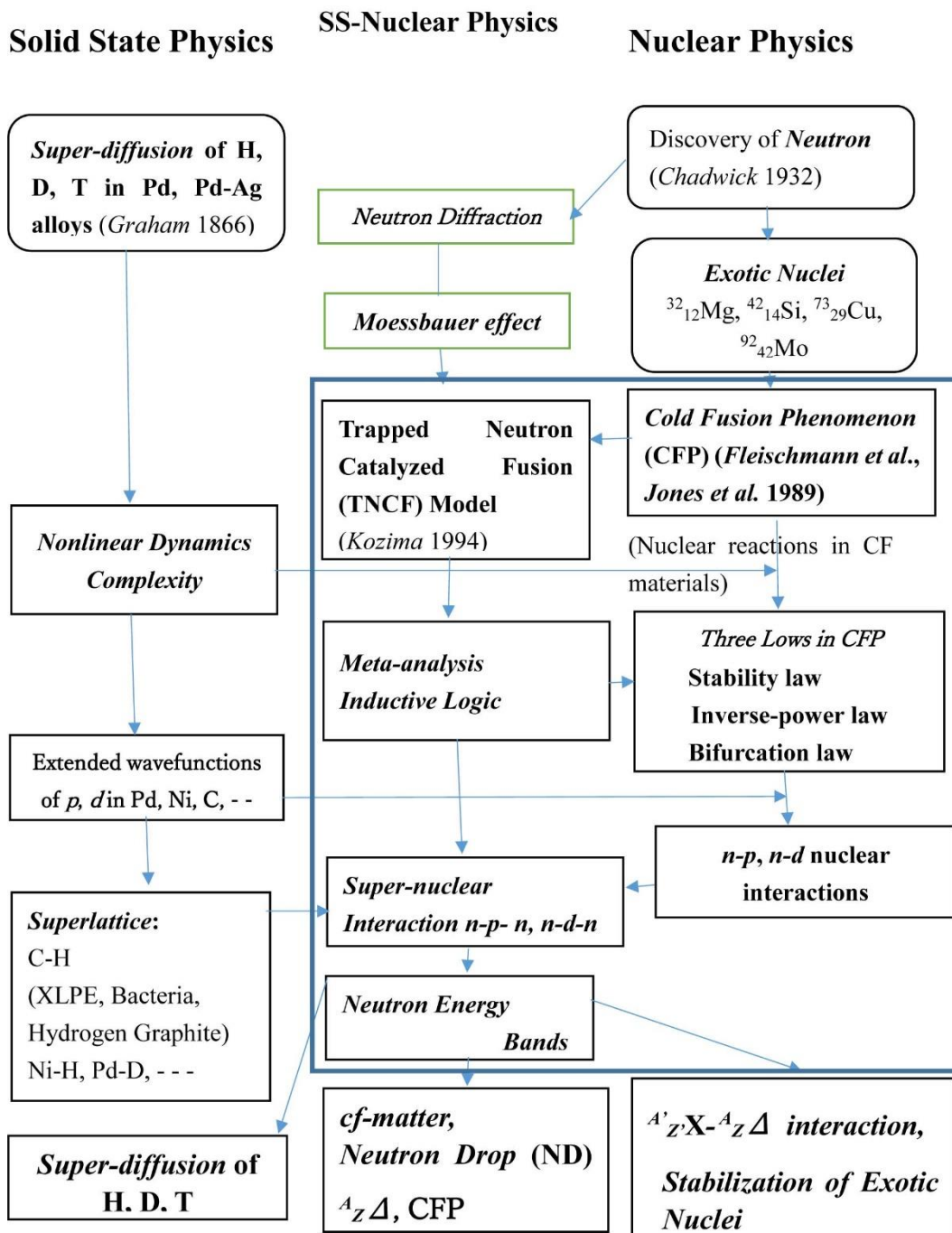


Fig. A1 Flowchart of the developments of the solids state-nuclear physics in relation to those of the solid state physics and the nuclear physics.

## Appendix B. Continental Drift vs. Cold Fusion Phenomenon

### Continental Drift

### Cold Fusion Phenomenon

#### 1. Phenomenon

1. The complementary arrangement of the facing sides of South America and Africa
2. Similar plant and animal [fossils](#) are found around the shores of different continents
3. The same animals being found on two continents
4. Widespread distribution of [Permo-Carboniferous](#) glacial sediments

1. Space distribution of Nuclear Transmutation products  $NT(r)$
2. Neutron energy spectrum  $n(\epsilon)$
3. Stabilization of unstable nuclei
4. Decrease of decay constants
5. Enormous excess energy  $Q$
6. Lowering of fission threshold energy

#### 2. Phenomenological Explanation

Continental drift

1. TNCF Model and
2. Neutron Drop (ND) Model

#### 3. Physical Bases of the Explanation

The theory of [plate tectonics](#) explains all following facts, including the movement of the continents, better than Wegener's theory.

1. Super-nuclear interaction of neutrons
2. Formation of neutron energy bands
3. Generation of the cf-matter at boundary regions
4. Formation of neutron drops in the cf-matter  ${}^A_Z\Delta$
5. Interaction of neutrons in the energy bands
6. TNCF and ND models explain almost all experimental data in CFP

Fig. B1 Explanation of the logical structure of the continental drift theory (left) in contrast to the case of the cold fusion phenomenon (CFP) (right).

## Appendix C. Experimental Data Sets Explained by the TNCF Model

Tables of experimental data sets of CFP in Pd/D/Li and Ni/H/K systems with explanation by the TNCF model.

**Table C-1** Pd/D/Li System and Others. Neutron Density  $n_n$  and Relations between the Numbers  $N_x$  of Event  $x$  Obtained by Theoretical Analysis of Experimental Data on TNCF Model ( $N_Q \equiv Q$  (MeV)/5 (MeV)). Typical value of the surface vs. volume ratio  $S/V$  ( $\text{cm}^{-1}$ ) of the sample is tabulated, also. Reference numbers are those of the original book. [Kozima 1998a] (Revised May, 2002) and the References is posted at CFRL website;

<http://www.kozima^cfrl/Books/bookse/bookse01.html>

Authors	System	$S/V$ $\text{cm}^{-1}$	Measured Quantities	$n_n$ $\text{cm}^{-3}$	Other Results (Remarks)
Fleischmann et al. <sup>1)</sup>	Pd/D/Li	6 ~40	$Q, t, n$ $N_t/N_n \sim 4 \times 10^7$ $N_Q/N_t \sim 0.25$	$\sim 10^9$	( $Q=10\text{W}/\text{cm}^3$ ) $N_t/N_n \sim 10^6$ $N_Q/N_t = 1.0$
Morrey et al. <sup>1-4)</sup>	Pd/D/Li	20	$Q, {}^4\text{He}$ ${}^4\text{He}$ in $\ell \leq 25\mu\text{m}$	$4.8 \times 10^8$	$N_Q/N_{He} \sim 5.4$ ( If 3% ${}^4\text{He}$ in Pd)
Packham <sup>43)</sup>	Pd/D/Li	40	$t$ in solution	$3.6 \times 10^7$	
Chien et al. <sup>43')</sup>	Pd/D/Li	4	${}^4\text{He}$ in surf. layer and $t$ , no ${}^3\text{He}$	$1.8 \times 10^6$	$N_t/N_{He} \sim 1$ (If few % ${}^4\text{He}$ in Pd)
Roulette <sup>177)</sup>	Pd/D/Li	63	$Q$	$\sim 10^{12}$	
Storms <sup>4)</sup>	Pd/D/Li	9	$t(1.8 \times 10^2 \text{Bq}/\text{m}\ell)$	$2.2 \times 10^7$	( $\tau=250\text{h}$ )
Storms <sup>4')</sup>	Pd/D/Li	22	$Q$ ( $Q_{max}=7\text{W}$ )	$5.5 \times 10^{10}$	( $\tau=120\text{h}$ )
Takahashi et al. <sup>5')</sup>	Pd/D/Li	2.7	$t, n$ $N_t/N_n \sim 6.7 \times 10^4$	$3 \times 10^5$	$N_t/N_n \sim$ $5.3 \times 10^5$
Miles et al. <sup>18')</sup>	Pd/D/Li	5	$Q, {}^4\text{He}$ ( $N_Q/N_{He}=1 \sim 10$ )	$\sim 10^{10}$	$N_Q/N_{He} \sim 5$
Okamoto et al. <sup>12')</sup>	Pd/D/Li	23	$Q, NT_D$ $\ell_0 \sim 1 \mu\text{m}$	$\sim 10^{10}$	$N_Q/N_{NT} \sim 1.4$ ( ${}^{27}\text{Al} \rightarrow {}^{28}\text{Si}$ ) (with ${}^{252}\text{Cf}$ )
Oya <sup>12-5)</sup>	Pd/D/Li	41	$Q, \gamma$ spectrum	$3.0 \times 10^9$	(with ${}^{252}\text{Cf}$ )
Arata. et al. <sup>14)</sup>	Pd/D/Li	7.5 $\times 10^4$	$Q, {}^4\text{He}$ ( $10^{20} \sim 10^{21}$ $\text{cm}^{-3}$ ) $N_Q/N_{He} \sim 6$	$\sim 10^{12}$	(Assume $t$ channeling in Pd wall)
McKubre <sup>3)</sup>	Pd/D/Li	125	$Q$ (& Formula)	$\sim 10^{10}$	Qualit. explan.
Passell <sup>377)</sup>	Pd/D/Li	400	$NT_D$	$1.1 \times 10^9$	$N_{NT}/N_Q = 2$
Cravens <sup>247)</sup>	Pd/H/Li	4000	$Q$ ( $Q_{out}/Q_{in}=3.8$ )	$8.5 \times 10^9$	(If PdD exists)
Bockris <sup>43)</sup>	Pd/D/Li	5.3	$t, {}^4\text{He}; N_t/N_{He} \sim 240$	$3.2 \times 10^6$	$N_t/N_{He} \sim 8$
Lipson <sup>15-4)</sup>	Pd/D/Na	200	$\gamma$ ( $E_\gamma=6.25\text{MeV}$ )	$4 \times 10^5$	If effic. =1%
Will <sup>45)</sup>	Pd/D <sub>2</sub> SO <sub>4</sub>	21	$t(1.8 \times 10^5/\text{cm}^2\text{s})$	$3.5 \times 10^7$	(If $\ell_0 \sim 10\mu\text{m}$ )
Cellucci et al. <sup>5177)</sup>	Pd/D/Li	40	$Q, {}^4\text{He}$ $N_Q/N_{He}=1 \sim 5$	$2.2 \times 10^9$	(If $Q=5\text{W}$ ) $N_Q/N_{He}=1$
Celani <sup>3277)</sup>	Pd/D/Li	400	$Q$ ( $Q_{max}=7 \text{W}$ )	$1.0 \times 10^{12}$	(If 200% output)
Ota <sup>53)</sup>	Pd/D/Li	10	$Q$ (113%)	$3.5 \times 10^{10}$	( $\tau=220 \text{h}$ )
Gozzi <sup>5177)</sup>	Pd/D/Li	14	$Q, t, {}^4\text{He}$	$\sim 10^{11}$	( $\tau \sim 10^3\text{h}$ )
Bush <sup>27')</sup>	Ag/Pd/Li	2000	$Q$ ( $Q_{max}=6\text{W}$ )	$1.1 \times 10^9$	( $\tau=54\text{d}$ , Film)
Mizuno 26-4)	Pd/D/Li (If Cr in Pd)	3.4	$Q, NT_D$ $\ell \leq 2 \mu\text{m}$ )	$2.6 \times 10^8$	$\tau=30\text{d}$ , Pd $1\text{cm}\phi \times 10\text{cm}$
Iwamura <sup>17)</sup>	PdD <sub>x</sub>	20	$n$ (400/s), $t$	$3.9 \times 10^8$	$4.4 \times 10^6 t/\text{s}$
Itoh <sup>17)</sup>	PdD <sub>x</sub>	13.3	$n$ (22/m), $t$	$8.7 \times 10^7$	$7.3 \times 10^{10} t/\text{s}$
Itoh <sup>177)</sup>	PdD <sub>x</sub>	13.3	$n$ ( $2.1 \times 10^3/\text{s}$ )	$3.9 \times 10^8$	
Iwamura 1777)	PdD <sub>x</sub>	20	$Q$ (4 W) $NT_F$ (Ti, Cr etc.)	$3.3 \times 10^{10}$	( $NT_F?$ unexplained)
Miley <sup>65)</sup>	Pd/H/Li	150	$NT_F$ (Ni, Zn, ...)	$4.5 \times 10^{12}$	
Dash <sup>59)</sup>	Pd/D, H <sub>2</sub> SO <sub>4</sub>	57	$Q, NT_D$	$\sim 10^{12}$	Pt $\rightarrow$ Au
Szpak et al. <sup>79-9)</sup>	Pd/D/Li	$10^3(?)$	$t$	$\sim 10^2$	Electroplated Pd
Clarke et al. <sup>80')</sup>	Pd/D/Li	0.26(?)	( $Q$ ), $t$	$\sim 10^{10}$	Pd black <sup>14)</sup>
Kozima <sup>203)</sup>	Pd/D, H/Li	200	$n$ ( $2.5 \times 10^{-4}/\text{s}$ )	$2.5 \times 10^2$	Effic. =0.44%

**Table C-2** Ni/H/K System and Others. Neutron Density  $n_n$  and Relations between the Numbers  $N_x$  of Event  $x$  Obtained by Theoretical Analysis of Experimental Data on TNCF Model ( $N_Q \equiv Q(\text{MeV})/5(\text{MeV})$ ). Typical value of the surface vs. volume ratio  $S/V(\text{cm}^{-1})$  of the sample is tabulated, also. Reference numbers are those of the original book. [Kozima 1998a] (Revised May, 2002) and the References is posted at CFRL website;

<http://www.kozima^cfri/Books/bookse/bookse01.html>

Authors	System	$S/V$ $\text{cm}^{-1}$	Measured Quantities	$n_n$ $\text{cm}^{-3}$	Other Results (Remarks)
Jones <sup>2)</sup>	Ti/D/Li	8.1	$n$ (2.45 MeV)	$3.1 \times 10^{11}$	
Mills <sup>25)</sup>	Ni/H/K	160	$Q$ (0.13 W)	$3.4 \times 10^{10}$	
Bush <sup>27)</sup>	Ni/H/K	$\sim 160$	$NT_D(\text{Ca})$	$5.3 \times 10^{10}$	$N_Q/N_{NT} \sim 3.5$ if $\tau=0$ for $^{40}\text{K}$ )
	Ni/H/Na	$\sim 160$	$NT_D(\text{Mg})$	$5.3 \times 10^{11}$	
Bush <sup>27')</sup>	Ni/H/Rb	$\sim 10^4$	$NT_D(\text{Sr})$	$1.6 \times 10^7$	$N_Q/N_{NT} \sim 3$
Savvatimova et al. <sup>34')</sup>	Pd/D <sub>2</sub>	100	$NT_D(\text{Ag})$	$9 \times 10^{10}$	
Bockris et al. <sup>43-6)</sup>	Pd/H/		$NT_F(\text{Mg, Si, Cs, Fe, etc. in } 1\mu\text{m layer})$	$3.0 \times 10^{11}$	Only Fe(10% of Pd) is taken up.
Alekseev <sup>44')</sup>	Mo/D <sub>2</sub>	4.1	$t$ ( $\sim 10^7/\text{s}$ )	$1.8 \times 10^7$	(If MoD)
Romodanov et al. <sup>44''')</sup>	TiC/D	4.1	$t$ ( $\sim 10^6/\text{s}$ )	$\sim 10^6$	(D/Ti $\sim$ 0.5 assumed)
Reifenschweiler <sup>38')</sup>	TiT <sub>0.0035</sub>	$7 \times 10^5$	$\beta$ decay reduction	$1.1 \times 10^9$	( $T=0 \sim 450^\circ\text{C}$ )
Dufour <sup>7)</sup>	Pd,SS/D <sub>2</sub> Pd,SS/H <sub>2</sub>	48	$Q, t, n$	$9.2 \times 10^{11}$ $4.0 \times 10^9$	(D(H)/Pd $\sim$ 1 is assumed)
Claytor <sup>9)</sup>	Pd/D <sub>2</sub>	400	$t$ (12.5 nCi/h)	$1.6 \times 10^{13}$	(If D/Pd $\sim$ 0.5)
Srinivasan <sup>16)</sup>	Ti/D <sub>2</sub>	1500	$t$ ( $t/d \sim 10^{-5}$ )	$1.9 \times 10^8$	(Aged plate)
De Ninno <sup>6)</sup>	Ti/D <sub>2</sub>	440	$n, t$	$1.2 \times 10^6$	(D/Ti=1,1w)
Focardi <sup>23)</sup>	Ni/H <sub>2</sub>	8.2	$Q$	$3.0 \times 10^{12}$	(If $N_p=10^{21}$ )
Oriani <sup>52)</sup>	SrCeO <sub>3</sub> /D <sub>2</sub>	22	$Q \sim 0.7\text{W}$	$4.0 \times 10^{10}$	$V=0.31\text{cm}^3$
Notoya <sup>35'')</sup>	Ni/D,H/K	$3.4 \times 10^4$	$Q$ (0.9 W), $t$	$2.4 \times 10^{13}$	(If $1/2 t$ is in liquid)
Notoya <sup>35-4)</sup>	Ni/D,H/K	same	$NT_D(\text{Ca})$	$1.4 \times 10^9$	(Sintered Ni)
Yamada <sup>54)</sup>	Pd/D <sub>2</sub>	185	$n, NT_D(\text{C})$	$2.0 \times 10^{12}$	
Cuevas <sup>55)</sup>	TiD <sub>1.5</sub>	134	$n$ (102 n/s)	$5.4 \times 10^{11}$	
Niedra <sup>56)</sup>	Ni/H/K	80	$Q$ (11.4 W)	$1.4 \times 10^9$	5km $\times$ 0.5mm $\phi$
Ohmori <sup>22'')</sup>	Au/H/K	200	$Q, NT_F(\text{Fe})$	$\sim 10^{11}$	(Au plate)
Li <sup>57)</sup>	Pd/D <sub>2</sub>	185	$Q$	$1.6 \times 10^{12}$	(Pd wire)
Qiao <sup>57')</sup>	Pd/H <sub>2</sub>	185	$NT_F(\text{Zn})$	$3.8 \times 10^{10}$	(40%NT in 1y)
Bressani <sup>58')</sup>	Ti/D <sub>2</sub>	$\leq 10^3?$	$n$ ( $\epsilon$ )	$10^4 - 10^7$	(Ti shaving)
Miley <sup>65')</sup>	Ni/H/Li	50	$NT_D(\text{Fe, Cr, } \dots)$	$1.7 \times 10^{12}$	
Botta <sup>58'')</sup>	Pd/D <sub>2</sub>	$\leq 10^3?$	$^4\text{He}$	$7 \times 10^{12}$	(0.1 mm Pd sheet)
Coupland et al <sup>81)</sup>	Pd/H,D	$\sim 4$	$\Delta(^7\text{Li}/^6\text{Li})=60-90\%$ if $(^7\text{Li}/^6\text{Li})_0=12.5$	$3.5-4.1 \times 10^8$	Pd rod returned by F. and P. <sup>1)</sup>
Passell <sup>3-6)</sup>	Pd/H <sub>2</sub>	185(?)	$\Delta(^7\text{Li}/^6\text{Li})=100\%$	$4.4 \times 10^8$	Pd wire <sup>57-3)</sup>

## Acknowledgement

The author would like to express his thanks to all people who had helped his work in this field in these more than 30 years since the year of 1989. Especially, he is thankful for the members of the former Kozima's Laboratory in the Shizuoka University and of the present Cold Fusion Research Laboratory. His thanks are especially to people who introduced him into and taught him physics since his high school days. Especially, he would like to point out following names who influenced his study very much. The late Mr. Yozo Hayashi, a physics teacher at the Tatebayashi High School, Gunma Prefecture, the late Prof. Yasutaro Takahashi at the Tokyo University of Science, the late Prof. Toshinosuke Muto at the Tokyo University, the late Dr. Kiyoe Kato at the Shizuoka University, the late Dr. Koji Husimi at the Nagoya University, and the late Dr. John Dash at the Portland State University. Finally, he is indebted to his wife Takako for her understanding and help in his work for more than 50 years.

## References

- [Anderson 1939] H. L. Anderson, E. Fermi, and Leo Szilárd. "Neutron production and absorption in uranium," *Physical Review*, **56**, 284–286 (1939).
- [Blatt 1952] J.M. Blatt and V.F. Weisskopf, *Theoretical Nuclear Physics*, John Wiley and sons, New York, 1952. ISBN-10: 0-471-08019-5.
- [Bohr 1969] A. Bohr and B.R. Mottelson, *Nuclear Structure I*, Benjamin, New York, 1969. ASIN: B0000EG4S6
- [Bradley 1932] A.J. Bradley and A.H. Jay, "The formation of Superlattices in Alloys in Iron and Aluminium". *Proc. R. Soc. A*. **136** (829): 210–232 (1932).
- [Caurier 2005] E. Caurier, G. Martínez-Pinedo, F. Nowacki, A. Poves and A. P. Zukeri, "The Shell Model as a Unified View of Nuclear Structure," *Rev. Mod. Phys.*, **77**, 427 – 488 (2005), ISSN 0034-6861.
- [Chen 1974] F.F. Chen, *Introduction to Plasma Physics*, Plenum Press, New York, 1974, ISBN 0-306-30755-3.
- [Cizewski 2010] J.A. Cizewski, K.L. Jones, R.L. Kozub, S.D. Pain and the ORRUBA/RIBENS Collaboration, "Single-particle Structure of Neutron-rich Nuclei," *Journal of Physics: Conference Series*, **239** (2010) 012007, doi:10.1088/1742-6596/239/1/012007.
- [Fleischmann 1989] M. Fleischmann, S. Pons and M. Hawkins, "Electrochemically induced Nuclear Fusion of Deuterium," *J. Electroanal. Chem.*, **261**, 301 – 308 (1989).
- [Frauenfelder 1962] H. Frauenfelder, *The Moessbauer Effect*, W.A. Benjamin Inc., New

- York, 1962, Library of Congress Catalogue Number 61-18181.
- [Fukai 2005] Y. Fukai, *The Metal-Hydrogen System – Basic Bulk Properties*, Springer, Berlin, 2005. USBN-10 3-540-00494-7.
- [Gould 1977] S.J. Gould, *Ever Since Darwin – Reflections in Natural History –*, W.W. Norton & Co., New York, 1977, ISBN 0-393-00917-3.
- [Graham 1866] [Graham 1866] T. Graham, *Philos. Trans. R. Soc. London*, **156**, p. 415 (1866).
- [Hino 1998] M. Hino, N. Achiwa, S. Tasaki, T. Ebisawa, T. Akiyoshi and T. Kawai, “Observation of Quasi-bound States of Neutron in Fabry-Perot Magnetic Thin Film Resonator using Larmor Precession,” *Physica B*, Vol. **241 – 243**, pp. 1083 – 1085 (1998). The revised and enlarged version of this paper is published in the following journal: M. Hino, N. Achiwa, S. Tasaki, T. Ebisawa, T. Kawai and D. Yamazaki, T. Kawai and D. Yamazaki, “Measurement of Spin-precession Angles of Resonant Tunneling Neutrons,” *Phys. Rev.*, **A61**, 013607-1 – 8 (2000).
- [Iwamura 2018] Y. Iwamura and other 16 authors, “Reproducibility on Anomalous Heat Generation by Metal Nanocomposites and Hydrogen Isotope Gas,” *Proc. JCF18*, pp. 32 – 44(2018), ISSN 2187-2260. [http://jcfrs.org/proc\\_jcf.html](http://jcfrs.org/proc_jcf.html)
- [Kitamura 2016] A. Kitamura, E. F. Marano, A. Takahashi, R. Seto, T. Yokose, A. Taniike and Y. Furuyama, “Heat evolution from zirconia-supported Ni-based nano-composite samples under exposure to hydrogen isotope gas”, *Proc. JCF16*, pp. 1-16 (2016), ISSN 2187-2260. [http://jcfrs.org/proc\\_jcf.html](http://jcfrs.org/proc_jcf.html)
- [Kitamura 2018] A. Kitamura and other 16 authors, “Comparison of excess heat evolution from zirconia-supported Pd-Ni nanocomposite samples with different Pd/Ni ratio under exposure to hydrogen isotope gases,” *Proc. JCF18*, pp. 14 – 31 (2018), ISSN 2187-2260. [http://jcfrs.org/proc\\_jcf.html](http://jcfrs.org/proc_jcf.html)
- [Kittel 1976] C. Kittel, *Introduction to Solid State Physics*, Fifth Edition, John Wiley & Sons, 1976, ISBN 0-471-49024-5.
- [Knight 1949] W.D. Knight, “Nuclear Magnetic Resonance Shift in Metals,” *Physical Review*, **76** (8): 1259–1260 (1949).
- [Knight 1956] W.D. Knight, “Electron Paramagnetism and Nuclear Magnetic Resonance in Metals,” in *Solid State Physics, Advances in Research and Applications*, Edit. F. Seitz and D. Turnbull, Vol. 2, pp. 93 – 136 (1956), Library of Congress Catalog Card Number: 55-12299.
- [Kothari 1959] L.S. Kothari and K.S. Singwi, “Interaction of Thermal Neutrons with Solids,” in *Solid State Physics, Advances in Research and Applications*, Edit. F. Seitz and D. Turnbull, Vol. 8, pp. 109 – 190 (1959), Library of Congress Catalog Card Number: 55-

12200.

[Kozima 1990] H. Kozima, S. Oe, K. Hasegawa, H. Suganuma, M. Fujii, T. Onojima, K. Sekido and M. Yasuda, “Experimental Investigation of the Electrochemically Induced Nuclear Fusion,” *Report of Faculty of Science, Shizuoka University*, **24**, pp. 29 -34 (1990), ISSN 0583-0923.

[Kozima 1994] H. Kozima, “Trapped Neutron Catalyzed Fusion of Deuterons and Protons in Inhomogeneous Solids,” *Transact. Fusion Technol.*, **26**, 508 – 515 (1994), ISSN: 0748-1896.

[Kozima 1998a] H. Kozima, *Discovery of the Cold Fusion Phenomenon – Development of Solid State-Nuclear Physics and the Energy Crisis in the 21<sup>st</sup> Century –*, Ohtake Shuppan Inc., 1998, ISBN 4-87186-044-2. The “References” in this book is posted at the CFRL (Cold Fusion Research Laboratory) Website;

<http://www.kozima^cfrl.com/Books/bookse/bookse.html>

[Kozima 1998b] H. Kozima, “Neutron Band in Solids,” *J. Phys. Soc. Japan* **67**, 3310 – 3311 (1998), ISSN 0031-9015. And also *Elemental Energy (Cold Fusion)* **28**, 30 – 34 (1998).

[Kozima 2000] H. Kozima. “Neutron Drop: Condensation of Neutrons in Metal Hydrides and Deuterides”, *Fusion, Technol.* **37**, 253 - 258 (2000), ISSN 0748-1896.

[Kozima 2004] H. Kozima, “Quantum Physics of Cold Fusion Phenomenon,” *Developments in Quantum Physics Researches – 2004*, pp. 167 – 196, Ed. V. Krasnoholovets, Nova Science Publishers, Inc., New York, 2004. ISBN 1-59454-003-9

[Kozima 2006a] H. Kozima, *The Science of the Cold Fusion Phenomenon, – In Search of the Physics and Chemistry behind Complex Experimental Data Sets –*, 1<sup>st</sup> Edition, Elsevier, Amsterdam, 2006, ISBN-13: 978-0-08045-110-7, ISBN-10: 0-080-45110-1.

[Kozima 2006b] H. Kozima, “Cold Fusion Phenomenon and Solid State Nuclear Physics,” *Proc. ICCF11*, pp. 769 – 775 (2006), ISBN 981-256-640-6.

[Kozima 2008] H. Kozima and H. Date, “Nuclear Transmutations in Polyethylene (XLPE) Films and Water Tree Generation in Them,” *Proc. ICCF14*, pp. 618 – 622 (2010), ISBN 978-0-578-06694-3.

[Kozima 2009] H. Kozima, “Non-localized Proton/Deuteron Wavefunctions and Neutron Bands in Transition-metal Hydrides/Deuterides,” *Proc. JCF9*, pp. 84 – 93 (2009), ISSN 2187-2260. [http://jcfrs.org/proc\\_jcf.html](http://jcfrs.org/proc_jcf.html)

[Kozima 2011] H. Kozima, “Localization of Nuclear Reactions in the Cold Fusion Phenomenon,” *Proc. JCF11*. pp. 59 –69 (2011), ISSN 2187-2260.

[http://jcfrs.org/proc\\_jcf.html](http://jcfrs.org/proc_jcf.html)

[Kozima 2012] H. Kozima, “Three Laws in the Cold Fusion Phenomenon and Their

Physical Meaning,” *Proc. JCF12* (Kobe, Japan, December 17 – 18, 2011), pp. 101 – 114 (2012), ISSN 2187-2260. [http://jcfirs.org/proc\\_jcf.html](http://jcfirs.org/proc_jcf.html)

[Kozima 2013a] H. Kozima, “Characteristics of Solid-State Nuclear Track Detectors for Heavy Charged Particles – A Review,” *Proc. JCF13* **13-12**, pp. 57 – 75 (2013), ISSN 2187-2260. [http://jcfirs.org/proc\\_jcf.html](http://jcfirs.org/proc_jcf.html)

[Kozima 2013b] H. Kozima, “Cold Fusion Phenomenon in Open, Nonequilibrium, Multi-component Systems – Self-organization of Optimum Structure,” *Proc. JCF13* **13-19**, pp. 134 - 157 (2013), ISSN 2187-2260.

[Kozima 2014a] H. Kozima and K. Kaki, “Atomic Nucleus and Neutron—Nuclear Physics Revisited with the Viewpoint of the Cold Fusion Phenomenon,” *Proc. JCF14*:**14-5**, pp. 47 -76 (2014), ISSN 2187-2260. [http://jcfirs.org/proc\\_jcf.html](http://jcfirs.org/proc_jcf.html)

[Kozima 2014b] H. Kozima, “Nuclear Transmutations (NTs) in Cold Fusion Phenomenon (CFP) and Nuclear Physics,” *Proc. JCF14*:**14-15**, pp. 168 - 202 (2014). ISSN 2187-2260. [http://jcfirs.org/file/proc\\_jcf.html](http://jcfirs.org/file/proc_jcf.html)

[Kozima 2015] H. Kozima, “The Nuclear Transmutations (NTs) in Carbon-Hydrogen Systems (Hydrogen Graphite, XLPE and Microbial Cultures),” *From the History of Cold Fusion Research*, **8**, pp. 1 – 23 (June 2015):

<http://www.kozima^cfri.com/Papers/paperf/paperf.html>.

[Kozima 2016a] H. Kozima and K. Kaki, “The Cold Fusion Phenomenon and Neutrons in Solids,” *Proc. JCF16*, **16-14**, 158 – 198 (2016), ISSN 2187-2260.

[Kozima 2016b] H. Kozima, “Biotransmutation as a Cold Fusion Phenomenon,” *Proc. JCF16*, **16-18**, pp. 216 – 239 (2016), ISSN 2187-2260.

[Kozima 2017] H. Kozima, “The Sociology of the Cold Fusion Research,” *Proc. JCF17*, pp. 148-219 (2017), ISSN 2187-2260.

[Kozima 2018] H. Kozima, “Nuclear Transmutations and Stabilization of Unstable Nuclei in the Cold Fusion Phenomenon,” *Reports of CFRL (Cold Fusion Research Laboratory)*, **18-1**, pp. 1 – 32 (June, 2018);

<http://www.kozima^cfri.com/Papers/paperr/paperr.html>.

The contracted version of this paper with the same title is published as *J. Condensed Matter Nucl. Sci.* **28**, 28 – 49 (2019), ISSN 2227-3123 in the *Proceedings of the International Conference on the Application of Microorganisms for the Radioactive Waste Treatment* posted at the CMNS website; <http://www.iscmns.org/CMNS/CMNS.htm>

This *Proceedings* is posted at LENR website also;

<https://www.lenr-canr.org/acrobat/BiberianJPjcondensedza.pdf>

[Kozima 2019a] H. Kozima, “Inductive Logic and Meta-analysis in the Cold Fusion Phenomenon,” *Proc. JCF19*, **19-14** (2019), ISSN 2187-2260 (to be published).

- [Kozima 2019b] *The Science of the Cold Fusion Phenomenon, – In Search of the Physics and Chemistry behind Complex Experimental Data Sets –*, 2<sup>nd</sup> Revised Edition, Elsevier, Amsterdam, 2018 (in preparation). Main revised sections in this version marked by an asterisk (\*) in the Contents of the book are posted at the CFRL website prior to the publication; <http://www.kozima^cfrl.com/Books/bookse/bookse.html>
- [Lietz 2008] H. Lietz, “Status of the Field of Condensed Matter Nuclear Science”, *Working Paper*, Mittweida University, August 2008.
- [Morfouace 2014] P. Morfouace and 19 others, “Single-particle Strength in Neutron-rich <sup>69</sup>Cu,” *Acta Physica Polonica*, **B45**, 243 – 248 (2014).
- [McKubre 1993] M.C.H. McKubre, S. Crouch-Baker, Riley, S.I. Smedley and F.L. Tanzella, "Excess Power Observed in Electrochemical Studies of the D/Pd System," *Proc. ICCF3* (Oct. 21 – 25, 1992, Nagoya, Japan) pp. 5 - 19, Universal Academy Press, Inc., Tokyo, 1993. ISSN 0915-8502.
- [Miley 1996a] G.H. Miley and J.A. Patterson, “Nuclear Transmutations in Thin-Film Nickel Coatings undergoing Electrolysis,” *J. New Energy (Proc. 2<sup>nd</sup> International Low Energy Nuclear Reactions Conference)*, **1 – 3**, pp. 5 – 30 (1996).
- [Miley 1996b] G.H. Miley, G. Narne, M.J. Williams, J.A. Patterson, J. Nix, D. Cravens and H. Hora, “Quantitative Observation of Transmutation Products occurring in Thin-Film Coated Microspheres during Electrolysis,” *Proc. ICCF6*, pp. 629 – 644 (1996).
- [Mössbauer 1958] R.L. Mössbauer, "Kernresonanzfluoreszenz von Gammastrahlung in Ir<sup>191</sup>". *Zeitschrift für Physik A* (in German), **151** (2): 124–143 (1958).
- [Negele 1973] J.W. Negele and D. Vautherin, “Neutron Star Matter at Sub-nuclear Densities,” *Nuclear Physics*, A207, 298 – 320 (1973).
- [Notoya 1993] R. Notoya, “Cold Fusion by Electrolysis in a Light Water-Potassium Carbonate Solution with a Nickel Electrodes,” *Fusion Technol.*, **24**, 202 – 204 (1993), ISSN 0748-1896.
- [Notoya 1994a] R. Notoya, “Alkali-Hydrogen Cold Fusion accompanied by 31H Production on Ni,” *Trans. Fusion Technol.*, **26**, 205 – 208 (1994), ISSN 0748-1896.
- [Notoya 1994b] R. Notoya, Y. Noya and T. Ohnishi, “Tritium Generation and Large Excess Heat Evolution by Electrolysis in Light and Heavy Water – Potassium Carbonate Solutions with Ni Electrodes,” *Fusion Technol.*, **26**, 179 – 183 (1994), ISSN 0748-1896.
- [Ohmori 2016] T. Ohmori, “Anomalous Reactions induced by Light and Heavy Water Electrolysis,” in *New Topics in Electrochemistry Research*, Ed. M. Nunez, pp. 47 – 84, Nova Science Publisher, 2016, ISBN 1-60021-015-5.
- [Plackett 1958] R.L. Plackett, The Principle of the Arithmetic Mean," *Biometrika*, **45**, pp. 130 – 135 (1958). Also published in *Studies in the History of Probability and Statistics*,

pp. 121 – 126, 1970, Eds. E.S. Pearson and M.G. Kendall, Griffin, London, ISBN 0-85264-193-1.

[Price 1962] P.B. Price and R.M. Walker, “A New Track Detector for Heavy Particle Studies,” *Phys. Lett.* **3**, 113 – 115 (1962).

[Puska 1984] M.J. Puska and R.M. Nieminen, “Theory of Hydrogen and Helium Impurities in Metals,” *Phys. Rev.* **29B**, pp. 5382 – 5397 (1984).

[Sahin 2015] E. Sahin and 73 others, “Shell Evolution Beyond  $N = 40$ :  $^{69,71,73}\text{Cu}$ ,” *Phys. Rev.*, **C91**, 0343021-1 – 9 (2015).

[Sharp 2013] D.K. Sharp and 19 others, “Neutron Single-particle Strength outside the  $N=50$  Core,” *Phys. Rev.*, **C 87**, 014312-1 – 11 (2013).

[Scheckenhofer 1977] H. Scheckenhofer and A. Steyerl, “Diffraction and Mirror Reflection of Ultracold Neutrons,” *Phys. Rev. Lett.*, **39**, 1310 – 1312 (1977).

[Seitz 1940] F. Seitz, *The Modern Theory of Solids*, McGraw Hill, New York, 1940, ISBN-10: 9780070560307.

[Seitz 1956] F. Seitz and J.S. Koehler, “Displacement of Atoms During Irradiation,” in *Solid State Physics – Advances in Research and Applications*, Vol. 2, pp. 305 – 448 (1956), Ed. F. Seitz and D. Turnbull, Academic Press, 1959, Library of Congress Catalog Card Number 55-12299.

[Shull 1956] C.G. Shull and E.O. Wollan, “Applications of Neutron Diffraction to Solid State Problems,” in *Solid State Physics, Advances in Research and Applications*, Vol. 2, Edit. F. Seitz and D. Turnbull, pp. 137 – 217 (1956), Academic Press, 1956, Library of Congress Catalog Number: 55-12299.

[Shull 1995] C.G. Shull, “Early development of neutron scattering,” *Rev. Mod. Phys.*, **67** 753–757 (1995), ISSN 0034-6861.

[Silk 1959] E.C.H. Silk and R.S. Barnes, “Examination of Fission Fragment Tracks with an Electron Microscope,” *Phil. Mag.* **4**, 970 – 972 (1959).

[Silsbee 1964] R.H. Silsbee and D.B. Fitchen, “Optical Analogs of the Mössbauer Effect in Solids,” *Rev. Mod. Phys.*, **36**, 432 – 436 (1964).

[Sorum 1955] C.H. Sorum, *Elementals of General Chemistry*, 2<sup>nd</sup> edition, Prentice-Hall, Inc., 1955, Library of Congress catalog Card Number 63-9842.

[Springer 1978] T. Springer, “Investigation of Vibrations in Metal Hydrides by Neutron Spectroscopy,” in *Hydrogen Metals I* (Ed. G. Alefeld and J. Voelkl), pp. 75 – 100 (1978).

[Steinhauser 1980] K.A. Steinhauser, A. Steyerl, H. Scheckenhofer, and S.S. Malik, “Observation of Quasibound States of the Neutron in Matter,” *Phys. Rev. Lett.*, **44**, 1306 – 1309 (1980).

[Storms 2007] E. Storms, *The Science of Low Energy Nuclear Reaction – A*

*Comprehensive Compilation of Evidence and Explanations about Cold Fusion* –, World Scientific, Singapore, 2007, ISBN-10 981-270-620-8.

[Stroberg 2015] S.R. Stroberg and 18 others, “Neutron Single-particle Strength in Silicon Isotopes: Constraining the Driving Forces of Shell Evolution,” arXiv:1504.02329v1 [nucl-ex] 9 Apr 2015..

[Tsutani 2003] K. Tsutani, “Examination of the Evidence in EBM (evidence-based medicine),” *Therapeutic Research* (0289-8020), 24, No. 8, pp. 1415-1422 (2003) (in Japanese). [Japanese title: EBM におけるエビデンスの吟味(解説)]

[Voelkl 1978] J. Voelkl and G. Alefeld, “Diffusion of Hydrogen in Metals,” in *Hydrogen in Metals I*, G. Alefeld and J. Voelkl ed., pp. 321 – 348. Springer, Berlin, 1978, ISBN 978-3-662-30846-2.

[Walker 2008] E. Walker, A.V. Hernandez and M.W. Kattan, “*Meta-analysis: Its strengths and limitations*”. *Cleve. Clinic. J Med.*, **75** (6), pp. 431– 439 (2008), [PMID 18595551](https://pubmed.ncbi.nlm.nih.gov/18595551/).

[Wicke 1978] E. Wicke and H. Brodowsky, “Hydrogen in Palladium and Palladium Alloys,” in *Hydrogen in Metals II* (Ed. G. Alefeld and J. Voelkl), pp. 73 – 155 (1978).

# Microstructure of Pd rod electrode during long-term electrolysis in 0.1 M LiOD and during repeated cathodic and anodic electrolysis in glycerin-phosphoric acid: Behavior of void related with vacancy-cluster

Hiroo NUMATA † †: (email: hiroonumata@gmail.com)

**Abstract** Long-term electrolysis of a thick Pd electrode in 0.1 M LiOD was performed. Some techniques to conduct clean and stable electrolysis are described. The post-electrolysis Pd electrode revealed a surface morphology with voids and two long faults without any cracks. To understand the evolution of this morphology, the physicochemical properties of hydrated Pd were studied by *in situ* potentiometric, resistance, and dilatometric measurements. The results of the microstructural changes, particularly the void behavior, were further analyzed by also considering the known characteristics of the H–Pd system.

**Keywords:** Pd, cold fusion, deuterium, electrode potential, resistance, dilation, void, hydrogen pressure-composition diagram, material science, lattice defect, vacancy

## 1. Morphology of deuterated thick Pd rod during long-term electrolysis in 0.1 M LiOD

### Introduction

Since Fleishmann and Pons [1] and Jones *et al.* [2] reported the possibility of cold fusion during electrolytic loading of deuterium in Pd at ambient temperatures, much work on reproducing nuclear fusion in condensed matter has been carried out [3–4]. In spite of much efforts to duplicate data of cold fusion experiments, there has been unsolved issue yet why some researchers encounter irreproducible experimental results. We assume that the poor reproducibility of cold fusion experiments has been attributed to localization of the reactive region and insufficient understanding of both optimal sample pretreatment methods and deuterium loading behavior. This report focuses on the electrolysis method for cold fusion experiments where deuterium charging is conducted by electrolysis in heavy water on a Pd electrode.

In Section 1, we describe the results of deuterium absorption on a well-annealed, thick Pd rod during long-term electrolysis in 0.1 M LiOD, accompanied with morphology observation of post-electrolysis Pd electrode. To improve the reproducibility of cold fusion experiments, a sample pretreatment method and experimental apparatus that enable a stable and clean long-term experiment are described. Takagi *et al.* observed a significant count rate of neutron (CRN) over background during long-term electrolysis on a Pd in 0.1 M LiOD at current densities of 0.04 to 0.10 A/cm<sup>2</sup> [5–6]. Microscopic observation of post-electrolysis Pd showed that long-term electrolysis for *ca.* 6 months did not show any surface crack but the anomaly in grain growth. Later we compare the surface and internal morphologies of post-electrolysis Pd sample with those of natural phenomenon of the earth, and discuss peculiar morphologies observed in deuterated Pd electrode.

The evidence of a cold fusion reaction in condensed matter can be found explicitly during deuterium charging in a Pd electrode. Then, the nuclear fusion reaction would be brought about by means of high pressure within a solid. However in an equilibrium state, the pressure is no greater than ten or several tens of atmosphere, which is not sufficient for this case. In a nonequilibrium state, e.g., crack formation might provide an

explanation. Since a cold fusion reaction would have to be accomplished by deuterium absorption in a Pd electrode along the generation of miscellaneous defects, the phase-changes and microstructural changes due to D absorption (i.e., D loading) are of interest, particularly with respect to the microstructural changes underneath the Pd surface. In Section 2 for a precise understanding of phase-changes and microstructural changes of a Pd electrode during H (D) absorption, the physicochemical properties of hydrated Pd have been studied by *in situ* potentiometric, resistance and dilatometric measurements. The results of microstructural changes were further analyzed with reference to the knowledge of metal–H interaction under a stress field.

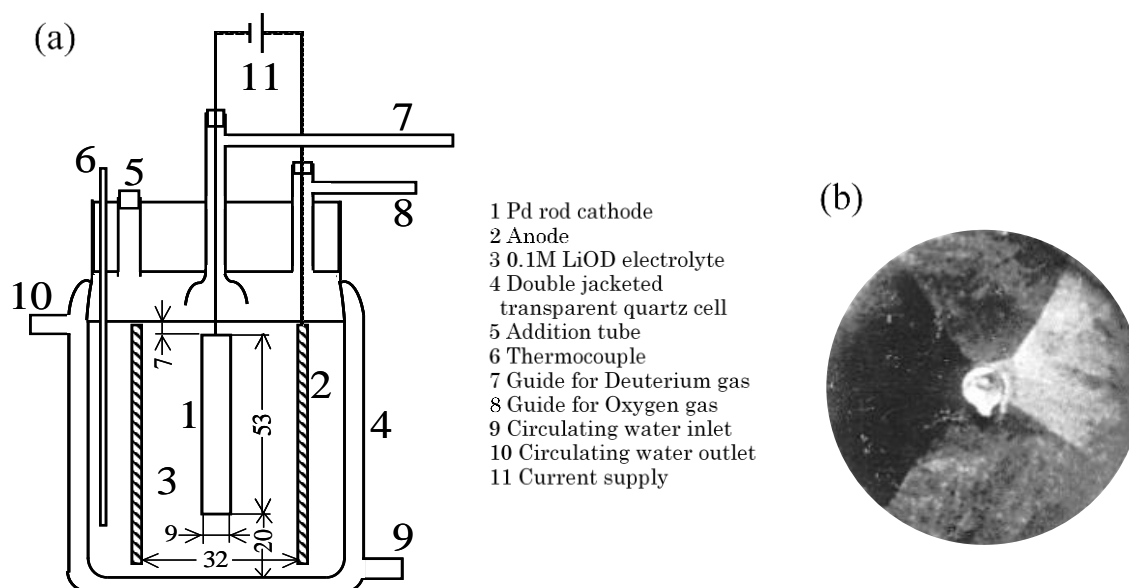
### Experimental

Cold fusion experiments were conducted at ambient temperatures by the electrolysis of heavy water on a Pd electrode and on other stable metals, such as Ni and Ti. An electrolytic cell, especially the dimensions and arrangement of the electrode, counter electrode, and electrolyte, is shown in Fig. 1a. The components of the measurement systems with regard to excess heat generation, neutron emission, and isothermal water bath to control the cell temperature are not shown. The experimental apparatus and detailed procedures are described below. The basic features of a good cell design are

- long-term preservation of pure electrolyte and clean electrolytic cell conditions,
- ensuring stable current supply lead for the Pd rod, and
- a stable reference electrode.

Moreover, a simple system without recombiner catalysts was devised. Therefore, the source of contamination was corrosion products from the surface of the cell components, that is, transparent quartz, bottom surface of a silicon rubber stopper, gold plating, dimensional stable like anode and Inconel 600 thermocouple sheath, which might be exposed to caustic alkali liquid and its film. In this experiment, for long-term the electrochemical cell, electrodes, and the accessories were kept clean, and thus the contaminants could mostly be attributed to periodic D<sub>2</sub>O replenishing.

Electrolyte: A 0.1 M LiOD solution was prepared by the addition of Li<sub>2</sub>O (Wako Pure



Figs 1a and b. Schematic diagram of electrolytic cell for deuterium absorption on a Pd electrode in 0.1 M LiOD (a), and Pd electrode's optical micrograph of cross-sectional surface area of electrode (b). The unit is in mm.

Chemicals: 95%) to D<sub>2</sub>O (Merck: 99.8%, CEA: 99.8%, and Isotech: 99.9%). The concentration of the LiOD solution was substantially increased during electrolysis by pouring a small amount of 0.1 M LiOD into the cell every day to replenish the exhausted solution. During the long-term electrolysis, incremental fills were made with pure heavy water to minimize the effect of electrolyte concentration on the electrochemical systems.

Electrolytic cell (about 130 mL content): The experimental cell was made of transparent quartz and had a water jacket. The temperature in the jacket was controlled at 40 and 50 ± 0.5 °C. The cell container needs to be corrosion resistant to the caustic hot aqueous solution, and hence Teflon could be satisfactory. As a result, transparent quartz was preferred here over conventional Pyrex and nontransparent quartz. The upper part of the cell had a silicone rubber stopper, where the working, reference, and counter electrodes and accessories (addition tube and the guide for the thermocouple) were mounted. The electrode potential was referred the potential of dynamic type ( $\alpha + \beta$ ) PdD reference electrode. The guide for the counter electrode served as the gas outlet port.

Electrode and electric leading: A gold-plated Ti rod (3 mm  $\phi$ ) served as the electric leading. The Ti rod was pretreated by abrasion and Ni strike plating before gold plating. It was screwed into the upper end of the Pd electrode. First trials of an electric leading, which were prepared by a Pd or Pt wire welded to a Pd electrode, were unsuccessful. The spot-welding breakdown caused by a mismatch between the Pd deformation and the leading due to deuterium absorption was frequently experienced.

Pd plates and thin rod electrodes were purchased from a conventional metal company. The as-received Pd electrodes were further processed by a preliminary treatment before use. On the other hand, the thick Pd rod was made by casting: high-purity Pd ingots were cast into a high-purity alumina tube in an argon flow (2 L/min). A high-frequency inductive furnace (100 kW, 30 kHz) was used for melting and casting. The heating rate was 30 °C/min for the first 50 min, followed by 3.6 °C/min for the next 50–80 min, until around 1600 °C when the Pd ingots melt. The Pd melt was kept at this temperature for 120 min. During the cooling phase, the cooling rate was 2.8 °C/min for the first 50 min, followed by 7.6 °C/min for the next 50–200 min. Subsequently the Pd cast electrodes exhibited highly grown grains, which was confirmed by optical microscopic observations.

Configuration of the working electrode and the counter electrode: The working electrode was placed approximately in the center of the cylindrical space circumscribed by the counter electrode (a mixed oxide of Pd and Rh). This ensures that the local current density on the surface of the working electrode is homogenous. Such an ideal cylindrical

Table 1. Experimental conditions of Exp. 1 and Exp. 2: electrode dimension, pretreatment and current density.

<b>Exp. 1: Dimension of electrode 9.0 <math>\phi</math>, 53 mm long</b>		
Run No.	Current, mAcm <sup>-2</sup>	Pretreatments
1st	0.05–40	Cast, 800 °C anneal (10 <sup>-6</sup> Torr) Acid treatment
	40–500	
2nd	40	Polishing, Acid treatment, Evacuation, Evacuation, Polishing, Acid treatment
3rd	40	
4th	40	
<b>Exp. 2: Dimension of electrode 21 <math>\phi</math>, 32 mm long</b>		
1st	0.05–102.4	Cast, 800 °C anneal (10 <sup>-6</sup> Torr) D <sub>2</sub> gas charge, Acid treatment

geometry facilitates D absorption, that is, the  $\alpha$  and  $\beta$  phases appearance is concentric, and therefore the stress state of the electrode is a function of radial distance (radial symmetry). If the electrode system is not cylindrically symmetric, an unsymmetrical stress evolved that causes unusual bending even if the applied composition and temperatures are the same for the differently shaped Pd electrodes.

We successfully performed non-intermittent electrolysis for 2 months and approximately for 6 months with two experimental runs, referred to as Exp. 1 and Exp. 2, respectively. The electrode geometry for Exp. 1 was 9 mm  $\phi$  and 5.3 cm long; that for Exp. 2 was 21 mm  $\phi$  and 3.2 cm long (Table 1). Following are the characteristics of both the experimental procedures [5–6]: (1) cast and thick Pd rod electrode, (2) pretreatment of the Pd electrode, (3) preparation of the gas phase for the absorption of D<sub>2</sub> (D/Pd = 0.36), (4) stepwise increase in electrolysis current density, and (5) temperature cycle.

The surface pretreatment and electrolysis conditions are shown in Table 1, and the results of neutron measurement are described elsewhere [5–6].

Microscopic observation: The sample surfaces were observed with an optical microscope and a scanning electron microscope (JEOL T-330, 20 kV). Microscopic observation of the electrode was made by sectioning the rod along the traverse and radial directions. The sectioned cross-sectional area was polished using a 6  $\mu$ m diamond paste. Then, it was lightly etched by dilute hydrochloric acid for optical microscopic observation.

## Results and discussion

### 1.1 Microstructure of thick Pd Rod and dilation under long-term electrolysis - Exp. 1

For the measurement of the diameter, a sample was dismantled from the cell after pausing the electrolysis. Measurements were taken at three different heights (top, middle and bottom as shown in Fig. 2). Then, the electrode was carefully reinstalled, and this procedure was repeated four times (see Table 1), where the duration periods ranged 2 months or less.

In Fig. 2 the dilation of the Pd electrode was plotted against the run number. For the first run, the dilation at the bottom end shows a maximum of 7%, while those in the upper regions exhibited a lesser dilation than that at the bottom. During the 2nd to 4th run the values at these positions asymptotically approached 7.8–8.3%. It is noted that a significant count rate of neutron (CRN) and an energy spectrum of 2.45 MeV appeared in the 1st run, where the largest dilatation occurred especially during the 1st run [5–6]. Although we have found no explanation for the relationship between the neutron emission and the largest expansion of a material, it is helpful in understanding phenomenon inside of the specimen through metallographic observation.

The microstructure of the cross-sectional surface area of the apex is shown in Fig. 1b. As shown in Fig. 1b, the sample as a whole consisted of four columnar grains (the cross-sectioned disk divided into four quadrants), each of which looked like they have grown inside from a crucible wall during cooling, from a metallographic aspect. Since such a

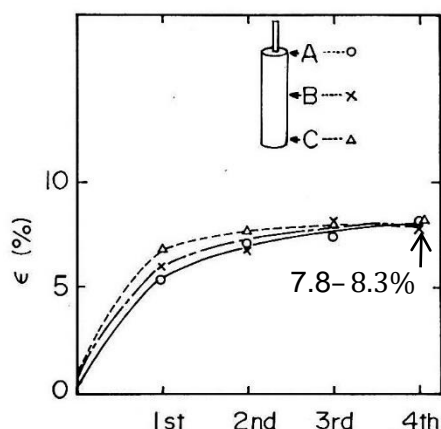
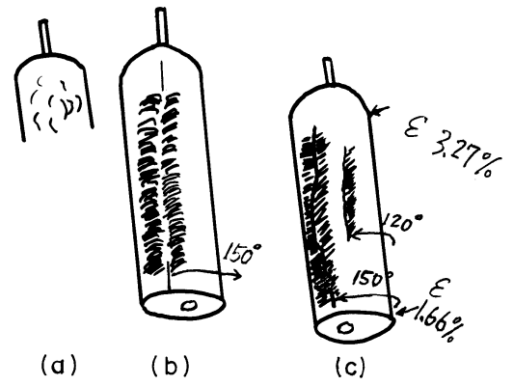


Fig. 2. Radial dilation:  $\epsilon$  % of post-electrolysis Pd electrode at three positions (A, B and C) during 1st to 4th run.

peculiar grain structure could not be obtained by conventional metal forming, another mechanism for grain boundary change was considered. The optical micrograph of the four columnar grains imply that long prisms have grown longitudinally along the electrode center. However, this explanation was unexpected since the temperatures of the electrode and those of the outside of the counter electrode showed no significant change corresponding to a heat burst. Hence, this is acceptable only when the small heat evolution in the interior lasts a long time to promote abnormal grain growth. Coupland *et al.* [7] found recrystallized grains near the area of electrical connection. The recrystallization temperature of the hydrated



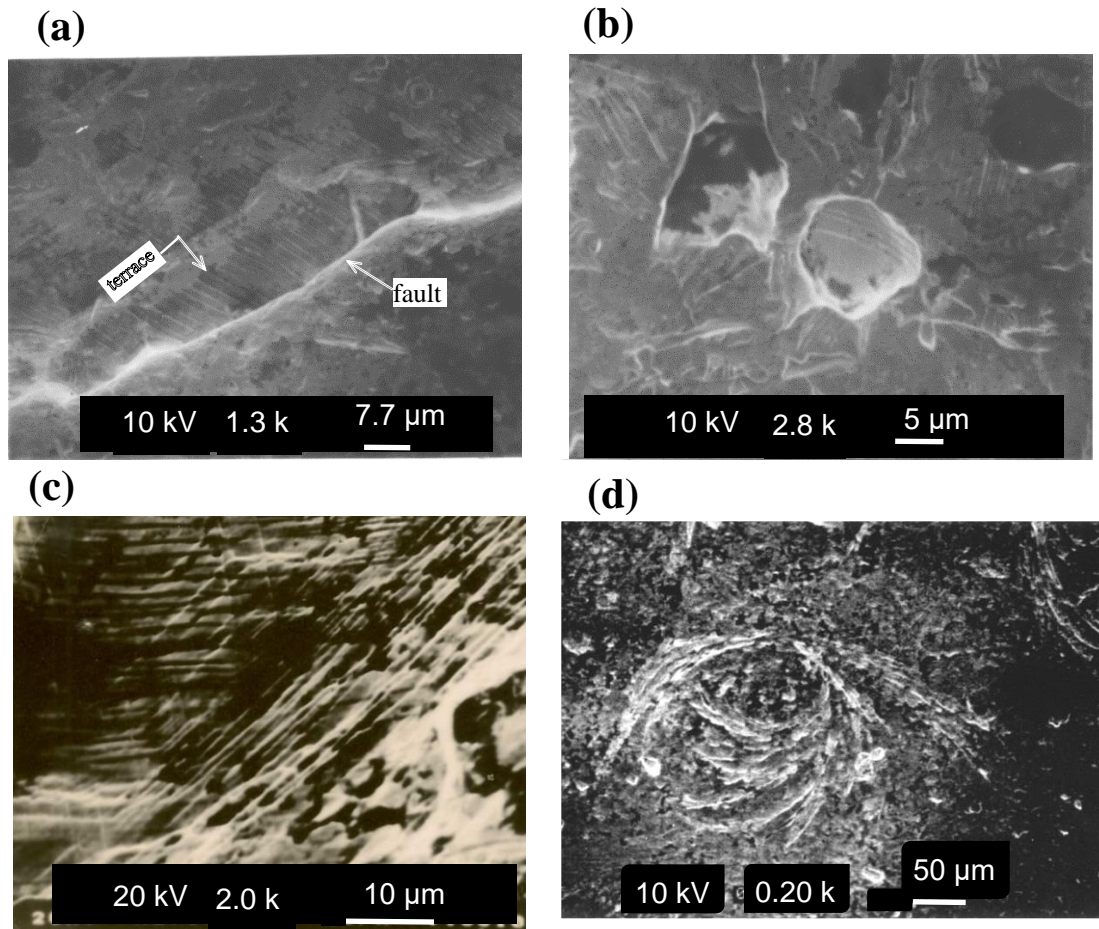
Figs 3a–c. Surface appearance of post-electrolysis Pd electrode showing blister (a), feather pattern, and center line indicates reference position (b) and two, long and short faults (c).

Pd was determined where the sample was subjected to high pressure distortion [8]. The grain growth of vanadium nanocrystalline in a hydrogen atmosphere was accelerated, where hydrogen could assist the grain growth by reducing the formation energy of vacancies [9]. Considering the high CRN observed, the heat evolution in the interior is moderate, resulting in the symmetrical grain structure.

### 1.2 Microstructure of thick Pd Rod under long-term electrolysis - Exp. 2

Visual observation of the electrode surfaces is characterized by three different morphologies, which are schematically shown in Figs 3a, b, and c. We found no surface crack but two faults (see Fig. 3c): (a) marked blisters and (b) blisters with a feather-like pattern arranged in two arrays [5]. These morphologies are located at 120° and 150° right turns from the reference position, (b). Thus, there appeared two line imperfections: a long fault and a center line of the feather pattern all over the surface. In the view of the cross-sectional area (see Fig. 5), the line imperfections, which traverse along the interior of the rod, thrust out one side at the fault and the other side at the center of the feather.

The SEM image taken before the chemical etching pretreatment partly showed a plain terrace with slip bands, partly covered by a gray overlayer along the long fault (see Fig. 4a) [10]. On the other hand, the long fault gathers holes, as shown in Fig. 4b. It was found that these holes concentrated near the fault line, which was substantiated by measuring the hole distribution profiles (hole density plot vs. distance from fault line) at three positions along the long fault [5]. Thus, it is considered that both morphologies—faults and holes—are relevant. Thus, the microstructure of deuterated Pd as a whole shows an inhomogeneous structure, a core and blanket as schematically illustrated by the optical microscopic observation (on the right side of Fig. 5) and Figs 4a and b. It consists of two big columnar grains (core) in the interior and columnar grains with random orientations near the surface (blanket). It seems that the latter grain structure remained unchanged throughout the long-term electrolysis, while the core was recrystallized resulting in grain growth. During the long-term deuterization, the lattice of the two big crystals expands in different directions aligned in the center, causing a fault and/or regularly arranged holes on the surface. Then, the holes formed around a fault, whereupon the deuterium gas along with the reaction products of the inside gushed out.



Figs 4a–d. SEM of Pd electrode surface showing exposed terrace along the long fault (a), holes on Pd electrode surface (b), double slip (c) and vortex which appeared on Pd electrode surface (d). The middle number at the bottom panel indicates the magnification in thousands.

It is significant to compare the formation process of the long fault and blisters (holes) on the Pd surface with those of a crater and faults: the natural phenomena and mantle movement inside the earth (see the left of Fig. 5). It is known that the earth evolves heat continuously in the interior. The mantle movement thereby induces cleavages in the crust, accompanied by craters and faults, as shown in the left of Fig. 5. This phenomenon is similar to the misoriented Pd grains causing a fault on the blanket, as shown in the right of Fig. 5. That is, both movements of the mantle and the deuterated Pd grains (core) are consistent, and hence the hole formation around the long fault on the Pd surface is attributable to gas evolution, such as the volcano gas in a volcanic eruption. Hence, we can explain the microstructure of the Pd electrode; two large grains in the interior, surrounded by random columnar grains, can be attributable to the occurrence of heat evolution and plastic deformation in the interior. Thus, comparison of the morphologies between the geological features on the earth and the deuterated Pd reveals several phenomenological similarities. Moreover, in both cases the surface layers (i.e., Plate (crust) and Pd grains (blanket)) exhibit faults induced by mantle and Pd grains (core) movements conjugated with slow heat evolution in both the interiors.

Recently, the Kobe earthquake was categorized as an active-fault type, which

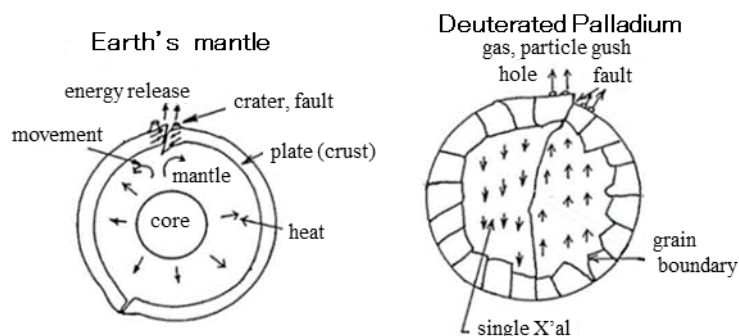


Fig. 5. Mechanism of surface holes formed along the fault of a Pd rod during long-term electrolysis in 0.1 M LiOD.

appeared as a trace of faults on the ground. The anomalous emission of energetic particles was reported before the earthquake and was confirmed by the analysis of a jet-like cloud, which evolved vertically from the ground. It could be reasonable to suppose that the energetic particles emission observed was a precursor to giant ground slippage that generated active-faults on the earth's surface [11]. Here, if we accept such energetic particles emission as the precursor of active-faults accompanied with an earthquake on the earth, the enormous emission of energetic particles observed as evidence of a cold fusion reaction could be closely related with faults and holes observed on the deuterated Pd surface. It could be significant to consider the cold fusion phenomena involving a cold fusion reaction, based on the phenomenological analyses referred to in the report [11], because some similarities are found between the behavior of a deuterated Pd and geological phenomena on the earth as shown above.

Figure 4c shows the other morphology of the double slip of the surface. It is elucidated that two morphologies, including the blister and its surrounding slip bands, are identified similar to those linked to the 3rd stage in the fcc single-crystal stress-strain curve [12]. This means that the Pd electrode could be locally experienced under a high stress/strain condition. As the pretreatment, the Pd electrode was annealed well, and thereby crystal grain growth was thoroughly occurred. Thus, the material could behave like a defect-free crystal within those narrow areas. It is inferred that the  $\epsilon$  of the corresponding area is over 0.6 (this value is estimated from Cu, which is similar to the well-annealed Pd because of the similar modulus of elasticity). On the other hand, the diameter of the post-electrolysis electrode (i.e., whole Pd electrode dimension) was measured at three different heights. As is shown in the results of Exp. 1, the dilations of the Pd electrode diameter exhibited an  $\epsilon$  value of 0.07 in the first run and asymptotically approached 0.078–0.083 during the 2nd to the 4th run. These values are almost 10 times lower than the estimated value, which implies that the area subjected to high stress exhibiting high strain is characterized as “local” because a lower strain was observed on the whole electrode.

Figure 4d shows a significant morphology, termed “vortex,” on the surface of the thick Pd electrode rod after long-term electrolysis in 0.1 M LiOD [13]. It is not the substance that adhered onto the surface, but a material on which the pattern was deeply impressed in the shape of a ditch. The formation mechanism of this morphology was investigated using PC simulation. Although a precise description is not shown here, the vortex formation on the Pd electrodes is deduced from the scavenger process 1 and 2 of the N-cycle model, as shown in Fig. 10 of Ref. 14. The N-cycle reaction model was proposed to understand the cold fusion related phenomena involving a cold fusion

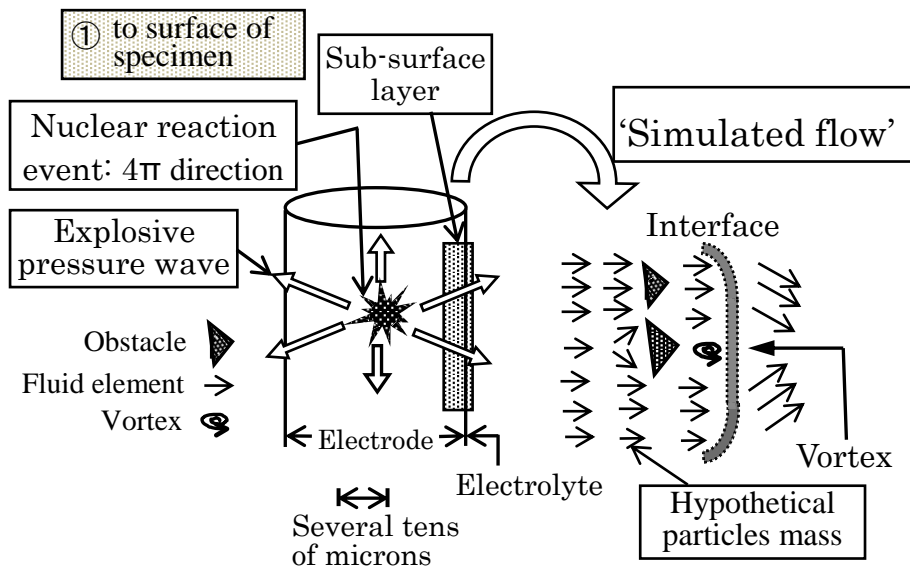
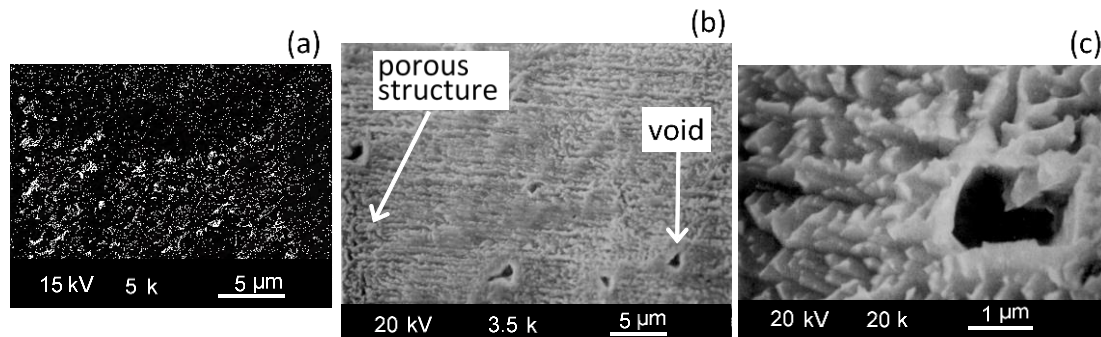


Fig. 6. Perspective view of model of vortex evolution by hypothetical particles mass motion.

reaction [13–18]. On simulation, hypothetical particle mass (HPM) might evolve as a result of the cold fusion reaction, which coincidentally gains momentum converted by the energy of the cold fusion reaction. According to the scavenger process, such synchronized HPM spout out with sufficient energy where the flows are expressed as “simulated flows” as shown in Fig. 6, normal to the electrode interface. At present, a primitive pattern of the locus of the rotating particles has been obtained by Lattice Gas Cellular Automata simulation. Using the discretization method for 3D domain possessing a cylindrical magnetic field, the ejected particles exhibited a helical trajectory appearing at the trace of the vortex on the surface [19].

*SEM views of the electrode interior* Figures 7a, b and c show SEM images of the cross-sectional surface of the deuterated Pd electrode (Exp. 2). In Fig. 7c the enlarged image of a void is characterized by sharp wall and surrounded by non porous structure. In Fig. 7b the whole matrix is composed of voids and circumference like blanket, and nanoporous structure distributed over the rest of the voids areas. For morphology evolution, the characteristic feature of nanoporous structure (Fig. 7a) closely resembles



Figs 7a–c. SEM of cross-sectional surface of a deuterated Pd electrode showing porous structure (a), porous structure and voids (b) and void and circumference (c). The middle number at the bottom panel indicates the magnification in thousands.

the morphology of nanoporous metal by dealloying, therefore the feature might reflect some phase transformation. It is seen that the overall image of voids (see Fig. 7b) is similar to the matrix of Ni-H system where H absorption is performed under high H pressure [20].

We assume the cold fusion reaction is a complicated phenomenon. Thus, our experiments have been focused on understanding the individual phenomena that make up the cold fusion phenomenon. N-cycle model was proposed introducing the above consideration [14-16]. It consists of 4 sequential processes: absorption/compression-triggering-reaction-scavenging, taking into account of the correspondence to long-term electrolysis of a thick Pd rod. Here, the process of reaction exhibits excess heat generation, neutron emission and the miscellaneous reaction products as a result of cold fusion reaction. While the absorption/compression process means making up reaction vessel possessing prerequisite items for the reaction occurrence. In the scavenging very many holes along the fault line were identified to discharge port of the reaction products. Now our experiments have been conducted to elucidate the morphologies of post-electrolysis Pd and to analyze the loading behavior and the lattice defect formation of hydrated Pd. During the study with respect to these two processes we could elucidate the cold fusion reaction mechanism and improve the reproducibility of the experiments.

## **2. Microstructural change of Pd rod during repeated cathodic and anodic electrolysis in glycerin-phosphoric acid**

### **Introduction**

Since McKubre *et al.* [21] reported that reproducible excess heat generation was closely linked to achieving high D/Pd, the subject of loading behavior (D/Pd ratio) has attracted attention. Along with the high D/Pd loading behavior, Storms determined the precise D/Pd ratio by measuring the released O<sub>2</sub> volume and demonstrated that surface cracks played an important role in the deloading behavior of  $\beta$ -PdD [22]. It is suggested that the cold fusion experiments were encountered by irreproducible data, which could be attributable to the diffusion of D<sub>2</sub> through surface cracks and unidentified impurities covering the surface. It is also suggested that for a precise understanding of phase change and surface and cross-sectional morphologies of deuterated Pd, *in situ* measurements of the electrode potential, dilation, and resistance are of interest under well-controlled hydrogen absorption [14]. In addition, our model predicted that the reaction vessel surrounded by the strained region was the precursor to the cold fusion reaction. Owing to the recent cold fusion research, the anomaly substantially has become a D atom transfer in the specified solid, apart from achieving a high D/Pd ratio. In this section, the experimental data of a Pd-H system are considered to be identical to those of a Pd-D system, as long as the theme is concerned with material items.

### **Experimental**

The absorption/desorption of hydrogen in Pd rod electrodes (0.8 and 2 m diameters, 50 mm length, and 99.95% purity) was performed by applying galvanostatic cathodic and anodic pulse currents, with current densities  $< 2 \times 10^{-3}$  A/cm<sup>2</sup>. The electrolyte was composed of glycerin and phosphoric acid (2:1 in volume ratio) [23]. The temperature was kept constant at  $40 \pm 0.5$  °C. The electrolytic cell and the apparatus for *in situ* measurements of potential, dilation, and resistance are described elsewhere [14]. An as-received Pd rod was pretreated according to our conventional experimental procedures. *In situ* measurements are better realized to ensure exact coincidence among the measured

variables.

It is known that the interaction between the dissolved atoms and the surrounding materials often bring about a lattice strain in materials. The apparent partial molar volume [ $d(\Delta l/l_0)/dx$ ] (abbreviated as “apparent molar volume”) was calculated from  $3V_M$  ( $V_M$  being the molar volume of the metal) multiplied by the slope of the dilation as a function of the H/Pd ratio. Peisl compiled the lattice expansion data of metal–hydrogen systems and demonstrated elastic interaction via the distortion fields as an important item [25].

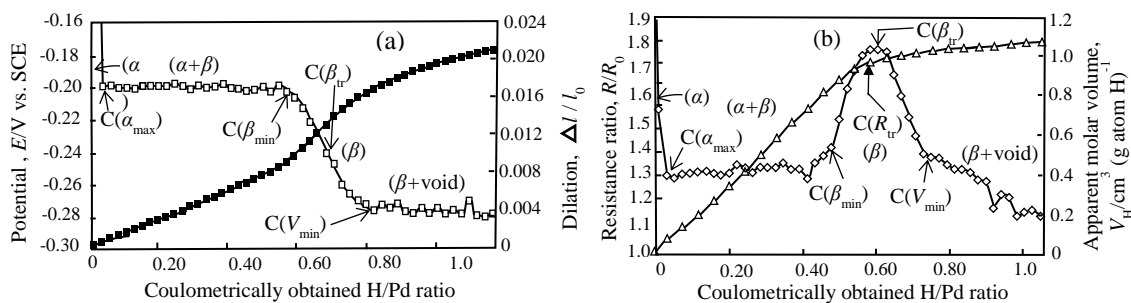
## Results and discussion

### 2.1 First absorption of H in Pd ( $x < 0.8$ ) in the C mode

Figure 8a shows the potential and dilation changes, and Fig. 8b shows plots of the resistance and apparent molar volume [ $d(\Delta l/l_0)/dx$ ] changes as a function of  $x$  under the first C mode. The term “first” means that the sample is characterized as free from bearing deformation due to hydrogen absorption/desorption reaction. In Figs 8a and b, the concentration  $\alpha_{\max}$  is the limit of the  $\alpha$  phase,  $\beta_{\min}$  is the limit of the  $(\alpha + \beta)$  phase coexistence,  $\beta_{\text{tr}}$  is the transition from the  $\beta$  phase to  $\beta + \text{PdH}_{2-x}$ ,  $V_{\min}$  is the onset of the  $(\beta + \text{void})$  coexistence region, and  $R_{\text{tr}}$  is the transition from increasing resistance to a damped resistance. Figs 8a and b also show  $\alpha$  single,  $(\alpha + \beta)$  phase coexistence,  $\beta$  single, and  $(\beta + \text{void})$  coexistence regions.

We now describe the coincidence of the potential, resistance, dilation, and apparent molar volume. As shown in Fig. 8a, the potential decreases with increasing  $x$  (H/Pd ratio) within the single  $\alpha$  phase and reaches a constant value corresponding to the  $(\alpha + \beta)$  phase coexistence (two-phase coexistence region). Meanwhile, the resistance (see Fig. 8b) monotonically increases, showing a slight deviation from the exact proportionality to  $x$ . Although the resistance curve is not shown at very low concentrations, it rises steeply, and the slope of the resistance as a function of  $x$  becomes small at the onset of the  $(\alpha + \beta)$  phase coexistence. For  $x > 0.55$ , the slope in the resistance curve begins to decrease and levels off at the point of inflection ( $R_{\text{tr}}$ ). Furthermore, it approaches a limiting value of 1.8 for  $x > 0.80$ . This behavior appeared only in the first absorption of the C mode. The samples subjected to repeated hydrogen absorption/desorption exhibited almost the same behavior up to the  $\beta$  phase, but above  $R_{\text{tr}}$ , they flatten at 1.7 (see Fig. 19b of Ref. 14). The difference in the resistance behavior above  $R_{\text{tr}}$  is attributed to the contribution of unrecovered absorbed hydrogen. Thus, during the first absorption/desorption, a small amount of hydrogen remained trapped near the surface, whose interstitial sites are already occupied and therefore do not contribute to the resistance change [26].

The values of the apparent molar volume obtained from Fig. 8b are  $1.64 \text{ cm}^3/\text{mol}$  for the  $\alpha$  single phase (this value was obtained from the dilation ( $\Delta l/l_0$ ) vs.  $x$  plot at  $x < 0.10$ )



Figs 8a and b. The C mode potential, dilation, resistance, and apparent molar volume as a function  $x$  of the first C mode absorption at  $40^\circ\text{C}$ . (a) Potential ( $\square$ ) and dilation ( $\blacksquare$ ) as a function of  $x$ ; (b) resistance ( $\triangle$ ) and apparent molar volume ( $\diamond$ ) as a function of  $x$ .

and  $0.40 \text{ cm}^3/\text{mol}$  for the  $(\alpha + \beta)$  phase coexistence. For two-phase coexistence, the values do not vary with increasing  $x$ , where the absorption presumably occurs in a homogeneous structure free from voids and cracks, in contrast to the repeated C mode, as described below. The potential in Fig. 8a shows a Nernstian behavior ( $\alpha$  single phase), the constant value of the  $(\alpha + \beta)$  phase coexistence, the transition toward a less noble direction ( $\beta_{\min} \sim V_{\min}$ ), and the next constant value of the  $(\beta + \text{void})$  coexistence, where the apparent molar volume follows two constant values corresponding to the  $\alpha$  phase and  $(\alpha + \beta)$  phase coexistence ( $1.64$  and  $0.40 \text{ cm}^3/\text{mol}$ ). At  $x < \beta_{\min}$ , the coincidence between the phases defined by the potential ranges and the apparent molar volume of the corresponding phases seems well enough. Tripodi *et al.* investigated the effect of hydrogen insertion on the resistance and strain of a Pd electrode under a constant mechanical stress [27]. They showed that the strains due to mechanical stress and lattice expansion were separated from the total strain measured. The resistivity difference between the annealed and as-drawn samples is attributed to the resultant mechanical strains. During hydrogenation cycles, the strain before hydrogen deloading and that of residual value were similarly explained in connection with the resistivity.

At  $x > \beta_{\min}$ , the strange behavior of apparent molar volume accompanied by the potential shift is explained as follows: If the hydrogen absorption proceeds, as in the first C mode, the potential might decrease in accordance with Nernst's equation and concurrently the apparent molar volume recovers to  $1.64 \text{ cm}^3/\text{mol}$  (absorption in the octahedral sites of Pd). However, the experimental data did not show ideal behavior; hence, we could draw the following interpretation. Above  $\beta_{\min}$ , the predominant absorption of the octahedral occupation is disturbed by a precipitation of  $\text{PdH}_{2-x}$  ( $0 < x \leq 1$ ) because of the occupation of tetrahedral sites [28]. Then, through  $\beta_{\text{tr}}$ , the increased pressure (corresponding to the decreased potential) allows the unstable precipitates to decompose to  $\text{PdH}_{1-x}$  and hydrogen gas. On this occasion, hydrogen evolution in the matrix causes void formation. Above  $R_{\text{tr}}$  (between  $\beta_{\text{tr}}$  and  $V_{\min}$ ), the apparent molar volume drops concurrently with the transition from  $\text{PdH}_{2-x}$  precipitation to absorption in voids when the resistance curve levels off (see Fig. 8b). Here, the resistance did not respond to void formation because the size of the void was larger than the mean free path of the conduction electrons, which means that the resistance was not sensitive to the existence of voids. Such a new phase different from the  $\beta$  phase is proposed by Mizuno *et al.* [29] and Storms [22].

## **2.2 Coincidence of two hydrogen states in the repeated C mode with the characteristic hydrogen states: defects induced by the interaction of hydrogen and applied stress**

The study of hydrogen states by thermal desorption analysis (TDA) combined with techniques such as secondary ion mass spectrometry elucidated that the two desorption peaks of hydrogen were a peak at low temperatures ( $100 \text{ }^\circ\text{C}$  or  $< 200 \text{ }^\circ\text{C}$ ; termed peak 1) and another peak at more than  $200\text{--}400 \text{ }^\circ\text{C}$  (peak 2) in a hydrogen desorption profile. Further analysis of hydrogen states clarified that peak 1 is diffusible, that is, spontaneous desorption occurs around  $30 \text{ }^\circ\text{C}$ , and that peak 2 is nondiffusible at ambient temperature. Peak 1 is the hydrogen state termed "weak trap site" and peak 2 is termed "strong trap site." Table 2 summarizes the two hydrogen desorption peaks (peak 1 and peak 2) and our two peaks ( $\alpha + \beta$  phase coexistence and  $(\beta + \text{void})$  coexistence phase) where the correspondence between the two hydrogen peaks and our two-phase coexistences is evaluated. Note that peak 1 considerably affects hydrogen embrittlement susceptibility, while peak 2 exhibits no effect on the embrittlement [30].

Table 2. Two hydrogen desorption peaks in TDA profile and two-phase coexistence during the C mode. The correspondence between two experimental results is also indicated.

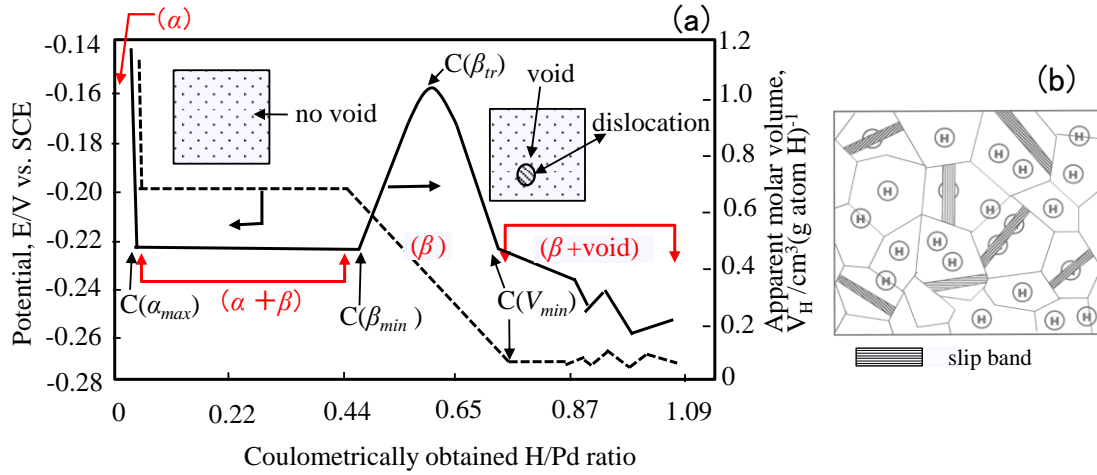
H content		← low	high → ( $\beta_{\min}$ )
Two phases coexistence during C mode (This study)	Type	( $\alpha+\beta$ ) phase coexistence	( $\beta$ +void) coexistence phase
	Absorption site	Dislocation	Void + void/ $\beta$ phase matrix boundary, vacancy
	Correspondence	↕	↕
Two H desorption peaks in TDA profile	Type	Peak 1	Peak 2
	Trap site	Weak trap site (diffusible)	Strong trap site (nondiffusible)
		Brittle (H-induced crystal defect)	–

In Fig. 19 of Ref. 14, during the repeated C mode, two characteristic ( $\alpha + \beta$ ) phase coexistence and ( $\beta + \text{void}$ ) coexistence regions appeared, where the former phase transformation proceeds accompanied by a high density of defects and vacancies. Such a change of materials might exhibit brittleness. Furthermore, the repetition of the C mode shows the enlargement of the ( $\alpha + \beta$ ) phase coexistence region, and the incremental charge in  $x$  (see Ref. 14) corresponds to the charges for the saturation of these voids and the absorption in high-defect density areas. Thus, in the ( $\alpha + \beta$ ) phase coexistence, the brittleness, the enlargement of the corresponding region, and hydrogen absorption accompanied by a high density of defects coincides with the hydrogen state that corresponds to peak 1—diffusible and trapped in dislocations.

On the other hand, taking into account the consequences of the hydrogen absorption process (see Table 2), the latter ( $\beta + \text{void}$ ) coexistence region might correspond to the nondiffusible hydrogen state (peak 2). It is known that this peak is attributable to the hydrogen strongly trapped by dislocations at the ferrite/cementite boundary where the cementite is regarded as precipitates in the ferrite matrix. If we accept void as a phase, that is, precipitate, absorption of hydrogen in high-defect density areas might coincide with the situation of peak 2. Again, high-defect density areas around voids correspond to dislocations surrounding precipitates/matrix. These results are schematically illustrated in Fig. 9.

### 2.3 Microstructural changes by taking into consideration of adsorption/desorption process

Figure 9a shows the schematics of microstructural changes (shown in the insets) and the *in situ* measurements of potential and apparent molar volume during the first absorption as a function of  $x$ . In Fig. 9a during the first H absorption, the insets are the microstructure without void in the ( $\alpha + \beta$ ) phase coexistence region, and that with a small volume of voids in ( $\beta + \text{void}$ ) coexistence region. Next, we consider the repeated C mode absorption followed by desorption, where hydrogen adsorbed once is desorbed electrochemically. When that occurs, the microstructure shows the H absorption of matrix with a large volume of voids in the corresponding two regions. Aforementioned, the adsorbate characterized as diffusible hydrogen was trapped in the field of tensile stress, which exists in a weak trap potential and such hydrogen easily diffuses out of matrix. Subsequently, defects, i.e., dislocations introduced during former absorption remain. Thus, the evolution of slip bands occurred as illustrated in Fig. 9b.



Figs 9a and b. Schematics of the in-situ measurements of potential (dotted line) and apparent molar volume (solid line) of 1st repetitions as a function of  $x$  (a); schematic illustration of slip bands developed within crystal grains during H absorption/desorption (b).

#### 2.4 Macro void behavior during hydrogen absorption/desorption

Numata *et al.* reported that a significant number of micro voids was formed during the repeated C mode in glycerin and phosphoric acid [14]. Even if a Pd electrode was not subjected to the repeated H absorption/desorption, surface voids arrayed along the faults were confirmed by SEM observation of post-electrolysis Pd electrode (see Fig.4). Alternatively, even with a low concentration of vacancy, macro voids could be formed through nanoscale micro voids in the case of iron [32]. Then, H-vacancy clusters as a resource of nanoscale voids are of interest to evaluate the influence of H absorption/desorption on the macro voids behavior. Note that the microstructure discussed here does not refer to the phenomena arising through the propagation of the dislocation but rather to voids, therefore the state is at  $x > \beta_{\min}$  including ( $\beta + \text{void}$ ) coexistence region.

First our target of this study is to elucidate the anomaly of the relationship between apparent molar volume increase to  $\sim 1.1$  at  $x \beta_{tr}$  followed by a drop and concurrent resistance level off attaining 1.8 at  $x > \beta_{\min}$  (see Fig. 8b). Here, we describe the data and evaluation of *in situ* measurements of the electrode potential, dilation, and resistance to shed light on the microstructural changes.

When a cathodic current is supplied to a metal electrode equipped in an electrochemical cell, hydrogen atoms adsorb on the electrode surface and diffuse into the sample bulk. On reversing the current hydrogen atoms can be desorbed out of the sample. The hydrogen atoms dissolved within a vacancy thereby diffuses outwards while the vacancies and/or defects remain irrespective their microstructural changes.

Considering the H gas in a gas phase that is in equilibrium with the H within an electrode, the H pressure can be calculated as:

$$pH_2 = \exp[-(E + E_{SCE})(2F/RT)] \quad (1)$$

where  $pH_2$  is the H equivalent pressure and  $E_{SCE}$  is the potential of the reference electrode. Figure 10 shows the equivalent H pressure at more than  $x$  0.01 where the two-phase coexistence pressure,  $0.05 \times 10^5$  Pa, coincides with that obtained from the Pd–H isotherm at 40 °C. When the state is turned into the  $\beta$  phase, i.e.,  $x > \beta_{\min}$ , the equivalent H pressure

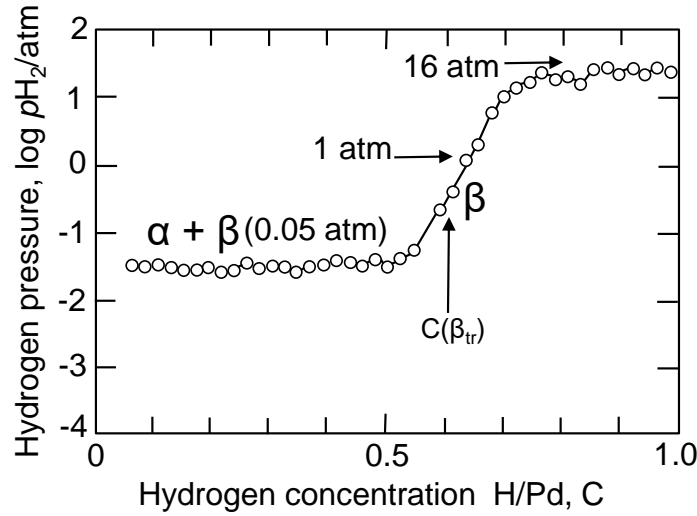


Fig. 10. Equivalent H pressure as a function of the H/Pd ratio at 40 °C.

again begins to increase until a final pressure of  $16 \times 10^5$  Pa has been reached. Provided that given H pressure means equilibrium of the activity of H occupying interstitial sites with the H gas in voids, the H pressure increase at around  $\beta_{tr}$  causes the transformation from nanoscale to macro voids. At that time, the peak in apparent molar volume and changes in resistance are, qualitatively speaking, consistent with macro void formation [14].

### 2.5 Vacancy-cluster formation accompanied with solute segregation during hydrogen absorption/desorption

Superabundant vacancy (SAV) was first discovered by Fukai and his group, which was characterized with a gradual contraction of the lattice parameters of Ni and Pd hydrides under high H pressure and at high temperature [33–34]. The vacancy concentration amounts to many order of magnitude higher than that of room temperature. Kirchheim analyzed the formation of SAV based on the thermodynamic consideration taking into account changes of the defect energy by solute segregation [35]. According to Kirchheim paper the solute excess at a defect is calculated through new Gibbs-Wagner's definition as:

$$\Gamma_A = \left. \frac{\partial n_A}{\partial a} \right|_{T, V, \mu_A, n_B} \quad \text{Gibbs-Wagner equation} \quad (2)$$

$\Gamma_A$  : excess of A at the defect,  $\mu_A$ : chemical potential of A atom (solute) in solvent B atom,  $a$  : interface area,  $n_A$ : number of A atom,  $n_B$  : number of B atom.

For vacancies the excess:  $\Gamma_A^V$  is equal to the number of Z (H atoms residing in a vacancy). The value of Z of Pd powder deformed by high pressure torsion is most probably 6 where H/Pd ratio reached 0.78 [36].

Next, our discussion will be focused on the microstructural changes, i.e., void behavior related with vacancy-cluster, and then the behavior of electrode potential of hydrated Pd combined with  $n_V$ : vacancy concentration is evaluated. First the value of  $n_V$  is obtained as 0.20 from the tangential value of dilation at  $x \beta_{min}$  using  $x_{cl} = 3 \times (\Delta a/a) / -0.36$  ( $\Delta a/a$ : lattice contraction) [37]. This value corresponds to an upper bound because the tangential value for calculation tends to decrease as the H absorption progresses. It's

worth noting that the electrolytic H absorption exhibits considerably high vacancy concentration immediately after the cessation of the ( $\alpha + \beta$ ) phase coexistence region. Hence, it is suggested that the formation of vacancy is mostly attributed to lattice defects and in parallel the migration of vacancy from the surface would be slower due to low temperature hydration.

On the other hand, Harada *et al.* reported the values of  $n_V$  as a function of  $x$  (up to  $x = 1$ ) under high H pressure of 3.0–5.0 G Pa and high temperature of 920–1120 K [37]. At  $x < 0.6$ , the vacancy concentration is small but not negligible. Over  $x = 0.6$ , it exhibits an increase linearly with  $x$ , reaching maximum concentration 0.12. From knowledges as an experimentalist, there might exist discrepancies in sample preparation between high temperature gas phase atmosphere and hydrogenation at around room temperature. As shown in Fig. 8, the ( $\alpha + \beta$ ) phase coexistence shifts to the single  $\beta$  phase at  $x = 0.55$ , even more than  $x = 0.6$  the increase of  $n_V$  confirmed in gas phase measurement. Therefore in our experiment  $x > \beta_{\min}$   $n_V$  is already 0.20 over maximum value of 0.12, which implies the transformation from vacancies to micro or macro voids.

Finally, it is emphasized that *in situ* potentiometric, resistance and dilatometric measurements combined with the electrochemical discharge for accurate H loading are advantageous because experimental explanation can be free from an effect due to high temperature/quenching process, high pressure deformation and an exposure to high vacuum atmosphere for a sample preparation. Furthermore, it is necessary to collect new experimental results obtained by developed experimental technique and improve more deep understanding of the phenomenon.

## Conclusion

We summarize our study as follows:

1. Long-term electrolysis for well annealed thick Pd rods (9.0 and 21 mm diameters) in 0.1 M LiOD was performed. Microscopic observation of post-electrolysis Pd electrode showed the surface morphology of surface holes, two long faults without any crack. The formation of the characteristic microstructure was explained as similar to miscellaneous geologic phenomena, such as earthquake and active fault formation.
2. *In situ* potentiometric, resistance and dilatometric measurements of Pd electrode were performed to elucidate the elemental steps of electrochemical hydrogen absorption. During the first C mode, the potential of Pd exhibited the structural phase changes: the  $\alpha$  phase, the ( $\alpha + \beta$ ) phase coexistence, fine PdH<sub>2-x</sub> precipitates (void formation) and finally ( $\beta + \text{void}$ ) coexistence regions. During each stage, e.g., the ( $\alpha + \beta$ ) phase coexistence and ( $\beta + \text{void}$ ) coexistence regions, the resistance and apparent molar volume behave consistently appearing the phase transformation and resultant void formation.
3. Two hydrogen states concerning above the ( $\alpha + \beta$ ) phase and ( $\beta + \text{void}$ ) coexistence were clarified with the evolution of defects in the matrix with reference to the reports on TDA analysis.
4. Applying thermodynamic analysis to vacancy-H interaction, according to Kirchheim paper [35], we have examined preliminary source data, i.e., equilibrium H pressure and  $n_V$ . Next the data is needed to evaluate the following equation:

$$\Delta n_A = (n_A)_{\text{high}} - (n_A)_{\text{low}} = (\text{H/Pd})_{\text{high}} - (\text{H/Pd})_{\text{low}} \text{ under given } \mu_A$$

where the subscripts high and low denote high and low vacancy concentrations, respectively.

### Acknowledgments

The author would like to thank to Messrs. T. Ooi, A. Nakajima, M. Ban and Profs I. Ohno and the late R. Takagi of Tokyo Institute of Technology for co-operative work.

### References

- 1 M. Fleischmann, S. Pons and M. Hawkins, *J. Electroanal. Chem.* 261, **301** (1989).
- 2 S. E. Jones *et al.*, *Nature* **338**, 737 (1989).
- 3 A. De Ninno *et al.*, *Europhys. Lett.* 9, 221 (1989).
- 4 H. O. Menlove *et al.*, *J. Fusion Energy*, 9, 495 (1990).
- 5 H. Numata, R. Takagi, I. Ohno, K. Kawamura and S. Haruyama, *Conf. Proc. Vol.33, ACCF2* “The Science of Cold Fusion” pp.71(1991).
- 6 R. Takagi, H. Numata, I. Ohno, K. Kawamura and S. Haruyama, *Fusion Technol.* **19**, 2135 (1991).
- 7 D. Coupland, M. Doyle, J. Jenkins, J. Notton, R. Potter, and D. Thompson, *Proc. 1st Annual Conf. on Cold Fusion* pp.299, Utah (1990).
- 8 M. Krystian, D. Setman, B. Mingler, G. Krexner and M.J. Zehetbauer, *Scripta Mater.* **62**, 49 (2010).
- 9 M. Martin, A. Pundt and R. Kirchheim, *Acta Mater.* 155, 262 (2018).
- 10 The ‘fault’ usually means a kind of geological phenomenon, however, we expressed such morphology as fault because of similarity between the experimental result and the knowledge of geology. In metallurgy the feature of ‘fault’ is coincident with ‘surface steps due to multiple slip’. In the experiments one long slip line thrusting the specimen center was observed, which was meet with usual tensile loading test.
- 11 Photograph of the trace of cloud formed by high energy particles emission on the ground was taken at 8 days before giant Kobe earthquake on Jan.17 1995 (by photographer T. Sugi-e). The research work with this phenomenon has been extensively carried out by Y. Enomoto *et al.*, referred to: Y. Enomoto, *Chishitu News*, no.523 63 (1998) (in Japanese).
- 12 H. Numata, *Proc. JCF17* 40 (2017).
- 13 H. Numata and M. Ban, *ICCF12* Yokohama Japan, 411 (2005).
- 14 H. Numata and I. Ohno, *Fusion Technol.* **38**, 206 (2000).
- 15 H. Numata, *Proc. Conf. 3rd New Hydrogen Energy Basic Research* pp.55 (1996).
- 16 H. Numata and I. Ohno, *ICCF6* Toya Japan **vol.1**, 213 (1997).
- 17 H. Numata, in Book “Cyber X” No.11, pp.37 (1999) Kougakusha (in Japanese).
- 18 A. Takahashi, H. Numata, H. Yamada, Y. Iwamura, T. Ohmori, T. Mizuno and T. Akimoto, “Nuclear Reaction Study in Condensed Matter No. 1”, Chap. 4, pp.124 (1999) Kougakusha (in Japanese).
- 19 H. Numata and M. Ban, *Proc. JCF11* 70 (2011).
- 20 H. Osono, T. Kino, Y. Kurokawa and Y. Fukai, *J. Alloys Compd.* **231**, 41 (1995).
- 21 M.C.H. McKubre, S. Crouch-Baker, R. C. Roche-Filho, S. I. Smedley, F. L. Tanzella, T. O. Passell, *Proc. Fifth Int. Conf. on Cold Fusion*, 9-13 Apr. 1995, Monte Carlo, Monaco, pp. 17.
- 22 E. Storms, *J. Alloys and Compounds* **268**, 89 (1998).
- 23 R. Kirchheim, *Acta Metal.* **29**, 835 (1981).
- 24 It is useful to conduct electrolysis for determining precise D/Pd ratio during absorption and desorption runs, where the value of D/Pd is converted by the charges thrown by a current supply. Concurrently measured electrode potential exhibits the changes of crystallinity of a surface, i.e., phase, composition, equilibrium H pressure inside, etc.

- 25 H. Peisl, Hydrogen in Metals (Ed. G. Alfeld and J. Völkl), **Vol.1**, Springer, Berlin, pp.53 (1978).
- 26 K. Kandasamy, F.A. Lewis and S.G. McKee, Surface Coating Technol. **35**, 93 (1988).
- 27 P. Tripodi, N. Armanet, V. Asarisi, A. Avveduto, A. Marmigi, J.P. Biberian and J.D. Vinko, Phys. Lett. **A 373**, 4301 (2009).
- 28 M. Pitt and E. Gray, Europhys. Lett. **64**, 344 (2003).
- 29 T. Mizuno and M. Enyo, *Modern Aspects of Electrochemistry*, **No.30**, pp.480, R.E. White *et al.* Eds., Plenum Press, New York (1996).
- 30 K. Takai, G. Yamauchi, M. Nakamura, M. Nagumo, J. Japan Inst. Met. Mater. **62**, 267 (1998).
- 31 T. Doshida, M. Nakamura, H. Saito, T. Sawada and K. Takai, Acta Mater. **61**, 7755 (2013).
- 32 M. Nagumo and K. Miyamoto, J. Japan Inst. Met. Mater. **45**, 1309 (1981).
- 33 Y. Fukai, Y. Ishii, Y. Goto, and K. Watanabe, J. Alloys Comp. **313**, 121 (2000).
- 34 Y. Fukai, Y. Kurokawa and H. Hiraoka, J. Japan Inst. Metals **61**, 663 (1997).
- 35 R. Kirchheim, Acta Mater. **55**, 5129 and 5139 (2007).
- 36 M. Krystian, D. Setman, B. Mingler, G. Krexner and M. Zehetbauer, Scripta Mater. **62**, 49 (2010).
- 37 S. Harada, S. Yokota, Y. Ishii, Y. Shizuku, M. Kanazawa and Y. Fukai, J. Alloys Comp. **404-406**, 247 (2005).

## **Characteristics of the Nuclear Reactions in the Cold Fusion**

### **Phenomenon**

Hideo Kozima and Hiroshi Yamada\*

Cold Fusion Research Laboratory, Shizuoka 421-1202 Japan

E-mail: [hjrfq930@ybb.ne.jp](mailto:hjrfq930@ybb.ne.jp)

\* Iwate University, Morioka 020-8551 Japan

### **Abstract**

The cold fusion phenomenon is characterized by nuclear reactions in CF materials, i.e. materials including hydrogen isotopes (H or/and D) with high concentration, with no mechanisms to accelerate particles in them. The CF materials are not confined to deuterium but also protium systems and classified into three groups; (1) metallic materials include transition-metal hydrides (e.g. NiH<sub>x</sub>, AuH<sub>x</sub>) and deuterides (e.g. PdD<sub>x</sub>, TiD<sub>x</sub>), (2) carbonic materials include hydrogen graphite (HC<sub>x</sub>) and XLPE (cross-linked polyethylene) and (3) biological materials include microorganisms, microbial cultures and biological tissues or organs.

Looking for the common cause of nuclear reactions in these CF materials, we have to notice the characteristics of the nuclear reactions in the CFP very different from the nuclear reactions in free space investigated extensively in nuclear physics. In free space, the liberated energy of a nuclear reaction, the energy difference between the initial and the final states, is carried out by a particle or two; the energy difference is in general of a few MeV.

On the other hand, the nuclear reactions in the CFP where the liberated energy is more than eight orders of magnitude larger than the thermal energy of the particles in the system, show, in general, no emission of high energy particles, especially photons which are probable to be observed if emitted in CF materials. It should be noticed also that there is generation of new elements with large shifts of proton numbers from those of the preexisting elements in the system and emission of neutrons with energies up to more than 10 MeV.

These characteristics of nuclear reactions in the CFP have been consistently explained by our phenomenological approach with using the TNCF and the ND models.

In this paper, we investigated experimental data sets on the nuclear transmutations obtained recently in these about 15 years using our model (the ND model), confirmed our approach and obtained further evidences characteristics of the nuclear reactions in the CFP.

**Key words:** cold fusion phenomenon, nuclear transmutation, TNCF model, ND model, metal-hydrogen superlattice, neutron drop, biotransmutation, Stabilization of Unstable Nuclei,

## 1. Introduction

It has elapsed almost 30 years since the discovery of the first evidence of the cold fusion phenomenon (CFP) in PdD<sub>x</sub>, the first CF material, i.e. materials where occurs the CFP, by Fleischmann et al. in 1989 [Fleischmann 1989]. They presupposed the *fusion reactions* of two deuterons in the solid solution PdD<sub>x</sub> resulting in three branching decay products in free space written down as follows;



The experimental data full of variety in their characteristics had shown that the presupposed reactions (1.1) – (1.3) could not be fundamental for the CFP. We have had to look for causes of nuclear reactions for whole events observed in the CF materials including the data by Fleischmann et al. Even if the fusion reactions of two deuterons are not fundamental for the events observed in CF materials, we would like to call the observed events as a whole the *cold fusion phenomenon (CFP)* appropriate for them in the solid state-nuclear physics keeping a scent of historical reminiscence.

It should be kept in our mind that we had observed the CFP only in solids but not in liquids among the condensed matters including a great deal of hydrogen isotopes (protium and/or deuterium) comparable to the host elements, hitherto. We may be able to classify the CF materials, materials where observed the CFP, into three groups according to the properties of host elements; (1) metallic materials include transition-metal hydrides (e.g. NiH<sub>x</sub>, AuH<sub>x</sub>) and deuterides (e.g. PdD<sub>x</sub>, TiD<sub>x</sub>), (2) carbonic materials including hydrogen graphite (HC<sub>x</sub>) and XLPE (cross-linked polyethylene) and (3) biological materials including microorganisms, microbial cultures and biological tissues or organs. Each CF materials in these groups are composed of the metal (carbon)-hydrogen superlattice (superlattice with a sublattice of host elements and another of hydrogen isotopes) [Kozima 2018] and have specific characteristics for the nuclear transmutations occurring there.

It is also necessary to notice that we have observed the CFP only in these CF materials at dynamical but not at static conditions. This characteristic may be related to the

complexity supposed to be in the CF materials [Kozima 2012a, 2015 (Sec. 3.8)].

It is a remarkable characteristic of the CFP that there is a threshold value of the average density of hydrogen isotopes in the CF materials for the occurrence of the CFP. For transition metal hydrides (and deuterides) with a ratio  $x_1$  of the concentration  $C_H$  of H (or D) and that  $C_M$  of the host element M (M = Ti, Ni, Pd, Au, Pt, - -),  $x_1 = C_H / C_M$ , it is necessary to have  $x_1$  larger than a threshold value  $x_{1th} \approx 0.8$ ,  $x_1 \geq x_{1th} \approx 0.8$ . Let us call the ratio  $x_1$  the *concentration index*, or *Index 1*.

It is convenient to define the second index, *Index 2*,  $x_2$ , for the CFP specifying the metal-hydrogen superlattice in the case of transition metal hydrides (deuterides) and the carbon-hydrogen superlattice in the case of carbon-hydrogen system (XLPE and microorganisms). The Index 2, the *superlattice index*  $x_2$ , is defined as the proportion of the superlattice to the whole CF material. It is essential to increase  $x_2$  in an experiment for realization of the CFP.

As a whole, there are two important indices characterizing the CF materials for the CFP;

- (1) *The concentration index*  $x_1$  (Index 1), defined as  $x_1 = C_H / C_M$  where  $C_H$  is the concentration of H (or D) and  $C_M$  is the concentration of the host element M (M = Ti, Ni, Pd, Au, Pt, - -). (Threshold value of  $x_1$  for the CFP is supposed to be  $x_{1th} \approx 0.8$ )
- (2) *The superlattice index*  $x_2$  (Index 2), defined as the proportion of the superlattice to the whole CF material. ( $0 \leq x_2 \leq 1$ )

The irreproducibility, or the qualitative reproducibility, of events in the CFP is a characteristic to be considered seriously in the research of science in this field. One reason for this characteristic is the complexity in formation of the CF materials as discussed in the paper published before [Kozima 2013]; the self-organization of the optimum metal-hydrogen superlattice is an uncontrollable process and the same state of the CF material does not exist forever.

Another cause of the qualitative reproducibility is related to the result of nuclear reactions in the CFP. The nuclear energy liberated in the nuclear reactions is more than 5 MeV, in general, about 8 orders of magnitude larger than the thermal energy, about 25 meV at room temperature, of particles of the CF material where occurs the CFP. The liberated nuclear energy is distributed among particles around the place where occurs the reaction and the temperature of that region becomes very high to melt the CF material there; several examples of melting of the reaction region have been often observed as shown, e.g. in our book [Kozima 2006 (Fig. 2.3)] and a paper by Ohmori [Ohmori 2016 (Fig. 34)]. The change of the structure by the nuclear reaction in the CFP makes it

impossible to obtain the same result for the sample under the same macroscopic experimental condition.

These characteristics have to be kept in our mind when we look for the causes of the CFP based on the experimental facts obtained in this field in about 30 years.

In this paper, we concentrate our discussion on a characteristic of the nuclear transmutations in the CFP, the large shifts of  $A$  and  $Z$  from those of pre-existed nuclei in the CF materials,

In Section 2, we give a brief explanation of experimental results in the CFP. In Section 3, the nuclear transmutation and the stabilization of unstable nuclei investigated hitherto are explained briefly [Kozima 1998, 2006, 2018]. The nuclear transmutations with large changes of  $A$  and  $Z$  published before 1998 had been discussed in relation to the participation of nuclear fissions in the CFP already [Kozima 1998 (Sec. 9.2), 2006 (Sec. 2.5), 2014b (Sec. 2.4)]. In Section 4, we investigate the 25 experimental data sets obtained until 2017 from a new point of view for the data. The analysis of these data sets with the ND model will show the ability of the model to give a unified understanding of the CFP. In Section 5, the inductive logic and the meta-analysis necessary to investigate the CFP conditioned by complexity are briefly discussed leaving the full discussion to another paper [Kozima 2019a]. In Section 6, Conclusion, it is confirmed that the explanation of the CFP by the ND model, including the investigation of the nuclear transmutations analyzed in this paper, gives a foundation of the science of the CFP.

In Appendix A, we noticed some problems in the experiments on the nuclear transmutation. In Appendix B, we have given some key concepts used in our analysis on the product nuclei of the nuclear transmutation.

## 2. Experimental Results in the Cold Fusion Phenomenon (CFP)

It is interesting to see the ubiquitous appearance of the CFP in various CF materials as shown in Table 2.1.

Table 2.1. Systems and Obtained Evidences of the CFP: Host solids, agents, experimental methods, direct and indirect evidence, cumulative and dissipative observables are tabulated.  $Q$  and NT express excess energy and the nuclear transmutation, respectively. The direct evidence of nuclear reactions in the CFP is the dependences of reaction products on their energy ( $\varepsilon$ ) and position ( $\mathbf{r}$ ), the decrease of decay constants of radioactive nuclides, the decrease of fission threshold energy of compound nuclei.

Host solids	C, Pd, Ti, Ni, Au, Pt, KCl + LiCl, ReBa <sub>2</sub> Cu <sub>3</sub> O <sub>7</sub> , Na <sub>x</sub> WO <sub>3</sub> , KD <sub>2</sub> PO <sub>4</sub> , TGS (triglycine sulfate), SrCe <sub>a</sub> Y <sub>b</sub> Nb <sub>c</sub> O <sub>d</sub> , XLPE (cross linked polyethylene), Biological Systems (microbial cultures)
Agents	$n, d, p, {}^6_3\text{Li}, {}^{10}_3\text{B}, {}^{12}_6\text{C}, {}^{39}_{19}\text{K}, {}^{85}_{37}\text{Rb}, {}^{87}_{37}\text{Rb}$
Experiments	Electrolysis, Liquid contact, Gas discharge, Gas contact
Direct evidences of nuclear reaction	Gamma ray spectrum $\gamma(\varepsilon)$ , Neutron energy spectrum $n(\varepsilon)$ , Space distribution of NT products $\text{NT}(\mathbf{r})$ , Stabilization of unstable nuclei (Decrease of decay constants), lowering of fission threshold energy
Indirect evidences of nuclear reaction	Excess energy $Q$ , Number of neutrons $N_n$ , Amounts of tritium atom $N_t$ , helium-4 atom* $N_{\text{He4}}$ , NT products ( $\text{NT}_D, \text{NT}_F, \text{NT}_A$ ), X-ray spectrum $X(\varepsilon)$
Cumulative observables	$\text{NT}(\mathbf{r})$ , amount of tritium atom $N_t$ , helium-4* $N_{\text{He4}}$ ,
Dissipative observables	Excess energy $Q$ , neutron energy spectrum $n(\varepsilon)$ , number of neutrons $N_n$ , Gamma ray spectrum $\gamma(\varepsilon)$ , X-ray spectrum $X(\varepsilon)$ ,

A remarkable characteristic of the nuclear reactions in the CFP is the fact that there are observed no gamma radiations accompanied to the nuclear reactions producing transmuted nuclei in contrast to the case in free space where are observed always any radiation such as gamma, beta and alphas with energies liberated by the nuclear reaction [Kozima 1998, 2006, 2017b]. Furthermore, there is another remarkable characteristic of the nuclear transmutations in the CFP that the generation of new elements  ${}^A_Z\text{X}$  with large shifts of the mass number  $A$  and the proton number  $Z$  from those of elements pre-existed in the CF materials. It is also noticed that the observed distribution of  ${}^A_Z\text{X}$  over the proton number  $Z$  is in accordance with the abundances of elements in the universe [Kozima 2006, 2012b, Suess 1956, Trimble 1975].

Because it is out of the question to assume fusion reactions between charged nuclei in solids at near room temperature without any acceleration mechanisms as discussed already in our book [Kozima 2006 (Sec. 3.4)], it is our common sense in nuclear physics to assume participation of neutrons to explain the occurrence of nuclear reactions in CF materials. We have proposed models (TNCF model and its extended version the ND (neutron drop) model) with an adjustable parameter  $n_n$  to explain the CFP. We have been successful to give unified systematic explanation of diverse and complex experimental data in this field [Kozima 1994, 1998, 2006].

The quantum mechanical investigation of the neutron-proton (and neutron-deuteron)

interaction in CF materials has given an explanation of the origin of the trapped neutrons assumed in the TNCF model [Kozima 2006 (Secs. 2.4 and 3.7)]. The existence of neutrons as the cf-matter [Kozima 2006 (Sec. 2.4.2)] in the CF materials composed of a superlattice of host elements and hydrogen isotopes justified the progress of the TNCF model into the ND model, an extended version of the former.

It should be noticed that the CF materials include biological systems, nuclear transmutations in them had been noticed more than 200 years ago [US AMTL 1978, Kushi 1994, Kozima 1998 (Section 10.1), 2018]. These biological systems have been cultivated recently to include microbial cultures [Vysotskii 1996, 2015] that are discussed briefly in Section 2 leaving full discussion in the previous paper [Kozima 2016b, 2018].

We must reconsider the role of the deductive and inductive logics in science at the beginning of the 21<sup>st</sup> century when a new branch in science characterized by complexity has been excavated in these 20 – 30 years. It is also noticed that the analysis of experimental data should be reconsidered taking up the meta-analysis used effectively in modern medical science. We give a brief overview on this problem in this paper leaving full discussions to another paper [Kozima 2019a].

In short, the roots of the fruitless battle fought between people in favor of CFP and those opposed to it have been in the two causes. (1) The deductive logic we have been accustomed to it in science since the dawn of the modern science in the 18<sup>th</sup> century based on the linear dynamics, and (2) Ignorance of the meta-analysis which is effective to analyze complicated data observed independently in similar samples by several researchers as discussed in another paper extensively [Kozima 2019a].

Since the development of the non-linear dynamics in the second half of 20<sup>th</sup> century, we have to realize the fact that the cause does not necessarily determine the effect in this real world where almost all phenomena are governed by non-linear dynamics. However, this fact has almost been put out of our discussion on the reality of the CFP in these almost 30 years.

In relation to the following discussion on the nuclear transmutation, we have to give a word to the fact that it is very difficult to determine the mass  $A$  and proton  $Z$  numbers of an unknown nuclide exactly even by the latest techniques such as TOF SIMS and we have given an overview of the recent technique in Appendix A.

### **3. Experimental Results on the Nuclear Transmutation and Stabilization of Unstable Nuclei in the Cold Fusion Phenomenon**

The nuclear transmutations in the cold fusion phenomenon (CFP) occur mainly in near-surface regions of the CF materials with width of about a few micrometers. Variety

of the products of the nuclear transmutation ranges very wide and we need to classify them by some standards to investigate them systematically.

### 3.1 Nuclear Transmutations in the CFP

The nuclear transmutations (NTs) are classified into four kinds according to the mechanism to produce new nuclides from the original nuclei in the CF material; NT<sub>A</sub> (nuclear transmutation by absorption), NT<sub>D</sub> (nuclear transmutation by decay), NT<sub>F</sub> (nuclear transmutation by fission), and NT<sub>T</sub> (nuclear transmutation by transformation) in our model [Kozima 2006 (*Section 2.5 Nuclear Transmutations*), 2014c].

The stabilization of unstable nuclei (including decay-time shortening of unstable nuclei) observed in the CFP has mainly been successfully explained by the NT<sub>D</sub> even if other mechanisms are not necessarily excluded. We will give explanation on the stabilization of unstable nuclei in this Section along the line of the explanation made in our papers with use of the NT<sub>D</sub> [Kozima 2018].

#### 3.1.1 Nuclear Transmutations in TiD<sub>x</sub>, PdD<sub>x</sub> and NiH<sub>x</sub>

The experimental data sets showing nuclear transmutations along with other observables such as excess energy  $Q$ , neutron emission  $n$ , and tritium  $t$ , had been analyzed by the TNCF model [Kozima 1998, 2004, 2006]. The results of the analyses had shown the applicability of the model to explain the CFP as a whole; the parameter  $n_n$  is determined as in between  $10^8 - 10^{12} \text{ cm}^{-3}$  and the theoretical ratio  $N_a/N_b|_{\text{th}}$  of the numbers  $N_a$  and  $N_b$  of events  $a$  and  $b$  is in accordance with the experimental ratio  $N_a/N_b|_{\text{ex}}$  in a factor 3 [Kozima 1998 (Tables 11.2 and 11.3), 2006 (Tables 2.2 and 2.3)];

$$N_a/N_b|_{\text{th}} = m N_a/N_b|_{\text{ex}} (m \leq 3).$$

The nuclear transmutations of Ti and Pd in cathodes were observed in electrolytic experiments where their isotopic ratios had been determined. The analyses of these results were given by the TNCF model giving semi-quantitative explanation [Kozima 2006 (Appendix C7)]

It is interesting to notice that the products of the nuclear transmutations in PdD<sub>x</sub> and in NiH<sub>x</sub> show different characteristics each other. In the former, the nuclear transmutation seems to occur rather quiet manner and the transmuted nuclei have  $A$  and  $Z$  a little different from those of pre-existed nuclei in the system. In the latter, however, we observe transmuted nuclei with  $A$  and  $Z$  with large difference from those of pre-existed nuclei (e.g. [Miley 1996a, 1996b], [Kozima 2006 (Appendix C6)]). In the words of our approach, the former is explicable with the original TNCF model by absorption of single neutron and the latter needs neutron drops to explain the experimental results.

The distinction of the mechanisms in PdD<sub>x</sub> and NiH<sub>x</sub> to explain the nuclear transmutations occurring in them may have its origin in the difference of numbers of neutrons in the neutron bands. In the former, there is a few neutrons in the neutron band and nuclear reactions occur mainly by absorption of single neutron. In the latter, there are a lot of neutrons to form the cf-matter and neutron drops in it and they participate to induce nuclear transmutations. The distinction of the neutron bands in PdD<sub>x</sub> and NiH<sub>x</sub> speculated above should be explained by quantum mechanical estimation using concrete parameters of both materials.

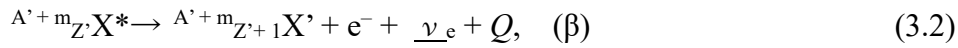
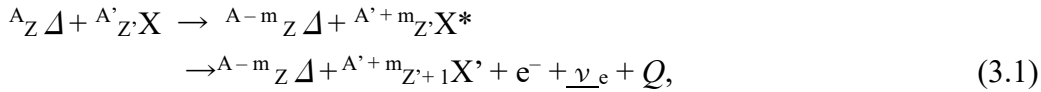
The nuclear transmutation in hydrogen carbon CH<sub>x</sub> [Kozima 2012c] which will be discussed briefly in Sec. 3.3 below seems to resemble NiH<sub>x</sub> in the production of new nuclei with large shifts of *A* and *Z*.

### 3.2 Stabilization of Unstable Nuclei in the CFP

We have given explanation on the stabilization of unstable nuclei (including decay-time shortening) in the CFP as follows [Kozima 2006 (*Sec. 2.5.1.1 Decay Time Shortening*), 2018].

#### 3.2.1 Decay-Time Shortening

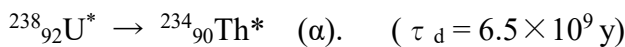
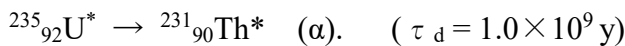
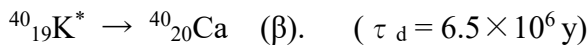
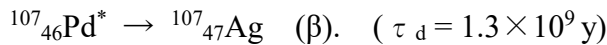
In general, the explanations of the mechanisms of the nuclear transmutations by decay (NT<sub>D</sub>) with absorption of several neutrons are given by the following reaction formulae:



where  $\alpha$  and  $\beta$  in parentheses designate types of the decay.

In these nuclear transmutations, there are several cases where the decay-times  $\tau_d$  of the intermediate compound nuclide  ${}^A_ZX^*$  are very long of orders of  $10^6$  to  $10^9$  years ( $10^{12}$  –  $10^{15}$  s) in free space. The time elapsed in experiments is at most several months ( $\approx 10^5$  s). Therefore, if the decay products with such long decay-times in free space are observed, there should be drastic shortening of the decay-times (or stabilization of unstable nuclei).

Following compound nuclei correspond to this case [Kozima 2018]:



#### 3.2.2 Nuclear Transmutation in Actinoid Hydrides and Deuterides

Experimental data sets on actinoid hydrides and deuterides prepared by electrolysis and glow discharge have been analyzed and explained using the TNCF model [Kozima 2014b, 2018]. The experimental data have shown that these hydrides and deuterides are classified into the CF materials where occurs the CFP and the observed events are understood by nuclear reactions common to those observed in CF materials, mainly transition-metal hydrides and deuterides. Details of the analysis on the data for the nuclear transmutation in actinoid hydrides and deuterides were given in our previous paper [Kozima 2014b].

### 3.3 Nuclear Transmutation in Hydrogen Graphite HC<sub>x</sub>

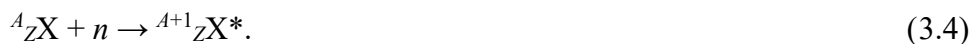
The experimental data obtained in the arc discharge between graphite electrodes in water has given wonderful results showing generation of various elements including Si, S, Cl, K, Ca, Ti, Cr, Mn, Co, Ni, Cu, Zn besides Fe, the most abundant element. We had given explanation of this event using the TNCF and ND models [Kozima 2012c, 2015] and its brief explanation was given in our recent paper [Kozima 2018].

### 3.4 Nuclear Transmutation in XLPE

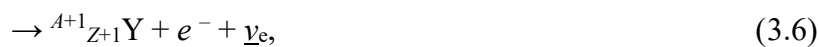
Similarly, we can contemplate appearance of neutron energy bands in XLPE by the mechanism shown in our books [Kozima 1998 (Fig. 12.3), 2006]. The rather regular structure of the carbon-hydrogen array in XLPE [Kozima 2010a (Fig. 5)] suggests similar mechanism of super-nuclear interaction among neutrons in different lattice nuclei to form the neutron energy bands as discussed in our recent paper [Kozima 2010a, 2016b]. The explanation of nuclear transmutations observed in XLPE using the TNCF and ND models was given in our previous paper [Kozima 2010a].

### 3.5 Characteristics of Biotransmutation

Allowing application of the TNCF model to the problems of biotransmutation, we can use following reactions between a trapped neutron  $n$  and a nucleus  ${}^A_ZX$  at or in the surface of a bacterium or a biological tissue [Kozima 2016b]:



In this reaction formula,  ${}^{A+1}_ZX^*$  is an excited state of the nucleus  ${}^{A+1}_ZX$  which will decay through following several channels in free space;



where  $\bar{\nu}_e$  is an anti-electron neutrino,  $\gamma$  is a photon (in free space) and Y, Y' and Y'' are daughter nuclides of the reactions. In the CF materials, the liberated energy emitted as the *photon*  $\gamma$  in the free space is supposed to be absorbed by the cf-matter composed of neutrons in the neutron energy band and its energy dissipates into *phonons* to heat the system as a whole [Kozima 2006 (Section 3.7.5)].

The details of the above discussions on these problems had been given in our recent paper [Kozima 2018].

### **3.6 Lack of Gamma Emission in the Nuclear Reactions in the CFP**

In the history of the cold fusion research, the origin of the nuclear products observed in this field had been supposed to be the nuclear fusion reactions between two deuterons as shown in Eqs. (1.1) – (1.3). And therefore, the lack of gamma radiation from the CF materials where observed nuclear products, excess energy, neutron, tritium and nuclear transmutation was the center of dispute as briefly surveyed in our report [Kozima 2017b].

There are few data showing emission of gamma photons in the CF materials as summarized in our book [Kozima 1998 (Sec. 6.3)] and a recent experiment in XLPE by Kumazawa et al. [Kumazawa 2007].

To explain this characteristic of the CFP, the lack of gamma emission in nuclear reactions in the CF material, it is necessary to use a new mechanism for the nuclear reactions for the CFP. One of the possible mechanisms to this requirement is our ND model where the liberated energy of the nuclear reaction is shared by the cf-matter and then dissipated into the thermal energy of the CF material. This idea has been assumed throughout in our books and papers (e.g. [Kozima 1998 (Sec. 12.8c), 2006 (Sec. 2.10, Sec. 2.2.2.1)]).

## **4. Nuclear Reactions generating Nuclei with Large Shifts of $A$ and $Z$ from those of Pre-existed Nuclides**

The nuclear transmutations in the CF materials without any mechanisms of acceleration are astonishing events themselves as surveyed in Section 2. In addition to this fact, we have had more surprising facts that there were generated nuclides with the mass number  $A$  and the proton number  $Z$  shifted largely from those of pre-existed ones in the CF materials; an extraordinary example is such heavy element as lead (Pb) in Ni [Miley 1996a (Fig. 2), Kozima 2006 (Fig. 2.7)]. It was troublesome events to explain them for scientists accustomed to the nuclear physics developed in the 20<sup>th</sup> century.

As we have shown in our books [Kozima 19998, 2006] and papers [Kozima 2005, 2013, 2015, 2017a, 2018], a great diversity of experimental data sets has consistently

been explained by the TNCF model and the ND model where existence of the trapped neutrons with a density  $n_n$  is assumed as a fundamental premise.

We have used the TNCF model to explain the nuclear transmutation when the shifts of the proton and nucleon numbers  $Z$  and  $A$  were 1 or 2; absorption of a neutron by a nucleus in the system followed by a decay process has explained the generation of the transmuted nuclei [Kozima 1998].

We have used the ND model to explain the nuclear transmutations with large shifts of  $A$  and  $Z$  in several experimental data sets already in our books and papers [Kozima 1998 (Secs. 9.2, 11, and 12), 2006 (Secs. 2.5.3, 2.5.4, and 2.5.5), 2014a, 2014c]. In these explanation of the nuclear transmutations with larger shifts of  $Z$  and  $A$  than two units by the ND model, we assumed participation of a neutron drop  ${}^A_Z\Delta$  with  $A$  and  $Z$  larger than two [Kozima 2005, 2006].

Theoretically, the possible existence of the trapped neutrons and neutron drops in the CF materials has been explained by the quantum mechanical investigation of the nuclear interaction between a neutron in lattice nucleus and a proton/deuteron at interstitial site. It has been shown existence of the *super-nuclear interaction* among neutrons in different lattice nuclei mediated by interstitial protons/deuterons which results in formation of the neutron energy bands and the neutron drops in them [Kozima 2006, 2014a, 2014c].

These explanations of nuclear transmutations observed in the CFP using our models have given reality of existence of neutrons in the CF materials that caused extraordinary phenomenon not observed in free space. However, the extraordinary events in the CF materials should be investigated thoroughly to give detailed explanation acceptable to scientists accustomed to the nuclear physics developed in free space. To extend our explanation to experimental data sets obtained recently, we have taken up 25 data sets further in this paper and analyze them by our ND model to show further the applicability of the model and accordingly reality of the new state of neutrons in the CF materials not noticed before.

#### **4.1 Recent Experimental Facts of Nuclear Reactions generating Nuclides with $A$ and $Z$ shifted largely from those of Pre-existed Ones**

We had given the results of analyses on the experimental data sets where observed nuclear transmutations in our books and papers [Kozima 1998 (Chapters 9 and 10), 2006 (Section 2.5), 2017a, 2018]. There have appeared many experimental data sets in the field of the CFP more than those we have given our analyses as those cited above. From our point of view, those data not analyzed yet are within our range of analysis and we will give some examples of our analysis on the recent data in this section.

We show some of the recent experimental data selected by our standard in Tables 4.1 – 4.8 tabulated according to different parameters. The correspondence of the References to the experimental data tabulated in these tables (e.g. 1) for K<sup>1)</sup>) to the References in this paper (e.g. [Sasaki 2002]) is given at the end of Table 4.7 (e.g. as 1) [Sasaki 2002]).

Each table gives the products of the nuclear transmutation in terms of a characteristic of the experiment where the product elements were determined. We can see from these tables that there are diversity of nuclear transmutations in the CFP depending on the various factors of the experiment.

Table 4.1 Detected elements with large isotopic shifts, classified by the method of analysis. (References in this table are correlated to References in this paper at the end of Table 4.7).

Method of analysis	Detected elements
SIMS	S <sup>12)</sup> Cr <sup>10)</sup> Sr <sup>7)</sup> Pd <sup>8)9)10)</sup>
TOF-SIMS	Li <sup>14)</sup> K <sup>1)13)</sup> Ti <sup>6)</sup> Cr <sup>3)6)</sup> Fe <sup>3)12)</sup> Ni <sup>16)</sup> Pd <sup>2)4)</sup>
NAA	Zn <sup>11)</sup> Ag <sup>15)</sup>
ICP-MS	Si <sup>12)</sup> Pb <sup>5)</sup>

Table 4.2 Detected elements with large isotopic shifts, classified by the experimental method. (References in this table are correlated to References in this paper at the end of Table 4.7).

Experimental method	Detected elements
Electrolysis	Si <sup>12)</sup> K <sup>1)13)</sup> Cr <sup>10)</sup> Fe <sup>12)</sup> Ni <sup>16)</sup> Sr <sup>7)</sup> Pd <sup>2)4)8)10)</sup> Ag <sup>15)</sup> Pb <sup>5)</sup>
Gas discharge	Pd <sup>9)</sup>
Gas permeation, exposure	Li <sup>14)</sup> Si <sup>12)</sup> S <sup>12)</sup> Ti <sup>6)</sup> Cr <sup>3)6)</sup> Fe <sup>3)12)</sup> Zn <sup>11)</sup>

Table 4.3 Detected elements with large isotopic shifts, classified by the test sample. (References in this table are correlated to References in this paper at the end of Table 4.7).

Test sample	Detected elements
Pd	Li <sup>14)</sup> Si <sup>12)</sup> S <sup>12)</sup> Ti <sup>6)</sup> Cr <sup>3)6)10)</sup> Fe <sup>3)12)</sup> Zn <sup>11)</sup> Pd <sup>2)4)8)9)10)</sup> Pb <sup>5)</sup>
Ni	Ni <sup>16)</sup> Sr <sup>7)</sup> Ag <sup>15)</sup>
Co	K <sup>1)</sup>
Re	K <sup>13)</sup>

Table 4.4 Detected elements with large isotopic shifts, classified by the environment atom. (References in this table are correlated to References in this paper at the end of Table 4.7).

Environment atom	Detected elements
D	Li <sup>14)</sup> Si <sup>12)</sup> S <sup>12)</sup> K <sup>13)</sup> Cr <sup>10)</sup> Fe <sup>12)</sup> Zn <sup>11)</sup> Pd <sup>8)10)</sup> Pb <sup>5)</sup>
H	Li <sup>14)</sup> K <sup>1)13)</sup> Ti <sup>6)</sup> Cr <sup>3)6)</sup> Fe <sup>3)</sup> Ni <sup>16)</sup> Sr <sup>7)</sup> Pd <sup>2)4)</sup> Ag <sup>15)</sup>
Xe/Ar mixture	Pd <sup>9)</sup>

Table 4.5 Detected elements with large isotopic shifts, classified by  $\Delta Z(\geq 2)$ . (References in this table are correlated to References in this paper at the end of Table 4.7).

$\Delta Z(\geq 2)$	Detected elements
2	La <sup>20)</sup> Os <sup>23)</sup>
3	K <sup>24)</sup> Ir <sup>22)</sup>
4	Mo <sup>17)18)21)</sup> Pr <sup>17)19)23)25)</sup> Pt <sup>23)</sup>
6	F <sup>12)</sup> Mg <sup>12)</sup> Sm <sup>23)</sup>
8	Si <sup>12)</sup>
10	Al <sup>12)</sup> S <sup>12)</sup>

To see the relation of changes of the nucleon number  $A$  and the proton number  $Z$  of the generated nuclides from the pre-existed host nuclei, we tabulated  $\Delta Z(> 2)$  and  $(\Delta A)_{\min}$  (or  $(\Delta A)_{\max}$ ) of transmuted nuclei in Table 4.6 (or Table 4.7). There are no experimental data of the isotopic distribution of the transmuted nuclei and, therefore, we have to satisfy with the  $(\Delta A)_{\min}$  and  $(\Delta A)_{\max}$  values.

The relation of these results with the magic number of atomic nuclei is qualitatively investigated in Appendix B.

Table 4.6 Detected elements with large isotopic shifts, classified by  $\Delta Z(\geq 2)$  vs. the minimum value of the shift of the nucleon number  $(\Delta A)_{\min}$ . (References in this table are correlated to References in this paper as shown at the end of Table 4.7).

		$(\Delta A)_{\min}$					
		3	4	5	8	10	11–20
$\Delta Z$	2		La <sup>20</sup> Os <sup>23</sup> )				
	3	K <sup>24</sup> )		Ir <sup>22</sup> )			
	4		P <sup>23</sup> )		Mo <sup>17</sup> 18)21) Pr <sup>17</sup> 19)23)25)		
	6						F <sup>12</sup> ) Mg <sup>12</sup> ) Sm <sup>23</sup> )
	8						Si <sup>12</sup> )
	10						Al <sup>12</sup> ) S <sup>12</sup> )

Table 4.7 Detected elements with large isotopic shifts, classified by  $\Delta Z (\geq 2)$  vs. the maximum value of the shift of the nucleon number  $(\Delta A)_{\max}$ . (References in this table are correlated to References in this paper as shown at the end of this Table).

		$(\Delta A)_{\max}$						
		4	7	8	10	11	12	13–24
$\Delta Z$	2	La <sup>20</sup> )			Os <sup>23</sup> )			
	3		K <sup>24</sup> )			Ir <sup>22</sup> )		
	4			Pr <sup>17</sup> 19)23)25)	Pt <sup>23</sup> )		Mo <sup>17</sup> 18)21)	
	6							F <sup>12</sup> ) Mg <sup>12</sup> ) Sm <sup>23</sup> )
	8							Si <sup>12</sup> )
	10							Al <sup>12</sup> ) S <sup>12</sup> )

### Correspondence of References in Tables 4.1 – 4.7 to the References in this paper.

1) [Sasaki 2002], 2) [Ohmori 2002], 3) [Onodera 2002], 4) [Ohmori 2003a], 5) [Celani 2003], 6) [Yamada 2003], 7) [Bush 1994], 8) [Dash 1996], 9) [Savvatimova 1996], 10) [Mizuno 1996], 11) [Passell 2000], 12) [Iwamura 2000], 13) [Ohmori 2003b], 14) [Passell

2003], 15) [Violante 2003], 16) [Rajeev 2017], 17) [Sakano 2004], 18) [Celani 2006], 19) [Higashiyama 2006], 20) [Yamada 2006], 21) [Yamaguchi 2008], 22) [Kitamura 2009], 23) [Iwamura 2013], 24) [Esko 2014], 25) [Takahashi 2014].

The results of the experiments tabulated in Tables 4.6 and 4.7 seem to show a possibility of very large changes of  $\Delta A$  which had been already noticed before and explained as results of nuclear fissions [Kozima 2006 (Sec. 2.5.3)]. About this point, further discussion is given in Appendix B.

## **4.2 Explanation of the Experimental Data by the TNCF and ND Models**

As we have given the explanation of the nuclear transmutations in our papers and books published before and in the preceding section in this paper, it is possible to understand the nuclear transmutations as a whole by our model assuming trapped neutrons in the CF materials. We give a further definitive explanation for some of experimental data discussed above in this section.

### **4.2a Overall results of the nuclear transmutation obtained recent experiments.**

The typical experimental data sets tabulated in Table 2.1 have been analyzed and published already in our books and papers [Kozima 1998, 2006, 2017a, 2018]. In these explanation of the data sets tabulated in Table 2.1 and the explanation given in Section 4.1, we could apply successfully our TNCF and ND models assuming absorption of the single neutron or the neutron drop by a nucleus in the system.

It is, however, interesting to take up the data by Rajeev et al. in the next subsection and give our investigation on their data in relation to our knowledge obtained in analyses on the previous data sets.

### **4.2b Experimental Data by Rajeev et al. obtained in the Ni-H System**

Rajeev et al. have observed nuclear transmutations in Ni/H<sub>2</sub>O (D<sub>2</sub>O) + K<sub>2</sub>CO<sub>3</sub>/Pt system [Rajeev 2017]. They used EDS (Energy Dispersive Spectroscopy) for elemental analysis of the Ni cathode used in the experiments of dc electrolysis with the electric current of 4 V and 100 A for about 2 weeks with a daily run time of 8 h in average.

The EDS analysis showed that a whole of such new elements as O, K, Fe, Cu, Rh, Zr and Pb had appeared on the cathode. The apparent concentration of the elements varied from just over a percent for K and Pb up to about 10% for Rh and 20% for Cu. The sample was then taken to a ToF-SIMS (Time of Flight Secondary Ion Mass Spectrometer) for

isotopic analysis. This analysis also showed that a set of such new elements as O, K, Ca, Si, Mg, Mn, Zn, Zr, Rh and Pb had appeared on the nickel wire. The Ni itself was found to have the following isotopes,  $^{58}\text{Ni}$ ,  $^{60}\text{Ni}$  and  $^{62}\text{Ni}$ , with isotopic concentration ratios differing significantly from the natural ratios of Ni. It was clear that the concentrations of  $^{60}\text{Ni}$  and  $^{62}\text{Ni}$  in the electrolyzed Ni had gone down compared to the concentration of  $^{58}\text{Ni}$ .

#### 4.2b-1 Generation of New Elements

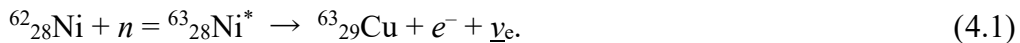
We summarized the experimental result by Rajeev et al. in Table 4.8 below. The inconsistency in the results of EDS and ToF-SIMS should be understood as the dispersion of data depending on the position in the analyzed Ni cathode and also on the characteristics of both techniques.

The amounts of copper (Cu) and rhodium (Rh) are remarkable not saying the expected detection of oxygen (O) and potassium (K) that are in the electrolyte.

It is easy to give an explanation for new elements using the ND model. We give here only two examples of our explanation for Cu and Rh.

##### (a) Copper (Cu)

To obtain copper  $^{63}_{29}\text{Cu}$  and  $^{65}_{29}\text{Cu}$  from  $^{58}_{28}\text{Ni}$ ,  $^{60}_{28}\text{Ni}$ ,  $^{61}_{28}\text{Ni}$ ,  $^{62}_{28}\text{Ni}$ ,  $^{64}_{28}\text{Ni}$ , it is necessary to increase  $Z$  by 1 and  $A$  by 1 – 5 in general. The neutron drops  $^A_Z\Delta$  ( $A = 1 - 5$ ,  $Z = 0$  or 1) are responsible to these transmutations in our ND model. The most probable reaction will be, e.g. in the case of  $^{63}_{29}\text{Cu}$  production, by the reaction (3.6) or (4.1) below;



The decay time of  $^{63}_{28}\text{Ni}$  is 100.1 y in free space but we can expect the acceleration of the decay by cf-matter as proposed already [Kozima 2006 (Sec. 2.5.1.1), 2018].

Table 4.8 Nuclides determined by EDS and ToF-SIMS techniques by Rajeev et al. in Ni-H electrolysis experiments [Rajeev 2017]. The cathode material, nickel (Ni), is placed in the second row in this Table. The concentration (%) of the element determined by EDS is shown in the second column. Mass numbers were not necessarily determined. Chemical symbols are in bold face when the elements were detected by both techniques.

Z	Symbol	%	Isotopes
28	Ni		$^{58}_{28}\text{Ni}$ , $^{60}_{28}\text{Ni}$ , $^{61}_{28}\text{Ni}$ , $^{62}_{28}\text{Ni}$ , $^{64}_{28}\text{Ni}$ ,
8	O		$^{16}_8\text{O}$ , $^{17}_8\text{O}$ , $^{18}_8\text{O}$ ,
12	Mg		$^{24}_{12}\text{Mg}$ , $^{25}_{12}\text{Mg}$ , $^{26}_{12}\text{Mg}$ ,
14	Si		$^{28}_{14}\text{Si}$ , $^{29}_{14}\text{Si}$ , $^{30}_{14}\text{Si}$ ,
19	K	1	$^{39}_{19}\text{K}$ , $^{40}_{19}\text{K}$ , $^{41}_{19}\text{K}$ ,
20	Ca		$^{40}_{20}\text{Ca}$ , $^{42}_{20}\text{Ca}$ , $^{43}_{20}\text{Ca}$ , $^{44}_{20}\text{Ca}$ , $^{46}_{20}\text{Ca}$ , $^{48}_{20}\text{Ca}$ ,
25	Mn		$^{55}_{25}\text{Mn}$
26	Fe		$^{54}_{26}\text{Fe}$ , $^{56}_{26}\text{Fe}$ , $^{57}_{26}\text{Fe}$ ,
29	Cu	20	$^{63}_{29}\text{Cu}$ , $^{65}_{29}\text{Cu}$ ,
30	Zn		$^{64}_{30}\text{Zn}$ , $^{66}_{30}\text{Zn}$ , $^{67}_{30}\text{Zn}$ , $^{68}_{30}\text{Zn}$ , $^{70}_{30}\text{Zn}$ ,
40	Zr		$^{91}_{40}\text{Zr}$ , $^{92}_{40}\text{Zr}$ , $^{94}_{40}\text{Zr}$ , $^{96}_{40}\text{Zr}$ ,
45	Rh	10	$^{103}_{45}\text{Rh}$
82	Pb		$^{204}_{82}\text{Pb}$ , $^{206}_{82}\text{Pb}$ , $^{207}_{82}\text{Pb}$ , $^{208}_{82}\text{Pb}$ ,

#### (b) Rhodium (Rh)

To obtain  $^{103}_{45}\text{Rh}$  from nickel isotopes in the cathode, we need large increase of  $Z$  by 17 and  $A$  by 39 – 45. It is possible to explain this transmutation by an absorption of a large neutron drop  $^A_Z\Delta$  ( $A = 39 - 45$ ,  $Z = 17$ ) or by multiple absorptions of smaller neutron drops, e.g.  $^A_Z\Delta$  ( $A = 20 - 26$ ,  $Z = 10$ ) and  $^{A'}_{Z'}\Delta$  ( $A' = 19$ ,  $Z' = 7$ ) even if this is too artificial. Anyway, the cf-matter works effectively to induce various nuclear transmutations as shown above also in a previous book and papers [Kozima 2006, 2014c, 2018]

#### 4.2b-2 Change of Isotope Ratios of Ni

The experimental data by Rajeev et al. [Rajeev 2017] have shown the decrease of  $^{60}\text{Ni}$  and  $^{62}\text{Ni}$  compared to the concentration of  $^{58}\text{Ni}$ . There have had several experimental data sets showing shifts of isotopic ratios of generated elements in Ti, Ni and Pd. We have given successful explanations of quantitative relations between observed isotopes using the TNCF model. One of the successful explanations are given in our book using a single-neutron absorption by the nucleus of host metal element followed by a decay of the intermediate nucleus [Kozima 2006 (Appendix C7)].

We would like to apply the same recipe to the data obtained by Rajeev et al. The absorption cross-section of a thermal neutron by Ni isotopes are given in Table 4.9.

Table 4.9 Absorption cross-section  $\sigma_{n\text{-Ni}}$  (barns) of a thermal neutron by  ${}^A_{28}\text{Ni}$  isotopes.

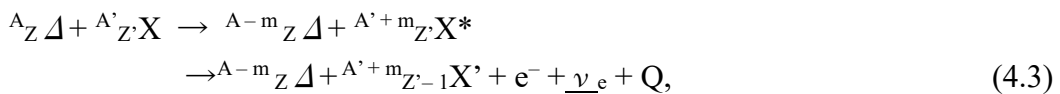
$A$	<b>58</b>	<b>60</b>	61	<b>62</b>	64
$\sigma_{n\text{-Ni}}$ (barns)	4.503	2.900	2.509	14.20	1.480

It is concluded that the single neutron process is not applicable to this case as follows. If the nickel nuclei at lattice points absorb a neutron (single neutron process) and their concentrations change according to Eq. (4.1) in the cases of  ${}^A_{28}\text{Ni}$  ( $A = 58$  and  $62$ ) or according to Eq. (4.2) below in the case of  ${}^A_{28}\text{Ni}$  ( $A = 60$ ),  ${}^{58}_{28}\text{Ni}$  decreases faster than  ${}^{60}_{28}\text{Ni}$  due to the difference of the absorption cross-section. This is in contradiction to the experimental data and the mechanism by single neutron absorption is not applicable in this case.



Therefore, we have to rely on the neutron drop absorption to explain the data of the isotope shifts for Ni in this experiment. The idea of the neutron drop to treat the large changes of  $A$  and  $Z$  had been suggested by the simulation calculation of in neutron star matter by Negele et al. [Negele 1973] and successfully applied to explain the nuclear transmutations observed in CFP [Kozima 2006]. Of which model, the TNCF or the ND models, we should use for the explanation of the experimental result depend on the situation of the experiment where the nuclear transmutation is observed

It is interesting to notice here the difference of NiH and PdD systems in terms of the nuclear transmutations in the CFP. Generally speaking, the nuclear transmutations in the PdD systems are explained by the mechanism where a single neutron participates in the nuclear reactions. On the other hand, the nuclear transmutations in the NiH systems are explained not by the single neutron mechanism but by the neutron drop mechanism Eq. (3.1) or (4.3) below;



In relation to this characteristics of nuclear transmutations in PdD and NiH systems, we have noticed the density of trapped neutrons determined in the TNCF model is smaller in the former than in the latter system. The dependence of the nuclear transmutations on the CF material are discussed in the next subsection 4.2c.

#### 4.2c Nuclear Transmutations depending on the CF Materials

As noticed on the end of the previous subsection, the density of trapped neutrons determined by the TNCF model is, generally speaking, smaller in the PdD systems than in the NiH systems. This tendency is shown in our books (e.g. [Kozima 1998 (Tables 11.2

and 11.3), 2006 (Tables 2.2 and 2.3)] and papers (e.g. [Kozima 2019b (Tables C1 and C2)]. It seems that the cf-matter formed in the NiH systems has more dense neutron density than in the PdD systems. To see the tendency more clearly, we tabulated the values of the density of the trapped neutrons  $n_n$  in Pd/D/Li in Table 4.10 and those in Ni/H/K, Ti/D/Li and other systems in Tables 4.11 from our analyses cited above.

Table 4.10 The density of the parameter  $n_n$  in the TNCF model determined by experimental data on the Pd/D/Li system [Kozima 2006 (Table 2.2), 2019b (Table C1)].

Experiment	1	2	3	4	5	6	7	8	9	10
$n_n$	$10^9$	$4.8 \times 10^8$	$3.6 \times 10^7$	$1.8 \times 10^6$	$10^{12}$	$2.2 \times 10^7$	$5.5 \times 10^{10}$	$3 \times 10^5$	$10^{10}$	$10^{10}$

Experiment	11	12	13	14	15	16	17	18	19	20
$n_n$	$3.0 \times 10^9$	$10^{12}$	$10^{10}$	$1.1 \times 10^9$	$8.5 \times 10^9$	$3.2 \times 10^6$	$4 \times 10^5$	$3.5 \times 10^7$	$2.2 \times 10^9$	$10^{13}$

Experiment	21	22	23	24	25	26	27	28
$n_n$	$3.5 \times 10^{10}$	$\times 10^{11}$	$1.1 \times 10^9$	$2.6 \times 10^8$	$3.9 \times 10^8$	$8.7 \times 10^7$	$3.9 \times 10^8$	$3.1 \times 10^{10}$

Table 4.11 The density of the parameter  $n_n$  in the TNCF model determined by experimental data on the Ni/H/K (**Experiments 1 – 9**, in bold face), Ti/D/Li (Experiments 10 – 15) and other systems [Kozima 2006 (Table 2.3), 2019b (Table C2)]. (Experiments is contracted as Exp. in this Table.)

Exp.	<b>1</b>	<b>2</b>	<b>3</b>	<b>4</b>	<b>5</b>	<b>6</b>	<b>7</b>	<b>8</b>	<b>9</b>	10
$n_n$	<b><math>3.4 \times 10^8</math></b>	<b><math>5.3 \times 10^{10}</math></b>	<b><math>5.3 \times 10^{11}</math></b>	<b><math>1.6 \times 10^7</math></b>	<b><math>3 \times 10^{12}</math></b>	<b><math>2.4 \times 10^{13}</math></b>	<b><math>1.4 \times 10^9</math></b>	<b><math>1.4 \times 10^9</math></b>	<b><math>1.7 \times 10^{12}</math></b>	$3.1 \times 10^{11}$

Exp.	11	12	13	14	15	16	17	18	19
$n_n$	$1.1 \times 10^9$	$1.9 \times 10^8$	$1.2 \times 10^6$	$5.4 \times 10^{11}$	$10^7$	$9 \times 10^{10}$	$6.5 \times 10^{11}$	$1.8 \times 10^7$	$10^6$

Exp.	20	21	22	23	24	25	26	27	28
$n_n$	$9.2 \times 10^{11}$	$4.0 \times 10^9$	$1.6 \times 10^{13}$	$4.0 \times 10^{10}$	$2.0 \times 10^{12}$	$10^{11}$	$1.6 \times 10^{10}$	$3.8 \times 10^{10}$	$7 \times 10^{12}$

From above tables, we can see the tendency of the larger values of the parameter  $n_n$  in the Ni/H/K system (Table 4.11, Experiments 1 – 9) than in the Pd/D/Li system (Table 4.10). The nuclear transmutations with large changes of  $A$  and  $Z$  are also observed frequently in the former than in the latter systems as we have already shown in our books [Kozima 1998 (Section 9.2), 2006 (Section 2.5)]. About this problem, we have excellent data sets obtained by Miley et al. which we have to consult for further investigation [Miley 1996a, 1996b].

We have noticed the general tendency that the generation of excess energy lasts longer in PdD than in NiH systems and the nuclear transmutations with large shifts of  $A$  and  $Z$  occur more frequent in NiH than in PdD systems. The above facts observed in the value of the parameter  $n_n$  might be the cause of these tendencies; the violent reactions occurred in the cf-matter with higher density result in higher elevation of the temperature of the CF material and then in destruction of the metal-hydrogen superlattice which induce the CFP.

### **4.3 Stability Law for the Generation of Nuclides by the Cold Fusion Phenomenon (CFP)**

On the end of this Section, we want to refer to a recent data of the abundances of the chemical elements in the universe [Trimble 1975] not used in our analysis of “the stability law” in our previous work [Kozima 2006 (Sec. 2.11), 2012b].

We had noticed a regularity or a law in the relation of the abundance of transmuted nuclei  $N_{ob}$  vs. their mass numbers  $A$  in the CFP corresponding to the abundances of elements in the universe ( $\log_{10}H$ ) vs. their mass number  $A$  [Suess 1956]. This relation in the CFP is called “*the stability law for the generation of nuclides in the CFP*” [Kozima 2006 (Sec. 2.11), 2012b].

The new paper on the origin and abundances of the chemical elements [Trimble 1975] had compared the data of Suess and Urey [[Suess 1956] with more recent one [Cameron 1968] and had concluded that there was a little difference as follows even if that did not influence the conclusion of the “stability law” induced in our paper [Kozima 2012b]; “In fact the standard abundances have been remarkably stable. Only 8 elements out of the 81 tabulated had abundances which changed by factors of 3 or more between 1956 and 1968: C, Ga, and Pb were revised upward by factors of 3, 4, and 8.5, respectively, and Be, La, Sm, Ta, and W downward by factors of 25, 4, 3, 3, and 3, respectively.” [Trimble 1975].

The revision of Pb upwards by the factor 8.5 and of Be downwards by the factor 25 are favorable for the “stability law” improving the coincidence of  $N_{ob}$  and  $\log_{10}H$ .

## 5. Inductive Logic and Meta-analysis in the CFP

We would like to give a short explanation here on the methods of analysis of complex data obtained in the CFP; the inductive logic and the meta-analysis.

The induction of the stability law for the generation of nuclides by the CFP depended on the so-called meta-analysis popular recently in the medical science even if it had been used in the time of the 18<sup>th</sup> century [Plackett 1958]. We give an extensive explanation of the statistical analysis used to induce the stability law in another paper presented at this Conference [Kozima 2019a].

Since the development of the modern science in the 16<sup>th</sup> century, the physics developed according to the deductive logic guided by fundamental principles governing simple systems described by the linear dynamics. The natural history used widely in science before the rise of modern science had been forgotten as an old-fashioned thinking pattern. However, we have to reconsider the logic useful in investigation of nature. In nature, the nonlinear interactions are ubiquitous and therefore complexity prevails as revealed by the nonlinear dynamics. The inductive logic should be an effective logic to investigate phenomena occurring in complicated systems governed by nonlinear interactions as discussed in another paper presented at this Conference [Kozima 2019a].

## 6. Conclusion

The nuclear reactions in the CFP including the nuclear transmutation are wonderful phenomena difficult to understand in the traditional solid-state physics and nuclear physics. The confusion in scientists since the discovery of the cold fusion phenomenon in 1989 has shown the overwhelming influence of the deductive logic, established in the modern science since the 17<sup>th</sup> century, on this problem as seen in the history of the CFP [Kozima 2017b, 2019a].

To understand the complex experimental data obtained in the CFP consistently, we have to depend on the phenomenological approach to the CFP using the TNCF model (trapped neutron catalyzed fusion model) [Kozima 1994, 1998] depending on a kind of the meta-analysis and then on the quantum mechanics to investigate the premises used in the model [Kozima 2006]. The TNCF model proposed in 1994 was successful to explain various events observed in the CFP qualitatively and sometimes semi-quantitatively [Kozima 1998]. The consistent explanation of experimental facts by the model has shown reality of the assumed participation of neutrons in the nuclear reactions in the CF materials where the CFP has been observed. The quantum mechanical investigation of the nuclear interaction between lattice nuclei and interstitial protons or deuterons has

shown a new feature of the interaction among lattice nuclei in the CF materials (the super-nuclear interaction) [Kozima 2006].

The nuclear transmutations with large shifts of the proton number  $Z$  and the nucleon number  $A$  from those of preexisted nuclei in the system have been observed very often especially in NiH systems [Kozima 2006 (Sec. 2.5)] which asked us to extend the TNCF model to the ND model (neutron drop model) suggested by nuclear physics of the neutron star matter [Negele 1973]. The basis of the neutron drop in cf-matter was given by the neutron energy band due to the super-nuclear interaction between neutrons in different lattice nuclei [Kozima 2006 (Sec. 3.7), 2013].

It is valuable to point out the use of the meta-analysis in such complex situations as medical fields where they call the analysis “EBM” or “Systematic Review.” The analysis of the data sets in CFP performed in our works [Kozima 1998, 2006] could be classified into the meta-analysis as shown in another paper presented at this Conference [Kozima 2019a] where we have given an extensive investigation of the meta-analysis in the CF research. We have also noticed that the logic used in our explanation of the CFP by the TNCF model is classified into the inductive logic rather than the deductive logic prevalently used in the modern science developed after the 17<sup>th</sup> century. These points were discussed furthermore in other papers presented at this Conference [Kozima 2019a, 2019b].

We have given examples of nuclear transmutations in metal-hydrogen systems in Section 2. In addition to these examples obtained in metal-hydrogen systems, there are nuclear transmutations and decay-time shortening in the carbon-hydrogen systems as introduced above in Section 3. The consistent explanation of various events in the metal-hydrogen and the carbon-hydrogen systems was given in our recent paper [Kozima 2018]. It was pointed out that we can contemplate application of the CFP to the nuclear waste treatment as discussed there. It may be possible to imagine a fantastic dream to have some microorganisms that obtain their energy from unstable nuclei destabilizing them by the mechanism we had known in the biotransmutation summarized in that paper. Biological systems are a source of miracles we have had in past and will have in future.

In Section 4, we have given a novel analysis of the nuclear transmutations with large shifts of  $A$  and  $Z$  obtained recently until 2017. The result of the analysis has confirmed the amazing characteristics of nuclear reactions occurring in the CFP very different from those in free space investigated hitherto in the nuclear physics and also has shown availability of our phenomenological approach using the TNCF and the ND models.

In conclusion, the whole data obtained in our theoretical investigation of the CFP published in our books and papers before, including the new analysis of the nuclear

transmutations observed in recent almost 20 years given in this paper have shown clearly the effectiveness of our phenomenological approach with the TNCF and ND models. It means that the existence of the neutron energy bands in the CF materials and participation of the neutrons in them are becoming realistic furthermore. We have to conclude that the CFP is a typical phenomenon in the solid state-nuclear physics where has appeared a new interaction between the host elements and interstitial hydrogen isotopes. The CFP will have a vast field of development in future as discussed in our paper [Kozima 2019b].

## **Appendices**

Appendix A.

*On the Determination of Proton and Nucleon Numbers in Cold Fusion Experiments*

Appendix B.

*Neutron Drop, Nuclear Fission, and Magic Number*

### **Appendix A. On the Determination of Proton and Nucleon Numbers in Cold Fusion Experiments**

We have given an analysis of recent experimental data sets on the nuclear transmutation using the phenomenological model proposed by one of the authors (H.K.) in 1994. In the analysis, we have trusted in the data presented in papers even when there are no description of details about the method of determination of nuclides observed in the experiment. We have followed this principle according to the spirit of the meta-analysis explained in another paper presented at this Conference [Kozima 2019a].

It is well-known, however, that the determination of the proton and nucleon numbers of unknown nucleus is very difficult. Therefore, the credibility of the analysis given in this paper largely depends on the raw materials. We hope that the papers reporting the determination of new nuclides present clearly the methods of analysis used in their analyses.

We have an example to be referred in relation to this problem. Narita et al. have found the uncertainty in determining the abundance is up to 20 %, and no clear dependence on the surface morphology [Narita 2011]. In this paper, the authors summarized knowledge about the TOF-SIMS at that time and we are able to obtain precious know-hows from this paper.

The paper reporting experimental results on the nuclear transmutation needs to fulfill following critical issues.

1. Well-documented experimental techniques and detailed analysis methods of raw data.
2. Well-selected valuable data to avoid the mountain of data useless for the analysis.
3. Presenting sufficient raw data in all the valuable data.
4. Simply-designed but sophisticated figures and tables made from the raw data.

## **Appendix B. Neutron Drop, Nuclear Fission, and Magic Number**

The neutron drops  ${}^A_Z\Delta$  participating in the generation of elements tabulated in Tables 4.6 and 4.7 (tabulated according to  $\Delta Z (> 2)$  vs.  $(\Delta A)_{\min}$  and  $\Delta Z (> 2)$  vs.  $(\Delta A)_{\max}$ , respectively) are interesting in terms of the interpretation of the nuclear transmutations with large shifts of  $A$  and  $Z$  by the nuclear fission given before [Kozima 2006 (Section 2.5.3)].

The data obtained by Miley et al. [Miley 1996a, 1996b] shows resemblance of the distribution of the generated elements on the atomic number to the distributions of fission products observed for  ${}^{233}\text{U} + n$ ,  ${}^{235}\text{U} + n$  and  ${}^{239}\text{Pu} + n$  reactions. We have suggested a possible interpretation of a part of the data obtained by Miley et al. [Miley 1996a, 1996b]; “occurrence of fissions of nuclides with atomic number  $Z$  of about 40” in terms of fission reactions [Kozima 2006 (Sec. 2.5.3)]. At that time, we have set the other part aside saying “the upper two peaks show decrease of heights with increase of  $Z$  (except Pb) that may be attributed to another cause.”

The data tabulated in Tables 4.6 and 4.7 show a possibility of absorption of such neutron drops  ${}^A_Z\Delta$  with large numbers of  $A$  and  $Z$  up to  $A = 20 - 24$  and  $Z = 6 - 10$  in the case of recent experiments in Pd systems. Then, we may have a possibility to interpret the data by Miley et al. as a whole (including the upper peaks in their data) by combination of the absorption of a neutron drop with large values of  $A$  and  $Z$  and succeeding fission of the composite nucleus.

It is desirable to have experimental data identifying the definite combination of the initial and final nuclides of a nuclear transmutation determining the neutron drop  ${}^A_Z\Delta$  participating to the reaction. Then, we can know static and dynamical properties of the neutron drop formed in a cf-matter in a CF material as we could determine the density  $n_n$  of the trapped neutrons from the data of nuclear transmutations with changes of  $A$  and  $Z$  by 1 [Kozima 1998 (Tables 11.2 and 11.3)]. We may be able to know that the rather stable

formation of the neutron drop corresponds to the nuclides with a magic number of atomic nucleus and then that the neutron drop model gives the foundation for the stability law of generated nuclei formulated in the Three Laws of the CFP [Kozima 2012b].

It is a recent tendency of experiments to perform them in Pd systems rather than in Ni systems and there are more data in the former showing remarkable data on the nuclear transmutation. However, the experimental data in the whole history of CF research show the nuclear transmutation has been observed also in Ni systems. We may be able to expect similar experimental data of nuclear transmutations in Ni systems even if there are more difficulties in this system to handle samples than in Pd systems.

### **Acknowledgement**

The authors would like to express their thanks to Dr. Masayoshi Ohmori for his valuable discussions during this work.

### **References**

- [Baym 1971] G. Baym, H.A. Bethe and C.J. Pethick, "Neutron Star Matter," *Nuclear Phys.*, **A175**, pp. 225 – 271 (1971).
- [Bush 1994] R. Bush and R. Eagleton, "Evidence for Electrolytically Induced Transmutation and Radioactivity Correlated with Excess Heat in Electrolytic Cells with Light Water Rubidium Salt Electrolytes," *Proc. ICCF4*, Vol. 2, pp. 2/1 – 2/19 (1994), TR-104188-V3 (EPRI, Palo Alto, California, USA).
- [Cameron 1968] A.G.W. Cameron, in *Origin and Distribution of the Elements*, edited by L. H. Ahrens (Pergamon, Oxford), p. 125 (1968).
- [Celani 2003] F. Celani, A. Spallone, et al., "Further Tests on Composition and Isotopic Anomalies when Pd Thin Cathode are Electrolyzed in Acidic C<sub>2</sub>H<sub>5</sub>OD/D<sub>2</sub>O Mixtures added with Th-Hg Salts at Micromolar Concentration," *Proc. JCF5*, pp. 41 – 45 (2003), ISSN 2187-2260.
- [Celani 2006] F. Celani, A. Spallone, and other 18 authors, "Thermal and Isotopic Anomalies when Pd Cathodes are electrolyzed in Electrolytes containing Th-Hg Salts dissolved at Micromolar Concentration in C<sub>2</sub>H<sub>5</sub>OD/D<sub>2</sub>O Mixtures," *Proc. ICCF10*, pp. 379–397 (2006), ISBN 981-256-564-7.
- [Dash 1996] J. Dash, "Chemical Changes and Excess Heat caused by Electrolysis with H<sub>2</sub>SO<sub>4</sub>-D<sub>2</sub>O Electrolyte," *Proc. ICCF6*, pp. 477 – 481 (1996), NEDO and Institute of Applied Energy.

- [Dash 2005] J. Dash and D. Chicea, "Changes in the Radioactivity, Topography, and Surface Composition of Uranium after Hydrogen Loading by Aqueous Electrolysis," *Proc. ICCF10* pp. 463 – 474 (2005), ISBN 981-256-564-7.
- [Esko 2014] E. Esko, "Anomalous Metals in Electrified Vacuum," *J. CMNS, Vol. 13 (Proc. ICCF17)*, pp. 114–117 (2014), ISSN 2227-3123.
- [Fleischmann 1989] M. Fleischmann, S. Pons and M. Hawkins, "Electrochemically induced Nuclear Fusion of Deuterium," *J. Electroanal. Chem.*, **261**, 301 – 308 (1989).
- [Higashiyama 2006] T. Higashiyama, H. Miyamaru, A. Takahashi, M. Sakano, "Replication of MHI Transmutation Experiment by D<sub>2</sub> Gas Permeation through Pd Complex," *Proc. ICCF10*, pp.447–454 (2006), ISBN 981-256-564-7.
- [Iwamura 2000] Y. Iwamura, T. Itoh and M. Sakano, "Nuclear Products and Their Time Dependence induced by Continuous Diffusion through Multi-layer Palladium containing Low Work Function Material," *Proc. ICCF8*, pp. 141 – 146 (2000), ISBN 88-7794-256-8.
- [Iwamura 2013] Y. Iwamura, S. Tsuruga, T. Itoh, "Increase of Transmutation Products in Deuterium Permeation Induced Transmutation," *Proc. JCF13*, pp. 196–213 (2013), ISSN 2187-2260.
- [Kitamura 2009] A. Kitamura, T. Yamaguchi, T. Nohmi, Y. Sasaki, Y. Miyoshi, A. Taniike, Y. Furuyama and A. Takahashi, "CMNS Research Progressing in Kobe University – Deuterium Permeation and Absorption –," *Proc. JCF9*, pp. 17–22 (2009), ISSN 2187-2260.
- [Kozima 1994] H. Kozima, "Trapped Neutron Catalysed Fusion of Deuterons and Protons in Inhomogeneous Solids," *Trans. Fusion Technol.* **26**, 508 - 515 (1994), ISSN 0748-1896.
- [Kozima 1996] H. Kozima, K. Hiroe, M. Nomura and M. Ohta, "Elemental Transmutation in Biological and Chemical Systems," *Cold Fusion*, **16**, 30 – 32 (1996), ISSN 1074-5610, <http://www.kozima^cfrl.com/Papers/paperc/paperc.html>.
- [Kozima 1998] H. Kozima, *Discovery of the Cold Fusion Phenomenon*, Ohtake Shuppan Inc., Tokyo, Japan, 1998. ISBN: 4-87186-044-2.
- [Kozima 2000a] H. Kozima, "Electroanalytical Chemistry in Cold Fusion Phenomenon," in *Recent Research Developments in Electroanalytical Chemistry*, pp. 35 – 46, ed. S.G. Pandalai, Transworld Research Network, 2000, ISBN 81-86486-94-8. This paper is posted at the CFRL website:  
<http://www.kozima^cfrl.com/Papers/papere/papere.html>
- [Kozima 2000b] H. Kozima, "Neutron Drop; Condensation of Neutrons in Metal Hydrides and Deuterides," *Fusion Technology*, **37**, 253 – 258 (2000), ISBN 0748-1896.
- [Kozima 2004] H. Kozima, "Quantum Physics of Cold Fusion Phenomenon," in

- Development of Quantum Physics Researches – 2004*, pp. 167 – 196 (F. Columbus and V. Krasnoholovets, ed.), Nova Science Publishers Inc., New York, ISBN 1-59454-003-9.
- [Kozima 2005] H. Kozima, “Cold Fusion Phenomenon,” *Rep. Fac. Science, Shizuoka University*, 39, pp. 21 – 90 (2005), ISSN 05830923.
- [Kozima 2006] H. Kozima, *The Science of the Cold Fusion Phenomenon*, Elsevier Science, 2006, ISBN-10: 0-08-045110-1.
- [Kozima 2010a] H. Kozima and H. Date, “Nuclear Transmutations in Polyethylene (XLPE) Films and Water Tree Generation in Them” *Proc. ICCF14* (August 10 – 15, 2008, Washington D.C., U.S.A.), pp. 618 – 622 (2010), ISBN 978-0-578-06694-3.
- [Kozima 2010b] H. Kozima, “Complexity in the Cold Fusion Phenomenon,” *Proc. ICCF14*, pp. 613 – 617 (2010), ISBN 978-0-578-06694-3.
- [Kozima 2012a] H. Kozima, “Cold Fusion Phenomenon in Open, Nonequilibrium, Multi-component Systems,” *Reports of CFRL (Cold Fusion Research Laboratory)* **12-1**, pp. 1 – 14 (January, 2012); <http://www.kozima^cfrl.com/Papers/paperr/paperr.html>
- [Kozima 2012b] H. Kozima, “Three Laws in the Cold Fusion Phenomenon and Their Physical Meaning,” *Proc. JCF12*, pp. 101 – 114 (2012), ISSN 2187-2260, [http://jcfirs.org//proc\\_jcf.html](http://jcfirs.org//proc_jcf.html).
- [Kozima 2012c] H. Kozima and M. Tada, “The Cold Fusion Phenomenon in Hydrogen-Graphite” *Proc. JCF12*, pp. 77 – 92 (2012), ISSN 2187-2260, [http://jcfirs.org//proc\\_jcf.html](http://jcfirs.org//proc_jcf.html).
- [Kozima 2013] H. Kozima, “Cold Fusion Phenomenon in Open, Nonequilibrium, Multi-component Systems – Self-organization of Optimum Structure,” *Proc. JCF13* **13-19**, pp. 134 - 157 (2013), ISSN 2187-2260. [http://jcfirs.org//proc\\_jcf.html](http://jcfirs.org//proc_jcf.html).
- [Kozima 2014a] H. Kozima and K. Kaki, “Atomic Nucleus and Neutron — Nuclear Physics Revisited with the Viewpoint of the Cold Fusion Phenomenon,” *Proc. JCF14*:**14-5**, pp. 47 - 76 (2014). ISSN 2187-2260.
- [Kozima 2014b] H. Kozima, “Nuclear Transmutation in Actinoid Hydrides and Deuterides,” *Proc. JCF14*, **14-6**, pp. 77 – 94 (2014), ISSN 2187-2260, [http://jcfirs.org/proc\\_jcf.html](http://jcfirs.org/proc_jcf.html).
- [Kozima 2014c] H. Kozima, “Nuclear Transmutations (NTs) in Cold Fusion Phenomenon (CFP) and Nuclear Physics,” *Proc. JCF14*, **14-15**, pp. 168 - 202 (2014), ISSN 2187-2260, [http://jcfirs.org/proc\\_jcf.html](http://jcfirs.org/proc_jcf.html). Also *Reports of CFRL (Cold Fusion Research Laboratory)*, **14-3**, 1 – 35 (March 2014): <http://www.kozima^cfrl.com/Papers/paperr/paperr.html>.
- [Kozima 2015] H. Kozima, “From the History of CF Research – A Review of the Typical Papers on the Cold Fusion Phenomenon –,” *Proc. JCF16*, **16-13**, pp. 116 - 157 (2016),

ISSN 2187-2260, [http://jcfirs.org/proc\\_jcf.html](http://jcfirs.org/proc_jcf.html).

[Kozima 2016a] H. Kozima, “Nuclear Transmutations in Polyethylene (XLPE) Films and Water Tree Generation in Them (2),” *Proc. JCF16*, **16-17**, 210 – 215 (2016), ISSN 2187-2260, [http://jcfirs.org/proc\\_jcf.html](http://jcfirs.org/proc_jcf.html).

[Kozima 2016b] H. Kozima, “Biotransmutation as a Cold Fusion Phenomenon,” *Proc. JCF16*, **16-18**, 216 - 239 (2016), ISSN 2187-2260, [http://jcfirs.org/proc\\_jcf.html](http://jcfirs.org/proc_jcf.html).

[Kozima 2017a] H. Kozima, M. Ohmori and M. Ohta, “Nuclear Transmutations in Critical and Supra-critical Electrolysis with Graphite, Pd, W, Re, Pt and Au Cathodes Analyzed by the TNCF Model,” *Proc. JCF17*, **17-12**, pp. 89 - 147 (2017), ISSN 2187-2260, [http://jcfirs.org/proc\\_jcf.html](http://jcfirs.org/proc_jcf.html).

[Kozima 2017b] H. Kozima, “The Sociology of the Cold Fusion Phenomenon – An Essay –,” *Proc. JCF17*, **17-13**, pp. 148 - 219 (2017), ISSN 2187-2260.  
[http://jcfirs.org/proc\\_jcf.html](http://jcfirs.org/proc_jcf.html).

[Kozima 2018] H. Kozima, “Nuclear Transmutations and Stabilization of Unstable Nuclei in the Cold Fusion Phenomenon,” *J. Condensed Matter Nucl. Sci.* **28**, 28 – 49 (2019), ISSN 2227-3123. <http://www.iscmns.org/CMNS/CMNS.htm>  
<https://www.lenr-canr.org/acrobat/BiberianJPjcondensedza.pdf>

The extended version of this paper with the same title is published as *Reports of CFRL (Cold Fusion Research Laboratory)*, **18-1**, pp. 1 – 32 (June, 2018);  
<http://www.kozima^cfrl.com/Papers/paperr/paperr.html>.

[Kozima 2019a] H. Kozima, “Inductive Logic and Meta-analysis in the Cold Fusion Phenomenon,” *Proc. JCF19*, **19-14** (2019), ISSN 2187-2260, ISSN 2187-2260 (to be published).

[Kozima 2019b] H. Kozima, “Development of the Solid State-Nuclear Physics,” *Proc. JCF19*, **19-15** (2019), ISSN 2187-2260 (to be published).

[Kumazawa 2007] 2. T. Kumazawa and R. Taniguchi, “Detection of Weak Radiation Involving Generation and Progress of Water Tree,” (in Japanese) *IEEJ Trans. FM*, **127**, 89 –96 (2007).

[Kushi 1994] M. Kushi, *The Philosopher’s Stone*, One Peaceful World Press, 1994.

[Miley 1996a] G.H. Miley, G. Narne, M.J. Williams, J.A. Patterson, J. Nix, D. Cravens, and H. Hora, “Quantitative Observation of Transmutation Products occurring in Thin-film Coated Microspheres during Electrolysis,” *Proc. ICCF6*, pp. 629 – 644 (1996).

[Miley 1996b] G.H. Miley and J.A. Patterson, “Nuclear Transmutations in Thin-film Nickel Coatings undergoing Electrolysis,” *Infinite Energy*, **9**, pp. 19 – 32 (1996).

[Mizuno 1996] T. Mizuno, T. Ohmori, T. Akimoto, K. Kurokawa, M. Kitaichi, K. Inoda, K. Azumi, S. Simokawa and M. Enyo, “Isotopic Distribution for the Elements evolved in

Palladium Cathode after Electrolysis in D<sub>2</sub>O Solution,” *Proc. ICCF6*, pp. 665 – 669 (1996), NEDO and Institute of Applied Energy.

[Nakamura 1993] K. Nakamura, *Self-developing Life – A story of Universality and Individuality* –, Tetsugaku-shobo, Tokyo, Japan, 1993, ISBN 4-88679-055-0. (In Japanese).

[Narita 2011] S. Narita, H. Yamada, H. Sasaki, H. Ougida, S. Sato, Y. Suzuki, “Systematic Uncertainties of Isotopic Abundance Measured by TOF-SIMS,” *Proc. JCF11*, pp. 36-40 (2011), ISSN 2187-2260.

[Negele 1973] J.W. Negele and D. Vautherin, “Neutron Star Matter at Sub-nuclear Densities,” *Nuclear Phys.*, **A207**, pp. 298 – 320 (1973).

[Ohmori 2002] T. Ohmori, S. Narita, H. Yamada, T. Mizuno and Y. Aoki, “Positive and negative energy evolution and new element production in critical electrolysis with Palladium electrode in K<sub>2</sub>CO<sub>3</sub>/H<sub>2</sub>O solution,” *Proc. JCF4*, pp. 22 – 26 (2002), ISSN 2187-2260.

[Ohmori 2003a] T. Ohmori, H. Yamada and S. Narita, “Anomalous Isotopic Distribution of Palladium Generated during the Light Water Critical Electrolysis on Palladium Electrodes,” *Proc. JCF5*, pp. 36 – 40 (2003), ISSN 2187-2260.

[Ohmori 2003b] T. Ohmori, H. Yamada, S. Narita and T. Mizuno, “Excess Energy and Anomalous Concentration of <sup>41</sup>K Isotopes in Potassium formed on/in a Re Electrode during the Plasma Electrolysis in K<sub>2</sub>CO<sub>3</sub>/H<sub>2</sub>O and K<sub>2</sub>CO<sub>3</sub>/D<sub>2</sub>O Solutions,” *Proc. ICCF9*, pp. 284 – 294 (2003), ISBN 7-302-06489-X.

[Ohmori 2016] T. Ohmori, “Anomalous Reactions Induced by Light and Heavy Water Electrolysis”, in *New Topics in Electrochemistry Research*, Ed. M. Nunez, pp. 47 – 84, Nova science publisher, 2016, ISBN: 1-60021-015-5.

[Onodera 2002] H. Onodera, S. Narita, H. Yamada, H. Suzuki, N. Tanaka, T. Nyui, “Analysis of Nuclear Products in Hydrogen Penetration through Palladium,” *Proc. JCF4*, pp. 42 – 45 (2002), ISSN 2187-2260.

[Passell 2000] T.O. Passell and R. George, “Trace Elements added to Palladium by Exposure to Gaseous Deuterium,” *Proc. ICCF8*, pp. 129 – 134 (2000), ISBN 88-7794-256-8.

[Passell 2003] T.O. Passell, “Evidence for Lithium-6 Depletion in Pd Exposed to Gaseous Deuterium and Hydrogen,” *Proc. ICCF9*, pp. 299 – 304 (2003), ISBN 7-302-06489-X.

[Plackett 1958] R.L. Plackett, “The Principle of the Arithmetic Mean,” *Biometrika*, **45**, Issue 1-2, pp. 130–135 (1958).

[Rajeev 2017] K. P. Rajeev and D. Gaur, “Evidence for Nuclear Transmutations in Ni-H Electrolysis,” *J. CMNS (Proc. ICCF20)* Vol. 24, pp.278 – 283 (2017), ISSN 2227-3123.

- [Sakano 2004] M. Sakano, S. Sakai, T. Itoh, Y. Iwamura and S. Kuribayashi, “Confirmation of Transmuted Elements on Pd Complexes using D<sub>2</sub> Gas Permeation Method,” *Proc. JCF5*, pp. 55–59 (2004), ISSN 2187-2260.
- [Sasaki 2002] S. Sasaki, T. Sato, T. Kubozono, S. Narita, H. Yamada and T. Ohmori, “Nuclear Reaction Occurring in Light Water Electrolysis on Gold and Cobalt,” *Proc. JCF4*, pp. 13 – 16 (2002), ISSN 2187-2260.
- [Savvatimova 1996] Savvatimova I. B., Senchukov A. D. and Chernov I. P. , “Transmutation Phenomena in the Palladium Cathode after Ions Irradiation at the Glow Discharge,” *Proc. ICCF6*, pp. 575 – 579 (1996), NEDO and Institute of Applied Energy.
- [Suess 1956] H.E. Suess and H.C. Urey, “Abundances of the Elements,” *Rev. Mod. Phys.*, **28**, 53 – 74 (1956), ISSN 0034-6861.
- [Takahashi 2014] N. Takahashi, S. Kosaka, T. Hioki and T. Motohiro, “Detection of Pr in Cs Ion-implanted Pd/CaO Multilayer Complexes with and without D<sub>2</sub> Gas Permeation,” *J. CMNS, Vol. 13 (Proc. ICCF17)*, pp. 579–585 (2014), ISSN 2227-3123.
- [Trimble 1975] V. Trimble, “The Origin and Abundances of the Chemical Elements,” *Rev. Mod. Phys.*, **47**, 877 – 976 (1975), ISSN 0034-6861.
- [Tsutani 2003] K. Tsutani, “Examination of Evidence in EBM,” *Therapeutic Research*, **24**, No. 8, pp. 1415 – 1422 (2003).
- [US AMTL 1978] U.S. Army Material Technology Laboratory, “Energy Development from Elemental Transmutations in Biological System,” 1978.
- [Violante 2003] V. Violante, P. Tripodi, D. Di Gioacchino, et al., “X-Ray Emission during Electrolysis of Light Water on Palladium and Nickel Films,” *Proc. ICCF9*, pp. 376 – 382 (2003), ISBN 7-302-06489-X.
- [Vysotskii 1996] V.I. Vysotskii, A.A. Kornikova and I.I. Samoylenko, “Experimental Discovery of the Phenomenon of Low-Energy Nuclear Transmutation of Isotopes (<sup>55</sup>Mn → <sup>57</sup>Fe) in Growing Biological Cultures,” *Proc. ICCF6*, pp. 687 – 693 (1996), NEDO and Institute of Advanced Energy.
- [Vysotskii 2015] V.I. Vysotskii and A.A. Kornilova, “Microbial Transmutation of Cs-137 and LENR in Growing Biological Systems,” *Current Science*, **108**, 636 – 641 (2015). (Increasing decay rate of Cs-137 isotope)
- [Walker 2008] E. Walker, A.V. Hernandez and M.W. Kattan, “Meta-analysis: Its Strengths and Limitations”. *Cleve. Clinic. J. Med.* **75** (6): 431–9, (2008), PMID 18595551.
- [Yamada 2003] H. Yamada, S. Narita, H. Onodera, H. Suzuki, N. Tanaka, T. Nyui and T. Ushirozawa, “Elemental Analysis on Pd-Foil after Hydrogen Permeation at Room Temperature by TOF-SIMS,” *Proc. JCF5*, pp. 69 – 73 (2003), ISSN 2187-2260.
- [Yamada 2006] H. Yamada, S. Narita, S. Taniguchi, T. Ushirozawa, S. Kurihara, M.

Higashizawa and M. Itagaki, "Producing an Element of Mass Number 137 on Multilayered Pd Sample with Small Amount of Cs by Deuterium Permeation," *Proc. JCF7*, pp. 28–32 (2006), ISSN 2187-2260.

[Yamaguchi 2008] T. Yamaguchi, Y. Sasaki, T. Nohmi, A. Taniike, Y. Furuyama, A. Kitamura and A. Takahashi, "Investigation of Nuclear Transmutation Using Multilayered CaO/X/Pd Samples Under Deuterium Permeation," *Proc. ICCF14*, pp. 195–202 (2008), ISBN 978-0-578-06694-3.